CHAPTER 1

INTRODUCTION

1.1 Optics Communication and Fiber Laser

The emergence of fiber-optic technology has provided many applications such as in laser based measurements and communications. Fiber optic was first developed during the 1960s, but the devices were extremely lossy (loss >1000 dB/km) for the modern standard. However, the situation changed drastically in the 1970s, when the progress in fabrication technology has resulted in a tremendous improvement where the fiber loss can be reduced down to 0.2 dB/km in the communication window of 1550 nm by the end of 1970s. This loss is limited mainly by the fundamental process of Rayleigh scattering. Hence, the availability of low loss silica fibers led to a revolution in the field of doped-fiber and optical fiber communications [1].

Despite the collapse of the Internet bubble at the beginning of the 21st century, there was an increase in demand for information technologies. At present, multimedia systems transmit not only voice, but they also exchange numerical data, text, image, video and others. The multiplicity of communication means such as videoconference, the Internet and videophone have dramatically increased the volume of information exchanged worldwide. The current growth of data transmission is facilitated by the advances of laser and fiber technologies. In the sixties, with the invention of the laser, the idea of using light

as an information carrier emerged. The continuous developments of optical components, such as optical fibers and amplifiers, made light an efficient means of transmitting and delivering information for backbones and wide area networks. To optimize the use of the bandwidth in optical fibers and to satisfy the bandwidth demand of future networks, multiplexing techniques that consist of merging several communications channels into one have been exploited [2]. The wavelength division multiplexing (WDM) techniques have shown to unlock the available fiber capacity and to increase the performances of broadband optical access networks. One of the essential components is the creation of new low-cost laser sources. Candidates for such applications are multi-wavelength fiber ring lasers as they have simple structure, are low cost, and have a multi-wavelength operation.

By employing a piece of doped fiber in a resonator and having it pumped by a diode laser, fiber lasers can be produced in the visible or infrared region of electromagnetic spectrum. The fiber lasers have some advantages compared to bulk-optics systems like compact size, high efficiency and high beam quality. The lasers in time-domain can be categorized into two groups “continuous wave fiber lasers” or “pulsed fiber lasers”, and in wavelength domain as single wavelength or multi-wavelength. Such lasers were made as early as 1976 and have remained an active topic of study since then [3, 4]. Fiber lasers can be used to generate CW radiation as well as ultra-short optical pulses. The nonlinear effects associated with the host fiber play a relatively small role in the case of CW operation until power levels exceed several watts. Various configurations with ring or Fabry-Perot geometry have been used for making lasers, each having its own advantages. In linear cavity fiber lasers, the mirrors can be replaced in various ways but the use of Fiber Bragg Gratings (FBGs) is very attractive because of their wavelength selective nature. Otherwise, no mirrors are needed in the ring cavity case as such a cavity can be made by using a directional fiber coupler for loop mirrors [5, 6]. Longitudinal mode interference in the laser

cavity can also be used to produce multiple lines. The fiber laser based on cavity operates efficiently and exhibits stable wide tunable range, narrow linewidth and could be tuned at high speed allowing fast component characterization. To date, many works on Erbium-doped fiber laser (EDFL) have been reported for single-wavelength and multi-wavelength operations. The EDFLs can operates either in C-band or L-band region when they are pumped at the wavelength of 0.98 μm or 1.48 μm due to the energy level difference between the meta-stable level and the ground state of the Erbium ion. However, this type of laser cannot operate at wavelengths beyond 1610 nm due to the excited state absorption (ESA) effect in the silica-host material. Furthermore, the long cavity length that is required for the EDFL makes them more susceptible to environmental influence and affects the stability of the laser [7]. In this work, compact fiber lasers are demonstrated using a Bismuth-based EDF (Bi-EDF) as the gain medium instead of the Silica-based. The Bi-EDF can be doped with a much higher concentration of Erbium ions than that in Si-EDF without introducing any deleterious ion quenching effects [8]. Therefore, a compact device can be achieved using this fiber. The Bi-EDF based fiber laser can also operate in the extended L-band region due to the suppression of ESA effect.

1.2 Overview on Multi-wavelength Fiber Lasers

Recently, multi-wavelength lasers have caused considerable interests due to their potential applications such as WDM systems, fiber sensors and fiber-optics instrumentations. Requirements for multi-wavelength sources include; stable multi-wavelength operation, high signal to noise ratio and channel power flattening. Compared to a system that uses a number of discrete semiconductor diode laser [9], it is physically simpler to produce a multiple wavelength source using a single gain medium including a

wavelength selective element. In order to define lasing wavelengths, wavelength selective comb filters have been included in the laser cavity. A multi-wavelength laser is highly desirable for the cost and size reduction, improvement of system integration and compatible with optical communication networks. For the past one decade or so, EDFs have been extensively studied and developed as a gain medium for the multi-wavelength laser.

In EDFL, the Erbium ions possess split Stark sublevels with multiple allowed transitions possibility of having oscillations at more than one wavelength. Therefore, the multi-transitions can be achieved in this fiber laser due to the depletion of Stark sub-levels which is selective and depends on the polarization of the wave. However, the outputs of the EDFLs are not stable at room temperature due to homogeneous broadening of lasing modes [2]. To increase the in-homogeneity one can cool Er^{+3} doped fiber at liquid nitrogen temperature [5, 6]. Generally, in order to produce the multi-wavelength, we have to employ intra-cavity filter in the EDFL cavity. In some works, a polarization controller (PC) is used in the cavity to change both the number of lasing lines and spacing of the multi-wavelength laser [10, 11].

There are also other methods to get simultaneous multi-wavelength outputs such as multi-wavelength Raman lasers [12, 13], multi-wavelength generation using semiconductor optical amplifiers (SOA) [14] and multi-wavelength Brillouin fiber lasers (BFLs) [15,16]. Special fibers such as dispersion compensating fibers (DCFs) have been used to increase the Raman gain in multi-wavelength Raman fiber lasers where the output power are limited only by the available pump sources [17]. Of the various approaches, the interest on the multi-wavelength fiber laser is increasing due to the improvements in number of lasing lines and power flatness. Furthermore, the BFL is easier to be generated due to the lower threshold pump power [18].

Brillouin fiber laser

Brillouin fiber lasers have been comprehensively investigated throughout the years due to their potential applications as coherent light sources and the sources of high microwave frequencies. The BFLs have a capability to produce a highly coherent light source with linewidth narrowing effect [18, 19]. The coherent light sources are an essential requirement for a variety of applications, such as coherent optical communication, coherent radar detection, interferometric sensing, and microwave photonics. The latter application arises because the Brillouin shift in fiber is typically of the order of 10 GHz at ~1.55 μm [20], so that the beat frequency between pump and Stokes is in the microwave range. The BFLs use a stimulated Brillouin scattering (SBS) effect in optical fiber to produce a highly coherent light source with linewidth narrowing effect [18, 19]. The SBS effect in single-mode fiber (SMF) enables multi-wavelength generation in BFL with constant spacing and narrow linewidth at room temperature. This effect is obtained from the interaction between the intense pump light and acoustic waves in a medium that resulted in a backward propagating Stokes once the Brillouin threshold is reached [1, 21].

However, the BEFL combines the gain from SBS and EDF. BEFL with 11 GHz Stokes shift in ring cavity and linear cavity BEFL have been demonstrated [6, 18]. The BEFLs consisting of a Fabry-Perot cavity exhibit features that are qualitatively different from those making use of a ring cavity. The difference occurs from the simultaneous presence of the forward and backward propagating components associated with the pump and Stokes waves. Higher order Stokes wave are generated through cascaded SBS, a process in which each successive Stokes component pumps the next order Stokes component after its power becomes large enough to reach the Brillouin threshold. At the same time, anti-Stokes components are generated through four-wave mixing (FWM) between co-propagating pump and Stokes waves [8]. However, the number of Stokes and

anti-Stokes lines is strongly depended on the pump power. The BEFL operation is also extremely sensitive to resonance detuning between the pump laser frequency and the Brillouin cavity mode.

FWM-based fiber laser

The multi-wavelength fiber laser with excellent stability and uniformity can be also achieved experimentally at room temperature using a FWM effect in the SMF. This fiber laser has a more stabilized output as a result of the balance between FWM effect and the mode competition effect of EDF, which is useful for applications in wavelength converters, optical parametric oscillator (OPO), determination of nonlinear parameters as well as multi-wavelength laser source for the WDM system [22-24].

1.3 Nonlinear Effects in Optical Fibers

Different nonlinear effects such as FWM [25], Self-phase modulation (SPM) [26], SBS [27] and Raman amplification [28] have been used in multi-wavelength fiber laser source generation. In this thesis, the multi-wavelength generations in two effects; SBS and FWM have been thoroughly investigated. This section briefly describes both effects.

SBS

Electrostriction is the tendency of materials to become compressed in the presence of an electric field. Electrostriction is of interest both as a mechanism leading to a third-order nonlinear optical response and as a coupling mechanism that leads to SBS [1]. SBS is a nonlinear effect that results from the interaction between intense pump light and acoustic waves in a SMF, thus giving rise to backward propagating frequency shifted light

[29]. The thermally excited acoustic waves generate an index grating that co-propagates with the pump at the acoustic velocity in the SMF. This moving grating reflects the pump light and causes the backscattered light to experience a frequency downshift of 11 GHz. SBS can easily take place in an optical fiber as a result of its small core diameter and low loss and requires the lowest power to be observed among all nonlinear phenomena in fibers. The cascaded Brillouin effect gives rise to higher order Stokes that can compete with one another giving rise to a broader microwave spectrum in multi-wavelength fiber laser generation.

FWM

Another nonlinear effect, which is due to the third-order electric susceptibility is called the optical Kerr effect. The FWM is a type of optical Kerr effect, and occurs when light of two or more different wavelengths is launched into a fiber. FWM is a kind of optical parametric oscillation [30]. The FWM phase-matching factor is dependent on the signal power [31]. Hence, phase matched FWM can result in the generation of new optical frequencies in fibers. In this case two photons of the pump source generate two sidebands which must be phase matched along the fiber length for optimum efficiency. However, it is difficult to maintain phase matching over a long length of fiber. Therefore, the FWM-based devices focus on applying highly nonlinear fibers such as dispersion-shifted fiber [32], dispersion compensating fiber and the photonic crystal fiber [33-35]. These fibers have a large nonlinear coefficient and thus only a short length is sufficient to introduce significant FWM effect. Multi-wavelength fiber laser can be achieved with a more stable output, cheaper and wider tenability using this type of fibers. Recently, a Bismuth oxide based fiber has been reported to have a high nonlinearity that opens the opportunity to implement a range of nonlinear devices with only a meter or less of the fiber. Another important

application of FWM is in wavelength conversion. The FWM also provides the basic technology for measuring the nonlinearity and chromatic dispersion parameters of optical fibers.

1.4 Optical Fiber Amplifiers

Optical fiber amplifiers have found widespread use not only in long distance point to point optical fiber links, but also in multi-access networks to compensate signal splitting losses. The features of optical amplifiers have led to many diverse applications, each having different design challenges [36]. The Erbium-doped fiber amplifier (EDFA) that is one type of rare-earth doped fiber amplifier is the most deployed fiber amplifier. As a practical amplification medium, EDFAs have been extensively studied due to their excellent gain operation due to Er^{3+} ion emission in the 1500 nm region [37]. Commercially, available EDFA is realized by the year 1992 after the introduction of laser diode pumped EDFA by M. Nakazawa et. al. in 1989 [38]. Since then, diode pumped EDFA has become a popular research field in optical communications.

However, the ideal amplifier should have high gain, high power conversion efficiency (PCE) and high saturated output power as well as low noise figure. In order to achieve high gain in L-band region, optimum long EDF should be used and this length makes handling of fiber spools difficult. Erbium ion concentration in silica fiber can only be increased up to 1,000 ppm, to reduce the EDF length and low loss characteristic that maintain the number of Erbium ion concentration in EDF. Recently, many researchers are looking into other alternative glass hosts for Erbium ions and Bismuth Oxide-based glass which is one of solutions to achieve a high concentration and compact EDFA. A broad band amplification

over C + L band or extended L-band have been reported in many literatures using fusion splice-able Bismuth oxide based Erbium doped fiber (Bi-EDF). Bi-EDF has the advantage of needing just a few meters the fiber for effective amplification in L-band region [39]. For instance, an efficient and low noise figure Bi-EDFA has been demonstrated with a broadband gain profile covering the wavelength region from 1530 nm to 1620 nm using a very short length of doped-fiber [40]. This fiber also has a higher nonlinearity property than other type of fibers, which opens the possibility to be used in BFL (BEFL) or FWM-based fiber laser.

Recently, Raman amplifiers and Raman fiber lasers also received considerable attention because they are easy to implement and they inherently allow any wavelength to be amplified. The appearance of band structure which places constraints upon the allowed photon states within the crystalline material offers the possibility of controlling the spontaneous emission process by engineering the material microstructure, which is significant for the design of novel lasers and amplifiers. Discrete Raman amplifiers with over 100 nm gain-bandwidth have already been demonstrated covering the S- and L-bands [33]. In this thesis, the Raman amplifier performance is also investigated in various types of fibers such as dispersion compensating fiber (DCF), photonics crystal fiber (PCF) and Bi-EDF. The Raman amplification is also used to assist in multi-wavelength generation of BFL [41].

1.5 Research Objectives

This thesis widely investigated the use of Bi-EDF as an alternative medium for optical amplification as well as applications in nonlinear fiber lasers. The Bismuth glass host provides the opportunity to be doped heavily with Erbium ions to allow a compact

optical amplifier design. One of the objectives of this work is to investigate the amplification characteristics of the Bi-EDFA in C-, L- and extended L-band region. Besides providing an efficient and broadband amplification, the Bi-EDF also exhibits a very high fiber nonlinearity, which can be used for realizing new nonlinear devices such as multi-wavelength as well as narrow linewidth fiber lasers. The main objective of this thesis is to demonstrate a multi-wavelength fiber laser with a dense number of lines, flat and stable output power as well as a constant spacing using the nonlinear effects in the Bi-EDF. This thesis details on the generation of multi-wavelength laser using a very short length of Bi-EDF based on either SBS or FWM effects.

1.6 Thesis Overview and Methodology of Research

This thesis comprehensively studies the Bi-EDF for optical amplification as well as applications in BEFL and FWM-based fiber laser. The Bi-EDF provides a very high Erbium ion concentration to allow a compact optical amplifier and fiber laser design. This thesis is organized into six chapters. The first chapter introduces the main topics such as optical communication, nonlinear effects and multi-wavelength fiber lasers.

Chapter 2 describes the literature review and background of the study. It also explains on the theory of nonlinear effects in optical fibers, optical amplifiers and fiber lasers. We also discussed on the SBS and FWM and its applications in multi-wavelength fiber laser generation as well as in determination of the nonlinear parameters of fibers. The brief description on the Bi-EDF is also presented in this chapter.

Chapter 3 is devoted to investigate the amplification characteristics of Bi-EDF for operation in C- and L-band regions. Compared to silica-based Erbium-doped fiber, this fiber only requires a gain medium as short as 215 cm for long wavelength band (L-band)

amplification and also capable to provide a wider gain bandwidth up to the extended L-band region. This chapter examines the gain, noise figure, conversion efficiency of the Bi-EDFA. The performance of fiber Raman amplifier is also investigated for various pumping schemes and gain media.

Besides providing an efficient and broadband amplification, the Bi-EDF also exhibits a very high fiber nonlinearity, which can be used for realizing new nonlinear devices such as multi-wavelength as well as narrow linewidth fiber lasers. Chapter 4 demonstrates BEFLs under a new approach using a piece of Bi-EDF as both linear and nonlinear gains media for single-wavelength and multi-wavelength operations. The performance of the BEFL is investigated under various configurations. The multi-wavelength fiber laser produces a comb like output based on SBS effect. Multi-wavelength Brillouin/Raman Fiber Laser and its applications is also discussed at the end of this chapter.

Besides SBS, the FWM effect can also be used for multi-wavelength laser generation. Chapter 5 demonstrates a multi-wavelength laser using a Bi-EDF as a gain medium. In this chapter, a FWM effect is also investigated in various types of fibers including the Bismuth-based EDF, where the interaction between a pump and probe signals generate sidebands. The FWM effect is also used to estimate some of the nonlinear parameters such as nonlinear coefficient and refractive index coefficient of the Bi-EDF.

Chapter 6 is dedicated to summary and general conclusion of this study. The recommendation for further research work is also presented in this chapter. In appendix, the copy of the selected published papers during the PhD in which the author was actively involved is also included. The summary of this work is also presented in the following flow-chart. The flow-chart shows the methodology of this research work.

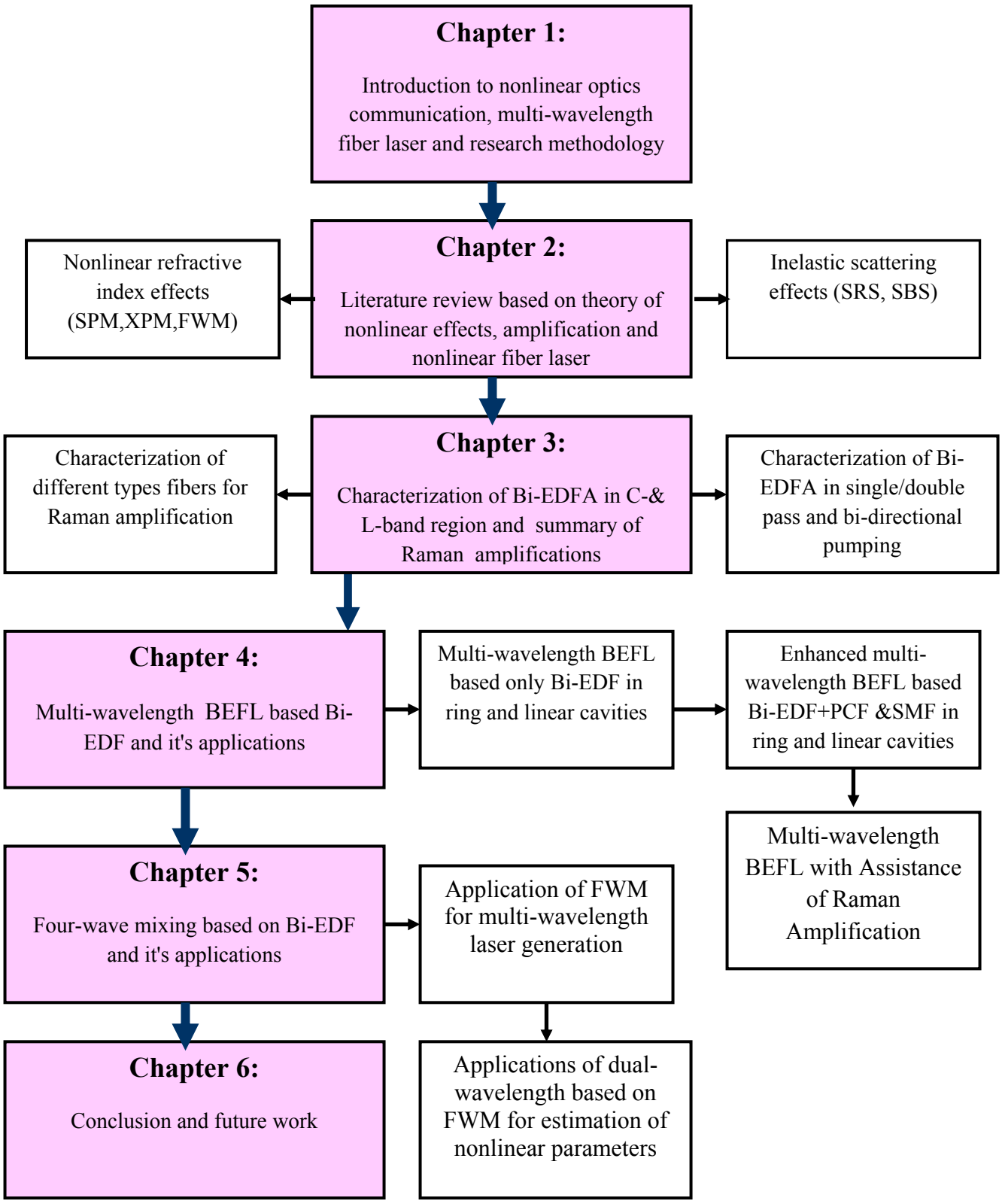

Figure 1.2: Methodology of research

REFERENCES

[1] R. W. Boyd, "Nonlinear Optics," Third edition, Academic Press, San Diego, 2007.

[2] M. Yamada, "Overview of Wideband Optical Fiber Amplification," NTT Technical, Vol.213, pp.63-66, 2002.

[3] K. O. Hill, B. S. Kawasaki, and D. C. Johnson, "CW Brillouin laser," Appl. Phys. Lett. Vol.28, pp.608, 1976.

[4] C. Montes, D. Bahloul, I. Bongrand, J. Botineau, G. Cheval, A. Mahmhoud, E. Picholle, and A. Picozzi, Self-pulsing and dynamic bistability in CW-pumped Brillouin fiber ring lasers, J. Opt. Soc. Am. Vol. 16, No. 6, pp. 932, 1999.

[5] P. W. France, "Optical fiber lasers and amplifiers," CRC Press Inc., Florida, 2000.

[6] G. P. Agrawal, " Nonlinear Fiber Optics,"Fourth edition, Academic Press, 2007.

[7] H. L. Liu, H. Y. Tam, W. H. Chung, P. K. A. Wai and N. Sugimoto, "La-codoped Bismuth-based Erbium-doped Fiber Ring laser bandwidth 80-nm Tuning Range," Photonics Technology Letters. Vol. 17, No. 2, pp. 297 – 299, 2005.

[8] N. Sugimoto, "Ultrafast optical switches and wavelength division multiplexing (WDM) amplifiers based on Bismuth oxide glasses," J. Am. Ceram. Soc., Vol.85, No.85, pp. 1083-1088, 2003.

[9] M. Ibsen, S. Alam, M. N. Zervas, A. B. Grudinin, and D.N. Payne, 8 and 16 Channel All-Fiber DFB Laser WDM Transmitters with Integrated Pump Redundancy, IEEE IEEE Photon. Technol. Lett. Vol. 11, No. 9, pp.1114-1116, 1999.

[10] N. Park, and P.F. Wysocki, "24-line multi-wavelength operation of erbium doped fiber ring laser," IEEE Photon. Technol. Lett., Vol. 8, pp.1459- 1561, (1996).

[11] S. Yamashita and T. Baba, "Multi-wavelength fiber lasers with tunable wavelength spacing," Opt. Fiber Commun. Conf., Anaheim,CA, 3, 2001.

[12] E. Yamada, H. Takara, T. Ohara, K. Sato, T. Morioka, K. Jinguji, M. Itoh and M. Ishii, " A high SNR, 150 ch supercontinum CW optical source with precise 25 GHz spacing for 10 Gbit/s DWDM systems," Opt. Fiber Commun. Conf., Anaheim, CA, 2001.

[13] F. Koch, P. C. Reeves-Hall, S. V. Chernikov and J. R. Taylor, " CW multiple wavelength, room temperature, Raman fiber ring laser with external 19 channel, 10 GHz pulse generation in a single electro-absorption modulator," Opt. Fiber Commun. Conf., Anaheim, CA, 3, 2001.

[14] N. Pleros, C. Bintjas, M. Kalyvas, G. Theophilopoulos, K. Yiannopoulos, S. Sygletos, and H. Avamopoulos, "Multiwavelength and power equalized SOA laser sources," IEEE Photon. Technol. Lett.,Vol. 14, pp.693-695, 2002.

[15] S. W. Harun, X. S. Cheng, N. K. Saat and H. S. Ahmad, "L-band Brillouin erbium fiber laser Electron," Lett. Vol. 4, pp.174–6, 2005.

[16] A. K. Zamzuri, M. A. Mahdi, A. Ahmad, and M. H. Al-Mansoori, "Flat amplitude multi-wavelength Brillouin–Raman comb fiber laser in Rayleigh-scattering-enhanced linear cavity," Opt. Express, Vol. 15, pp. 3000–5, 2007.

[17] M. J. Guy, S. V. Chernikov and J. R. Taylor, "Lossless transmission of 2 ps pulses over 45 km of standard fiber at 1.3 μm using distributed Raman amplification," Electron. Lett. Vol. 34, pp. 793–4, 1998.

[18] G. J. Cowle, W. H. Loh, R. J. Laming and D. Y. Stepanov, "Multi-wavelength operation of Brillouin/Erbium fiber laser with injection-locked seeding, Optical Fiber Communication Conf. OFC 97, pp. 34–5, 1997.

[19] M. P. Fok and C. Shu, "Spacing-adjustable multi-wavelength source from a stimulated Brillouin scattering assisted erbium-doped fiber laser" Opt. Express, Vol. 14, pp. 2618–24, 2006.

[20] A. Carter, K. Tankala, and B. Samson, "Optical Fibers for Industrial Laser Applications," Academic Press in an imprint of Elsevier, 2007.

[21] S. Yamashita and K. Hotata "Multi-wavelength erbium-doped fiber laser using intra-cavity etalon and cooled by liquid nitrogen," Electron. Lett. Vol. 32, pp. 1298–9, 1992.

[22] X. Liu **,** Self-stabilizing effect of four-wave mixing and its applications on multi-wavelength erbium-doped fiber lasers, Photonics technology letters IEEE, Vol. 17, No. 12, pp. 2541- 2543,2005.

[23] S. W. Harun, S. Shahi, H. Ahmad, "Bismuth erbium-doped fiber based multi-wavelength laser assisted by four-wave mixing process," IEICE Electronics Express, Vol. 6, No. 1, pp.40-43, 2009.

[24] A. Shtainhart, R. Segal, A. Tsherniak, "Wavelength division multiplexing," Networks, Radar Communication, 1999.

[25] X. Liu, X. Yang, F.Lu, J. Ng, X. Zhou, C. Lu, "Stable and uniform dual-wavelength erbium-doped fiber laser based on fiber Bragg gratings and photonic crystal fiber," Opt. Express ,Vol.13 ,pp.142, 2005.

[26] J. J. Veselka, S.K. Korotky, "A multiwavelength source having precise channel spacing for WDM systems," IEEE Photon. Technol. Lett. Vol.10, 1998.

[27] Y. J. Song, L. Zhan, J.H. Ji, Y. Su, Q.H. Ye, Y.X. Xia, "Self-seeded multi-wavelength Brillouin-erbium fiber laser," Opt. Lett. Vol. 30, pp.486-488, 2005.

[28] Y. G. Han, C. S. Kim, J. U. Kang, U. C. Paek, Y. Chung, " Multi-wavelength Raman Fiber-Ring Laser Based on Tunable Cascaded Long-Period Fiber Gratings," IEEE Photon. Technol. Lett. Vol.15, pp.383, 2003.

[29] G. P. Agrawal, "Applications of Nonlinear Fiber Optics," Academic press, 2001.

[30] J. E. Sharping, M. Fiorentino, A. Coker, P. Kumar, and R. S. Windeler, "Four-wave mixing in microstructure fiber," Opt. Lett. Vol. 26, pp.1048-1050, 2001.

[31] S. Pachnicke, J. Reichert, and E. Voges, "Impact of polarization-mode dispersion and fiber nonlinearities on four-wave mixing efficiency," OECC, 5F2-2-2, 2006.

[32] K. Inoue and H. Toba, "Wavelength conversion experiment using fiber four-wave mixing," IEEE Photon. Technol. Lett., Vol. 4, No.1, pp.69 – 72, 1992.

[33] Z. Yusoff, "Application of highly nonlinear holey fibres in optical communications," 2004.

[34] W. Belardi, J. H. Lee, K. Furusawa, P. Petropoulos, M. Ibsen, T. M. monro, and D. J. Richardson, "A 10 Gbit/s tunable wavelength converter based on four-wave mixing in highly nonlinear holey fiber," conference on optical communication in Europe, PD1.2, Copenhagen, Denmark, 2002.

[35] O. Aso, S. I. Arai, T. Yagi, M. Tadakuma, Y. Suzuki, S. Namiki, "Broadband four-wave mixing generation in short optical fibres," Electronics Letters, Vol. 36, No. 8, pp.709 – 711, 2000.

[36] G. Keiser, "Optical Fiber Communications," McGraw-Hill Series in Electrical and Computer Engineering, International Editions 2000.

[37] P. C. Becker, N. A. Olsson, J.R. Simpson, "Erbium-Doped Fiber Amplifiers," Academic Press, USA, 1999.

[38] M. Nakazawa, Y. kimura, and K. Suzuki, "Soliton amplification and transmission with Er^{3+} doped fiber repeater pumped by GaInAsP laser diode," Electron. Lett., Vol. 25, pp. 199-200, 1989.

[39] N. Sugimoto, T. Nagashima, T. Hasegawa, S. Ohara, K. Taira, K. Kikuchi, "Bismuth-based optical fiber with nonlinear coefficient," 2004**.**

[40] S. Tanabe, N. Sugimoto, S Ito, T. Hanada, "Broad-band 1.5 μm emission of Er^{3+} ions in Bismuth-based oxide glasses for potential WDM amplifier," J. Lumin, Vol. 87, pp. 670-672, 2000.

[41] A. K. Zamzuri, M. A. Mahdi, A. Ahmad, M. I. Md Ali, and M. H. Al-Mansoori, "Flat amplitude multi-wavelength Brillouin-Raman comb fibre laser in Raileigh-scattering enhanced linear cavity," Optics Express, Vol. 15, No. 6, pp. 3000-3005, 2007.

CHAPTER 2

LITERATURE REVIEWS ON NONLINEAR EFFECTS, AMPLIFICATION AND FIBER LASERS

2.1 Introduction

The terms linear and nonlinear, in optics, mean intensity independent and intensity dependent phenomena, respectively. Nonlinear effects in optical fibers occur due to the interaction between light and dielectric material [1]. The nonlinear effects can be divided into two categories. The first category arises due to the interaction of light waves with phonons which causes inelastic scattering phenomenon such as stimulated Raman scattering (SRS) and stimulated Brillouin scattering (SBS). The intensity of scattered light grows exponentially if the incident power exceeds a certain threshold value. The difference between Brillouin and Raman scattering is that the Brillouin generated phonons (acoustic) that are coherent and give rise to a macroscopic acoustic wave in the fiber, while in Raman scattering the phonons (optical) are incoherent and no macroscopic wave is generated. The second category is due to the change in the refractive index of the medium with optical intensity, which is responsible for the Kerr-effect. Depending upon the type of input signal, the Kerr-nonlinearity manifests itself in three different effects such as self-phase modulation (SPM), cross-phase modulation (XPM) and four-wave mixing (FWM).

The field of nonlinear fiber optics has generated a tremendous interest since 1990s and has grown considerably recently. It has led to a number of advances important from the

fundamental as well as the technological point of view. The observation of slow-light has been recently demonstrated in silica optical fibers by using the dispersion associated with laser induced amplification of a material resonance as is the case in SBS [2, 3] and SRS [4,5]. For applications involving SBS, it is desirable to have medium that has large Brillouin gain coefficient, g_B in order to reduce the threshold power and also the device length. Although many crystals and organic materials are reported to have large Brillouin gain coefficients [6], many are difficult to draw in the form of optical fibers. So far, a number of non-silica based fibers are successfully drawn into optical fibers, which include Tellurite, Bismuth and Chalcogenide glass fibers. These fibers are reported to have large nonlinear Kerr and Raman gain coefficients, and already found to have potential applications in high-speed optical signal processing [7, 8].

Recently, Bismuth-based Erbium-doped fibers (Bi-EDFs) have been extensively studied for use in compact amplifiers with short gain medium lengths. These fibers incorporate Lanthanum (La) ions to decrease the concentration quenching of the Erbium ions in the fiber [9], which in turn allows the Erbium ion concentration to be increased to above 1000 ppm. A fiber with such a high Erbium dopant concentration is expected to have enormous potentials in realizing compact EDFAs and EDFA-based devices. In this work, CW multi-wavelength lasers are demonstrated using the nonlinear effects in the Bi-EDF. This chapter reviews on the nonlinear effects that occur in a single-mode fiber and some background information about Bi-EDF. A literature survey on the experimental analysis, measurements, and applications of nonlinear fiber laser is then presented.

2.2 Nonlinear Effects in Optical Fibers

Nonlinear optics is the study of the interaction of intense laser light with matter [10]. This is caused by the anharmonic motion of bound electrons under the influence of the applied field. For a nonlinear material, the electric polarization **P** induced by electric dipoles is not linear in the electric field, but is described by the more general relation [11, 12]:

$$\mathbf{P} = \varepsilon_0 \chi^{(1)} : \mathbf{E} + \varepsilon_0 \chi^{(2)} : \mathbf{EE} + \varepsilon_0 \chi^{(3)} : \mathbf{EEE} + \dots \qquad (2.1)$$

where ε_0 is the vacuum permittivity and $\chi^{(n)}$ is the *n*-th order component of the electric susceptibility of the medium. The ":" symbol represents the scalar product between matrices. The relationship explicitly describes the *i*-th component for the vector *P* and also be expressed as

$$P_i = \varepsilon_0 \sum_{j=1}^{3} \chi_{ij}^{(1)} E_j + \varepsilon_0 \sum_{j=1}^{3} \sum_{k=1}^{3} \chi_{ijk}^{(2)} E_j E_k + \varepsilon_0 \sum_{j=1}^{3} \sum_{k=1}^{3} \sum_{l=1}^{3} \chi_{ijk}^{(2)} E_j E_k E_l + \dots \qquad (2.2)$$

where $i = 1, 2, 3$. It is often assumed that $P_1 = P_x$, i.e. the component parallel to *x* of the polarization field; $E_2 = E_y$ and so on. For a linear medium, only the first term of this equation is significant and its effects included through the refractive index *n* and the attenuation coefficient α in which the polarization varies linearly with the electric field. The quantities $\chi^{(2)}$ and $\chi^{(3)}$ are known as the second- and third-order nonlinear optical susceptibilities, respectively. $\chi^{(2)}$ is responsible for nonlinear processes such as second harmonic generation and sum frequency generation. For materials exhibiting a non-

negligible Kerr effect such as FWM, the third, $\chi^{(3)}$ term is significant, with the even-order terms typically falling out due to inversion symmetry of the Kerr medium.

In the next subsections, the nonlinear effects in optical fibres are divided into two categories namely; inelastic scattering (SRS, SBS), Kerr effects (SPM, XPM), and FWM that are relevant to this study and will be described in this thesis.

2.2.1 Inelastic Scattering Effects in Optical Fibers

An inelastic nonlinear effect is an effect that involves an energy transfer between the signal mode and the dielectric medium. Stimulated Brillouin scattering (SBS) refers to the interaction of an optical pulse with acoustic phonons, whereas stimulated Raman scattering (SRS) involves optical phonons. Both of these phenomenas are related to vibrational excitation modes of silica and transfer energy from the optical field to the nonlinear medium [13]. Besides that, both phenomena start to influence the signal close to their threshold power, when they become significant [1]. Different phonons cause some basic differences between the Raman and Brillouin effects. A fundamental difference is that SBS occurs mainly in the backward direction while SRS can occur in both directions [13].

Stimulated Raman Scattering (SRS)

The spontaneous Raman effect was first discovered by C. V. Raman in 1928 [14]. When light encounters molecules in the air, the predominant mode of scattering is elastic scattering, called the Rayleigh scattering. It is also possible for the incident electromagnetic wave to interact with the molecules in such a way that energy is either gained or lost so that the scattered photons are shifted in frequency. Such inelastic scattering is called Raman

scattering. The scattered radiation occurs over all directions and may also have observable changes in its polarization along with its wavelength as described in Figure 2.1. For polarizable molecules, the incident photon energy can excite vibrational modes of the molecules, yielding scattered photons which are diminished in energy by the amount of the vibrational transition energies. The light that is scattered to a lower frequency is called the Stokes and the light that is scattered to a higher frequency is so called the anti-Stokes.

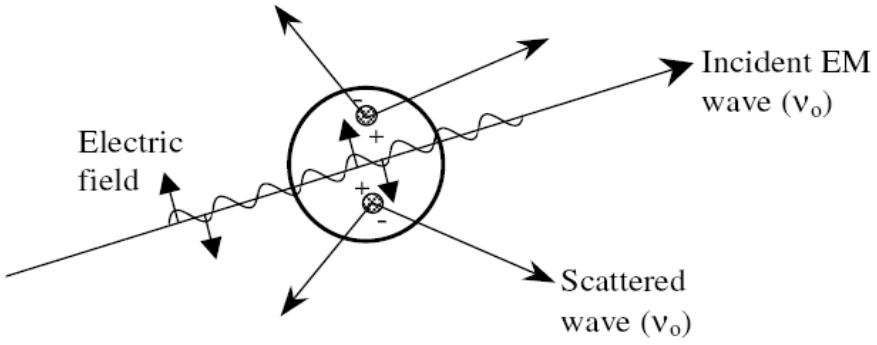

Figure 2.1: Light scattering by an induced dipole moment due to an incident EM wave [15].

These properties of spontaneous Raman scattering can also be described through use of an energy level diagram as shown in Figure 2.2. Raman Stokes scattering consists of a transition from the ground state E_1 to the final state E_2 by means of a virtual intermediate level associated with excited state $E' = h\omega + E_1$ in which this state is a virtual state, the system immediately decays to the final state E_2. Raman anti-Stokes scattering entails a transition from level E_2 to level E_1 with E' serving as the intermediate level. As a result, the final state E_2 has higher energy than the initial state E_1. The anti-Stokes lines are typically much weaker than the Stokes lines or the population of level E_2 is smaller than the population in level E_1 that is because of thermal equilibrium [10].

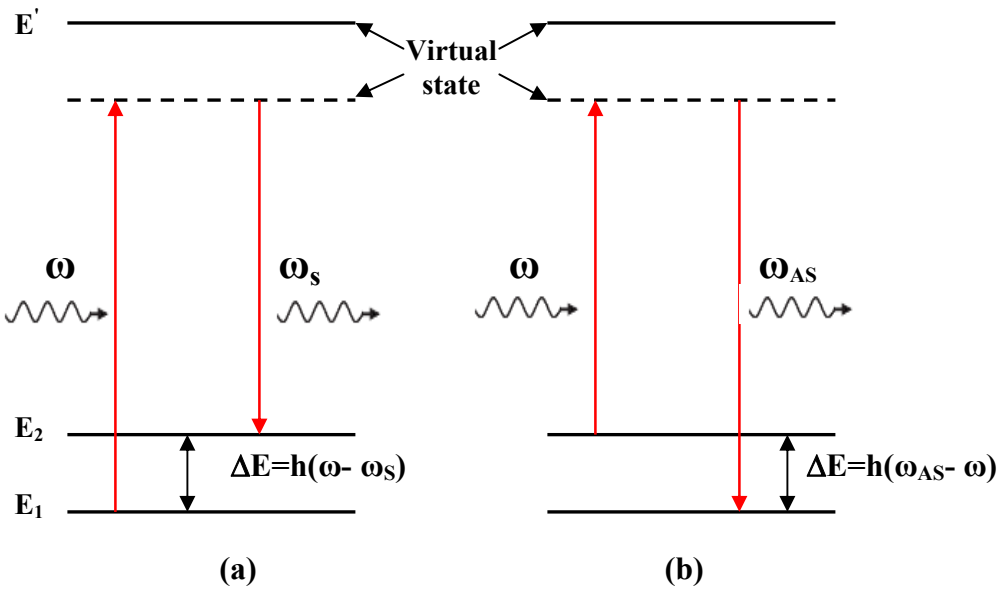

Figure 2.2: Energy level diagrams describing **(a)** Raman Stokes scattering and **(b)** Raman anti-Stokes scattering.

If the medium is excited under an intense laser beam that can modify its optical properties, the rather weak process of spontaneous Raman scattering can turn into a highly efficient scattering process SRS. Typical energy conversion into the Stokes frequency of more than ten percent can normally be observed [10]. The SRS arises from a transition between two vibrational states in the fiber material. This transition is induced by an incoming optical wave that involves optical phonons. Typically, only forward SRS is observed in optical fibers. Because optical phonons are much more energetic than acoustical phonons, SRS produces a larger downshift of the optical frequency in comparison with SBS. In silica, this downshift is about 13 THz, and the useful Raman gain bandwidth is several tera hertz [1]. In optical fibers this is the initial growth of the Stokes wave which can be described by a simple relation. For SRS, this relation is given by [11]

$$\frac{dI_s}{dz} = g_R I_p I_s \tag{2.3}$$

where I_s is the Stokes intensity, I_p is the pump intensity, and g_R is the Raman gain coefficient. It is possible to calculate an approximation for the threshold power level of the SRS as [1]

$$g_R P_{CR} \frac{L_{eff}}{A_{eff}} \approx 16 \tag{2.4}$$

where g_R is the Raman gain that is depends strongly on the composition of fiber core and used dopants; P_{CR} is the critical pump power required to reach the Raman threshold, A_{eff} is the effective area and the effective interaction length, L_{eff} is defined through

$$L_{\mathrm{eff}} = \frac{1}{\alpha}[1 - \exp(-\alpha L)] \tag{2.5}$$

which α is the fiber attenuation and L_{eff} is smaller than the fiber length L due to fiber attenuation. Thus polarization dependence of the Raman gain affects the performance of Raman amplifiers in several different ways [16]. The down-shifted co-polarized light radiates omnidirectionally, and that which reaches the receiver can introduce significant inter-channel crosstalk into the adjacent lower-frequency channels because the spectrum of this SRS component is very broad, as shown in Figure 2.3. For a given incident power level, the Raman effect is three orders of magnitude weaker than the Brillouin effect [17].

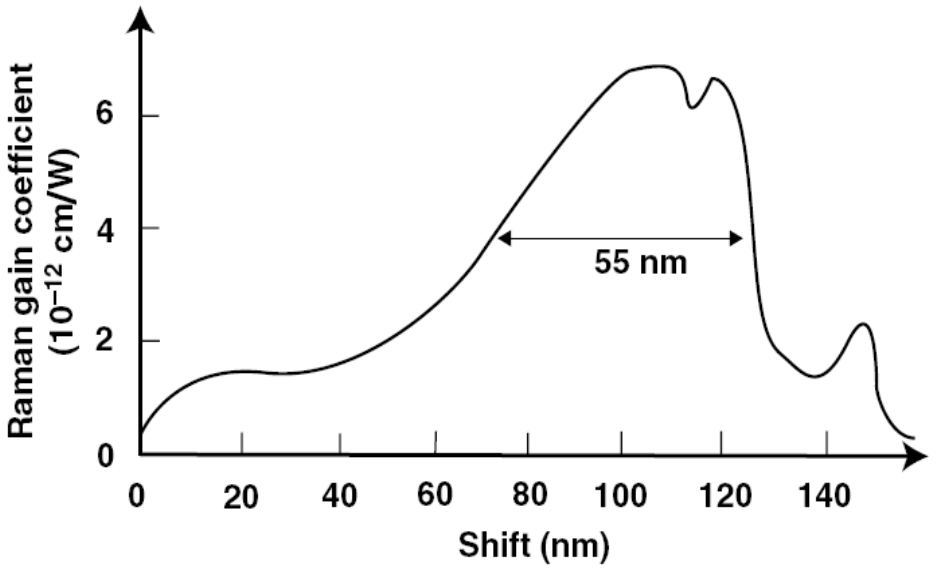

Figure 2.3: Spectrum of energy reradiated by stimulated Raman scattering [17].

However, the SRS is a nonlinear process that can also be exploited in Raman amplifiers and tunable Raman fiber lasers. Raman amplification with 1440 nm pumping will be discussed and used in the following chapters.

Stimulated Brillouin Scattering (SBS)

When a narrow band laser radiation is propagated through optical fiber, a part of the light is seen to scatter in the backward direction when the power exceeds a certain limit [11]. This nonlinear phenomenon which occurs at the lowest power, as low as a few mW in the small core of a single-mode fiber, is Stimulated Brillouin Scattering (SBS) [18] that was discovered by Leon Brillouin in 1922 [19]. He demonstrated that density fluctuations in condensed matter could cause light scattering. The SBS in optical fibers was first observed in 1972 and it has been studied extensively since then because of its implications for light wave systems [20]. It occurs when an optical power reaches the level that can generate

acoustic vibration in a nonlinear medium. The acoustic wave generated by the optical power affects the density of the material and thus changes its refractive index. This refractive index fluctuation can scatter light which is called the Brillouin scattering. Since the light wave are being scattered itself, it also generates the acoustic waves. Similar to SRS, SBS also generates a Stokes wave whose frequency is downshifted from an incident light by the amount set by the nonlinear medium, which the backscattering threshold is higher than the forward threshold. So, the energy can be transferred from a high-frequency channel to a low-frequency by SBS when the channel spacing equals to the Brillouin shift. Hence, the fact that acoustic phonons have much lower energies makes the frequency shift [21] in Brillouin scattering very small (~10 GHz or ~0.08 nm at 1550 nm). The scattered light is downshifted in frequency, because of the Doppler shift associated with a grating moving at the acoustic velocity [20]. However, the SBS can be useful to amplify a narrow band optical signal by propagating in a direction opposite to the pump. The principle of SBS is presented in Figure 2.4.

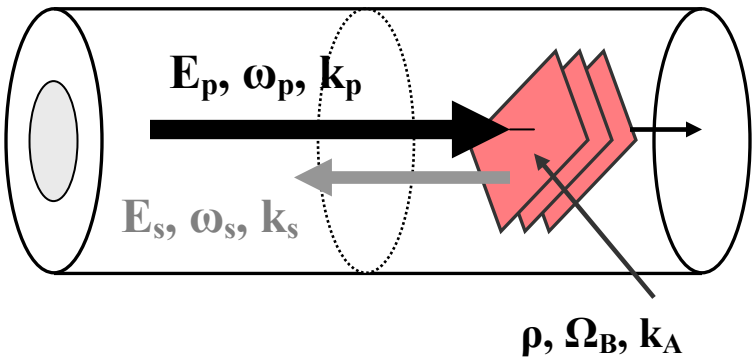

Figure 2.4: Schematic diagram of the SBS process in an optical fiber.

In Figure 2.4, ρ is the density of acoustic wave. Since the energy and momentum are conserved during these scattering events, the frequencies and wave vectors of the pump, scattered, and acoustic fields are given by following equations

$$k_A = k_p - k_s, \tag{2.6}$$

$$\Omega_B = \omega_p - \omega_s \tag{2.7}$$

where ω_p and ω_s are the frequencies, and k_p and k_s are the wave vectors, of the pump and Stokes waves, respectively. The frequency Ω_B and the wave vector k_A of the acoustic wave satisfy the standard dispersion relation

$$\Omega_B = \nu_A |k_A| \approx 2\nu_A |k_p| \sin(\theta/2), \tag{2.8}$$

where v_A is the speed of sound in the medium and θ is the angle between the pump and Stokes fields. However, in a single-mode fiber the relevant θ values are 0 and π. Hence, SBS occurs only in the backward direction with the Brillouin shift given by

$$\nu_B = \Omega_B / 2\pi = 2n v_A / \lambda_p \tag{2.9}$$

where n is the modal index or refractive index of fiber core at the pump wavelength λ_p [11, 22]. Since the scattering occurs in backward direction, the angle θ is π. By using v_A = 5.96 km/s and n=1.45 as typical values for silica fibers, the shift is found to be 11 GHz or 0.09 nm at 1550 nm region. The example of the SBS signals from a Bismuth-based Erbium-doped fiber (Bi-EDF) is shown in Figure 2.5. The peak at the lower wavelength is a BP signal, which is caused by the combination of Rayleigh scattering as well as the spurious reflections from connectors and splice joints. Some small ripples are also observed in the

figure, which may probably due to the limitation of resolution of the OSA. The longitudinal mode interference effect due to back reflection may also contribute to the observation. The Stokes signal due to the SBS is obtained at a down-shifted frequency as shown in Figure 2.5.

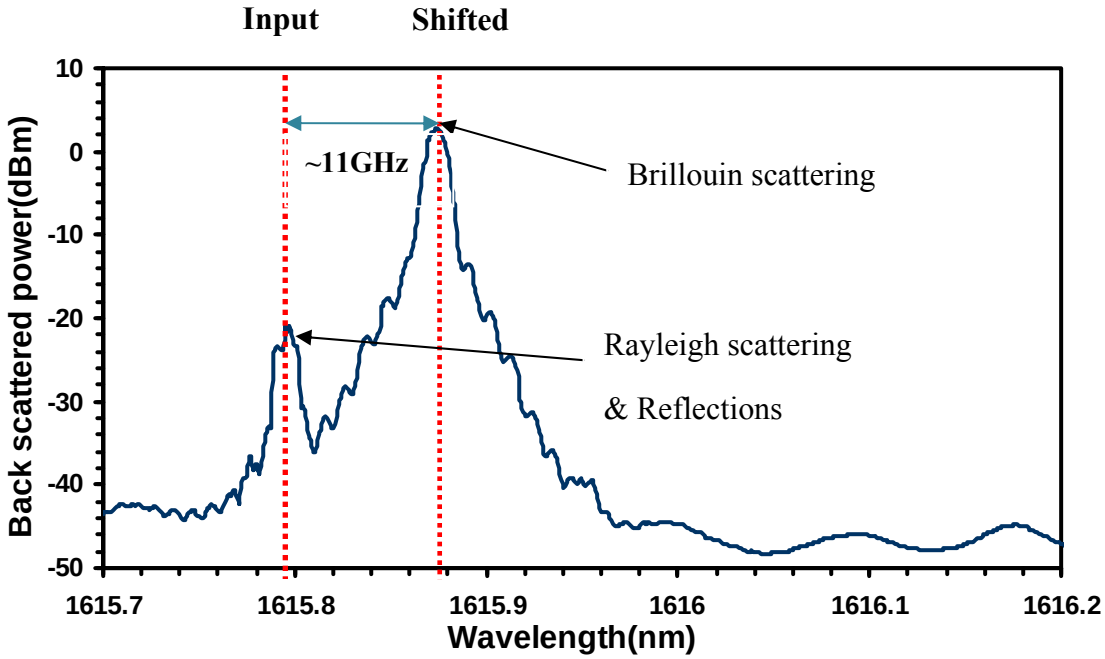

Figure 2.5: Spectrum of reflected light from 2.15m long Bi-EDF with input power of 150 mW and BP wavelength of 1615.8 nm.

The Brillouin gain spectrum, $g_B(\nu)$, which has a Lorentzian spectral shape can be also be determined by [11, 23]

$$g_B(\nu) = \frac{(\Delta\nu_B/2)^2}{(\nu-\nu_B)^2 + (\Delta\nu_B/2)^2} g_B(\nu_B) \qquad (2.10)$$

where $\Delta\nu_B$ is the 3dB spectral bandwidth that is related inversely to the decay time of acoustic phonons (-100 ns). The peak value of the Brillouin gain coefficient at $\nu = \nu_B$ can be evaluated using the following equation:

$$g_B(\nu_B) = \frac{2\pi n^7 p_{12}^2}{c\lambda_p^2 \rho_0 \upsilon_A \Delta\nu_B} \tag{2.11}$$

where p_{12} is the longitudinal electro-optic coefficient, ρ_0 is the density of the material and λ_p is the pump wavelength. The typical value of g_B for pure silica core fibre is $g_B = 5\times10^{-11}$ m/W. Both the Brillouin shift ν_B and the gain bandwidth $\Delta\nu_B$ can vary from fiber to fiber because of the presence of dopants in the fiber core [24].

The development of SBS in optical fibers is governed by a set of two coupled equations as follows [8]

$$\frac{dI_s}{dz} = \alpha_s I_s - g_B(\Omega) I_p I_s \tag{2.12}$$

$$\frac{dI_p}{dz} = -(\alpha_p I_p + g_B(\Omega) I_p I_s) \tag{2.13}$$

where the absorption coefficients α_s and α_p account for the fiber loss at the Stokes and pump frequencies, respectively. Two simplifications can be made because of the fact that the Brillouin shift is relatively small, as $\omega_p \approx \omega_s$ it follows that $\alpha_p \approx \alpha_s = \alpha$. We also assume that the Stokes and pump are co-polarized. If we assume that the pump is so intense compared with the Stokes, the pump depletion is neglected. Hence, the Stokes intensity inside the fibre is found to grow exponentially in the backward direction where I_0 is the pump intensity at $z = 0$ according to the relation

$$I_s(0) = I_s(L)\exp(g_B P_0 L_{eff} / A_{eff} - \alpha L) \qquad (2.14)$$

We used $P_0 = I_p(0)A_{eff}$, where P_0, effective area A_{eff} and L are the input pump power and length, respectively. In Eq. (2.14) the Stokes signal incident at $z = L$ grows in the backward direction as a result of SBS. In the case of a pump laser with a Lorentzian spectral profile, the Brillouin threshold can be written [11] as

$$P_{th}(mW) \cong \frac{21A_{eff}}{g_B(\nu_B)L_{eff}}(1+\frac{\Delta\nu_p}{\Delta\nu_B}) \qquad (2.15)$$

where $\Delta\nu_p$ is the frequency linewidth of the pump, $\Delta\nu_B$ is the spontaneous Brillouin linewidth. However, similar to that of finding the Raman threshold Eq. (2.4), the Brillouin threshold, by a good approximation, is summarized by

$$g_B(\nu_B)P_{th}\frac{L_{eff}}{A_{eff}} \approx 21 \qquad (2.16)$$

Using $g_B = 5\times10^{-11}$ m/W and $A_{eff} = 50\ \mu m^2$ as typical values, the threshold power P_{th} for the SBS onset can be as low as 1 mW for CW signals in the wavelength region near 1.55 μm [25]. In our experiment on a piece of 215cm long Bi-EDF that will be discussed in Chapter 4, P_{th} is obtained at approximately 3.2 mW, that leads to $g_B = 3.8\times10^{-7}$ m/W. This value is so much higher than the value obtained with the bulk silica, which is approximately 5×10^{-11} m/W. Abedin has also observed a strong SBS in $As^{39}Se^{61}$ single mode fiber with a gain coefficient of 6.0×10^{-9} m/W that is 134 times higher than that of silica fiber [25]. In this thesis, the SBS is used to generate a single and multi-wavelength laser sources that will be presented in chapter 4.

2.2.2 Nonlinear Refractive Index Effects or Kerr Effects

The Kerr effect or the quadratic electro-optic effect (QEO effect) was found in 1875 by John Kerr, a Scottish physicist. The effect describes a change in the refractive index of a material in response to an electric field. The index change is directly proportional to the square of the electric field instead of the magnitude of the field. In Kerr effect, the nonlinear phase shift induced by an intense and high power pump beam is used to change the transmission of a weak probe through a nonlinear medium [11]. Thus the change in the refractive index is proportional to the optical intensity. The overall refractive index is therefore a linear function of the optical intensity I [12]

$$n(I) = n + n_2 I \tag{2.17}$$

where

$$n_2 = \frac{3\eta_0}{n^2 \varepsilon_0} \chi^{(3)} \tag{2.18}$$

where n_2 is the second-order nonlinear refractive index, and I is the intensity of the wave. The refractive index change is thus proportional to the intensity of the light travelling through the medium. This effect is also a self-induced effect in which the phase velocity of the wave depends on the wave's own intensity [12]. This effect will become significant with very intense beams such as those from lasers. An intense beam of laser in a medium can provide the modulating electric field, without the need for an external field to be applied. In this case, the electric field is given by

$$E = E_{\omega} \cos(\omega t) \tag{2.19}$$

where E_ω is the amplitude of the wave stated. Combining this with the equation for polarization, and taking only linear terms and those in $\chi^{(3)}|E_\omega|^3$

$$P \approx \varepsilon_0(\chi^{(1)} + 3\chi^{(3)}|E_0|^2)E_\omega \cos(\omega t) \qquad (2.20)$$

The Kerr effect plays a significant role in the nonlinear processes of SPM, XPM, and FWM in optical fibers. The nonlinear coefficients of an optical fiber can also be measured using a method based on these effects [26, 27]. The magnitudes of these effects depend on the ratio n_2/A_{eff}, where n_2 is the nonlinear refractive index of the fiber and A_{eff} the effective area of the light mode. Furthermore, the process such as SPM can be used along with dispersion effect in optical fibers to produce optical solitons.

Self-phase Modulation (SPM) and Cross-phase Modulation (XPM)

The SPM is a nonlinear phenomena based on the Kerr effect in nonlinear optical media that leads to spectral broadening of optical pulses. In WDM systems, the refractive index nonlinearity gives rise to XPM, which converts power fluctuations in a particular wavelength channel to phase fluctuations in other co-propagating channels. This can be highly mitigated in WDM systems operating over standard non-dispersion shifted single-mode fiber; however, this nonlinearity can be a significant problem in WDM links operating at 10 Gbps and higher over dispersion-shifted fiber [28]. XPM is always accompanied by SPM and occurs because the effective refractive index seen by an optical beam in a nonlinear medium depends not only on the intensity of that beam but also on the intensity of other co-propagating beams [11]. Furthermore, when two CW intense signals with wavelength separation of $\Delta\lambda$ are launched into a fiber, SPM acts on the beat envelope to create sidebands in the frequency domain. Then, the optical power ratio of the input

signals (I_0) to the first sideband (I_1) is related to the nonlinear phase shift ϕ_{SPM} and can be used to deduce the value of n_2. When the chromatic dispersion is negligible, the power ratio for the central and first sideband can be expressed by using n-th order Bessel function J*n* as follows [11, 13]

$$\frac{I_0}{I_1} = \frac{J_0^2(\phi_{SPM}/2) + J_1^2(\phi_{SPM}/2)}{J_1^2(\phi_{SPM}/2) + J_2^2(\phi_{SPM}/2)} \tag{2.21}$$

The SPM effect can be used to determine a refractive index coefficient, n_2 of various kinds of optical fibers using a dual-wavelength continuous wave SPM-method [8] that was first introduced in 1993 [13]. The SPM effect produces a phase-shift that can be measured indirectly from the intensity peak heights of the dual wavelength source and the first harmonics that are generated by the SPM. Neglecting the dispersion, the field amplitude of a dual frequency optical signal out from the fiber can be expressed in terms of normalized amplitude along the fiber length L [11, 13] as

$$U(L,T) = U(0,T)\exp\left[i\,\phi_{NL}(L,T)\right] \tag{2.22}$$

where $U(0, T)$ is the field amplitude at $z = 0$, the SPM gives rise to an intensity-dependent nonlinear phase shift; ϕ_{NL} that increases with fiber length L, given by [11]

$$\phi_{NL}(L,T) = \left|U(0,T)\right|^2 (L_{eff}/L_{NL}) \tag{2.23}$$

where L_{eff} is the effective length, which is a function of the fiber losses and the nonlinear length as shown in the following equation

$$L_{NL} = (\gamma P_0)^{-1} \tag{2.24}$$

P_0 and γ are the peak power and nonlinear coefficient, respectively. If we ignore fiber losses, $\alpha = 0$, and then we achieved $L_{\text{eff}} = L$. The maximum phase shift $\phi_{\max}$ occurs at the pulse center located at $T = 0$ (T is pulse width) as a below:

$$\phi_{\max} = L_{eff} / L_{NL} = \gamma P_0 L_{eff} = \phi_{SPM} = \frac{2\omega_0 . n_2}{cA_{eff}} L_{eff} \overline{P} \tag{2.25}$$

where $\overline{P}$ shows the average launched power. Thus, the nonlinear parameters can be obtained by measuring the optical power ratio I_0/I_1 with various launched power and nonlinear phase shift due to SPM effect [29, 30]. It is therefore important to have a simple and accurate method for the determination of this ratio. On the other hand, the spectral broadening effect of SPM and XPM in optical fibers can be utilized to realize many nonlinear devices such as nonlinear optical loop mirrors [31], optical data de-multiplexers [32], nonlinear pulse switches [33], wavelength converters based on a nonlinear optical loop mirror [34] and many more.

Four-wave Mixing (FWM)

The origin of FWM lies in the nonlinear response of bound electrons of a material to an electromagnetic field. FWM is a type of optical Kerr effect and occur when two or more frequencies of light propagate through a medium. In quantum-mechanical terms, FWM occurs when photons from one or more waves are annihilated and new photons are created at different frequencies such that the net energy and momentum are conserved [35].

Providing that a condition known as phase matching is satisfied, light is generated at new frequencies by converting optical power at the original signal wavelengths [36].

The nonlinear effects can be involved as second-or third order processes depending on whether the second-order susceptibility $\chi^{(2)}$ or the third-order susceptibility $\chi^{(3)}$ is responsible for them. The second-order susceptibility $\chi^{(2)}$ vanishes for an isotropic medium in the dipole approximation. The third-order parametric processes involve, in general, nonlinear interaction among four optical waves and include the phenomena such as third harmonic generation, FWM, and parametric amplification [35-38]. Its main features can be understood by considering the third-order polarization term as shown in Eq.(2.14). Consider four optical waves oscillating at frequencies ω_1, ω_2, ω_3 and ω_4 linearly polarized along the same axis x. The total electric field can be written as

$$E = \frac{1}{2}\hat{x}\sum_{j=1}^{4} E_j \exp\left[i(k_j z - \omega_j t)\right] + c.c., \qquad (2.26)$$

where the propagation constant $k_j = n_j \omega_j / c$, n_j is the refractive index, and all four waves are assumed to be propagating in the same direction. If we express P_{NL} (the induced nonlinear polarization) in the same form as E using

$$P_{NL} = \frac{1}{2}\hat{x}\sum_{j=1}^{4} P_j \exp[i(k_j - \omega_j t)] + c.c., \qquad (2.27)$$

we find that P_j (j =1 to 4) consists of a large number of terms involving the products of three electric fields. For example, P_4 can be expressed as

$$P_4 = \frac{3\varepsilon_0}{4}\chi^{(3)}[|E_4|^2 E_4 + 2(|E_1|^2 + |E_4|^2 + |E_3|^2)E_4 + 2E_1E_2E_3\exp(i\theta_+) + 2E_1E_2E_3^*\exp(i\theta_-) + ...] \quad (2.28)$$

where θ_+ and θ_- are defined as

$$\theta_+ = (k_1 + k_2 + k_3 - k_4)z - (\omega_1 + \omega_2 + \omega_3 - \omega_4)t \quad (2.29)$$

$$\theta_- = (k_1 + k_2 - k_3 - k_4)z - (\omega_1 + \omega_2 - \omega_3 - \omega_4)t \quad (2.30)$$

The first four terms containing E_4 in Eq.(2.28) are responsible for the SPM and XPM effects. The remaining terms result from FWM. The efficiency of the FWM terms depends on the phase mismatch between E_4 and P_4 which is governed by θ_+ and θ_-.

One type of FWM corresponding to θ_+ can generate a new wave at the frequency $\omega_4 = \omega_1 + \omega_2 - \omega_3$; whenever three waves of frequencies ω_1, ω_2 and ω_3 co-propagate inside the fiber and three photons transferring energy to a single photon at frequency ω_4. Another type corresponds to the case in which two photon at frequencies ω_1 and ω_2 are annihilated, while two photons at frequencies ω_3 and ω_4 are created simultaneously such that; $\omega_1 + \omega_2 = \omega_3 + \omega_4$. The efficiency of this nonlinear interaction strongly depends on the phase-matching requirement, which is given by

$$\Delta k = k_3 + k_4 - k_1 - k_2 = (n_3\omega_3 + n_4\omega_4 - n_1\omega_1 - n_2\omega_2) = 0 \quad (2.31)$$

where k_j is the wave vector of the *jth* optical wave defined before. The degenerate case ($\omega_1 = \omega_2$), that is often useful for optical fibers can be initiated with a single pump beam. A strong pump wave at ω_1 creates two sidebands located at frequencies ω_3 and ω_4 with frequency shift, $\Omega s = \omega_1 - \omega_3 = \omega_4 - \omega_1$ (we assumed $\omega_3 < \omega_4$). If a weak signal at ω_3 is also

launched into the fiber with the pump, the signal is amplified while a new idler wave at ω_4 is generated [11]. Both the signal and idler waves experience gain through parametric amplification. Moreover, the phase of the idler wave is related to that of the signal wave through the phase-matching condition. For this reason, such a FWM process is also known as phase conjugation [20].

Figure 2.6 shows a simple example of mixing of two waves at frequency ω_1 and ω_2. When these waves are mixed up, they generate sidebands at ω_{112} or $(2\omega_1-\omega_2)$ and ω_{221} or $(2\omega_2-\omega_1)$. Similarly, three co-propagating waves will create nine new optical sideband waves at frequencies given by $\omega_{ijk} = \omega_i + \omega_j - \omega_k$ as shown in the figure. FWM has been investigated in many media including gases, semiconductors, crystals, and optical fibers. In particular, the large bandwidth, low loss, and long interaction lengths of optical fibers make them attractive for FWM.

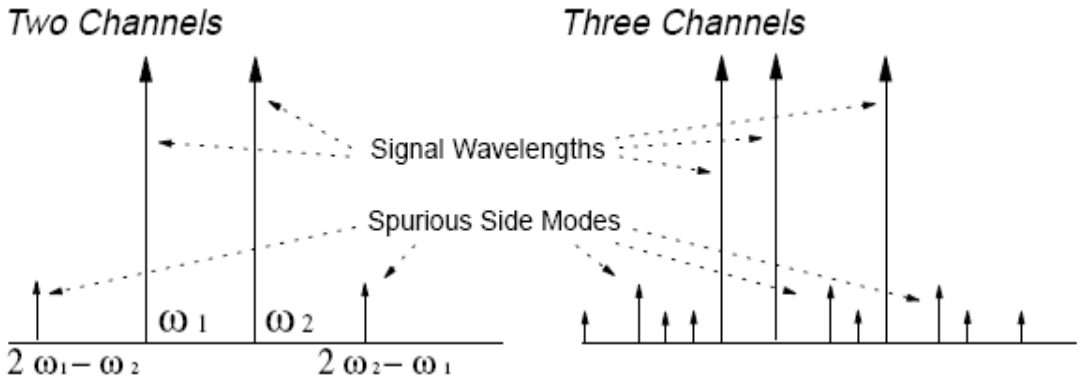

Figure 2.6: FWM effects in cases of partially degenerate (left) and non-degenerate (right) [39].

2.3 Applications of the Nonlinear Effects

Applications of the SBS

SBS has many possible applications in the areas of optics and optical communications such as narrow band amplification, lasing, sensing, phase conjugation and slow light generation [40]. SBS in optical fiber has been used for reduction of optical carrier of microwave signal [41-43]. When the power of a weakly intensity-modulated carrier exceeds the Brillouin threshold, it is converted to the backward propagating Stokes wave and is, therefore, selectively depleted. In such application, a single-mode Stokes wave is found to be more suitable compared with multimode in preventing the addition of noise [43]. Furthermore, Brillouin scattering is an efficient nondestructive and noncontact measurement method to obtain the wave properties of thin layers at hypersonic frequencies. This technique was applied for the nondestructive measurement of anisotropy and refractive indices of thin and polycrystalline ZnO films by introducing the Voigt function to obtain the Brillouin shift frequencies. The obtained refractive indices were similar with those of Abbe refractometer or the single crystal [44]. In another case, with the development of the very high contrast multi-pass interferometer it is now possible to perform measurements on very small and imperfect crystals and even on opaque materials where the penetration depth of the light is as low as a few wavelengths [45].

The effect of gamma-radiation on the physical properties of Brillouin scattering in commercially available optical fibers has been investigated up to very high total gamma doses. The frequency shift due to the ionizing radiation is about 5 MHz for the worst case. Distributed sensors based on stimulated Brillouin scattering can thus be considered to be radiation tolerant up to total doses of about 100 kGy, provided that the signal-to-noise ratio is kept at acceptable value. Distributed fiber sensors based on Brillouin spectral analysis

can be an efficient monitoring tool for nuclear facilities. Further work on different fibers with different dopant concentration types will indicate which fiber is more suitable for nuclear environments. In addition, the use of the radiation-induced Brillouin shift as a tool of analysis will certainly bring new perspectives in the understanding of the compaction mechanism in irradiated amorphous silica [46].

The Brillouin scattering method was also employed in a measurement of spectroscopic properties of materials [47]. The temperature variation changes the values of Brillouin shift. The SBS effect can also be used to generate narrow linewidth fiber laser as reported in many literatures [10, 12, 41] and also in this thesis. The Brillouin fiber laser (BFL) has many potential applications for WDM communications, fiber optic sensors and others.

Applications of the FWM

FWM in a nonlinear fiber can be used to achieve comb-like spectra for applications in wavelength converters [11, 48, 49], phase conjugators [50], optical parametric oscillator (OPO) [51], squeezing [52, 53], frequency metrology [54-57], multi-wavelength generation and spectroscopy [58]. Other interesting applications of FWM are for de-multiplexing of a time-division-multiplexed (TDM) signal [59] and spectral inversion that leads to the generation of a wave whose spectrum is the "mirror image" of that of the weak wave [60]. Two possible applications of FWM in a micro cavity are narrow line-width light sources (sub-MHz) which are insensitive to the pump laser line-width and frequency converters (>100 nm) through Raman-assisted FWM. From the perspective of quantum optics, FWM leads to the generation of squeezed states of light [61] and entangled photon pairs [62, 63]. FWM is applied in spectroscopy, most commonly in the form of coherent anti-Stokes Raman spectroscopy (CARS), where two input waves generate a detected signal with

slightly higher optical frequency. With a variable time delay between the input beams, it is also possible to measure excited-state lifetimes and rephrasing rates [64]. In theoretical physics, an important application of FWM is the measuring of the nonlinear coefficient [65], nonlinear index coefficient [1] and parameters that are employed in chapter 5**.**

Determination of the Nonlinear Coefficients in Fibers Using the FWM

The FWM is a phenomenon that must be avoided in DWDM transmission but FWM also provides the basic technology for measuring the nonlinearity, chromatic dispersion of optical fibers and a technique for measuring the nonlinear coefficient of optical fibers [66]. The magnitudes of optical Kerr effects depend on the nonlinear parameters like γ (nonlinear coefficient) and n_2 (nonlinear index coefficient) or n_2/A_{eff}. It is therefore important to have a simple and accurate method for the determination of these parameters. The nonlinear index coefficient n_2 in optical fibers is responsible for a large variety of nonlinear effects in optical fiber, such as SPM, XPM, FWM, and soliton formation. One of the important properties of n_2 is its dependence on the polarization state of the field in a long fiber, in which the polarization state varies during its propagation [67].

FWM effect produces sidebands whose amplitudes and frequencies depend on the nonlinear parameter, γ. When input wave is degenerated (λ_1 close to λ_2), then the power of FWM is described by [68]:

$$P_{FWM}= \eta P_S\gamma^2 P_P^2 \{1-\exp(-\alpha L)/\alpha\}^2= \eta P_S\gamma^2 P_P^2 (L_{eff})^2 \qquad (2.32)$$

where P_P is the input power of pump wave, P_S is the transmitted power of signal wave, L is the interaction length of FWM process. η is the FWM efficiency which depends on

wavelength difference between the pump and signal. In this analysis, we can select this value unit if the two input waves are close and near to a zero dispersion wavelength [69]. When the power of all channels is the same (P_0), FWM signal power can be also written as [70]

$$P_{FWM} = \frac{\eta}{9} d^2 \gamma^2 P_0^3 \exp(-\alpha L).L_{eff}^2 \qquad (2.33)$$

where d is the degeneracy factor (d = 3 and 6 in case of two and three channels respectively). In this case η is given by [71]

$$\eta = [\frac{n_2}{A_{eff}}.D(\Delta\lambda)^2]^2 \qquad (2.34)$$

where D is the dispersion parameter. The material dispersion arises due to the variation of the n of the core material as a function of wavelength. This causes a wavelength dependence of the group velocity of any given mode; that is, pulse spreading occurs even when different wavelengths follow the same path.

For this application, FWM efficiency can be written in terms of attenuation, α and mismatch parameter [70] as

$$\eta = \frac{\alpha^2}{\alpha^2 + \Delta\beta^2}[1 + \frac{4.\exp(-\alpha L).\sin^2(\Delta\beta.L/2)}{(1-\exp(-\alpha L))^2}] \qquad (2.35)$$

where the phase mismatch Δβ [66] is proportional with dispersion parameter D that lead to spreading the wave:

$$\Delta\beta = \frac{2\pi\lambda^2}{c}.D.\Delta f^2 = \beta_{probe} + \beta_{idler} - 2\beta_{pump} = -\frac{8\pi f_p^2}{c} D(f_p)(f_{probe} - f_p) \qquad (2.36)$$

with the dispersion parameter D according to following definition:

$$D = -\frac{2\pi c}{\lambda^2}\beta_2 \tag{2.37}$$

where β_2 is the group velocity dispersion parameter [70]. Hence, the coherence length can be defined as

$$L_{coh} = 2\pi/\Delta\beta = \lambda^2/\Delta\lambda \tag{2.38}$$

where $\Delta\beta$ is the maximum wave-vector mismatch that can be tolerated. If the length is less than the coherence length, significant FWM can occur. Therefore, the nonlinearity coefficient γ can only shift the P_{FWM} characteristic up or down, so FWM signal power can be used for measuring the dispersion of the optical fiber. By employing only two laser diodes by tuning range less than 1 nm and a proper length of the fiber, the dispersion parameter of the fiber can also be measured using

$$D = \frac{c}{\lambda^2.\Delta f^2.L} \tag{2.39}$$

where λ is the operating wavelength and Δf the channel spacing for which P_{FWM} reaches its first minimum[70 ,71]. Furthermore, the powers of the FWM sidebands in the experiment can be measured and the value is used to calculate nonlinear coefficient γ using the Eq. (2.32). By knowing the value of γ, nonlinear index coefficient, n_2 can be obtained according to the following equation:

$$\gamma = 2\pi n_2/\lambda A_{eff} \tag{2.40}$$

where λ is the input signal wavelength and A_{eff} is the effective area of the fiber.

The conversion efficiency G_c in the normal dispersion domain of the fiber can also be represented [11] based on γ as

$$G_c = \gamma^2 P_p^2 L^2 [\frac{\sin(gL)}{gL}]^2 \qquad (2.41)$$

where g is introduced as parametric gain, and can be obtained by

$$g = \sqrt{\frac{1}{4}\Delta\beta(\Delta\beta + 4\gamma P_p)} \qquad (2.42)$$

This equation shows that the conversion efficiency depends on pump power, phase matching condition and the γ. Finally, with FWM method, besides γ and $n_{2;}$ we can also estimate other parameters such as nonlinear phase shift $\Phi_{SPM,}$ chromatic dispersion coefficient and figure of merit (FOM = $\gamma.L_{eff}$) that is beyond the applications in this thesis.

2.4 Bismuth-based EDF for Optical Amplification and Nonlinear Devices

In this section, a new type of Erbium-doped fiber based on Bismuth oxide glass is introduced and its application in optical amplifier and nonlinear fiber laser is described. The Bi-EDF is a newly developed nonlinear fiber from Asahi Glass Company (AGC) [76-79], in Japan. The section gives a general overview of the Erbium-doped fiber amplifier.

2.4.1 Optical Fiber Amplifiers

Optical amplifiers are designed to boost the weakened signal to specific power level and prepare it for next transmission distance in optical communication. They are devices that amplify the optical signal directly without any conversion to an electric domain**.** All optical fiber amplifiers, using the principle of stimulated emission or inelastic scattering effects for amplification of incoming light**,** have been used in this thesis. However, the structure of optical fiber amplifier is similar to laser without an optical cavity, or one in which feedback from the cavity is suppressed. Two main categories of optical amplifiers are rare-earth doped fiber amplifiers, which are based on stimulated emission, and nonlinear optical amplifiers, which are based on phonon-photon interaction [12, 20].

Rare-earth Doped Fiber Amplifiers

The addition of rare earth ions into a silicate glass to produce laser action in a fiber was first shown in 1964 by Snitzer and Koester [72]. Rare earth element, such as Erbium, Ytterbium or Thulium, is doped in silica glass fibers for many practical applications, including fiber laser devices and amplifiers. These dopants are excited into a higher energy level by an optical signal, referred to as pump signal, at a wavelength lower than that of the communication signal. This allows the data signal to stimulate the excited atoms to release photons. Devices that provide gain must have low scattering losses, so the broader emission and absorption spectra of rare earth doped glasses lead to many applications [1].

In 1966 Fluoro-Phosphate glasses doped with Er^{+3} were also shown to produce laser oscillation at 1.55 μm [73]. The most popular example of doped fiber amplifiers is EDFA, where the core of silica fiber is doped with Erbium ions. EDFAs are very important device that allow significant improvements in the modern third window telecommunications

systems through the application of optical power amplifiers, signal repeaters, and low-noise preamplifiers. This amplifier typically provides gain amplification over the C-band (conventional band) and L-band that covers wavelengths from 1530 nm to 1600 nm, but recent EDFAs can also cover the extended L-band up to 1625 nm region [1, 28]. The broadband amplifications were achieved by using Bismuth-based Erbium-doped fiber amplifiers (Bi-EDFAs) with high Erbium ion concentration. The details on the Bi-EDFA that operates in both the C- and L-band regions will be discussed in chapter 3.

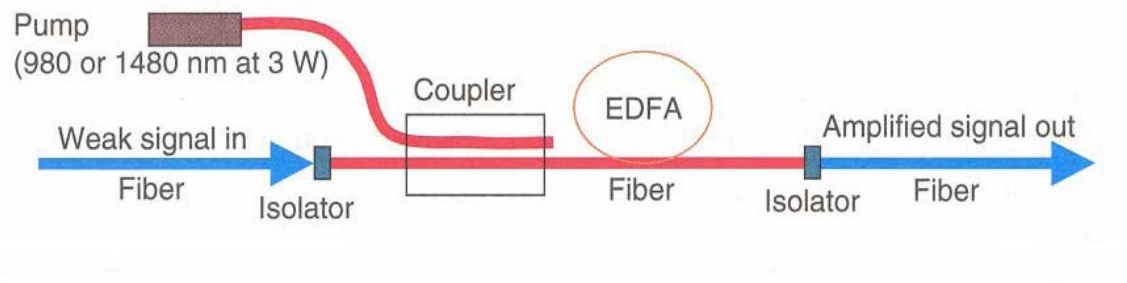

Figure 2.7: Schematic diagram for a standard EDFA.

Nonlinear Optical Amplifiers

The first observation of nonlinear optical amplifier (NOA) was made by Stolen and Ippen in 1973 [74]. Nonlinear optical amplifiers utilize inelastic scattering effects, such as SRS or SBS. The Brillouin and Raman scattering mechanisms are used to amplify signals beams in a fiber. The main emphasis was on Raman amplification, as Brillouin amplification has only a limited intrinsic bandwidth at 1550 nm. In particular, in Raman amplifiers, gain can be obtained over a large band (around 100 nm), but it is relatively small (10-15 dB) [75]. A major difference and advantage of NOA compared to EDFAs is that it occurs in the transmission fiber itself, distributed along the transmission path, but

uses a high-intensity pump signal. Pump power of several hundreds of milliwatts is also required for the Raman amplifiers. These amplifiers have also a low noise figure and sensitive to polarization. The configuration of the typical distributed Raman amplifier is shown in Figure 2.8, in which an optical circulator is used to inject Raman pump light into the gain medium.

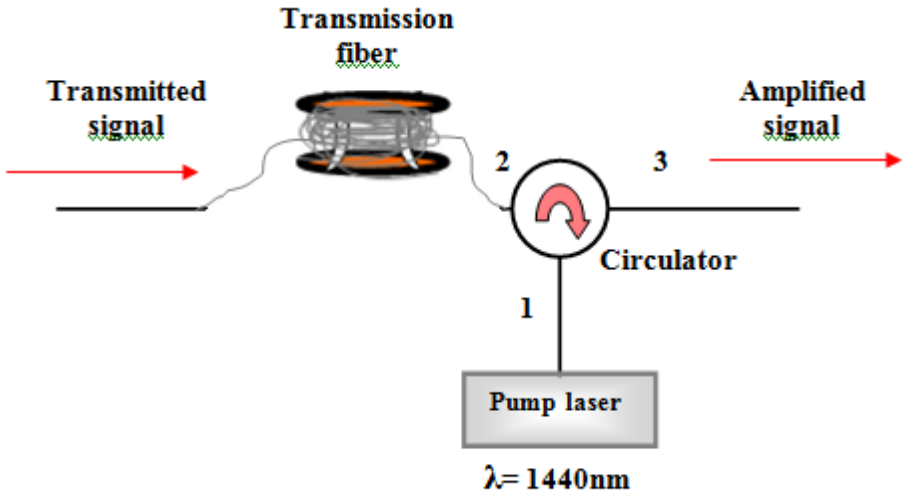

Figure 2.8: A typical nonlinear Raman optical amplifier configuration.

2.4.2 Background on the Bi-EDF

Bismuth oxide glass fiber such as Bi-EDF has a relatively higher refractive index, leading to a nonlinear refractive index to be so much higher than silica-based fiber. In glasses, various relevant properties as the refractive index can be tuned by the addition of heavy ions like lead or Bismuth. Heavy metal oxide glasses containing TeO_2, PbO, Ga_2O_3 and Bi_2O_3 are well known to show high refractive index [80]. The higher refractive index and with large Judd-Ofelt intensity parameter, Ω_6, of Bismuth-based glass results in larger

emission cross section and broader emission bandwidth which is desirable for WDM network systems [81]. However, due to high refractive index, the $^4I_{13/2}$ level lifetime is relatively shorter in Bismuth-based glass. In contrast to Chalcogenide fibers, Bismuth oxide fibers do not contain any toxic elements such as Pb, As, Se, Te [82- 84], and they have mechanical and thermal stability. It can be doped with much higher concentration of Erbium than silica without any negative effects and have been fabricated for optical fiber using these glasses for Bi-EDFA and nonlinear applications that will be extended in future chapters.

The basic structure of Bismuth Oxide is shown in Figure 2.9, which takes the fundamental crystalline structure of Bi_2O_3. The physical form of Bismuth oxide is a yellowish powder and it has melting temperature of 817^{o}C which is lower than silica glass. In this thesis, the Bi-EDF used has an Erbium ion concentrations of 3250 wt.ppm (weight parts per million) and La ion concentration of 4.4wt%. The Bi-EDF is co-doped with Lanthanum to suppress the concentration quenching of Erbium ions by increasing the distance of Erbium ions [85]. A fiber with such high Erbium dopant concentration is expected to have enormous potential in realizing a compact EDFAs and EDFA-based devices. The refractive indices of core and cladding of Bi-EDF are ~2.03 and ~2.02, respectively at 1.55 μm, while these values for single mode fiber (SMF) are around 1.45. The cross section of the Bi-EDF is shown in Figure 2.10. The Bismuth fiber also has a large value of normal group velocity dispersion (GVD), which is mainly due to the material dispersion of the high refractive index of the glass [86].

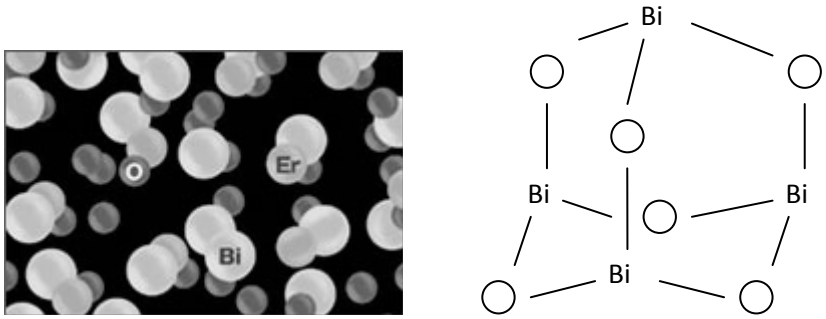

Figure 2.9: Illustration on the distribution of Erbium ions in Bismuth-based glass and basic structure of Bismuth oxide [87].

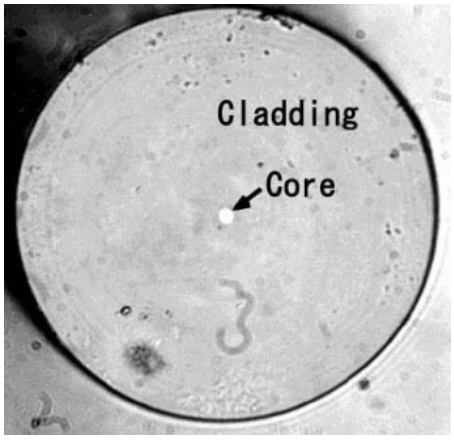

Figure 2.10: The cross-section picture of the Bi-EDF, provided by AGC.

The insertion loss of the Bi-EDF is estimated to be approximately 0.82 dB at 1550 nm using a cut-back method. The insertion loss is also due to splice loss between Bi-EDF and high numerical aperture (NA) of standard fibers (Corning HI980) as it is pre-angle spliced at 6^{o} by AGC as shown in Figure 2.11. The average splice loss was estimated to be less than 0.5 dB/point. Angled-cleaving is applied during splicing to suppress the reflection effect, which arises due to the large refractive index difference between the Bi-EDF and silica fiber [88]. The major problem of Bi-EDF is fusion splicing to standard silica fibers.

The melting point of Bi-EDF (~ 800°C) is much lower than that silica fiber (>1000 °C), therefore the commercial fusion splicers must be modified so that it can be used to fusion splice Bi-EDF to standard telecommunication fiber. Furthermore, the large refractive index difference (approximately 0.5~0.6) between Bi-EDF and SMF fiber introduces Fresnel reflection loss of about 2.8%. As shown in Figure 2.11, to avoid reflected light back to the fiber the incident angle θ_2, must be greater than θ_1, given in the following equation [89]

$$\theta_1 = 45^o - \frac{1}{2}\arcsin\left[\frac{n_{clad}}{n_{core}}\right] \qquad (2.43)$$

However, the incident angle should not be too large as it would increase the splicing loss between the SMF and Bi-EDF.

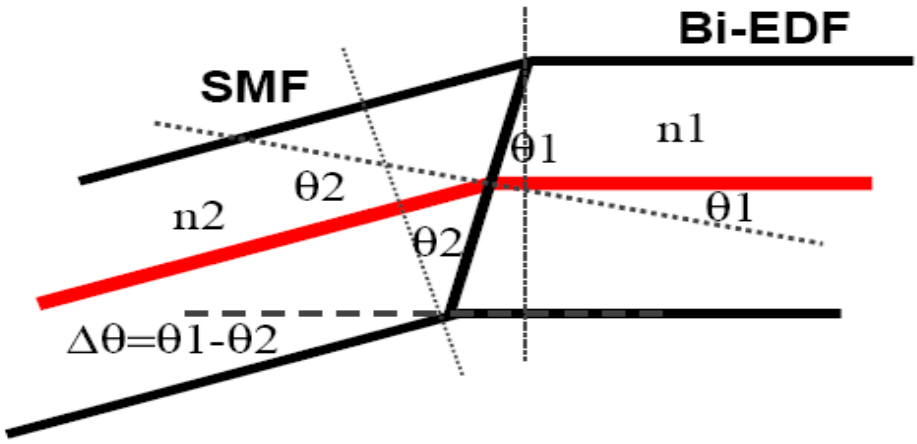

Figure 2.11: Angled splicing configuration between Bi-EDF and SMF. Silica fiber angle (θ_2) of 8.2° is optimum for Bismuth fiber angle (θ_1) of 6° [89].

Table 2.1 introduces the main physical properties of three lengths of the nonlinear Bi-EDF: 49cm, 181cm and 215cm that we employed in this thesis. The error values of the numerical aperture, core/cladding diameters and fiber optical loss are estimated to be less than ±0.05, ±0.2 μm and ±0.005 dB/m, respectively as reported in many literatures [10, 87, 89]. The NA of a fiber, essentially the contrast in index between the core and the cladding, is estimated to be 0.2. It is an important parameter that determines the mode-field diameter (MFD) and hence the effective area of the fundamental mode, with direct implications on the threshold power estimation for stimulated Brillouin scattering [90]. The $V\text{-}_{number}$ for a step-index fiber is a function of NA and the relation is given by

$$V = (\pi d/\lambda).NA \tag{2.44}$$

where d is the core diameter and a value of V= 2.405, or lower ($1.8<V<2.4$) indicates single mode behavior. Larger values of V indicate the potential for propagation of a higher number of modes. Using the NA and $V\text{-}_{number}$ values, the MFD (2 times of spot size) of the fundamental mode can be estimated and is given by [91]

$$MFD=d1/e^2=2\omega_0= d\times (0.65+1.619/V^{1.5}+2.879/V^6)=\frac{d}{\sqrt{\ln V}} \tag{2.45}$$

Also, the A_{eff} (the effective area) and γ (nonlinear coefficient) of the fiber are given by $A_{eff} = (\pi/4)(MFD)^2$ and Eq.(2.40), respectively. Hence, we have two approaches to enhance the fiber nonlinearity γ. One is to reduce the effective core area A_{eff} of the fiber and the other is to use a glass material whose n_2 is high. For example, the γ value of a standard single mode SiO_2 based fiber is $2.7W^{-1}km^{-1}$, and that of SiO_2-based holey fiber which has very small

A_{eff} is 60 $W^{-1}km^{-1}$[91]. The highest nonlinearity reported for a conventional fiber made from a Bismuth borate glass is 1360 $W^{-1}km^{-1}$ [92]. Even though the intrinsic material non-linearity of silica is not large (non-linear refractive index of silica, $n_2= 2\times10^{-20}$ m^2/W), the total amount of non-linearity can be significant owing to the substantial length and small effective area of the fiber waveguide. The non-linear index (n_2) at 1.55 μm were measured using the spectrally resolved by two beam coupling technique (SRTBC) as previously reported [93]. In this thesis, the n_2 value is calculated using Eq. (2.14) and the result will be compared with the value estimated from a FWM method, which will be discussed in chapter 5. Some of the physical properties of the Bi-EDF estimated in 1550 nm region is summarized in Table 2.1.

Table 2.1: The Bi-EDF parameters (at operating wavelength of 1.55 μm)

Type L(cm)	**Clad dia.(μm)**	**Core dia.(μm) MFD(μm)**	**Loss(dBm^{-1})**	**γ(w.km)-^{1}**	**n_2 (m^2/W)**	**$V_{-number}$**	**$A_{eff}(\mu m^2)$**
Bi-EDF 49 cm	124.5	5.4, 6.12	1.44@1.3μm	58.3	4.23×10^{-19}	2.18	29.4
Bi-EDF 181cm	125.1	5.1,6	1.51@1.3μm	58.87	4.1×10^{-19}	2.06	28.26
Bi-EDF 215 cm	125.7	5.4, 6.12	0.82@1.55 μm 1.18@1.48 μm	58.3	4.23×10^{-19}	2.18	29.4

2.4.3 Review on Previous Works Using a Bismuth Oxide Fiber

Several authors have recently studied on the properties of Bismuth borate glasses in a restricted composition range, un-doped [94], Er^{3+}-doped [95] or Nd^{3+}-doped [96]. Becker et.al. [97] showed that the refractive index of the Bismuth Borate glass can be widely varied, and Chen et al. proved that high luminescence efficiencies are possible, especially in Nd^{3+}-doped glass [96]. Tanabe et al. [98] showed for Er^{3+} doped Bi_2O_3 and SiO_2 glasses that the luminescence lifetime and efficiency decrease with increasing B_2O_3 content. Similar results were found by Yang et.al.[99] for Bi_2O_3 glasses. The Bi_2O_3-based high index glasses were designed and prepared to be used for highly nonlinear fiber and spectral broadening. Bismuth nonlinear fiber exhibits the highest nonlinear coefficient in the simple step-index type optical fibers reflecting the high nonlinear refractive index of the core glass. Recent progress for nonlinear applications indicates that the Bismuth oxide based fiber is the promising material because it has a high refractive index. Recently, Nagashima et al. developed a novel Bi_2O_3-based glass material which has high refractive index more than 2.2 at 1.55 μm and a suitable cladding glass material for the step-index structure with small A_{eff} [100]. These results indicate that the Bismuth-based nonlinear fiber (Bi-NLF) could be the best candidate for the practical nonlinear fibers used in all-optical processing. It can be fusion spliced and has a fast response when used as a Kerr switch [100]. Bi_2O_3 based EDF (Bi-EDF) exhibits broadband gain profile covering the wavelength region from 1530 nm to 1620 nm with quite short length fiber [101] that can provide amplification in both the C and L wavelength band of communications. The amplification characteristics of the Bi-EDFA will be described in detail in chapter 3.

Highly nonlinear Bismuth-oxide fiber can be also used for its smooth super-continuum generation that is suitable in broad spectra for a variety of applications including

frequency metrology [102], medical imaging [103], spectroscopy [104], characterization of broadband devices, such as photonic crystals [105,106], and communication systems. Such spectra can be generated either directly from ultrafast mode locked lasers [107,108] or in highly nonlinear fiber [109]. However, the large normal dispersion of the Bismuth fiber, provides the ultimate limit on spectral broadening, but is responsible for the smooth unstructured super-continuum product. Calculations indicate that the dispersion of the fiber is relatively flat, within 20%, over a large wavelength range of 1200 nm to 1800 nm [110]. Finally, the high nonlinear performance of Bi-EDF has been reported that leads to many applications in fiber laser devices [111-115]. The major nonlinear effects as introduced in the earlier section occurring inside all types of optical fibers, and are governed by the nonlinear parameter γ, defined in Eq.(2.41). Although, the majority of the fibers have a value of $\gamma \sim 1(W/km)^{-1}$, however, several new kinds of fibers may have a value γ of more than 10 $(W/km)^{-1}$ and this fiber is referred to as a highly nonlinear fiber [11].

2.5 Background on the Fiber Lasers

Fibers were primarily designed exclusively for the purpose of light transmission; however, their unique light guiding property quickly attracted them to other applications such as optical amplifiers and lasers. Optical fiber used as laser gain medium was first demonstrated in 1964 [116], shortly after the first laser appeared [117], the first fiber lasers were realized in 70s in both pulsed [118] and continuous-wave (CW) [119] forms. Fiber lasers (FLs) are normally referred to as lasers with optical rare-earth doped fibers as gain media. Some lasers with a semiconductor gain medium and a fiber cavity are also called fiber lasers. Different rare-earth ions, such as Erbium, Neodymium, and Ytterbium can be used to make FL over a wide operating wavelength range from 0.4 μm to 4 μm. A fiber

laser is pumped by a laser known as a pump with a spectral selection of radiation. Many configurations can be used for these lasers such as linear (Fabry-Perot cavity), ring and figure-of-eight configurations. The simplest way to create a FL is to attach a high reflecting mirror such as loop mirror, fiber Bragg grating (FBG), dielectric coating or WDM coupler to each end of the amplifying gain medium [120].

Fiber lasers have a lot of advantages compared to bulk lasers. They are compact and easy to build, to manipulate, and to transport. Fiber laser setups can be very robust when they are made with fibers only. They are easy to integrate and do not require any complex alignment or coupling. They are also less expensive and have the potential for high output powers (several kilowatts with double-clad fibers) with excellent beam quality [121, 122] due to high surface-to-volume ratio, thermal management and the guiding effect which avoids thermo-optical problems. These fiber lasers can also operate with small pump powers. Their axial mode separation can be small (2 to 100 MHz for optical lengths of 3 m to 150 m). On the other hand, FLs suffer from various problems such as; stability, power fluctuations, complicated temperature-dependent polarization evolution, and nonlinear effects which may limit performance. Significant dispersion effects can be detrimental due to long length of the fibers [123].

Besides the linear fiber lasers, inelastic nonlinear effects such as Brillouin and Raman scattering can also be used to produce nonlinear fiber lasers such as Brillouin and Raman fiber lasers (BFLs and RFLs). These types of lasers can operate at any operating wavelength depending on the availability of the pump laser. In BFL oscillation closed loop gain medium must exceed unity so that Brillouin amplification can over-compensate the cavity loss. The BFL oscillation can only happen at above a certain pump power that is referred to the SBS threshold power.

Brillouin Erbium Fiber Lasers (BEFLs)

Brillouin fiber lasers (BFLs) have been an attractive topic of research since 1976 [124,125]. The BFLs can be generated by using the Brillouin gain function, g_B in the fiber, if an optical fiber is placed inside a cavity. The SBS threshold power can be considerably reduced by placing longer length of optical fiber to generate BFL oscillations. Major important quantity in BFL generation is called the Brillouin shift, which is the difference in the BFL and BP frequencies, rather than the BFL and the BP frequencies [126], [127]. However, in BFL generation the optical circulators and optical couplers are normally used instead of mirrors as in Fabry-Perot lasers.

Cowle and Stepanov had firstly reported on the Brillouin Erbium fiber lasers (BEFLs) [128] that have been also developed in the same configurations of BFLs [129, 130]. When the fiber gain medium is pumped with a narrow linewidth laser source which is also known as a BP, a Stokes-shifted wave is generated in the reverse direction which is then amplified by the EDF. The BEFL can be obtained using a ring resonator, which normally consists of a circulator, a piece of SMF, output coupler, isolator and the EDFA. A Fabry-Perot cavity (linear cavity) can also be used, which requires two mirrors and two gain media between them. Fabry-Perot BEFLs (linear BEFLs) have some aspects qualitatively different from those making the usage of a ring cavity. This difference is due to the simultaneous attending of the forward and backward propagating components of the Brillouin pump (BP) and Brillouin Stokes (BS) in the cavity which will be described in chapter 4. Therefore, higher order Stokes waves generated through cascading SBS are readily performed in the linear cavity than in the ring one at the same conditions. On the other hand, in a ring cavity, even-order Stokes and anti-Stokes lines are observed with the transmitted BP in the forward direction in which they co-propagate with the BP whereas

odd-order Stokes and anti-Stokes line appear in the backward direction in comparison to BP due to the counter propagating feature of SBS process and the uni-directional aspect of the ring cavity [131]. However, by using linear cavities, it is easier to generate multiple lasing wavelengths due to the feature of the standing wave generation in them.

Multi-wavelength Fiber Lasers (MWFLs)

Another view of the fiber lasers is in multiple lasing wavelengths generation. The generated multiple lasing wavelengths have been advantageously utilized in the past few years in optical fiber sensors, optical component testing, and spectroscopy applications [132,133]. Perhaps the largest interest has arisen from the use of multiple lasing wavelengths in wavelength division multiplexing (WDM) and dense WDM (DWDM) optical transmission systems. Several researches have been done by using EDF lasers to produce multiple wavelengths with a constant wavelength spacing [134, 135]. In another approach, single mode operation of a compact multi-wavelength Erbium-Ytterbium fiber lasers (EYFL) have generated up to 29 wavelengths in a simple Fabry-Perot design.

A group of laser lines (comb) can also be produced by a multi-wavelength Brillouin fiber lasers (MWBFLs). The MWBFLs utilizes a nonlinear Brillouin gain in an optical fiber as a gain medium to generate a cascading Stokes lines. In the cascading process of SBS, each successive Stokes wave pumps the next-order Stokes wave after its power becomes large enough to satisfy the Brillouin threshold condition. At the same time, anti-Stokes waves are generated through FWM between co-propagating pump and Stokes waves. The hybrid of Brillouin Erbium fiber laser (BEFL) which manipulates narrow bandwidth of nonlinear Brillouin gain in an optical fiber to generate laser at the larger output power with assistance of EDFA [136]. The enhanced BEFL will be demonstrated in chapter 4 of this thesis using a short piece of Bi-EDF as the gain medium. The multi-wavelength laser

generation will also be proposed using a FWM effect in Chapter 5 of this thesis. The fiber lasers are less expensive and have received attention for numerous potential applications in optical communication for high output power, sensing, medicine, material processing, imaging, data storage, and laser ranging, over which they present the advantage of high brightness, excellent mode quality, highly efficient coupling into a single-mode fiber, and a far superior wavelength stability with temperature.

2.6 Comparison of the SBS Effects in Various Types of Fibers

In this thesis, we employed four types of the fibers for fiber laser applications. These fibers are a 215 cm long Bi-EDF, 20 m long PCF, 25 km long SMF and 7.7 km long dispersion compensating fiber (DCF). The Bi-EDF will be used as both linear and nonlinear gain medium in fiber laser applications. The fiber parameters are shown in Table 2.2, which were obtained from data sheet, calculations and other literatures. Figure 2.12 shows the experimental set-up to measure the SBS in the fibers. As shown in the figure, tunable laser source (TLS) is used to act as BP for the observation of SBS. A circulator is used to launch the BP signal and to monitor the back reflected signals. The backward propagating output is routed to the optical spectrum analyzer (OSA) via the optical circulator. The maximum available BP power is approximately 8 dBm.

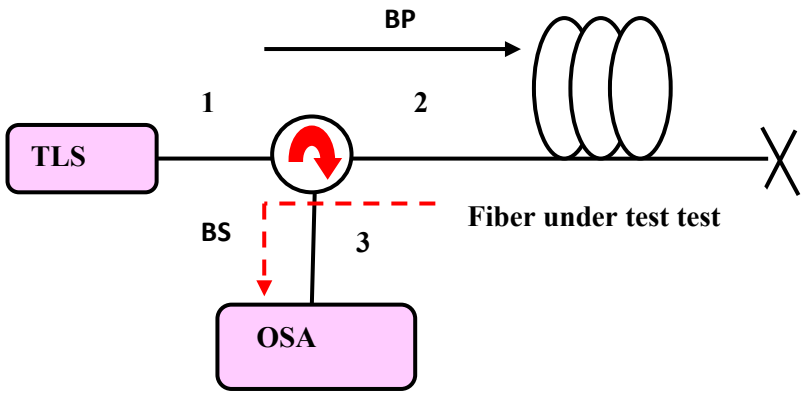

Figure 2.12: Experimental setup to observe the SBS effect.

Figure 2.13 shows the spectrum of the back-reflected signal from various fibers when the BP powers are varied from -8 dBm to 8 dBm in the optimum wavelength for every pieces of fibers. The Brillouin Stokes operates at a frequency separated from the BP frequency by the Brillouin shift, which is due to the Doppler effects. The inelastic scattering in the fiber produces a moving grating by electrostriction phenomenon, which in turn generates Doppler effects. As shown in the figure, the wavelength of the scattered signal is shifted from the pump wavelength by about 0.08 nm to the longer wavelength side. This wavelength shift confirms that it is actually the Brillouin scattering effect that is taking place in the PCF as the Brillouin shift in silica is normally about 10 GHz, which is approximately 0.08 nm if the input signal is set at L-band region. The Brillouin effect is more pronounced at higher BP power. The strongest SBS is observed in SMF with a spacing of 0.088 nm as shown in Figure 2.13(b). This is attributed to the SMF length which is the longest therefore the interaction between the gain medium and pump intensity is more pronounced. As shown in Figure 2.13(d), the SBS effect is slightly weaker in DCF compared to the SMF even though nonlinear coefficient characteristic is higher in this fiber.

This is attributed to the interaction length, which is around one third of the SMF as well as the fiber attenuation, which is higher in this fiber. The Brillouin effect is also more significant at longer wavelength, which is attributed to a lower loss of power at this region. Therefore a larger amount of BP power is transferred into the Stokes and anti-Stokes wavelength. The anti-Stokes is also observed at a shorter wavelength because of FWM between the BP and Stokes line. The small Brillouin scattering is observed in 20 m long PCF with symmetry Stokes and anti-Stokes as shown in Figure 2.13(a). The symmetry characteristic proves that the FWM effect is reasonably high in this fiber. However, the Brillouin scattering cannot be observed in the reduced lengths of Bi-EDF as shown in Figure 2.13(c). This is probably due to the Erbium dopant inside the fiber, which has absorbed the injected pump light.

Table 2.2: Physical fiber parameters

Fiber Type	PCF	Bi-EDF	DCF	SMF-28
Length(m)	20	2.15	7700	25000
Numerical Aperture (NA)	0.2	0.2	0.14	0.13
Core(μm)	4.8	5.4	4.58	8.3
Cladding(μm)	125	125.7	125	125
Mode field diameter(μm)	4.2	6.12	5.04	9.36
Zero dispersion wavelength(nm)	1040	1513	1276	1315
Cut off wavelength (nm)	1000	1180	1210	1200
Effective area(μm)^2	27.5	29.4	20	68.8
V-$_{number}$	1.94	2.18	2.71	2.28
Material	Pure silica	Bi_2o_3-Er doped	germanium and fluorine (Ge/F)	Pure silica
Insertion loss (dB)	~2@1.06μm ~1.5@1.55μm	0.82@1.55 μm 1.18@1.48 μm	0.5@1.55 μm	0.18@1.55 μm
g_B(m/W)	5×10^{-7}	3.8×10^{-7}	8.6×10^{-11}	2.5×10^{-11}
Chromatic dispersion @1550nm (ps/nm.Km)	~70	-120	-95	17.46
Refractive index of core/cladding at 1.55 μm	1.46/1.45	2.03/2.02	1.47/1.44	1.45/1.44
γ(w.km)-^{1}@1550nm	~33.8	~60	~6	~1

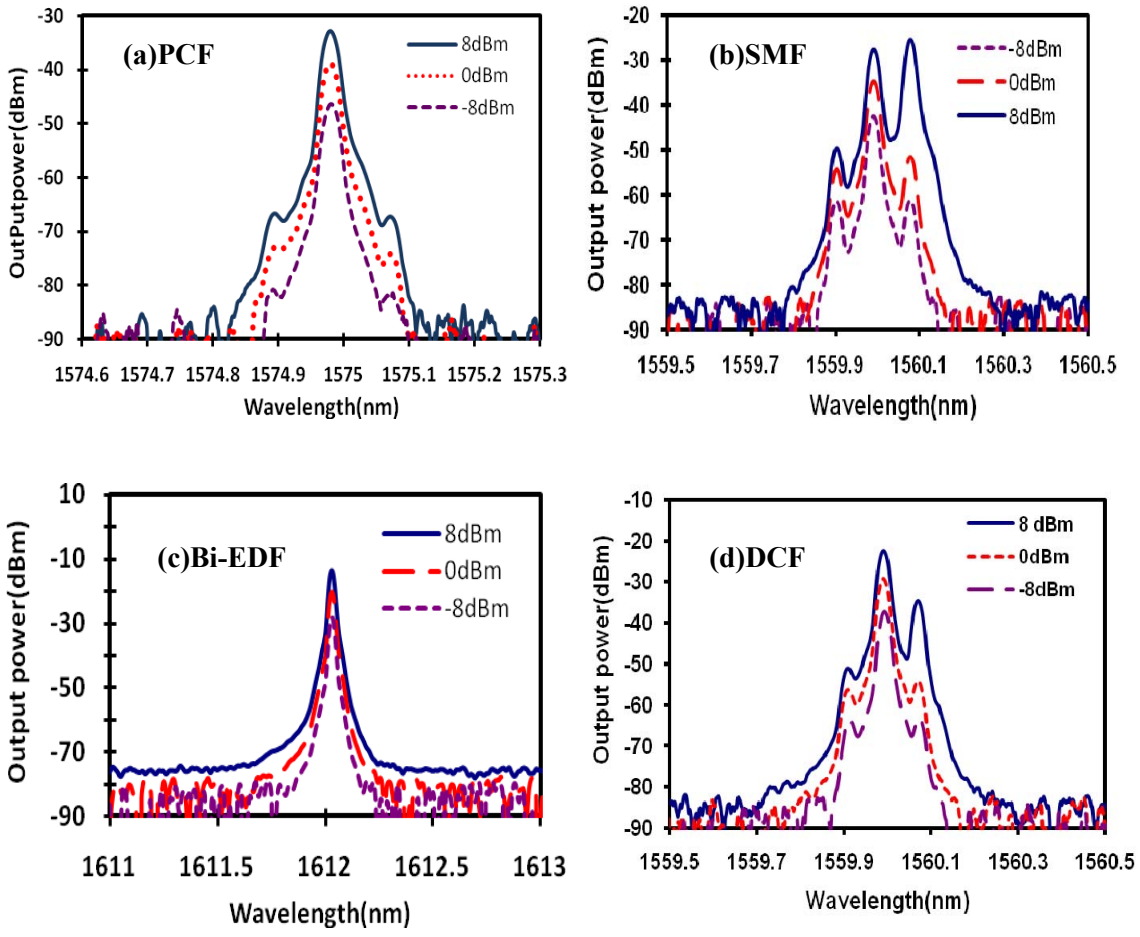

Figure 2.13: Optical spectrum of the Brillouin scattering effect in **(a)** PCF, **(b)** SMF, **(c)**Bi-EDF and **(d)** DCF.

REFERENCES

[1] M. J. F. Digonnet, " Rare Earth Doped Fiber Lasers and Amplifiers," Second edition, 1993.

[2] K.Y. Song, M.G. Herraez, L. Thevenaz, "Observation of pulse delaying and advancement in optical using stimulated Brillouin scattering," Opt. Exp., Vol.13, No. 3, pp.82-88, 2005.

[3] Y. Okawachi, M. S. Bigelow, J. E. Sharping, Z. Zhu, A. Schweinsberg, D. J. Gauthier, R.W. Boyd, A. L. Gaeta, "Tunable All-Optical Delays via Brillouin Slow Light in an Optical Fiber," Phys. Rev. Lett. Vol. 94, pp.5390, 2005.

[4] J. E. Sharping, Y. Okawachi, A.L. Gaeta, "Non-linear properties of Chalcogenide glasses and fibers ," Opt. Express. Vol.13, pp. 6092, 2005.

[5] D. Dahan, G. Eisenstein, "Tunable all optical delay via slow and fast light a route to all optical buffering," Opt. Express, Vol. 13, pp.6234-6249, 2005.

[6] H. Yoshida, M. Nakatsuka, H. Fujita, T. Sasaki, and K. Yoshida, "High-energy operation of a stimulated Brillouin scattering mirror in an L-Arginine phosphate monohydrate crystal," Appl. Opt. Vol.36, pp. 7783-7787,1997.

[7] J. H. Lee, T. Tanemura, T. Nagashima, T. Hasegawa, S. Ohara, N. Sugimoto, and K. Kikuchi, "Use of 1m Bi_2O_3 nonlinear fiber for 160-Gbit/s optical-time division demultiplexing based on polarization rotation and wavelength shift induced by cross-phase modulation," Opt. Lett. Vol. 30, pp.1267-1269, 2005.

[8] M. Asobe, T, Kanamori, and K. I. Kubodera, "Applications of highly nonlinear chalcogenide glass fibers in ultrafast all-optical switches," IEEE J. Quantum Electron. Vol. 29, pp.2325-2333, 1993.

[9] N. Sugimoto, K. Ochiai, T. Hirose, S. Ohara, Y. Fukasawa, Ultracompact gain block with Bi_2O_3-based Erbium-doped fiber. Jpn J Appl Phys. Vol. 43, pp.2551–2., 2004.

[10] R. W. Boyd, "Nonlinear Optics," Third edition, Academic Press, San Diego, CA, 2007.

[11] G. P. Agrawal, "Nonlinear Fiber Optics," Fourth edition, Academic press, New York, 2007.

[12] B. E. A. Saleh and M.C. Teich, "Fundamentals of Photonics," Copyright by John Wiley & Sons, Inc. 1999-2001.

[13] A. Lamminpaa, "Measurement of nonlinearity of optical fiber," 2003.

[14] C. V. Raman and K. S. Krishnan, "A new type of secondary radiation," Nature, Vol. 121, 1928.

[15] F. Forghieri, R.W. Tkach, A.R. Chraplyvy, Fiber nonlinearities and their impact on transmission systems, Opt. Fiber Telecommun. Vol.3, pp. 196–264,1997.

[16] C. Headley and G. P. Agrawal, "Raman Amplification in Fiber Optical communication Systems," Elsevier Academic Press, 2005.

[17] E. Paul and J. Green, "Fiber to the Home: The New Empowerment," by John Wiley & Sons, Inc. All rights reserved, 2006.

[18] E. P. Ippen and R.H. Stolen, "Stimulated Brillouin scattering in optical fibers," Appl. Phys. Lett. Vol. 21, pp.539-540 ,1972.

[19] L. Brillouin, "Diffusion de la lumiere et des rayons X par un corps transparent homogene: influence de l'agitation thermique," Annales de Physique, Vol. 17, pp. 88-122, 1922.

[20] G. P. Agrawal, “Applications of Nonlinear Fiber Optics,” Academic press, San Diego, California 92101-4495, USA, 2001.

[21] D. Cotter, “Stimulated Brillouin scattering in monomode optical fiber,” J. Opt. Commun. Vol. 4, pp.10, 1983.

[22] M. Nikles, L. Thevenaz, and P. A.Robert, “Brillouin gain spectrum characterization in single-mode optical fibers," Journal of Lightwave Technology, Vol. 15, pp.1842-1851, 1997.

[23] M. Suzuki and N. Edagawa, “Dispersion-Managed High-Capacity Ultra-Long-Haul Transmission, ” J. Lightwave Technol. Vol.21, pp.916 , 2003.

[24] G. P. Agrawal, “Light wave technology telecommunication,” by John Wiley & Sons, Inc. All rights reserved, pp.134-136, 2005.

[25] K. S. Abedin, “Observation of strong stimulated Brillouin scattering in single-mode As_2Se_3 Chalcogenide fiber,” Opt. Express, Vol. 13, pp.10266-10271, 2005.

[26] A. Fellegara, M. Artiglia, S. Andreasen, A. Melloni, F. Espunes, and S. Wabnitz, “Cost 241 intercomparison of nonlinear refractive index measurements in dispersion shifted optical fibers at 1550 nm,” Electr. Lett., Vol. 33, pp. 1168–71, 1997.

[27] Y. Namihira, K. Miyagi, K. Kaneshima, M. Tadakuma, C. Vinegoni, G. Pietra and K. Kawanami, “A Comparison of Six Techniques for Nonlinear Coefficient Measurements of various Single Mode Optical Fibers,” 2007.

[28] M. Yamada, “Overview of Wideband Optical Fiber Amplification,” NTT Technical, Vol. 213, pp.63-66, 2002.

[29] A. Boskovic, S. V. Chernikov, J. R. Taylor, L. Gruner-Nielsen, and O. A. Levring, “Direct continuous-wave measurement of n_2 in various types of telecommunication fiber at 1.55 μm,” Opt. Lett., Vol. 21, pp. 1965–7, 1996.

[30] T. Omae, K. Nakajima, and M. Ohashi, "Universal conditions for nonlinear refractive index n_2 estimation of dispersion compensating fibers by CW-SPM method," Optical fiber communications; OFC, Anaheim, p. TuH3, 2001.

[31] J. H. Lee, P. C. Teh, P. Petropoulos, M. Ibsen, and D. J. Richardson, "Reduction of interchannel interference noise in a two-channel, grating based OCDMA system using a nonlinear optical loop mirror," IEEE Photonics Technology Letters, Vol. 13, pp. 529-531, 2001.

[32] B. Olsson and D. J. Blumenthal, "All-optical demultiplexing using fiber cross-phase modulation (XPM) and optical filtering," IEEE Photonics Technology Letters, Vol. 13, pp. 875-877, 2001.

[33] V. E. Perlin and H. G. Winful, "Nonlinear pulse switching using cross-phase modulation and fiber Bragg gratings," IEEE Photonics Technology Letters, Vol. 13, pp. 960-962, 2001.

[34] J. Yu, X. Zheng, C. Peucheret, A. T. Clausen, H. N. Poulsen, and P. Jeppesen, "40-Gb/s all-optical wavelength conversion based on a nonlinear optical loop mirror," Journal of Lightwave Technology, Vol. 18, pp.1001-1003, 2000.

[35] Y. R. Shen, "The Principles of Nonlinear Optics ," Wiley, New York, 1984.

[36] J. A. Armstrong, N. Bloembergen, J. Ducuing, and P. S. Pershan, "Interactions between Light Waves in a Nonlinear Dielectric," Phys. Rev, Vol.127, pp.1918 ,1962.

[37] M. Schubert and B.Wilhelmi, "Nonlinear Optics and Quantum Electronics," Wiley, New York, 1986.

[38] P. N. Butcher and D. Cotter, "Elements of Nonlinear Optics," Cambridge University Press, Cambridge, UK, 1990.

[39] H. J. R. Dutton, "Understanding Optical Communications," International Technical Support Organization, 1998.

[40] E. P. Ippen and R. H. Stolen, "Stimulated Brillouin scattering in optical fibers," Appl. Phys. Lett. Vol. 21, pp.539-540, 1972.

[41] K. J. Williams and R. D. Esman, "Stimulated Brillouin scattering for improvement of microwave fibreoptic link efficiency," Electron. Lett.Vol.30, pp.1965-1966 ,1994.

[42] A. Loayssa, D. Benito, and M. J. Garde, "Optical carrier-suppression technique with a Brillouin-Erbium fiber laser," Opt. Lett., Vol. 25, pp.197-199, 2000.

[43] S. Norcia, S. Tonda-Goldstein, D. Dolfi, and J.-P. Huignard, "Efficient single-mode Brillouin finer laser for low-noise optical carrier reduction of microwave signals," Opt. Lett.,Vol. 28, pp.1888-1890 ,2003.

[44] M. Matsukawa, K. Shintani, S. Tomohiro and N. Ohtori, "Application of Brillouin scattering to the local anisotropy and birefringence measurements of thin layers," Ultrasonic journal, Vol. 44, No. 22, pp.1555-1559, 2006.

[45] J. Sandercock, "Some recent applications of brillouin scattering in solid state," Advances in Solid State Physics, Switzerland, Vol. 15, pp.183-202,1975.

[46] D. Alasia1, A. Fernandez, L. Abrardi,, B. Brichard and L. Thevenaz, **"**The effects of gamma-radiation on the properties of Brillouin scattering in standard Ge-doped ptical fibres**,"** Meas. Sci. Technol. Vol.17 , pp.1091–1094, 2006.

[47] D. Kasprowicz, M. Drozdowski, A. Majchrowski, E. Michalski, "Spectroscopic properties of KGd(WO4)2: (Er, Yb) single crystals studied by Brillouin scattering method," Optical Materials ,Vol. 30 , pp.152–154, 2007.

[48] K. Inoue and H. Toba, "Wavelength conversion experiment using fiber four-wave mixing," IEEE Photonics Technology Letters, Vol. 4, pp. 69-72, 1992.

[49] C. Dorman, I. Kucukkara, and J. P. Marangos, "Measurement of high conversion efficiency to 123.6-nm radiation in a four-wave-mixing scheme enhanced by electromagnetically induced transparency," Phys. Rev. A, Vol. 61, pp.3802-3806, 1999.

[50] A. Yariv, D. Fekete, and D. M. Pepper, "Compensation of channel dispersion by nonlinear optical phase conjugation," Optics Letters, Vol. 4, pp. 52-54, 1979.

[51] J. E. Sharping, M. Fiorentino, P. Kumar, and R. S. Windeler, "Optical parametric oscillator based on four-wave mixing in microstructure fiber," Optics Letters, Vol. 27, pp. 1675-1677, 2002.

[52] R. E. Slusher, L. W. Hollberg, B. Yurke, J. C. Mertz, and J. F. Valley, "Observation of squeezed states generated by four-wave mixing in an optical cavity," Phys. Rev. Lett. Vol.55, pp.2409-2412, 1985.

[53] M. D. Levenson, R. M. Shelby, and S. H. Perlmutter, "Squeezing of classical noise by nondegenerate four-wave mixing in an optical fiber," Opt. Lett. Vol.10, pp.514-516, 1985.

[54] D. J. Jones, S. A. Diddams, J. K. Ranka, A. Stentz, R. S. Windeler, J. L. Hall, and S. T. Cundiff, "Carrier-envelope phase control of femtosecond mode-locked lasers and direct optical frequency synthesis," Science Journal, Vol.288, pp.635-639, 2000.

[55] B. R. Washburn, S. A. Diddams, N. R. Newbury, J. W. Nicholson, M. F. Yan, and C. G. Jorgenson, "Phase-locked, Erbium-fiber-laser-based frequency comb in the near infrared," Opt. Lett. Vol.29, pp.250-252, 2004.

[56] S. A. Diddams, D. J. Jones, J. Ye, S. T. Cundiff, J. L. Hall, J. K. Ranka, R. S. Windeler, R. Holzwarth, T. Udem, and T. W. Hansch, "Direct link between microwave and optical frequencies with a 300 THz femtosecond laser comb," Phys. Rev. Lett. Vol. 84, pp.5102-5105, 2000.

[57] S. A. Diddams, D. J. Jones, J. Ye, S. T. Cundiff, J. L. Hall, J. K. Ranka, and R. S. Windeler, "Direct RF to optical frequency measurements with a femtosecond laser comb," IEEE Trans. Instrum. Meas. Vol.50, pp.552-555, 2001.

[58] J. C. Diels and W. Rudolph, "Ultrashort laser pulse phenomena," Academic Press ,1996.

[59] P. V. Mamyshev, "All-optical data regeneration based on self-phase modulation effect," in Proc. Eur. Conf. Optical Communication (ECOC), Madrid, Spain, Sep., Vol. 1, pp. 475–476, 1998.

[60] M. Bass, J. M. Enoch, E. W. Van Stryland and W. L. Wolfe, **"**Fiber Optics and Nonlinear Optics**,"** McGRAW-HILL, Vol. 4, 2001.

[61] G. P. Agrawal, "Fiber-Optics Communication Systems,"2nd. edition., Wiley, New York, 1997.

[62] M. J. Collett and C. W. Gardiner, "Squeezing of intracavity and traveling-wave light fields produced in parametric amplification" Phys. Rev. Vol. 30, pp.1386 ,1984.

[63] X. Li, J. Chen, P. Voss, J. E. Sharping, and P. Kumar, "All-fiber photon-pair source for quantum communications: Improved generation of correlated photons" Opt. Express, Vol. 12, pp.3737, 2004.

[64] X. M. Liu, “Four-wave mixing self-stability based on photonic crystal fiber and its applications on Erbium-doped fiber lasers,” Optics Communications 260, pp.554–559, 2006.

[65] K. Inoue, “Four-wave mixing in an optical fiber in the zero-dispersion wavelength region,” J. Lightwave Technol., Vol. 10, pp. 1553–1561, 1992.

[66] O. Aso, M. Tadakuma and S. Namiki , “Four-Wave Mixing in Optical Fibers and Its Applications ,” Furukawa Review, No. 19, pp.43-45, 2000.

[67] A.V. Ramprasad and M. Meenakshi , “Four-Wave Mixing on dense wavelength division multiplexing optical systems,” Vol.17, 2006.

[68] S. Ohara, N. Sugimoto, K. Ochiai, H. Hayashi, Y. Fukasawa, T. Hirose, T. Nagashima, M. Reyes, “Ultra-wideband amplifiers based on Bi_2O_3-EDFAs,” Optical Fiber Technology ,Vol.10 , pp.283–295, 2004.

[69] T. Hasegawa , T. Nagashima, N. Sugimoto , “Determination of nonlinear coefficient and group-velocity-dispersion of bismuth-based high nonlinear optical fiber by four-wave-mixing,” Asahi Glass Co., Ltd., Research Center, 1150, Hazawa-cho, Kanagawa-ku, Yokohama 221-8755, Optics Communications, Vol.281, pp.782–787, 2008.

[70] M. P. Nikodem, W. Żurawski, K. M. Abramski , “Four-Wave Mixing in Non-Zero Dispersion Shifted Fibers,” ICTON 2008.

[71] D. K. Mynbaev and L. L. Scheiner, “Fiber optic communications technology,” 2001.

[72] C. J. Koester, E. Snitzer, “Amplification in a fiber laser”, Appl. Opt. Vol.3, pp.1182 ,1964.

[73] F. Auzel, "Emission stimulatede Er^{+3} dans un verre fluorophosphate" C. R. Acad. Sci. B263, Vol.765,1966.

[74] R. H. Stolen and E. P. Ippen, "Raman gain in glass optical waveguides," Appl. Phys.Lett., Vol. 22, pp. 276–278, 1973.

[75] S. Namiki and Y. Emori, "Ultrabroad-band raman amplifiers pumped and ainequalized by wavelengrh-division-multiplexed high-power laser diodes," IEEE Journal of Selected Topics in Quantum Electronics, Vol. 7, No. 1, pp. 3–16, 2001.

[76] N. Sugimoto, "Ultrafast optical switches and wavelength division multiplexing (WDM) amplifiers based on Bismuth-oxide glasses," J. Am. Ceram. Soc. Vol. 85, pp.1083-1088, 2002.

[77] Y. Kuriowa, N. Sugimoto, K. Ochiai, S. Ohara, Y. Fukasawa, S. Ito, S. Tanabe, and T. Hanada, "Fusion spliceable and high efficient Bi_2O_3-based EDF for short length and broadband amplification pumped at 1480 nm," presented at Optical Fiber Communication Conference (OFC), TuI5 , 2001.

[78] K. Taira, K. Kikuchi, and N. Sugimoto, "Dispersion and pulse amplification characteristics of bismuth oxide-based Erbium-doped fiber amplifiers," Optical Amplifiers and Applications Conference (OAA), OTuC2, 2002.

[79] K. Kikuchi, K. Taira, and N. Sugimoto, "Highly nonlinear bismuth-oxide-based glass fibres for all-optical signal processing," Electron. Lett. Vol. 38, pp.156-157, 2002.

[80] N. Sugimoto, T. Nagashima, T. Hasegawa, S. Ohara, K. Taira, and K. Kikuchi, "Bismuth-based optical fiber with nonlinear coefficient of 1360 $W^{-1}km^{-1}$," Optical Fiber Communication Conference (OFC), Los Angeles, California, USA, 2004.

[81] N. Sugimoto, T. Hasegawa, T. Nagashima and S. Ohara, "Bi-based fibers for amplifiers and nonlinear applications, IEEE, pp.34-36, 2006.

[82] J. H. Yang, S. X. Dai, Y. F. Zhou, L. Wen, L. L. Hu, and Z. H. Jiang, "Spectroscopic Properties and Thermal Stability of Erbium-doped Bismuth-based Glass for Optical Amplifier," J. Appl. Phys., Vol. 93, No. 2, pp. 977-983, 2003.

[83] J. T. Gopinath, "Studies of third order nonlinearities in materials and devices for ultrafast lasers," Massachusetts institute of technology, 2005.

[84] N. Sugimoto, H. Kanbara, S. Fujiwara, K. Tanaka, Y. Shimizugawa, and K. Hirao, "Third-order optical nonlinearities and their ultrafast response in Bi_2O_3-B_2O_3-SiO_2 glasses," J. Opt. Soc. Am. B,Vol. 16, pp.1904-1908,1999.

[85] W. Y. Chong, "L-band Bismuth-based erbium-doped fiber amplifier", 2006.

[86] G. P. Agrawal, "Fiber-Optic Communication Systems," Third Edition, by John Wiley & Sons, 2002.

[87] Z. Jusoh, "C-band Bismuth-based Erbium-doped amplifier", M. Eng. thesis, University of Malaya, 2008.

[88] N. Sugitomo, "Recent Progress in Bi-EDF Technology," Asahi Glass Co.Ltd., 2005.

[89] S. Ohara, N. Sugimoto, K. Ochiai, H. Hayashi, Y. Fukasawa, T. Hirose, T. Nagashima, M. Reyes, "Ultra-wideband amplifiers based on Bi_2O_3-EDFAs," Optical Fiber Technology,Vol. 10, pp.283–295, 2004.

[90] J. S. Sanghera, C. M. Florea, L. B. Shaw, P. Pureza a, V.Q. Nguyen, M. Bashkansky, Z. Dutton, I.D. Agrawal., "Non-linear properties of Chalcogenide glasses and fibers Non-Crystalline Solids," Vol. 354, pp.462–467, 2008.

[91] W. J. Wadsworth, N. Joly, J.C. Knight, T.A. Birks, F. Biancalana, P.S.J. Russell, "Hollow core photonic crystal fibers for beam delivery," Opt. Express,Vol.12 No.8, pp.299, 2004.

[92] H. Sotobayashi, J. T. Gopinath, Y. Takushima, K. Hsu, and E. P. Ippen, "Broadband wavelength tunable, single frequency, and single polarization Bismuth Oxide-based Erbium-doped fiber laser," IEEE Photon. Technol. Lett., Vol. 16, No. 7, 2004.

[93] J. M. Harbold, F.O. Ilday, F.W. Wise, J.S. Sanghera, I.D. Aggarwal and B. Aitken, "Highly nonlinear Chalcogenide glasses for all optical switching," in: Proceedings of Int. Symp. On Photonic Glasses (ISPG 2002), Shanghai, China, Oct 14-17, SPIE, Vol. 5061, pp.143, 2003.

[94] P. Becker, "Thermal and optical properties of glasses of the system Bi_2O_3 – B_2O_3 ,"Cryst. Res. Technol.Vol.38, No.1, pp.74, 2003.

[95] Y. Chen, Y. Huang, M. Huang, R. Chen, Z. Luo, "Luminescence of Erbium-doped Bismuth–borate glasses," Opt. Mater. Vol. 25, No.7, pp.271, 2004.

[96] Y. Chen, Y. Huang, M. Huang, R. Chen, Z. Luo, J. Am. Ceram, "THz diffuse reflectance spectra of selected explosives and related compounds," Vol.19, No.6, pp.5790, ,2005.

[97] S. Tanabe, N. Sugimoto, S. Ito, T. Hanada, "Broad-band 1.5 μm emission of Er^{3+} ions in Bismuth-based oxide glasses for potential WDM amplifier," J . Lumin. Vol. 670, pp. 87–89, 2000.

[98] J.H. Yang, S.X. Dai, Y.F. Zhou, L. Wen, L.L. Hu, Z.H. Jiang, "Optical transitions and upconversion luminescence of Er^{3+}/Yb^{3+} codoped halide modified tellurite glasses," J. Appl. Phys. Vol. 95, pp. 3020, 2004.

[99] I. I. Oprea, H. Hesse, K. Betzler, "Luminescence of Erbium-doped bismuth–borate glasses," optical material, 2005.

[100] T. Nagashima, T. Hasegawa, S. Ohara, N. Sugimoto, K. Taira and K. Kikuchi, "Bi_2O_3-based highly nonlinear fiber with step index structure," Photonic West San Jose, pp.5350-7, 2004.

[101] N. Sugimoto, Y. Kuroiwa, K. Ochiai, S. Ohara, Y. Fukasawa, S. Ito, S. Tanabe, and T. Hanada, "Novel Short-length EDF for C+L Band Amplification," OAA2000 Quebec City, PDP3,2000.

[102] B. R. Washburn, S. A. Diddams, N. R. Newbury, J. W. Nicholson, M. F. Yan, C. G. Jorgenson, "Phaselocked, erbium-fiber-laser-based frequency comb in the near infrared," Opt. Lett. Vol. 29, pp.250-252, 2004.

[103] W. Drexler, U. Morgner, F. X. Kaertner, C. Pitris, S. A. Boppart, X. D. Li, E. P. Ippen, and J. G. Fujimoto, "In vivo ultrahigh-resolution optical coherence tomography," Opt. Lett. Vol. 24, pp.1221-1223,1999.

[104] J. Shah, "Ultrafast spectroscopy of semiconductors and semiconductor nanostructures," Springer Series in Solid-State Sciences 115, Springer, New York, New York, 1999.

[105] P. T. Rakich, J. T. Gopinath, H. Sotobayashi, C. W. Wong, S. G. Johnson, J. D. Joannopoulos, and E. P. Ippen, "Broadband supercontinuum-based measurements

of high-index contrast photonic bandgap devices from 1 to 2 μm," To be presented at LEOS (Lasers and Electro-Optic Society) Annual Meeting, Oct. 2004 .

[106] R. T. Neal, M. D. C. Charlton, G. J. Parker, C. E. Finlayson, M. C. Netti, and J. J. Baumberg, "Ultrabroadband transmission measurements on waveguides of silicon-rich silicon dioxide," Appl. Phys.Lett. Vol. 83, pp. 4598-4600, 2003.

[107] R. Ell, U. Morgner, F. X. Kaertner, J. G. Fujimoto, E. P. Ippen, V. Scheuer, G. Angelow, T. Tschudi, M. J. Lederer, A. Boiko, B Luther-Davies, "Generation of 5-fs pulses and octave-spanning spectra directly from a Ti:sapphire laser," Opt. Lett. Vol. 26, pp. 373-375, 2001.

[108] D. H. Sutter, G. Steinmeyer, L. Gallmann, N. Matuschek, F. Morier-Genoud, U. Keller, V. Scheuer, G. Angelow and T. Tschudi, "Semiconductor saturable-absorber mirror-assisted kerr-lens modelocked Ti:sapphire laser producing pulses in the two-cycle regime," Opt. Lett. Vol. 24, pp.631-633, 1999.

[109] J. W. Nicholson, M. F. Yan, P. Wisk, J. Fleming, F. DiMarcello, E. Monberg, A. Yablon, C. Jørgensen, and T. Veng, "All-fiber, octave-spanning supercontinuum," Opt. Lett. Vol. 28, pp.643-645, 2003.

[110] J. T. Gopinath, H.M. Shen, H. Sotobayashi, and E. P. Ippen, Highly nonlinear Bismuth-oxide fiber for smooth supercontinuum generation at 1.5 μm," Optical Society of America, 2004.

[111] S. W. Harun, S. Shahi, H. Ahmad, "A compact Brillouin /Erbium fiber laser," Opt. Lett, 33, pp.770-772, 2008.

[112] S. Shahi, S.W. Harun, N.S. Shahabuddin and M.R. Shirazi , H. Ahmad, "Multi-wavelength generation using a Bismuth-based EDF and Brillouin effect in a linear cavity configuration," Optics & Laser Technology, Vol. 41, pp.198-201,2009.

[113] H. Ahmad, S. Shahi, S. W. Harun, "Multi-wavelength laser generation with Bismuth-based Erbium-doped fiber," Optics Express, Vol. 17, No. 1, pp. 203-207, 2009.

[114] S. Shahi, S. W. Harun, and H. Ahmad, "Multi-wavelength Brillouin fiber laser using a holey fiber and a Bismuth-oxide based erbium-doped fiber," Laser Phys. Lett. Vol. 6, No. 6, pp. 454–457, 2009.

[115] S. Shahi, S. W. Harun, K. S. Lim, A.W. Naji and H. Ahmad, "Enhanced four-wave mixing efficiency of Bi-EDF in a new ring configuration for determination of nonlinear parameters," J. of Electromagn. Waves and Appl. (JEMWA), Vol. 23, pp.2397–2407, 2009.

[116] C. J. Koester and E. Snitzer, "Amplification in a fiber laser," Appl. Opt. Vol. 3, pp.1182-1186, 1964.

[117] T. H. Maiman, "Stimulated optical radiation in ruby masers," Nature Vol.187, pp. 493-494, 1960.

[118] J. Stone and C. A. Burrus, "Neodymium-doped silica lasers in end-pumped fiber geometry," Appl. Phys. Lett. Vol.23, pp.388-389, 1973.

[119] J. Stone and C. A. Burrus, "Neodymium-doped fiber lasers: room temperature cw operation with an injection laser pump," Appl. Opt. Vol.13, pp.1256-1258 ,1974.

[120] P. W. France, "Optical fiber lasers and amplifiers, " Blackie and son Ltd, 1991.

[121] L. Zenteno, "High-power double-clad fiber lasers," Journal of Lightwave Technology, Vol. 11, No. 9, pp. 1435–1446, 1993.

[122] J. Nilsson, S. U. Alam, J. A. Alvarez-Chavez, P. W. Turner, W. A. Clarkson, and A. B. Grudinin, "High-power and tunable operation Erbium-ytterbium co-doped

cladding-pumped fiber lasers," IEEE J. Quantum Electron., Vol. 39, No. 8, pp. 987–994, 2003.

[123] J. Vasseur, "Multi-wavelength laser sources for broadband optical access networks," 2006.

[124] K. O. Hill, B. S. Kawasaki, and D. C. Johnson, "CW Brillouin laser," Appl. Phys. Lett. Vol. 28, pp. 608-609, 1976.

[125] C. Montes, D. Bahloul, I. Bongrand, J. Botineau, G. Cheval, A. Mahmhoud, E. Picholle, and A. Picozzi, "Self-pulsing and dynamic ability in CW-pumped Brillouin fiber ring lasers," J. Opt. Soc. Am. B, Vol. 16, pp. 932-951, 1999.

[126] S. P. Smith, F. Zarinetchi, and S. Ezekiel, " Narrow-linewidth stimulated Brillouin fiber laser and applications," Opt. Lett., Vol. 16, pp. 393–395, 1991.

[127] M. R. Shirazi, S. W. Harun, M. Biglary, K. Thambiratnam, and H. Ahmad, "Effect of Brillouin pump linewidth on the performance of Brillouin Fiber Lasers," ISAST Transactions on Electronics and Signal Processing, Vol. 1, No. 1, pp. 30-32, 2007.

[128] G. J. Cowle and D. Y. Stepanov, "Hybrid Brillouin/erbium fiber laser," Opt. Lett.,Vol. 21, pp. 1250-1252, 1996.

[129] S. W. Harun, N. Tamchek, P. Poopalan and H. Ahmad, "L-band Brillouin- Erbium Fiber Laser", Laser Physics, Vol. 13, No. 9, pp. 1161-1163, 2003.

[130] D. S. Lim, H. K. Lee, K. H. Kim, S. B. Kang, J. T. Ahn, D. I. Chang, and M. Y.Jeon, "Figure-of-eight Brillouin/Erbium fibre lasers," Electron. Lett., Vol.34, pp. 2406-2407, 1998.

[131] M. R. Shirazi, M. Biglary, S. W. Harun, K. Thambiratnam, and H. Ahmad, "Bidirectional multiwavelength Brillouin fiber laser generation in a ring cavity," J. Opt. A: Pure Appl. Opt. Vol. 10, No.3, pp.34-36, 2008.

[132] Y. Han, T. V. A. Tran, S. Kim, and S. B. Lee, "Multiwavelength Raman-fiber-laser-based long-distance remote sensor for simultaneous measurement of strain and temperature," Opt. Lett. Vol. 30, pp. 1282-1284, 2005.

[133] A. During, C. Fossati, and M. Commandré, "Multiwavelength Imaging of Defects in Ultraviolet Optical Materials," Appl. Opt. Vol.41, pp. 3118-3126, 2002.

[134] E. Desurvive, J. L. Zyskind, and J. R. Simpson, "Spectral gain hole-burning at 1.53μm in Erbium-doped fiber amplifiers," IEEE Photon. Technol. Lett. Vol. 2, pp. 246-248, 1990.

[135] O. Graydon, W. H. Loh, R. L. Laming, and L. Dong, "Triple frequency operation of an Er-doped twin core fiber loop laser," IEEE Photon. Technol. Lett, Vol. 8, pp. 63-65, 1996.

[136] G. J. Cowle, and D. Yu. Stephanov, "Hybrid Brillouin/Erbium fiber laser,"Opt. Lett. Vol. 21, pp. 1250-1252, 1996.

CHAPTER 3

CHARACTERIZATION OF BISMUTH-BASED ERBIUM DOPED FIBER AMPLIFIERS AND RAMAN AMPLIFICATION

3.1 Introduction

The scattering and absorption mechanisms in an optical fiber can cause a progressive attenuation of light signals as they travel along a fiber. Because of this, the signal tends to lose power and cohesion, requiring the signal to undergo amplification and regeneration at certain intervals so that the receiver can appropriately deduce them. Because of this need, optical amplifiers now have become indispensable components in high-performance optical communication links [1] and are essential for increasing the scale and performance of communication systems [2]. For instance, EDFAs have demonstrated exceptionally high gains (>30dB) and low noise figures as well as showing an output power as high as 10 mW [3-5]. EDFAs can operate in both the C-band region from 1530 nm to 1560 nm and the L-band region from 1570 nm to 1620 nm, which coincidently is located in the low-fiber loss region.

Bismuth-doped glass has many attractive features which make them suitable as the core material of optical fibers. The near-infrared spectral regions with wide luminescence in the range from 1000 nm ~ 1600 nm and the long lifetime of luminescence make such fibers promising for the development of lasers and amplifiers [6]. Recently, Bi-EDFAs have been proposed for broadband signal amplification [7-9] using short gain medium lengths. Amplifications in both the C- and L-band region have been demonstrated using 22

cm and 26 cm long Bi-EDF respectively [7, 8]. A fiber with such a high Erbium dopant concentration is expected to have enormous potential in realizing a compact EDFAs and EDFA based devices [10]. In this thesis, the efficient 1480 nm pumped Bi-EDFA configurations are demonstrated in both C- and L-band regions. The Bi-EDFAs are then used to demonstrate fiber lasers using nonlinear effects in the fiber.

The optical amplification is due to stimulated emission process, which occurs when some external stimulant, such as a signal photon, causes an excited electron sitting at a higher energy level to drop to the ground state. The photon emitted in this process has the same energy (i.e., the same wavelength) as the incident signal photon and is in phase with it. This means their amplitudes add to produce a brighter light. For stimulated emission to occur there must be a population inversion of carriers, which means that there are more electrons in an excited state than in the ground state. Since this is not a normal condition, population inversion is achieved by supplying external energy to boost (pump) electrons to a higher energy level. The pump supplies energy to electrons in an active medium, which raises them to higher energy levels to produce a population inversion [1]. The fiber amplifiers investigated to date belong to three main categories [11]: Rare earth-doped fiber amplifiers, nonlinear fiber amplifiers and fiber optics parametric amplifiers (FOPAs) or four-wave mixing amplifiers. In EDFA and Raman fiber amplifier, pumping can be achieved in either or both propagation directions, while pumping must be forward in parametric fiber amplifiers and backward in Brillouin fiber amplifiers as imposed by phase matching.

In this chapter, the performances of the Bi-EDFAs and fiber Raman amplifiers (FRAs) with various pumping schemes and configurations are investigated. The Bi-EDFAs can operate in C and/or L band region from 1520 nm to 1620 nm for optical communication networks. The Bi-EDF used in all experiments is commercially available from Asahi Glass

Co. (AGC) and has an Er^{3+} ion concentration of 7.6×10^{25} ions/m^3 with a Lanthanum (La) ion co-dopant concentration of approximately 4.4 wt%. The La ions are incorporated to decrease the concentration quenching of the Erbium ions in the fiber. The fibers used have a core/cladding refractive index of 2.03/2.02 and a NA of 0.20, and is angle spliced to a single-mode fiber in order to reduce splice point reflections. The gain, noise figure, QCE and PCE of the Bi-EDFAs are investigated. The gain of FRAs can be obtained over any wavelength region, provided a suitable pump source is used. Multiple pump sources at different wavelengths can be used to shape and extend the Raman gain spectrum [12].

3.2 Absorption and Emission Characteristics of the Bi-EDF

Bismuth-based glass has several advantages over conventional silica-based glass as host material for Erbium-doped glass. Its ability to disperse Erbium ions has allowed Erbium ion doping of more than 3,000 ppm without significant concentration quenching effect as occurred in silica-based glass. The higher refractive index of Bismuth-based glass [13] results larger emission cross section and broader emission bandwidth which is desirable for WDM network systems. However, due to high refractive index, the $^4I_{13/2}$ level lifetime is relatively shorter in Bismuth-based glass. The host glass of the Bi-EDF is a Bismuth oxide. Figure 3.1 shows the measured and calculated emission cross-section using the McCumber theory and also the Si-EDF emission cross-section as a comparison [11]. The McCumber emission cross-section was calculated using absorption cross-sections provided by AGC, and it can be seen in the figure that the calculated emission cross-section agrees well with the experimental data. This optical emission peaks at the 1.53 μm, which is obtained due to the population inversion between energy level $^4I_{13/2}$ and $^4I_{15/2}$.

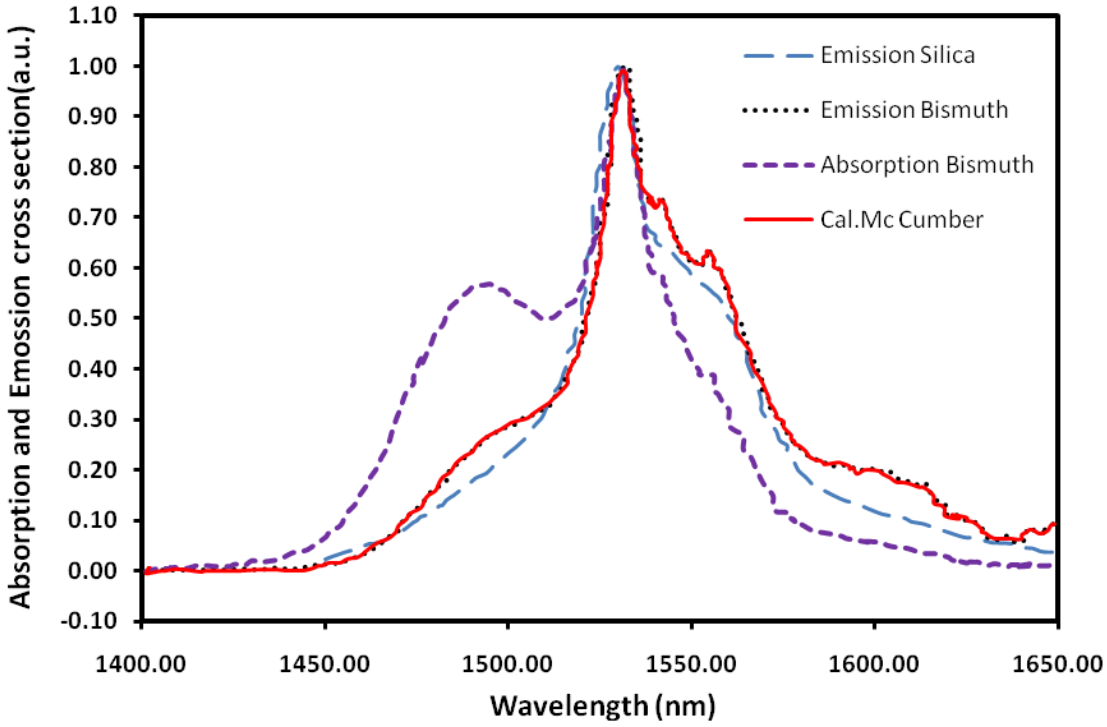

Figure 3.1: Absorption and emission cross-section of Bi-EDF and Si-EDF (The Bismuth absorption cross-section is obtained from AGC). The calculated Bismuth emission curve coincides very well with the measured curve [10].

Also from Figure 3.1, it can be seen that the Bi-EDF has wider emission spectra as compared to Si-EDF, especially at the longer wavelengths at 1620 nm because of its larger emission cross-section. The Si-EDF has a bandwidth of only 40 nm while the Bi-EDF bandwidth is almost double at 80 nm for the same emission intensity. The widening of the emission spectra is believed to be a result of the Stark level of the Er^{3+} ions in the Bi-EDF, which is separated to a larger degree due to the larger ligand field as shown by the absorption cross-section. As shown in Figure 3.1, despite the Bi-EDF having a higher absorption cross-section of 7.58×10^{-25} m^2 at the 1530 nm peak as compared to the Si-EDF absorption cross-section (which is only 4.39×10^{-26} m^2), the peak full-width half maximum (FWHM) of the Bi-EDF is narrower than the FWHM of the Si-EDF. This is due

to the larger inhomogeneous energy level degeneracy that the ligand field of the Bismuth host glass induced as a result of site to site variations, also known as the Stark effect [11], causing the widened optical transitions. Other elements such as Potassium oxide also have similar glass ability expander effects [14] and are used in the fabrication of Bi-EDF to obtain a broader amplification region. Therefore, this fiber allows a great broadband transmission capability and it is ideal for compact amplifier applications.

3.3 Amplification Principle and Numerical Model of Bi-EDFA

As a practical amplification medium, Er^{3+} doped fibers have been extensively studied due to their excellent gain operation around 1.5 μm in a loss minimum window of transmission silica fiber [15]. To get a phenomenological understanding of how an EDFA works, we need to look at the energy-level structure of Erbium. The Erbium atoms in silica are actually Er^{3+} ions, which are Erbium atoms that have lost three of their outer electrons. In describing the transitions of the outer electrons in these ions to higher energy states, it is common to refer the process as raising the ions to higher energy levels. Figures 3.2 and 3.3 show simplified energy-level diagrams and various energy-level transition processes of these Er^{3+} ions in silica glass. The two principal levels for telecommunication applications are a meta-stable level (the so-called $^4I_{13/2}$ level) and the $^4I_{11/2}$ pump level. The term meta-stable means that the lifetimes for transitions from this state to the ground state are very long compared to the lifetimes of the states that led to this level.

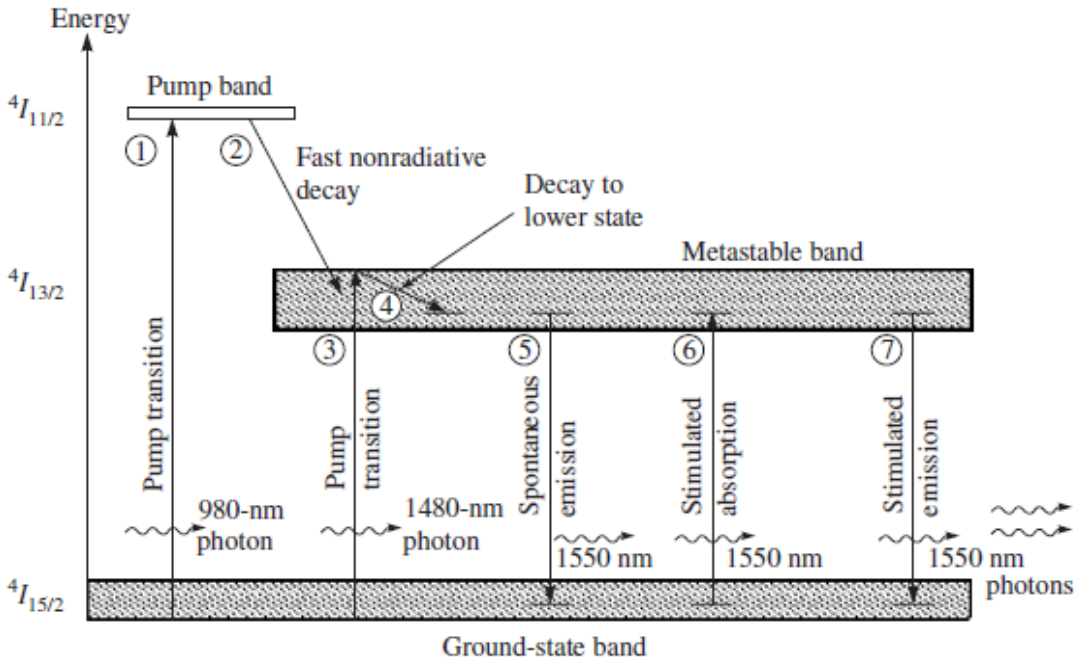

Figure 3.2: Simplified energy-level diagrams and various transition processes of Er^{3+} ions in silica [15].

As shown in Figure 3.3, the electron is excited by the pump from ground state ($^4I_{15/2}$) to excited state ($^4I_{11/2}$) and then non-radioactively transits to the meta-stable energy level ($^4I_{13/2}$).

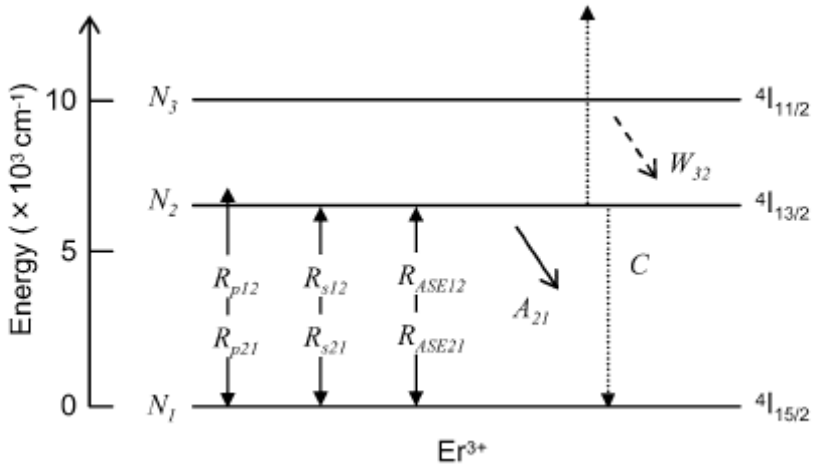

Figure 3.3: Energy level diagram of Er^{3+} and the relevant transitions [16].

Following that, it transits from the meta-stable level to the ground state with emission of 1550 nm photons. Assuming that the population densities of Er^{3+} ions at the $^4I_{15/2}$, $^4I_{13/2}$ and $^4I_{11/2}$ are N_1 , N_2 and N_3 , respectively, the steady- state rate equations for the Bi-EDFA system can be written as follows [16]:

$$\frac{dN_1}{dt} = (A_{21} + R_{S21} + R_{P21} + R_{ASE21})N_2 - (R_{S12} + R_{P12} + R_{ASE12})N_1 + CN_2^2 \quad (3.1)$$

$$\frac{dN_2}{dt} = -(A_{21} + R_{S21} + R_{P21} + R_{ASE21})N_2 + (R_{12} + R_{P12} + R_{ASE12})N_1 - 2CN_2^2 + W_{32}N_3 \quad (3.2)$$

$$\frac{dN_3}{dt} = -W_{32}N_3 + CN_2^2 \quad (3.3)$$

So, the total population density N is expressed as

$$N = N_1 + N_2 + N_3 \quad (3.4)$$

Here A_{21} is the spontaneous emission probability of the 1.55 μm band calculated by the Fuchtbauer–Ladenburg formula [17], and W_{32} is the non-radiative decay rate from the $^4I_{11/2}$ level that calculated by the measured lifetime. C is the corporative up-conversion coefficient evaluated by Snoek's method [18]. We neglect the non-radiative decay rate of the $^4I_{13/2}$ level and the spontaneous emission from the $^4I_{11/2}$ level because A_{21} and W_{32} are dominant in those levels. R represents the radiative decay rate of the signal, pump and ASE and is expressed as follows:

$$R_{S21} = \left(\frac{\sigma_S^E}{A_{eff} h \upsilon_S}\right) P_S \quad (3.5)$$

$$R_{S12} = (\frac{\sigma_S^A}{A_{eff} h\upsilon_S})P_S \tag{3.6}$$

$$R_{P21} = (\frac{\sigma_P^E}{A_{eff} h\upsilon_P})(P_p^+ + P_P^-) \tag{3.7}$$

$$R_{P12} = (\frac{\sigma_P^A}{A_{eff} h\upsilon_P})(P_p^+ + P_P^-) \tag{3.8}$$

$$R_{ASE21} = (\frac{\sigma_P^E}{A_{eff} h\upsilon_S})(P_{ASE}^+ + P_{ASE}^-) \tag{3.9}$$

$$R_{ASE21} = (\frac{\sigma_P^A}{A_{eff} h\upsilon_S})(P_{ASE}^+ + P_{ASE}^-) \tag{3.10}$$

where h, A_{eff} are the plank constant and effective area, respectively. $P_P^{\pm}$ and $P_{ASE}^{\pm}$ are the forward and backward propagating pump power and ASE powers while P_S, σ_P^E and σ_P^A are the signal power, emission and absorption cross sections at the pump wavelength, respectively. σ_P^E and σ_P^A are the functions of the input signals estimated from [10]. We assume that all the Er^{3+} ions excited to the $^4I_{9/2}$ levels by the cooperative up-conversion process relax to the $^4I_{11/2}$ immediately.

The evolution of the pump power, ASE powers and signal power along the Bi-EDF fiber (z) is given by [11]

$$\frac{dP_S}{dz} = \Gamma(\lambda_s)(\sigma_S^e N_2 - \sigma_S^a N_1) \times P_S - \alpha_S P_S \tag{3.11}$$

$$\frac{dP_P}{dz} = \Gamma(\lambda_P)(\sigma_P^e N_2 - \sigma_P^a N_1) \times P_P - \alpha_P P_P \tag{3.12}$$

$$\frac{dP_{ASE}(\lambda_{ASE})}{dz} = \Gamma(\lambda_{ASE})(\sigma_\lambda^e N_2 - \sigma_\lambda^a N_1) \times P_{ASE} + \Gamma(\lambda_{ASE}) h\nu\Delta\nu\sigma_\lambda^e N_3 - \alpha_{ASE} P_{ASE} \tag{3.13}$$

where Γ is the overlap factor of every wavelength [15] and α is the fiber background loss measured [11]. The subscripts s and ASE mean the signal and the ASE, respectively. In the ASE equation, $\Delta\nu$ represents the effective ASE bandwidth that is the resolution of the measuring device such as an OSA.

3.4 Gain and Noise Figure Performance of the Bi-EDFA

The gain of the Bi-EDFA is calculated by numerically solving E.qs (3.1) - (3.13) of the previous section. The parameters used in the calculations 3×10^8 m/s for the light speed c in vacuum, 6.626×10^{-34} m^2kg/s for the Planck's constant h, 2.7×10^{-6} m for the radius of the optical fiber and 8.5×10^{-24} for the C. The pump and input signal powers are fixed 150 mW and 10^{-3} mW, respectively; and the fiber background loss is 0.6 dB/m. All of the equation used for pump, signal and pump power are first order differential equations. We have used $P_P(z=0) = P_P$, $P_S(z=0) = P_S$ and $P_{ASE}(z=0) = 0$ as the boundary conditions on pump power, signal power and ASE spectral at input signal wavelength. To get accurate result a relaxation method is used by dividing fiber to many small segments of 10 cm long. The noise figure of the Bi-EDFA is calculated by this equation:

$$NF = 1/G + P_{ASE}/(G \times h \times \nu \times \Delta\nu) \qquad (3.14)$$

The experimental setup of the forward pumped Bi-EDFA is illustrated in Figure 3.4. It consists of a wavelength selective coupler (WSC), two optical isolators, one variable optical attenuator (VOA) and a piece of Bi-EDF. Both optical isolators are used to avoid the reflection and ensure unidirectional operation in the amplifier. The 1480 nm laser diode is used to pump the Bi-EDF. WSC is used to combine the pump light with 1550 nm signal.

Tunable laser source (TLS) is used in conjunction with OSA to characterize the Bi-EDFA. A VOA is incorporated immediately after the TLS to control the input signal power into the optical amplifier.

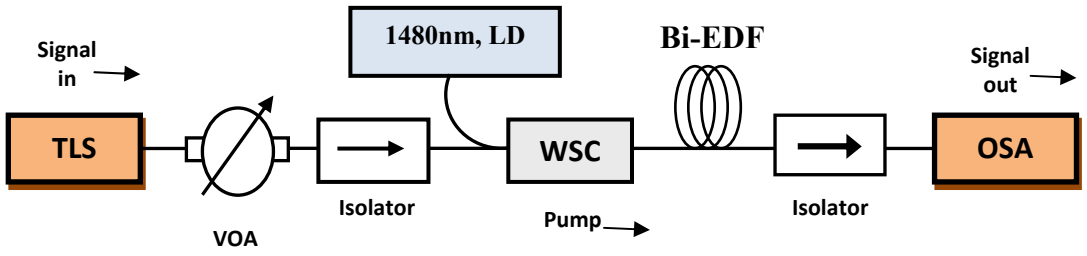

Figure 3.4: Experimental set-up for the forward pumped Bi-EDFA.

Figure 3.5 shows the calculated gain as a function of Bi-EDF's length at various input signal wavelength. In this calculation, the Erbium ion concentration and pump power are set at 7.6×10^{25} ions/m^3 and 150 mW, respectively. As shown in the figure, the maximum gains of 26 dB, 20 dB and 15 dB are obtained for 1530 nm, 1575 nm and 1615 nm at Bi-EDF's length of 1.0 m, 1.0 m and 1.5 m respectively. At a long Bi-EDF length, the gain of the Bi-EDFA shifts to the L-band as depicted in Figure 3.5. This is attributed to the quasi two level system effects in the Bi-EDFA, which the C-band photons are absorbed to emit at a longer wavelength. Figure 3.6 compares the experimental gain and noise figure characteristics of the Bi-EDFA with the theoretical values at the pump power of 150 mW and the Bi-EDF's length of 49 cm. The input signal power is fixed at -30 dBm. The gains are observed in both C- and L-band region with the higher gain is obtained at the C-band region ranging from 1530 nm to 1560 nm. It is shown that the calculated value is in good

agreement with the experimental measured one, verifying the feasibility of our theoretical model.

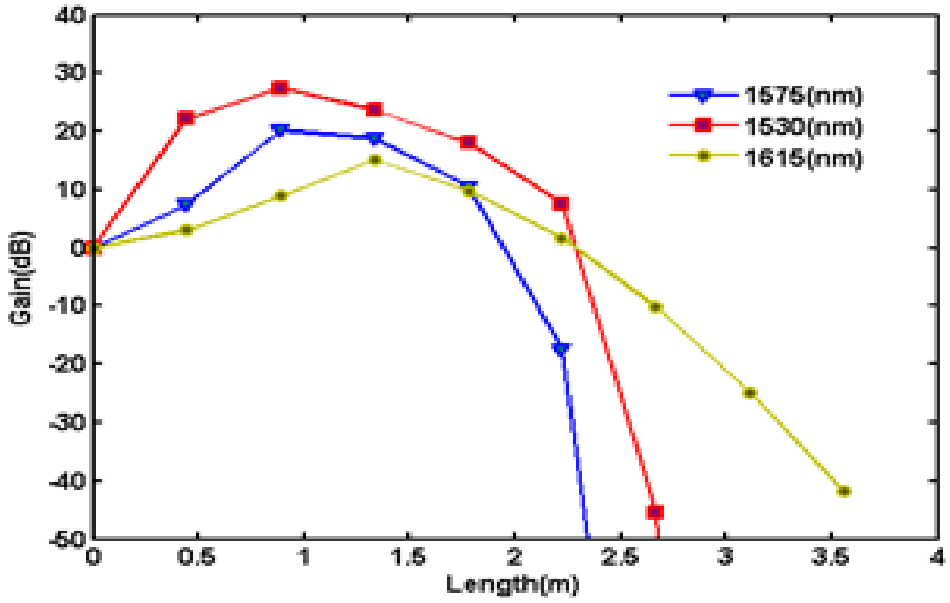

Figure 3.5: Variation of gain as a function of Bi-EDF's length for three different input signal wavelengths.

The theoretical and experimental gains of the Bi-EDFA are obtained within 20 dB to 23 dB at C-band region. The theoretical gain is flat within 35 nm bandwidth from 1530 nm to 1565 nm as shown in Figure 3.6. The slightly lower gain for the experimental results especially at longer wavelengths is expected due to the effect of multiple reflections from both the fiber splice points whereby the signal is reflected back into the Bi-EDF due to the large refractive index difference. This causes the increased cavity loss and spurious laser generation which suppresses the gain of the Bi-EDFA. As shown in Figure 3.6, the Bi-EDFA gain bandwidth covers until the extended L-band region and it is also much wider than that of the standard Si-EDFA. This is attributed to the suppression of Excited State Absorption (ESA) effect by the incorporation of La ions in the Bi-EDFA. The suppression of ESA reduces the dissipation of pump energy and increases the population inversion

especially at extended L-band region. The experimental noise figure is obtained at approximately 7 dB within the C-band region as shown in Figure 3.6. The high Erbium ion doping concentration and high insertion loss of the Bi-EDF incur a high noise figure for the Bi-EDFA. The theoretical noise figure is lower since the insertion loss of the Bi-EDF was ignored during simulation. Furthermore, we ignored the effect of strong excited state absorption (ESA) at longer wavelength region and also environmental effects like temperature on numerical gain and noise figure.

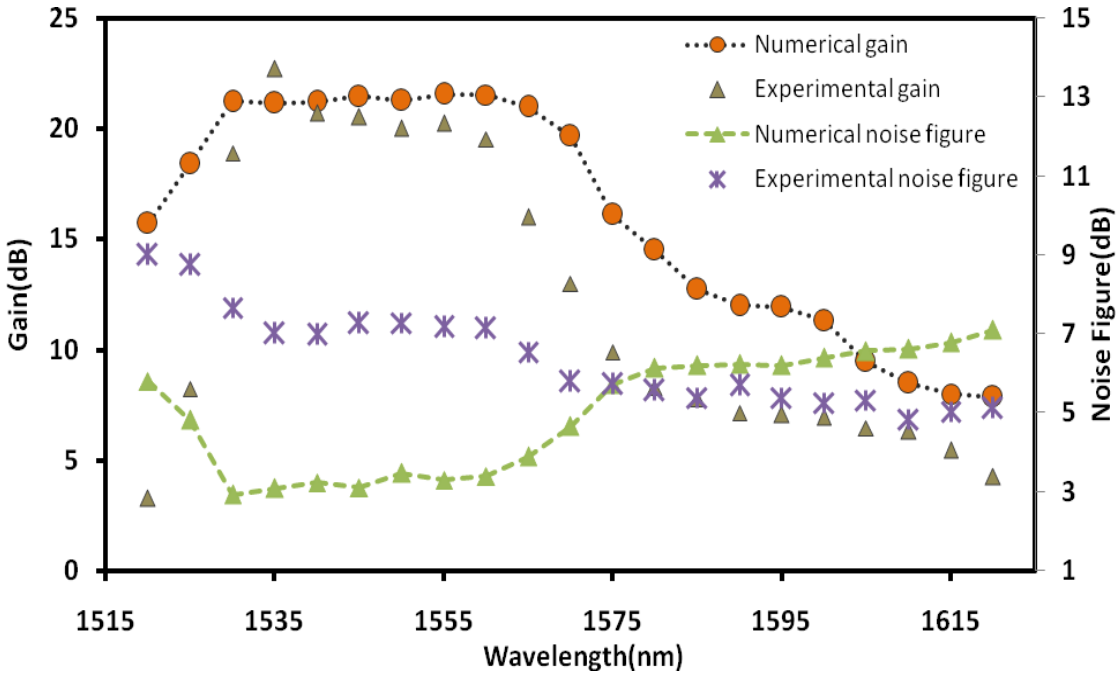

Figure 3.6: Comparison of calculated gain and noise figure with experimental results for the Bi-EDFA with 49 cm long Bi-EDF.

Figure 3.7 shows the theoretical gain spectrum of the Bi-EDF with variation of Bi-EDF length from 0 m to 1 m.

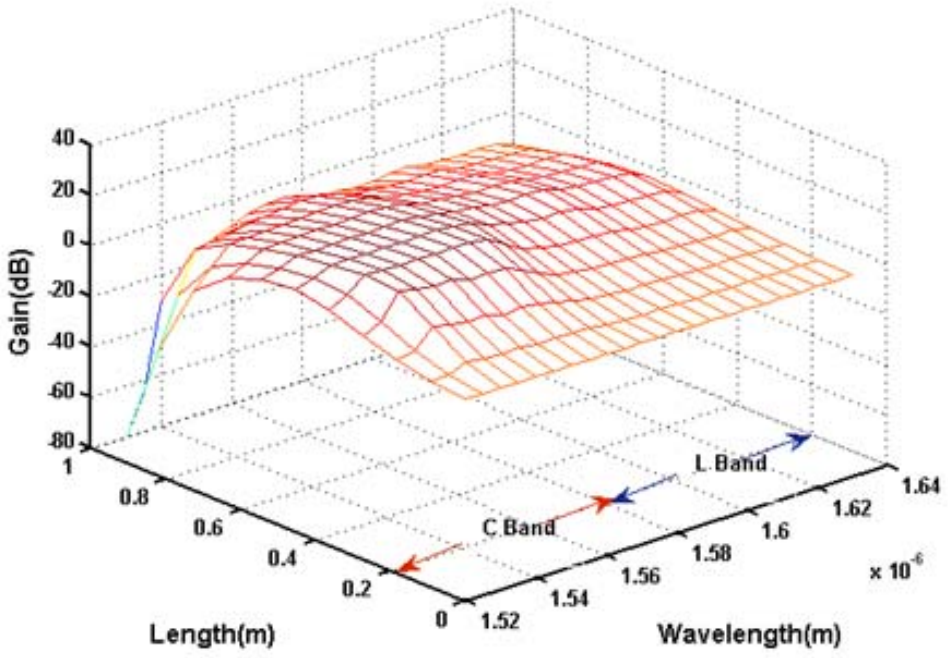

Figure 3.7: Theoretical gain versus input signal wavelength and Bi-EDF's length for the Bi-EDFA.

The input signal and pump powers are set at -30 dBm and 150 mW, respectively. As shown in Figure 3.7, the gain of the Bi-EDFA is remarkable in C-band with a shorter length of Bi-EDF and as the length increases the gain increment is more pronounced in L-band region. However, the optimum length for the Bi-EDFA to operate in C-band is around 0.5 m to 0.8 m.

3.5 Gain Spectrum

Figure 3.8 compares the gain spectra between the Bi-EDFA and Si-EDFA at input signal of -30 dBm. The length of the Bi-EDF is fixed at 215 cm (with an Erbium

concentration of 3250 ppm) while the lengths of the silica fiber are fixed at 8m and 16m (950 ppm). The 1480 nm pump power is fixed at 100 mW.

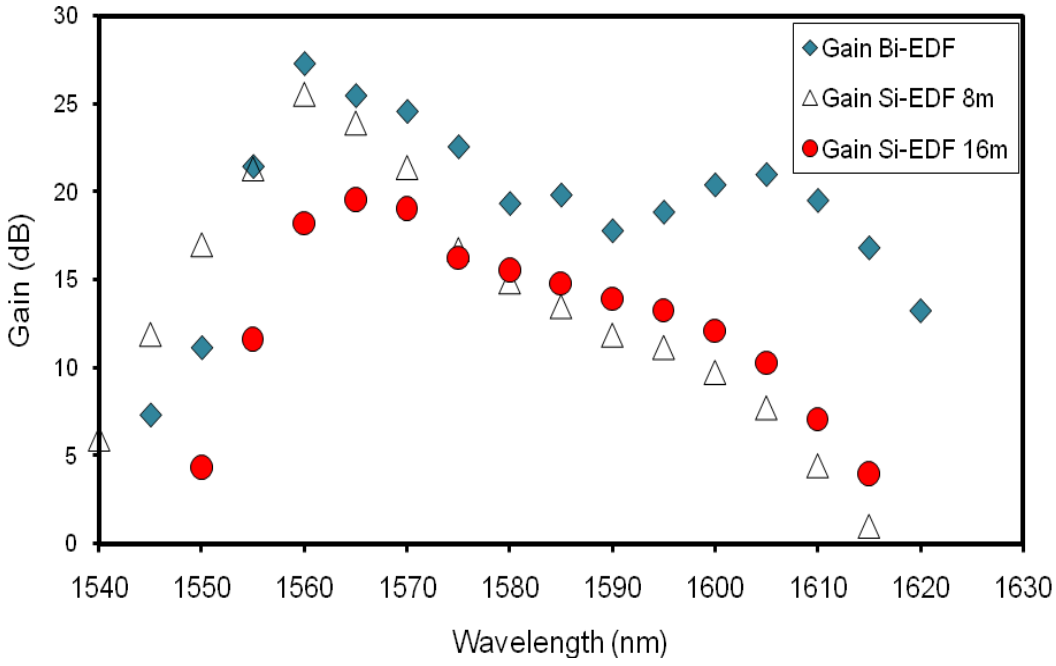

Figure 3.8: Comparison of the measured signal gain at input signal power of -30 dBm between Si-EDFA and Bi-EDFA. The 1480 nm pump power is fixed at 100 mW.

From Figure 3.8, the gain of the Bi-EDFA is seen to be much higher than that of Si-EDFA, especially at longer wavelength region. For instance, at 1600 nm, the gain of Bi-EDFA is 7 dB higher than that of the Si-EDFA (with 16 m long EDF). The Bi-EDFA gain bandwidth is also wider by about 15 nm than that of the Si-EDFA, to give the Bi-EDF gain bandwidth of approximately 80 nm spanning from 1540 nm up to 1620 nm. However, the high Erbium ions doping concentration and high insertion loss of the Bi-EDF when spliced to a conventional SMF incur a higher noise figure for the Bi-EDFA as shown in Figure 3.9. The gain spectrum shifts to a longer wavelength with the use of longer EDF, therefore the

gain is higher in extended L-band region (1600 nm) with 16 m Si-EDF compared to that of 8 m Si-EDF as depicted in Figure 3.8.

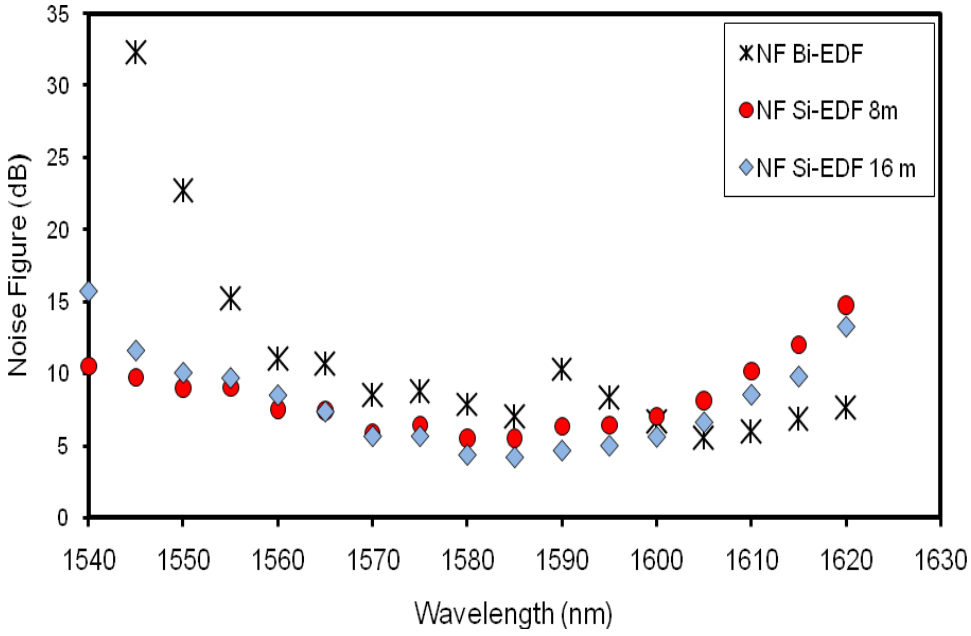

Figure 3.9: Comparison of the measured noise figure at input signal power of -30 dBm between Si-EDFA and Bi-EDFA. The 1480nm pump power is fixed at 100 mW.

This increased noise figure is attributed to the effect of multiple reflections from both the fibre splice points whereby the signal is reflected back into the Bi-EDF due to the large refractive index difference, causing Multi-Path Interference (MPI) noise [11]. As shown in Figure 3.9, the noise figure penalty of approximately 1~5dB is observed within wavelength region from 1560 nm to 1600 nm. However, at the longer wavelength region (>1600 nm), the noise figure is lower in the proposed Bi-EDFA due to the higher gain obtained.

3.6 Characterization of C-band Bi-EDFA

The performance of C-band EDFA, which is configured as in Figure 3.4 using a piece of 49cm long Bi-EDF is investigated. The fluorescence spectrum which is also known as ASE spectrum is first investigated as shown in Figure 3.10. This figure shows the C-band Bi-EDFA, which is pumped with both forward and backward scheme using 1480 nm laser diode. The forward ASE spectrum is measured longitudinally at the output end of the Bi-EDF using an OSA. The backward ASE spectrum is measured by incorporating an optical circulator at the input part of the Bi-EDFA to tap the backward propagating ASE. In the experiment, the pump power is fixed at 150 mW. The pump power used excites the Er^{3+} ions from ground state to the meta-stable level and creates a population inversion. The population inversion generates ASE spectrum, which is almost identical to the amplifier's gain profile [19]. The ASE power at the output end of the amplifier is given by [19]

$$P_{ASE} = n_{sp} h\nu \ BW \ (G-1) \qquad (3.15)$$

where G is the amplifier gain, BW is the bandwidth of ASE spectrum. The spontaneous emission factor n_{sp} is equal to 1 for ideal amplifiers with complete population inversion and otherwise is $1.4<n_{sp}<4$.

As shown in Figure 3.10, the forward and backward ASE have two peaks at 1535 nm and 1555 nm with the mean spectral power of -40.75 dBm and -26.71 dBm, respectively; that show the both ASE operates at C-band region. The spectrum peaks at 1535 nm, which coincides with the maximum emission region of Erbium ion in the EDF. A

small ripple is observed at the maximum peak region; in 1555 nm is due to the lasing effect due to back reflection, which oscillates in the cavity.

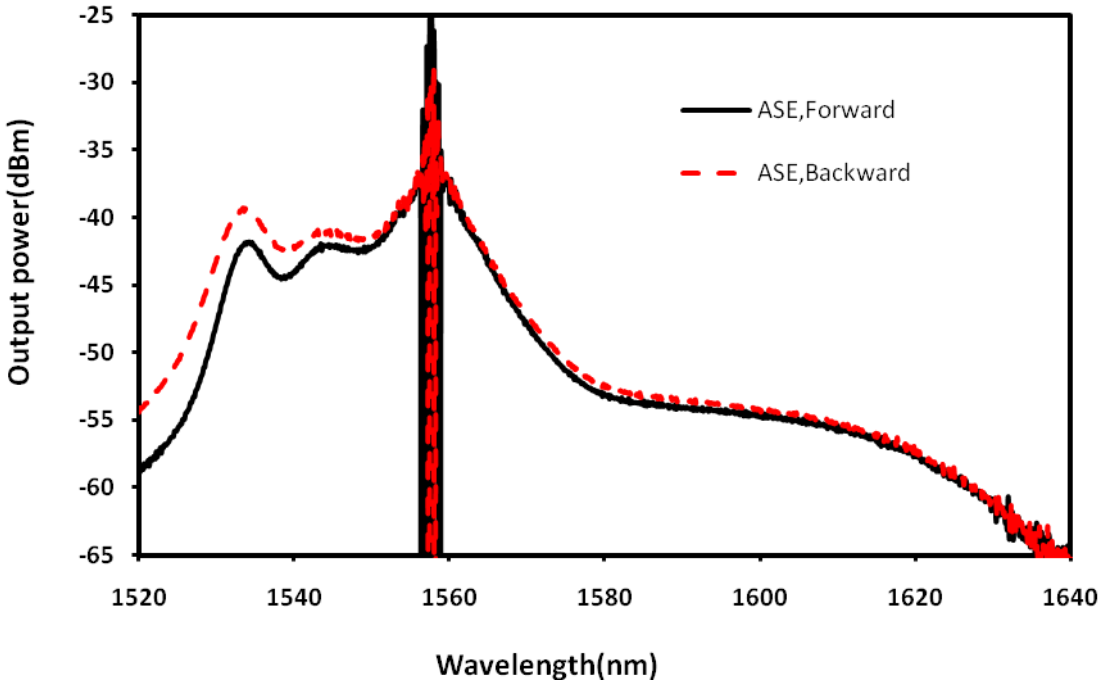

Figure 3.10: Fluorescence spectra of the C-band EDFA configured with 49 cm long Bi-EDF for both forward and backward pumping scheme.
The pump power is fixed at150 mW.

EDFAs that are operated in the saturation regime in order to yield maximized output signal power are referred to as power amplifier. For power EDFAs, one can define the power conversion efficiency (PCE) as the ratio [11]

$$PCE = \left(\frac{P_s^{out} - P_s^{in}}{P_p^{in}}\right) \qquad (3.16)$$

Figure 3.11 shows the PCE and quantum conversion efficiency (QCE) as a function of signal wavelength for the C-band Bi-EDFA. The QCE is pump wavelength independent and is calculated using the following equation [11]:

$$QCE = (\lambda_s / \lambda_p)(\frac{P_s^{out} - P_s^{in}}{P_p^{in}}) \tag{3.17}$$

where $\lambda_{p,s}$ are the pump and signal wavelengths, P_s^{out} and P_s^{in} are the signal output and input powers, respectively and P_p^{in} is the pump power. From energy conservation principles, the maximum value for the QCE is unity when

$$\frac{\lambda_p}{\lambda_s} = (\frac{P_s^{out} - P_s^{in}}{P_p^{in}}) \tag{3.18}$$

The highest QCE is determined by Eq. (3.13) to be approximately 17.9% at 1560 nm while the lowest QCE is calculated to be 0.9% at 1570 nm. The higher QCE in the Bi-EDF amplifier is due to the photon energy of the glass host is much lower than the Erbium ions energy gaps and this significantly reduces the pump photon energy loss to non-radiative emission [20]. The PCE has also maximum value of 17.1% at 1560 nm while lowest PCE is estimated to be 0.9% at 1570 nm. These results show that almost all the pump photons are converted to signal photons in the amplification process.

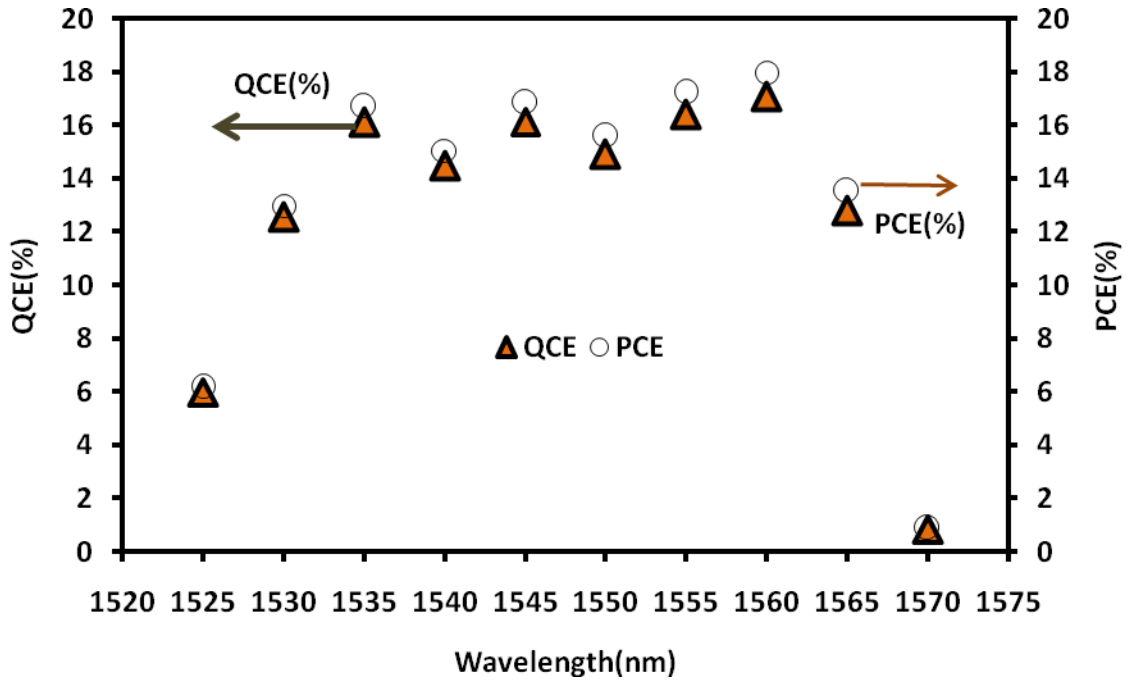

Figure 3.11: Measured QCE and PCE spectra of the C-band Bi-EDFA at input signal power of 0 dBm.

One of the most important parameter in optical amplifier is gain that referred to the ability of amplifier to amplify the power level of the input signals so that these signals can travel longer in optical fibers. Noise figure is also a crucial parameter for optical amplifiers because this effect is cumulative and it is an ultimate limiting factor in the number of amplifiers that can be concatenated and, therefore, the length of a fiber link without electronic signal regeneration. An optical amplifier should provide as high gain as possible and as low noise figure. In practice, signal can travel for up to 120 km between amplifiers. At longer distances of 600 km to 1,000 km the signal must be regenerated. In order to gauge the behavior of the Bi-EDF in optical amplification, then Bi-EDF optical amplifier characteristics and performance is evaluated by measuring the signal gain and noise figure. However, gain is actually limited by several physical effects such as the limit due to the

energy conversion principle and the finite number or Erbium ions existing in the medium. In practice, EDFA gain properties are also limited by commonly called second-order physical effects including pump ESA, self saturation by ASE, concentration quenching, and inhomogeneous broadening. Therefore, the optical gain, *G* is defined as

$$G(dB) = 10\log_{10}(\frac{P_{out} - P_{ASE}}{P_{in}}) \tag{3.19}$$

where P_{in} and P_{out} are the amplifier input and output signal powers respectively and P_{ASE} is the ASE power. An understanding of the net amplifier gain can be derived from an analysis of the gain from an individual 'slice' along the fiber.

In telecommunications, the noise figure is a measure of degradation of the Signal to Noise Ratio (SNR), caused by amplifier. Large noise figure can affect the transmission performance. ASE is the main contributor for noise figure other than thermal noise. Noise figure is defined as the ratio of the amplifier input SNR to its output SNR and is always greater than unity. SNR output is defined as the output of an ideal photo detector which is capable of converting each photon of incident light into electrical current and SNR input is referred to a shot noise but critical to be defined. Hence, noise figure is represented as

$$NF = \frac{(SNR)_{in}}{(SNR)_{out}} \tag{3.20}$$

The noise figure in decibel units can be described as

$$NF(dB) = 10\log_{10}\frac{(SNR)_{in}}{(SNR)_{out}} \tag{3.21}$$

In the experiment, the gain and noise figure are measured using an OSA, which uses the above equations in the calculation. The forward gain and noise figure characteristics against pump power at the input signal power of -30 dBm is shown in the Figure 3.12 (a) and (b), respectively. As shown in Figure 3.12 (a), the gain increases as the pump power increases. The gain starts to saturate at pump power of 80 mW. Maximum gain is achieved at 24.2 dB at the maximum pump power of 160 mW. The increase of pump power increases the population inversion in the Bi-EDF, which in turn increases the gain. The gain saturation is due to the limited amount of Erbium ion in the EDF. On the other hand, the noise figure for both the input signal powers of 1535 nm and 1555 nm reduces with increasing pump power as shown in Figure 3.12 (b). The minimum noise figure of 7.13 dB is obtained at the maximum power of 150 mW for input signal -30 dBm at 1555 nm. The noise figure is observed to depend on signal gain whereby noise figure is lower if the gain is higher.

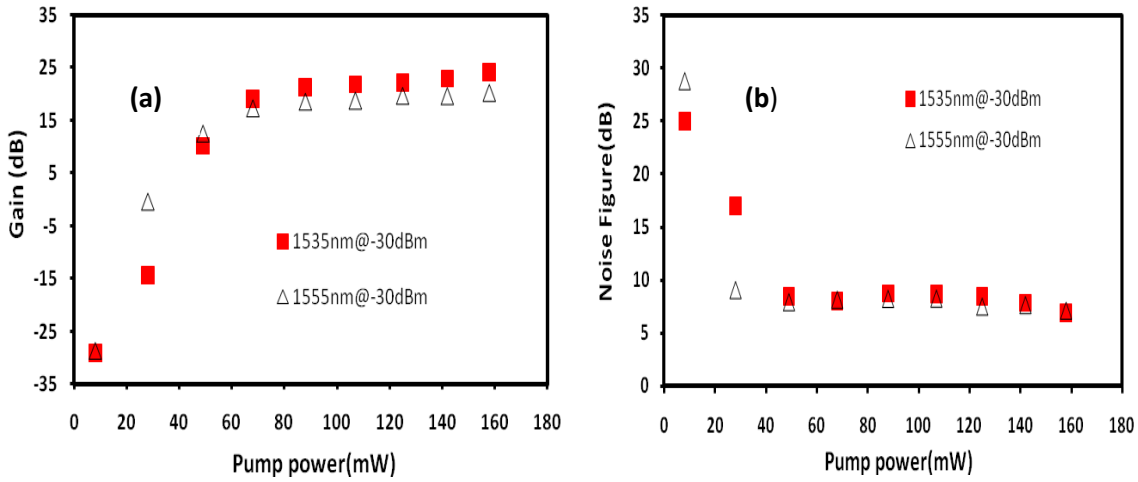

Figure 3.12: Forward **(a)** Gain and **(b)** Noise figure as a function of input pump power at a fixed signal wavelength of 1535 nm and 1555 nm.
The input signal power is fixed at -30 dBm.

Figure 3.13 shows the gain and noise figure spectra of the Bi-EDFA at input signal powers of -30 dBm and 0 dBm. The 1480 nm pump power is fixed at 150 mW in this experiment. At input signal power of -30 dBm, the gain peak of 22.7 dB is obtained at 1535 nm. The 3 dB bandwidth of the spectra is obtained at 30 nm (within wavelength region from 1530 nm to 1560 nm) and 40 nm (within wavelength region from 1530 nm to 1570 nm) for -30 dBm and 0 dBm input signal, respectively. At input signal of 0 dBm, a flat-gain of 11 dB is obtained with gain flatness of less than 1dB within the spectral bandwidth of 40 nm as shown in Figure 3.13. This shows that the length of Bi-EDF used (49cm) is optimum for C-band operation. Figure 3.14 shows the noise figure spectra at input signal powers of -30 dBm and 0 dBm. The maximum noise figure is observed at 1520 nm and reduces with increasing signal wavelengths. The minimum noise figure of 5.71 dB is obtained at input signal wavelength of 1575 nm. As shown in Figure 3.13, the gain is relatively smaller in lower and higher wavelength than 1530 nm to 1550 nm. This contributes to a lesser difference of noise figure value in this region as observed in Figure 3.14.

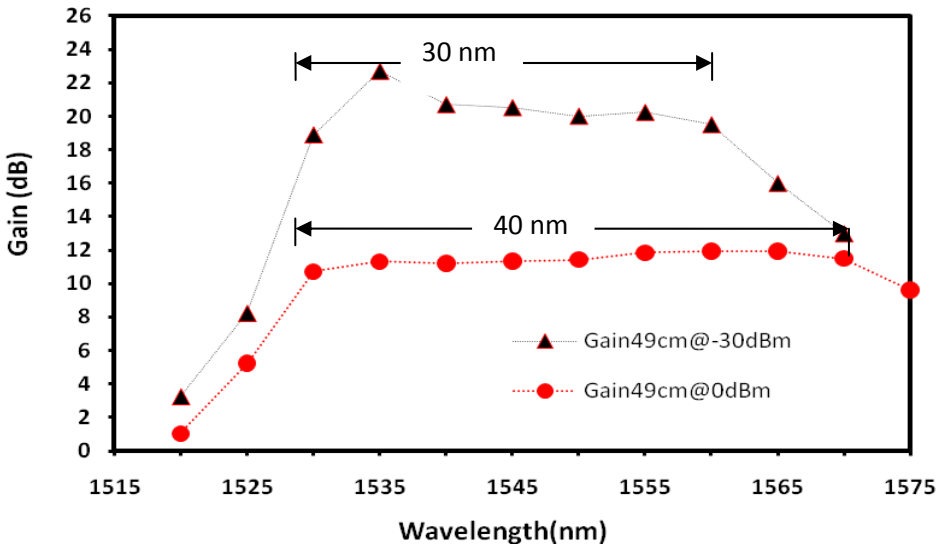

Figure 3.13: Forward gain of one-stage 49 cm Bi-EDFA as a function of different wavelengths measured by scan method. The -30 dBm and 0 dBm as input signal levels compared at fixed pump power of 150 mW.

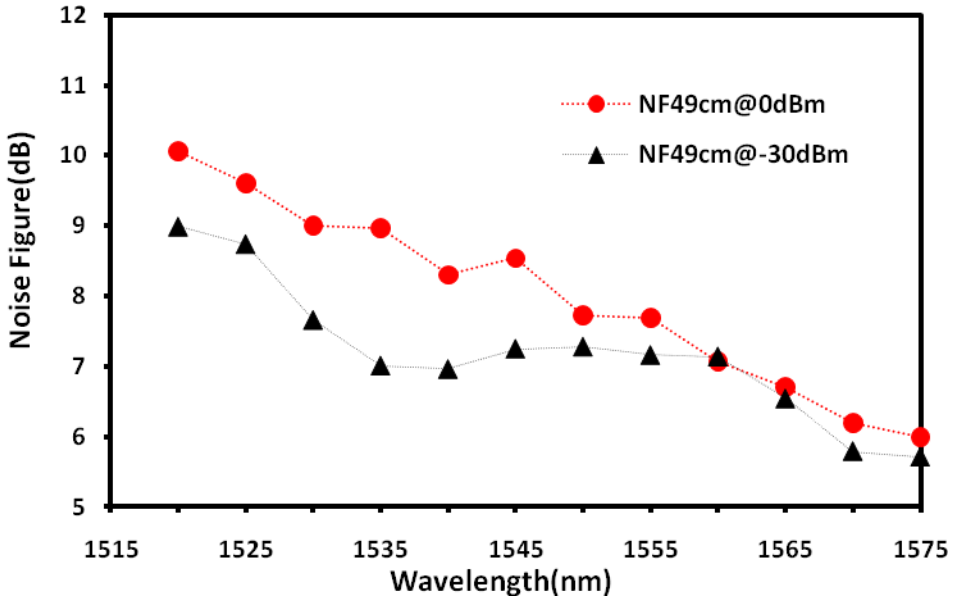

Figure 3.14: Forward noise figure of one-stage Bi-EDFA as a function of different wavelengths measured by scan method. The -30 dBm and 0 dBm as input signal levels compared at fixed pump power of 150 mW.

The performance of Bi-EDFA is also investigated with the backward pumping scheme as configured in Figure 3.15.

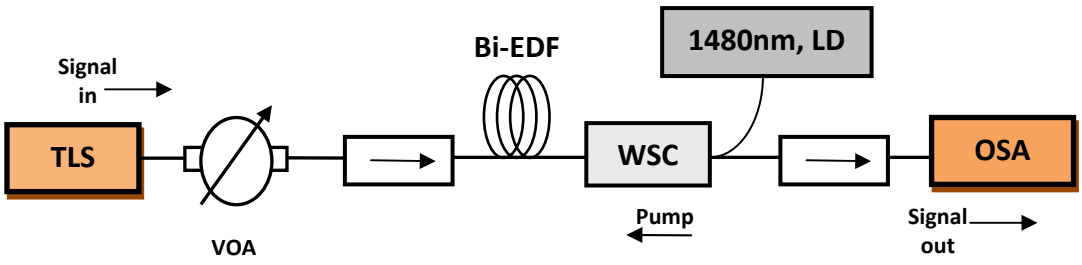

Figure 3.15: Configuration of the Bi-EDFA with the backward pumping scheme.

The gain and noise figure spectra of the Bi-EDFA is shown in Figure 3.16 for input signal powers of -30 dBm and 0 dBm using the same pump power of 150 mW.

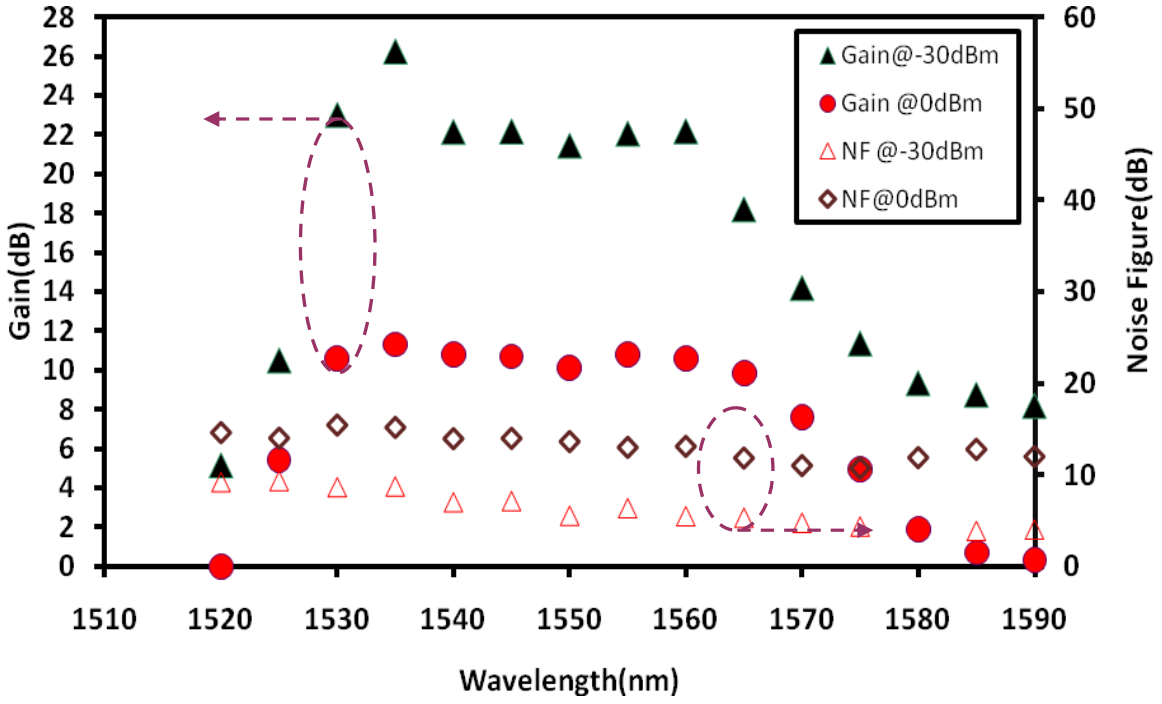

Figure 3.16: Gain and noise figure spectra of the backward pumped C-band Bi-EDFA at input signal powers of -30 dBm and 0 dBm. The 1480 nm pump power is fixed at 150 mW.

At input signal power of -30 dBm, the gain spectrum varies from 21.5 dB to 26.2 dB within a wavelength region from 1530 nm to 1565 nm, which is about 4 dB higher than that of the Bi-EDFA configured with the forward pumping. At input signal power of 0 dBm, the flat-gain spectrum peaks at 11.2 dB which is not much change in comparison with the forward one. The noise figure performance compared to constant forward pumping configuration is poor. However, the noise figure varies from 4.0 dB to 9.4 dB at input signal of -30 dBm. The large signal noise figure is higher than 10 dB at the input signal power of 0 dBm with increasing the pump power. This is contrast to forward pumping which is due to the domain of output ASE level factor which reduces the population inversion at input power of the amplifier.

3.7 Characterization of L-band Bi-EDFA

The performance of L-band Bi-EDFA, which is configured as in Figure 3.4 using a piece of 215 cm long Bi-EDF is also investigated. The Bi-EDF has an Erbium ion concentration of 3250 ppm. The 1480 nm pump power is fixed at 160 mW. Figure 3.17 shows the backward and forward ASE obtained from the L-band Bi-EDFA. The forward L-band ASE is obtained due to quasi-two-level operation, where the C-band ASE is absorbed to emit at L-band region. Fluorescence at wavelengths shorter than 1560 nm is too weak and is not detectable due to OSA sensitivity limitation. The weak C-band fluorescence is a result of high absorption of light in C-band region as shown in Figure 3.17.

The backward ASE has two peaks at 1532 nm and 1556 nm with the spectral power of -27.1 dBm and -27.5 dBm, respectively. The C-band ASE obtained from the input part of the Bi-EDF section is dominant in the backward ASE. The forward ASE operates at L-band region and peaks at 1608 nm with peak power of approximately -48.3 dBm. This indicates that the 215 cm Bi-EDF is capable to operate in the L-band region. The forward ASE has a relatively flat output spectrum between 1580 nm to 1610 nm, which indicates that the Bi-EDFA is possible to achieve a flat gain operation. The gain-flattened L-band Bi-EDFA is attractive for wavelength division multiplexing (WDM) applications.

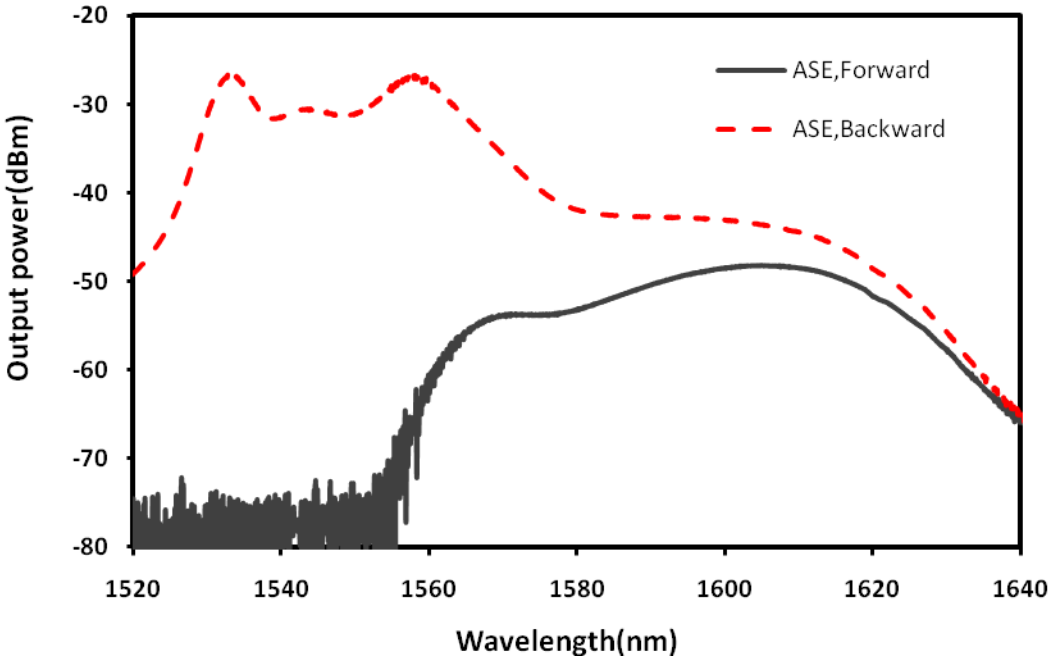

Figure 3.17: The forward and backward ASE spectrum from the Bi-EDFA with 215cm length of gain medium and 160 mW of the 1480 nm pump power**.**

As discussed in the previous section, the L-band Bi-EDFA performance can also be demonstrated in terms of optical PCE and QCE. Figure 3.18 shows the PCE and QCE as a function of input signal wavelength. As shown in the figure the highest QCE and PCE for 215 cm long of Bi-EDF are estimated to be approximately 23.7% and 25.7%, which is obtained at 1605 nm. The lowest QCE and PCE are calculated to be 11.1% and 11.7% respectively at 1570 nm.

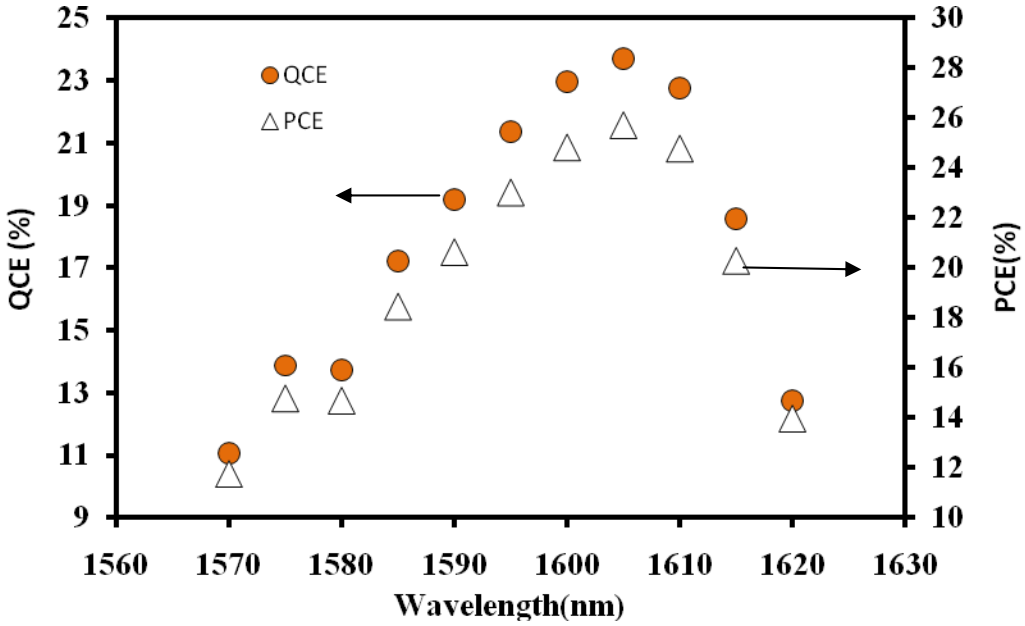

Figure 3.18: Measured QCE and PCE at 0 dBm input signal power from 1525 nm to 1570 nm for 215 cm of Bi-EDF.

Figure 3.19 (a) and (b) show the gain and noise figure characteristics as a function of input signal power at two different signal wavelengths of 1590 nm and 1610 nm. In the experiment, the pump power is fixed at 160 mW using a forward pumping scheme. As shown in Figure 3.19 (a), the gain reduces as the input signal power further increases. For instance, gain drop from the maximum value of 9.0 dB (at -40 dBm) to the minimum value of 4.4 dB (at -15 dBm) with input signal wavelength of 1590 nm. The saturation output power is obtained at input signal of -20 dBm. The saturation output power P_{sat}^{out} is, by definition, the output power at which the gain is 3-dB below its unsaturated value. The saturation output power P_{sat}^{out} should not be confused with the saturated output power, which some authors designate as the maximum output power that can be achieved with the EDFA, given an input signal P_s^{in}. In theory, this maximum output power can be, at most, as high as the input pump power when complete power conversion between pump and

signal occurs. The value of P_{sat}^{out} is more relevant to characterizing the EDFA, since it represents a threshold value for the transition between linear and nonlinear gain regimens of the amplifier [21]. While, for signal wavelength of 1610 nm the gain drops from its maximum value of 12.1 dB to the minimum value of 8.3 dB. The gain at 1610 nm signal is higher than 1590 nm signal by approximately 3.0 dB for all input signal powers tested as shown in Figure 3.19. It is attributed to the rate of energy transfer from C-band to L-band is higher at 1610 mW than at 1590 nm. The characteristic of noise figure versus input signal powers is also shown in Figure 3.19 (b) for both signal wavelengths of 1590 nm and 1610 nm. As shown in the figure, the noise figures are obtained at approximately 4 dB and 3.2 dB at the saturated gain region for input signal wavelengths of 1590 nm and 1610 nm, respectively. The figure shows that noise figure increases as the input signal power increases. At high input power the amplifier's gain is smaller and thus the noise figure increases.

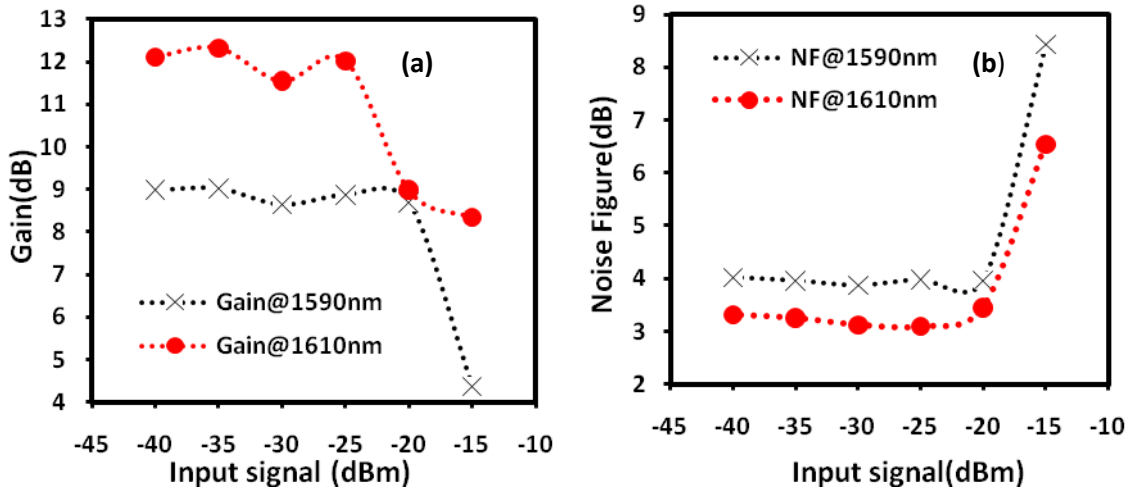

Figure 3.19: (a) Gain and **(b)** noise figure as a function of input power at a fixed signal wavelength of 1590 nm and 1610 nm.

The 1590 nm signal wavelength shows a higher noise figure compared to 1610 nm signal. This is attributed to the ASE level which is highest at 1590 nm region. The noise figure is governed by the following equation [11]:

$$NF = \frac{P_{ASE}}{h\nu G \Delta \nu_S} + \frac{1}{G} \tag{3.22}$$

where P_{ASE} is ASE power, h is Plank's constant, ν is signal frequency, $\Delta\nu_s$ is optical frequency band of photon detector system and G is signal gain. The equation shows that the noise figure is depended on the gain and ASE power values. The lower gain contributes to a higher noise figure. The power of ASE is highest at 1590 nm region, which contributes to a higher noise figure according to Eq. (3.22). The gain and noise figure characteristics against pump power at input signal power of -30 dBm is shown in the Figure 3.20. As shown in the figure, the gain increases as the pump power increases. The noise figure for both input signal powers at 1590 nm and 1610 nm reduces with increasing the pump power. The minimum noise figures of 3.8 dB are obtained at the maximum power of 160 mW for input signal of -30 dBm. The low loss Bi-EDFA can be used to increase the transmission length without repeater in optical networks. The maximum gain of 11.6 dB is obtained at 160 nm pump power.

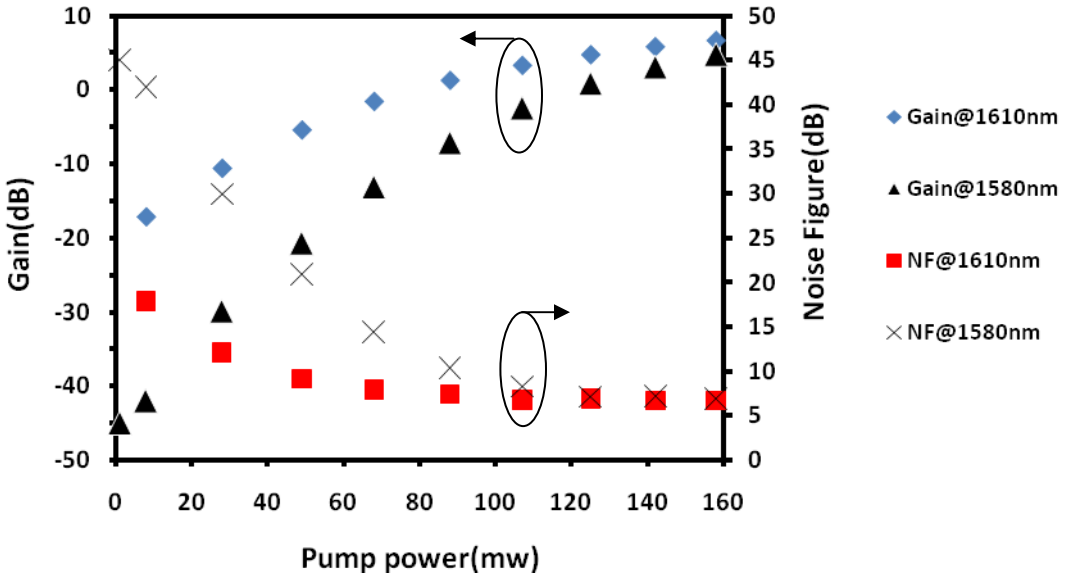

Figure 3.20: Gain and noise figure against 1480 nm pump power at a fixed signal wavelength of 1590 nm and 1610 nm. The input signal power is fixed at -30 dBm.

The gain and noise figure spectra at input signal powers of -30 dBm and 0 dBm are compared in Figure 3.21 for the forward pumping scheme. The pump power is fixed at 160 mW in this experiment. At input signal power of -30 dBm, the gain spectrum peaks 11.5 dB is obtained at 1610 nm, which is due to the energy transfer from the peak emission and absorption coefficient of the Erbium ion of 1530 nm. At input signal power of 0 dBm, the gain spectrum peaks is 7.3 dB at 1605 nm. The 3-dB gain bandwidth is obtained at more than 45 nm (1575 nm –1620 nm) with a small gain variation. On the other hand, the noise figure peaks at 1560 nm and reduces as the signal wavelength increases. The minimum noise figure of 3.2 dB is obtained at interval input signal wavelength 1610 nm to 1620 nm. These results show that the ESA of Erbium ion in Bi-EDF is shifted to longer wavelengths compared to other host. This enables Bi-EDF to exhibit high gain and low noise figure operation in the extended L-band. Therefore, the Bi-EDFA is suitable for the flat-gain operation, which covers both L-band and extended L-band regions.

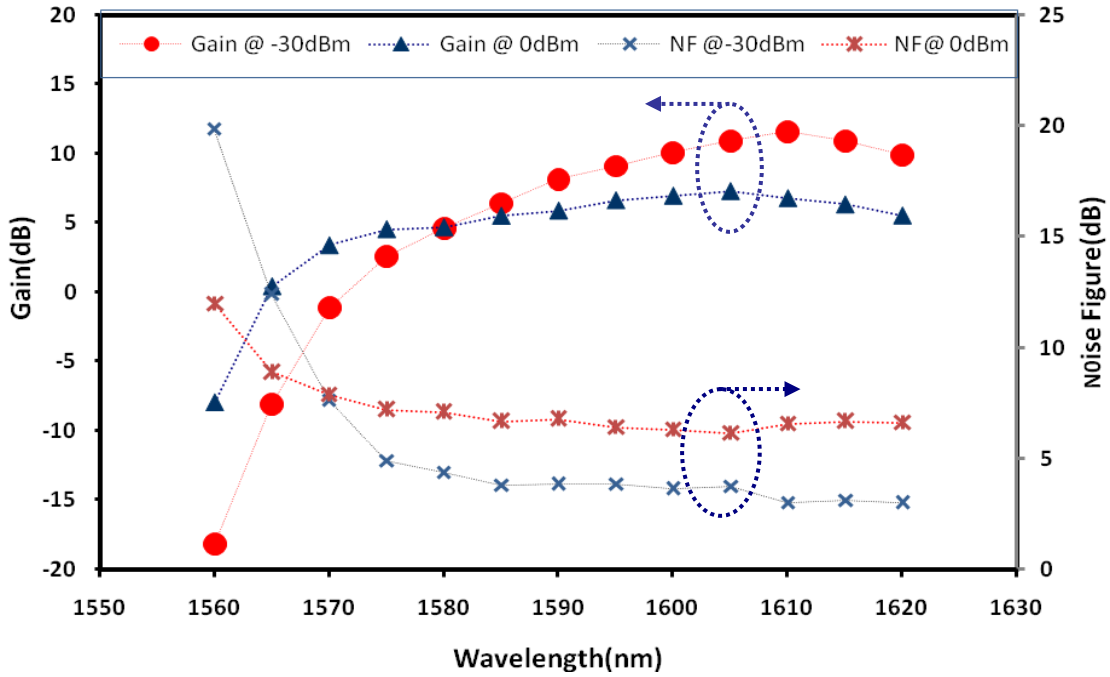

Figure 3.21: Gain and noise figure spectra of the forward pumped Bi-EDFA.

Finally, we demonstrate the gain and noise figure spectra of the Bi-EDFA configured using the backward pumping scheme of Figure 3.15.

Figure 3.22 shows the spectra at input signal powers of -30 dBm and 0 dBm when the pump power is fixed at 150 mW.

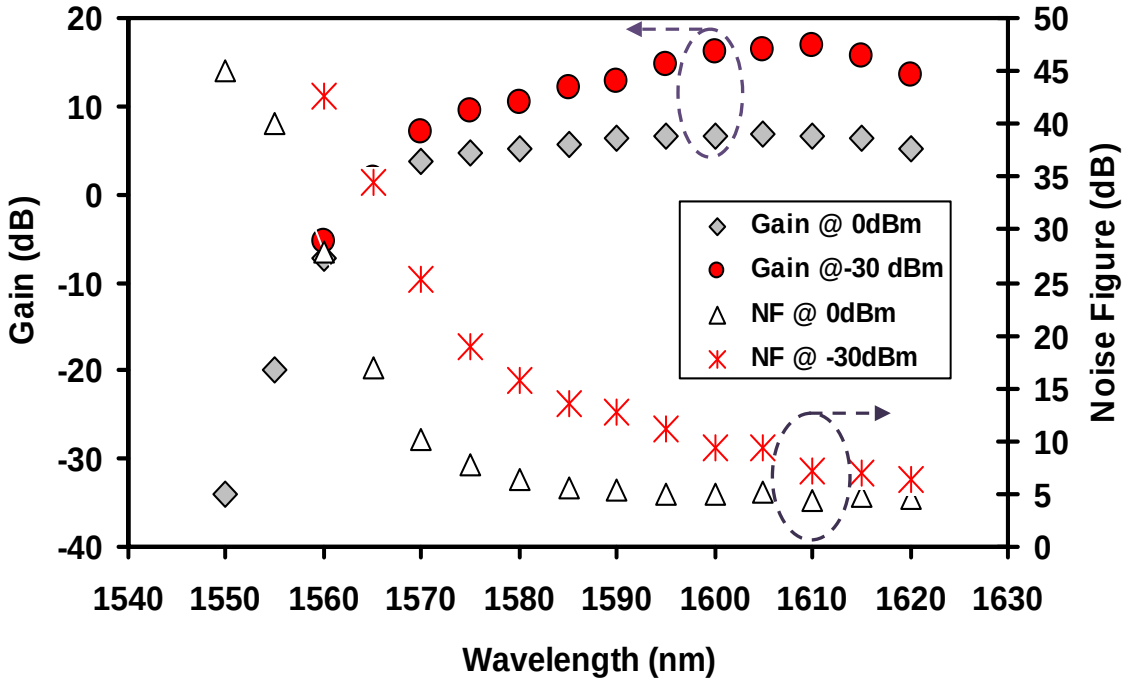

Figure 3.22: Gain and noise figure spectra of the backward pumped Bi-EDFA.

At input signal power of -30 dBm, the maximum gain of 16.9 dB is obtained at 1610 nm, which is approximately 5 dB higher than that of the forward pumping. At input signal power of 0 dBm, the maximum gain of 6.9 dB is obtained at 1605 nm that is not much different compared to that of the forward scheme. On the other hand, the minimum noise figure of 4.4 dB is observed at flat-gain region from 1580 nm to 1620 nm for the case of 0 dBm input power.

The noise figure is slightly higher with small input signal power of -30 dBm which is attributed to the high forward ASE level due to the back-ward pumping and inefficient ASE suppression by the small amplified signal in this length of Bi-EDF. However, the backward pumping provides a better gain compared to the forward pumping.

3.8 Double-pass Bi-EDFA

One of the methods to enhance the EDFA gain is via a double-pass technique [22]. The double-pass operation can be obtained by using a broadband reflector or mirror at the output end of the amplifier. This can be achieved using a broadband fiber Bragg grating (FBG), which is normally applied for the gain flattening applications [23]. In this study, a FBG with an appropriate loss response curve could be operated in double pass design amplifier, while this need can also be prepared by a circulator as a loop mirror. Figure 3.23 shows the configuration of the double-pass Bi-EDFA with the broadband FBG.

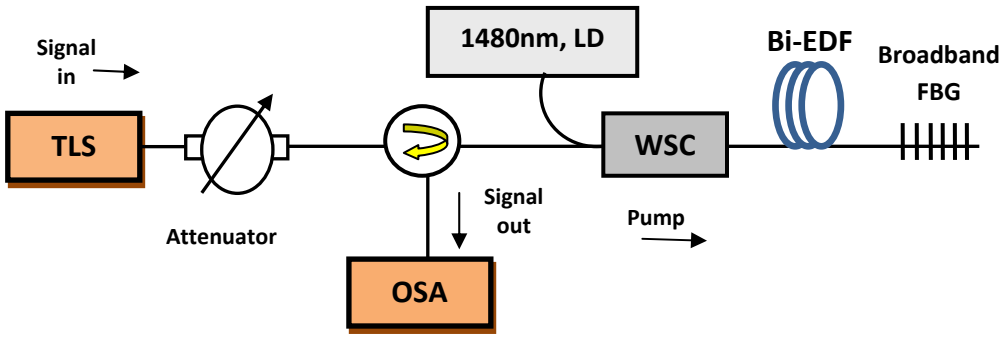

Figure 3.23: Configuration of the double-pass Bi-EDFA with a broadband FBG.

This amplifier employs 49 cm of Bi-EDF as a gain medium to operate in C-band region. The broadband FBG with a center wavelength of 1540 nm and a 3-dB bandwidth of 40 nm is used as the reflector. All elements in this experiment are the same with previous configurations except for the double-pass operation. Figure 3.24 shows the gain spectrum at different input signal powers of -30 dBm and 0 dBm. Pump power is fixed at 150 mW in this experiment.

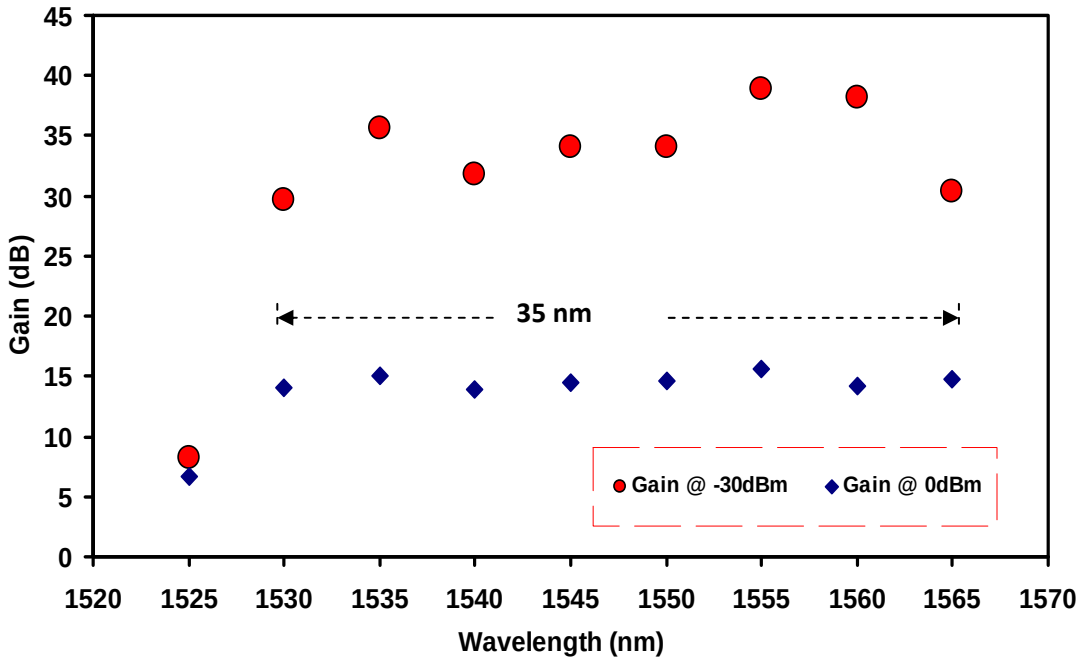

Figure 3.24: Gain spectra of the double-pass Bi-EDFA at different input signal powers of -30 dBm and 0 dBm. Pump power is fixed at 150 mW.

At input signal power of -30 dBm, the gain peaks of 35.7 dB and 39.0 dB are obtained at 1535 nm and 1555 nm, respectively. Compared with the single-pass operation (refer to Figure 3.13), the gain of the double-pass Bi-EDFA is increased by 13 dB at small input signal power. Furthermore, the flat-gain of 15.6 dB is obtained within the wavelength region from 1530 nm to 1565 nm (35 nm bandwidth) with gain variation of less than 1dB at input signal power of 0 dBm. The noise figure spectra at input signal powers of -30 dBm and 0 dBm are shown in the Figure 3.25.

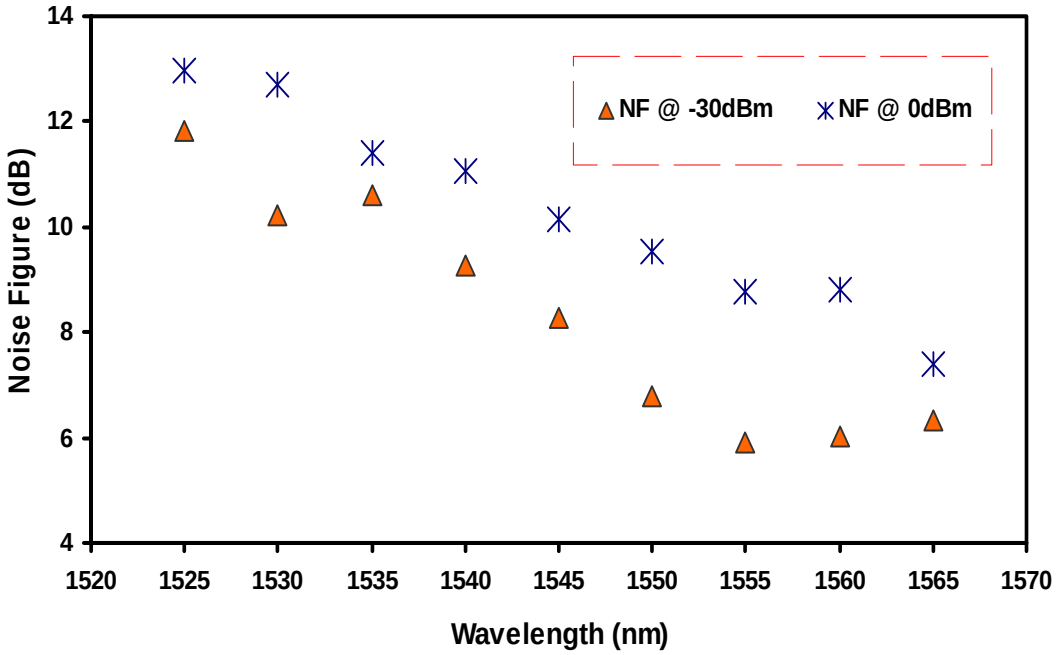

Figure 3.25: Noise figure spectra of the double-pass Bi-EDFA at different input signal powers of -30 dBm and 0 dBm. Pump power is fixed at 150 mW.

The maximum noise figure is observed at 1525 nm and it reduces with increasing signal wavelengths. The minimum noise figure of 5.9 dB is also obtained at input signal power -30 dBm and wavelength of 1555 nm. The noise figure in the double-pass Bi-EDFA is higher than that of the single-pass one (Figure 3.14). The increased noise figure is due to the double-propagation of signal in the gain medium, which increases the ASE at the input part of the amplifier. This will reduce the population inversion, which in turn increases the noise figure. In this thesis, we use the double-pass amplifier to improve the multi-wavelength generation in Raman /Brillouin fiber laser in chapter 4.

3.9 Bi-EDFA with a Bi-directional Pumping

Erbium-doped fiber amplifiers are inherently bi-directional in nature, as proposed by the presence of both forward and backward propagating ASE. The addition of uni-directional elements, such as isolators, removes the bi-directional amplification capability of a single Erbium-doped fiber amplifier [24]. The traditional EDFA (uni-directional signaling) can only amplify signals propagating in single-direction, because some isolators must be installed for eliminating the reflection of fiber discontinuities such as end faces and fusion points. In future communication networks, bi-directional transmission of signals may be desirable for capacity enhancement of existing systems or design flexibility and cost reduction of new systems [25]. In this section, the performance of the Bi-EDFA configured with bi-directional pumping is demonstrated.

The experimental setup of the bi-directional pumped Bi-EDFA is shown in Figure 3.26. The Bi-EDFA consists of two WSC, two optical isolators and a gain medium Bi-EDF. In the set-up, the Bi-EDF is pumped by two 1480 nm laser diodes. Both optical isolators are used to avoid the reflection and ensure uni-directional operation in the amplifier. Pump and signal beams were coupled with 1480/1550 nm WSC. A TLS is used in conjunction with an OSA for gain and noise figure measurements. A VOA is used to control the input signal power.

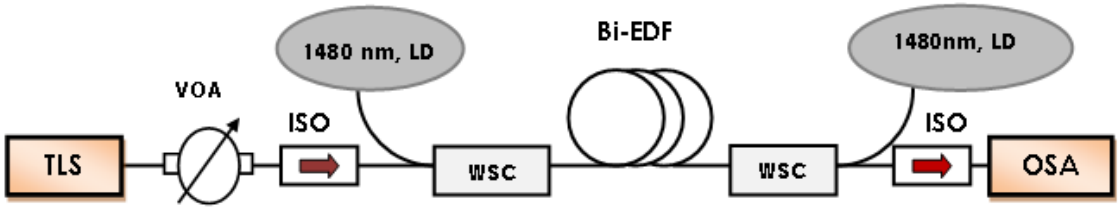

Figure 3.26: Experiment setup for the bi-directional pumped Bi-EDFA.

Figure 3.27 shows the forward ASE of the amplifier, which is measured by the OSA. The maximum ASE power of around -35 dBm is obtained at a wavelength region of 1570 nm with the pump power of 120 mW for each 1480 nm laser diodes. The ASE spectrum observed is the mixer of the backward and forward ASE and thus it covers both C-band and L-band wavelengths as shown in Figure 3.27. Then, the gain and noise figure spectra are measured by scanning the signal wavelength in the Bi-EDFA as shown in Figure 3.28. As shown in the figure, the gain operates in both C and L-band region with the maximum gain of 34 dB is obtained at around 1570 nm. This coincides with the peak of ASE spectrum, which is a result of energy transfer from C-band to L-band. The gain of more than 20 dB is obtained within a wavelength region from 1530 nm to 1620 nm, which actually covers from C-band to the extended L-band regions. On the other hand, the noise figure obtained is less than 9 dB at whole tested wavelengths as shown in Figure 3.28. The noise figure is relatively lower at the longer wavelength region due to the cavity loss, which is lower at the longer wavelength. Furthermore, the excited state absorption in longer wavelength lead to higher gain and lower noise. These results indicate that the Bi-EDFAs are promising candidates for practical wideband amplifiers. Furthermore, bi-directional Bi-EDFA has a higher gain in comparison to uni-directional pumping Bi-EDFA.

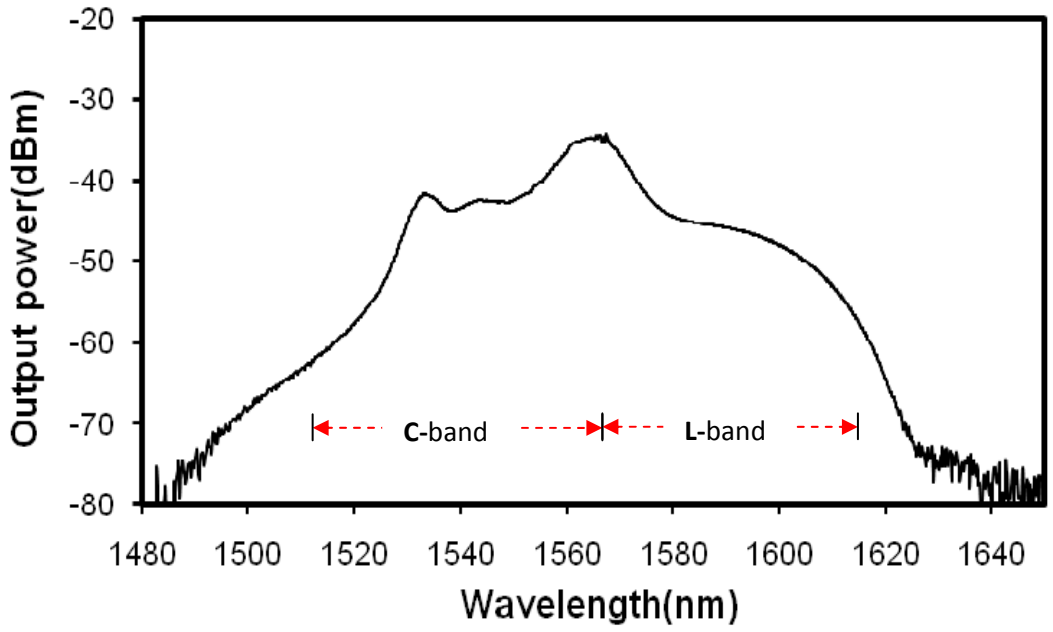

Figure 3.27: ASE spectrum of the bi-directional pumped Bi-EDFA.

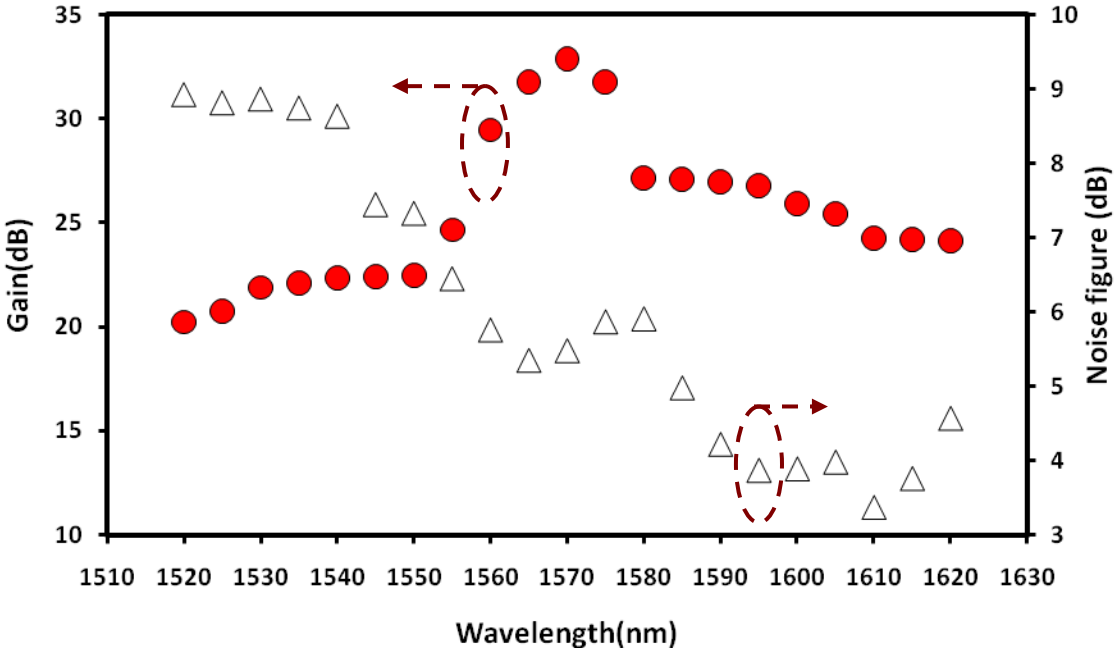

Figure 3.28: Gain and noise figure spectra of the bi-directional pumped Bi-EDFA at input signal power of -30 dBm. The total 1480 nm pump power is 240 mW.

Finally, the gain and noise figure characteristics as a function of input signal power are demonstrated for two different input signal wavelengths of 1560 nm and 1590 nm as shown in Figure 3.29. In this experiment, two pump powers are also fixed at 120 mW.

With an increasing input signal power, the gain drops from the maximum value of 33.0 dB (at -40 dBm) to the minimum value of 6.1 dB (at 0 dBm) at the input signal wavelength of 1560 nm. While, for signal wavelength of 1590 nm the gain drops from its maximum value of 28.0 dB to the minimum value of 7.9 dB.

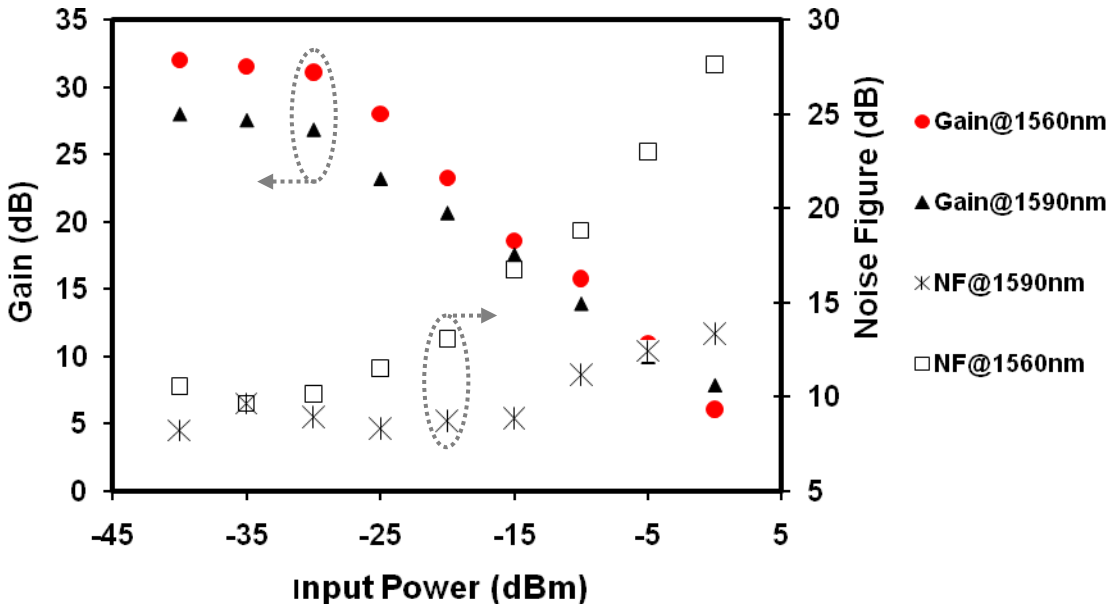

Figure 3.29: Gain and noise figure as a function of input signal power for the bi-directionally pumped Bi-EDFA. The signal wavelengths are fixed at 1560 nm and 1590 nm while the pump power for each pump is fixed at 120 mW.

These results show that the rate of energy transfer from the extend C-band to the extended L-band is not optimized. By optimizing this effect through the increase of pump power, the flat-gain is expected to be achieved in a wider amplification region, which covers from C-band to the extended L-band regions. On the other hand, the noise figure is

relatively lower at the longer wavelength as shown in Figure 3.29. This figure shows that the noise figure increases as the input signal power increases. At the input signal power near to -15 dBm and above the amplifier's gain is much smaller and thus increases the noise figure.

3.10 Raman Amplification

Raman amplifiers have attracted huge attention in recent years as the enabling technology for future long-haul, high-capacity optical communication systems. This is due to the fact that any wavelength within the transparency window of an optical fiber can be amplified by simply adjusting the pump wavelength [26, 27]. In typical applications for transmission systems, fiber Raman amplifiers showed superior performance, such as ultra-wide bandwidth, low noise, and suppressed nonlinearities [27]. Discrete Raman Amplifiers (DRAs), using Dispersion-Compensating Fiber (DCF) or Highly Nonlinear Fiber (HNLF), have also been shown to have good noise performance [28] and better signal power budget.

Owing to the low Raman conversion efficiency, Raman amplifier requires a significant amount of pump power and a longer interaction of the amplifying medium to achieve enough gain, which results in high cost. Therefore, it is important to enhance the gain efficiency when designing a DRA. The double-pass amplification technique can be also used to increase the efficiency of the signal gain [29]. In this structure, the signal light is reflected back into the same amplifying medium by either a broadband reflector or mirror. In this section, a Raman gain is investigated for various types of gain medium or fibers, which will be used in our experiments in the next chapters.

The most important parameter in characterizing Raman amplifiers is the Raman gain coefficient g_R, which is related to the cross section of spontaneous Raman scattering.

The Raman gain responds instantaneously to the Raman pump power. Therefore fluctuations in the Raman pump power; $P_P(z)$, causes the optical gain $G(z)$ to vary and will appear as Raman crosstalk to the desired signals. The optical gain $G(z)$ is related to the Raman gain as

$$G(z) = g_R \frac{P_P(z)}{A_{eff}} \tag{3.23}$$

which A_{eff} is the effective area of the pump beam inside the fiber. Hence, for Raman amplifiers, it is important to keep the pump at a constant power. Figure 3.30 shows the Raman gain spectrum in three types of optical fibers [29]. The frequency (or wavelength) difference between the pump and the signal photon ($v_p - v_s$) is called the Stokes shift, and in the standard transmission fibers with a Ge-doped core, the peak of this frequency shift is about 13.2 THz. According to Eq. (3.23) the ratio $C_R = g_R / A_{eff}$ is a measure indicating Raman-gain efficiency [30]. This ratio is depicted in Figure 3.30 for the three fibers, namely the standard silica single mode fibers (SMFs), Dispersion-Shifted Fibers (DSFs), and DCFs. In this research, only two types of fibres (DCF and SMF) will be useful for Raman /Brillouin amplification.

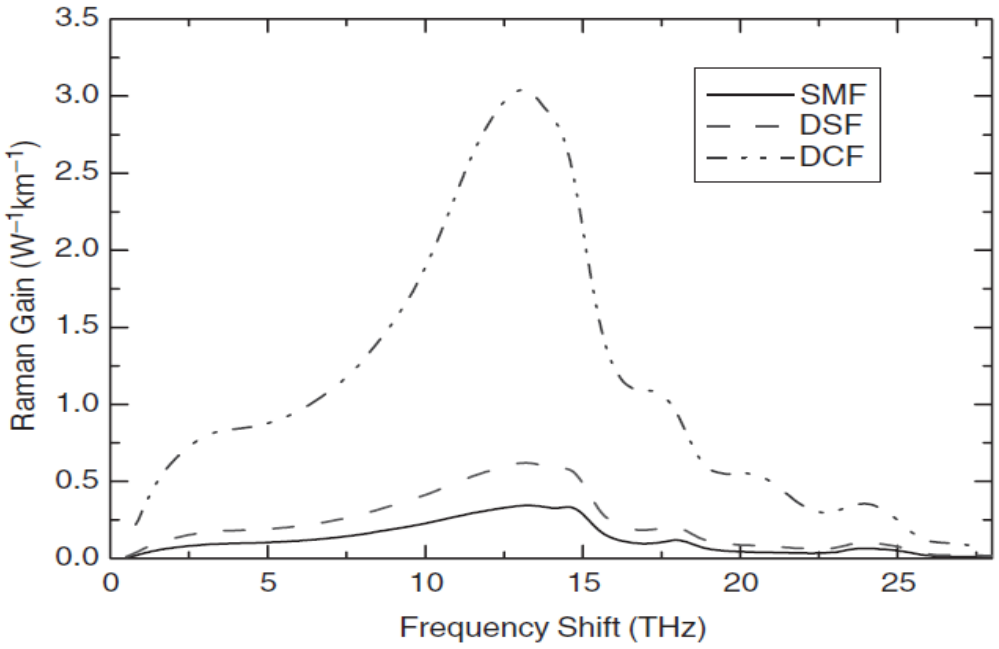

Figure 3.30: Raman gain profiles for a 1510 nm pump in three different fiber types SMF, DSF and DCF [29].

Another quantity of interest is the so-called on-off gain (defined as the ratio between output signal power with and without a pump) in a fiber when a pump power of P_{pump} is used and is given by [27]

$$G_{on-off} = \exp\left[C_R P_{pump} L_{eff}\right] \qquad (3.24)$$

where G_{on-off} in dB is proportional to both the Raman gain efficiency, C_R , and to the pump power as described in Eq. (3.24). Therefore, an increase in C_R allows for a similar reduction in required pump power for the same gain. The Raman gain also depends on the effective length, L_{eff}. However, the Raman gain efficiency of the fiber is independent of the pump power. Figure 3.31 shows the simple experimental setup for investigating of the Raman gain properties in different types of fibers that we will use in our study. The Raman pump

(RP) used operates at 1440 nm and has the maximum output power of 350 mW. The IWDM is used to combine the 1440 nm pump with input signal from tunable laser source (TLS). We compare the performance of Raman amplifiers with four types of fiber pieces (49 cm long Bi-EDF, 20 m long PCF, 25 km long SMF and 7.7 km long DCF) in this experiment. The output is characterized using an OSA.

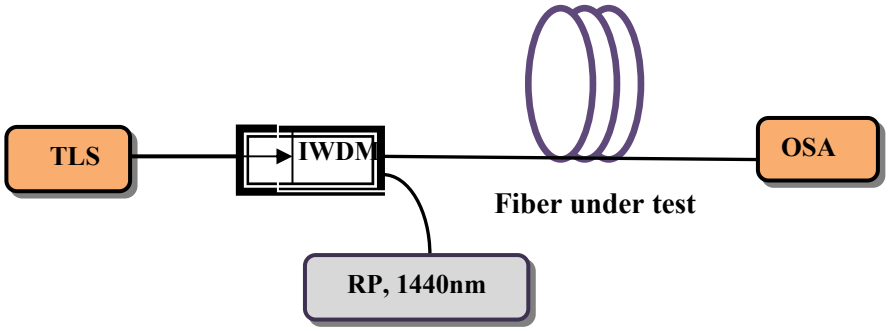

Figure 3.31: Schematic diagram for optical Raman gain measurement.

Figure 3.32 shows the gain spectrum of the Raman amplifier. As shown in the figure, the highest gain of 5.1 dB is obtained with DCF at 1540 nm region. With 25 km long SMF, a flat gain of approximately 3.0 dB is obtained at wavelength region from 1520 nm to 1550 nm region. No gains are observed with PCF and Bi-EDF. Because of Raman gain is more pronounced in higher pump power and optimum length. This is attributed to the fiber length which is too short to interact with the pump and generated stimulated Raman scattering. Some gain is negative due to the absorption effect in the fibers. These results show that the DCF is an efficient Raman gain medium. In communication network, DCF is normally used to compensate the group velocity dispersion (GVD) [31]. The DCF is attractive as a Raman gain medium for more versatile discrete Raman amplifiers with

larger net gains, because in addition to high Raman gain efficiency, it has a large absolute magnitude of dispersion. Also, nonlinear effects appear less detrimental in the presence of large dispersion. DCFs in WDM applications usually have an opposite sign of both dispersion and dispersion slope to compensate for the GVD over a wide band [32, 33].

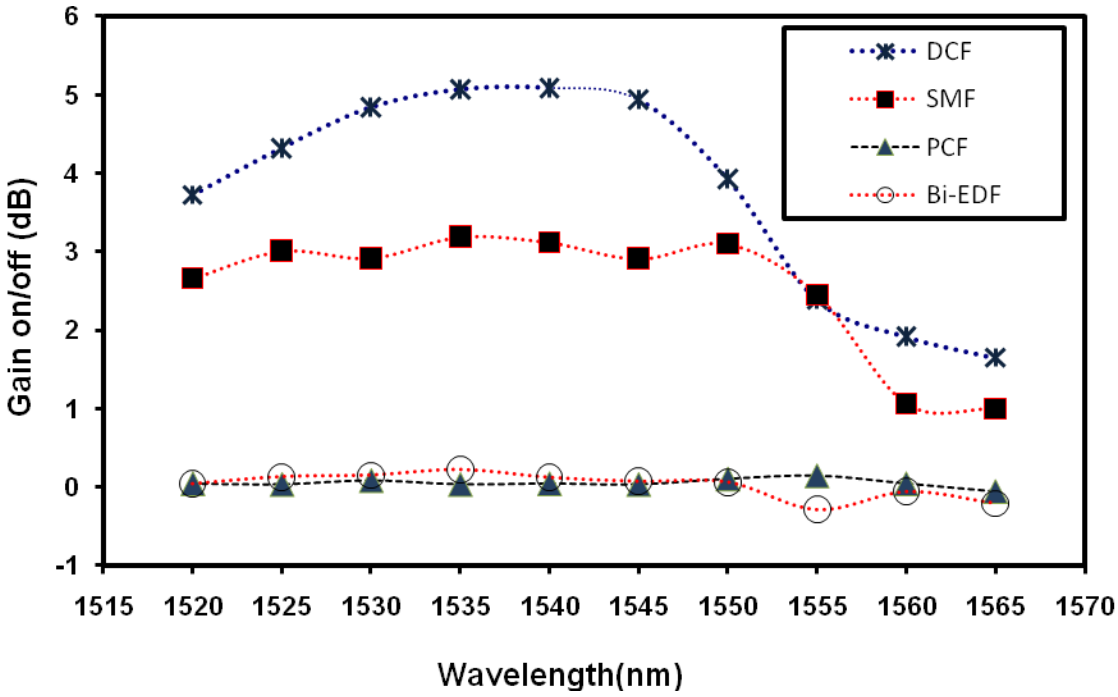

Figure 3.32: The comparison of on–off Raman gain spectra for four types of fiber pieces with input signal power of -3 dBm and pump power of 350 mW.

However, Raman amplifiers can be used to extend to bandwidth of WDM systems operating in the 1550 nm region. Hybrid Raman and EDF amplifiers made by combining Erbium doping with Raman gain have also been developed for the WDM applications [26].

REFERENCES

[1] G. Keiser, "Optical Communications Essentials," Copyright at the McGraw-Hill Companies, 2004.

[2] M. Yamada, "Overview of Wideband Optical Fiber Amplification Technologies," NTT Technical Review, Vol. 2, No. 12, pp.34, 2004.

[3] R. J. Mears, L. Reekie, I. M. Jauncey and D.N. Payne, "Low-noise Erbium-doped fibre amplifier at 1.54 μm," Electron. Lett., 23, pp.1026-1028,1987.

[4] R. I. Laming, P.M. Morkel, D.N. Payne and L. Reekie, "Noise in Erbium-doped fibre amplifiers," ECOC 88, Brighton, England, 1988.

[5] T. J. Whiteley and T.G. Hodgkinson, "1.54μm EP-doped fibre amplifier optically pumped at 807nm," European Conference on Optical Communication **(**ECOC 88*)*, Brighton, England, 1988.

[6] Y. S. Seo, Y. Fujimoto and M. Nakatsuka, "Simultaneous Amplification at Two Wavelengths Near 1300 nm in a 6.5-cm-Long Bismuth-Doped Silica Glass," IEEE Photonics Technology Letters, Vol.18, No.18, pp.1901-1903, 2006.

[7] N. Sugimoto, "Ultrafast optical switches and wavelength division multiplexing (WDM) amplifiers based on Bismuth oxide glasses," J. Am. Ceram. Soc., Vol.85, pp. 1083–1088, 2002.

[8] Y. Kuroiwa, et al., "Fusion spliceable and high efficient Bi_2O_3-based EDF for short length and broadband amplification pumped at 1480 nm," Proc. 26th Optical Fiber Communication Conference (OFC), Naheim, 2001.

[9] K. Taira, K. Kikuchi, and N. Sugimoto, "Dispersion and pulse amplification characteristics of Bismuth oxide-based Erbium doped fiber amplifiers," Proc. Optical Amplifiers and Applications Conference, Vancouver, Paper OTuC2, July 2002.

[10] S. W. Harun, N. Tamchek, S. Shahi, and H. Ahmad, "L-band amplification and multi-wavelength lasing with Bismuth based erbium doped fiber," Progress In Electromagnetics Research C, Vol. 6, pp.1–12, 2009.

[11] E. Desurvire, "Erbium-doped Fibre Amplifiers: Principle and Application," John Wiley & Son, New York, 1994.

[12] D. A. Chestnut, C. J. S. Dematos, P. C. R. Haland, J. R. Taylor, "High efficiency, dual-wavelength fibre Raman pump laser for U-band fibre Raman amplifiers," Optical and Quantum Electronics ,Vol. 34, pp.1025–1030, 2002.

[13] J. H. Yang, S. X. Dai, Y. F. Zhou, L. Wen, L. L. Hu, and Z. H. Jiang, "Spectroscopic Properties and Thermal Stability of Erbium-doped Bismuth based Glass for Optical Amplifier," J. Appl. Phys., Vol. 93, No. 2, pp. 977-983, 2003.

[14] S. Tanabe, T. Ohyagi, N. Soga and T. Hanada, "Compositional dependence of Judd-Ofelt parameters of Er^{3+} ions in alkali-metal borate glasses," Phys. Rev. B, Vol. 46, No. 6, pp.3305, 1992.

[15] H. Hayashi, N. Sugimoto, S. Tanabe and S. Ohara, "Effect of hydroxyl groups on Erbium-doped Bismuth-oxide-based glasses for fiber amplifiers," J. Appl. Phys., Vol.99, 2006.

[16] H. Hayashi, N. Sugimoto, S. Tanabe, "High-performance and wideband amplifier using Bismuth-oxide-based EDF with cascade configurations," Elsevier, Optical Fiber Technology, Vol. 12, pp. 282-287, 2006.

[17] W. L. Barnes, R. I. Laming, E. J. Tarbox, P. R. Mokel, "Absorption and emission cross section of Er^{3+} doped silica fiber," IEEE, J. Quantum Electronics, Vol. 27, pp. 1004-1010, 1991.

[18] E. Snokes, G. N. van den Hoven, A. Polman, "Cooperative upconversion in Erbium –implanted soda-lime silicate glass optical waveguides," J. opt. Soc. Am. B, Vol. 12, pp. 1468-1474, 1995.

[19] W. Y. Chong, "L-band Bismuth-based erbium-doped fiber amplifier," 2006.

[20] E. Desurvire, J. L. Zyskind and C. R. Giles, "Design optimization for efficient erbium-doped fibre amplifiers," IEEE Journal Lightwave Technol., Vol.8, pp.1730, 1990.

[21] M. J. F. Digonnet, "Rare Earth Doped Fiber Lasers and Amplifiers," 2001.

[22] C. L. Chang, L. Wang and Y.J. Chiang , "A dual pumped double-pass L-band EDFA with high gain and low noise," Optics Communications, Vol. 267, No. 1, pp. 108-112, 2006.

[23] M. R. Molhtar, "Bragg grating for optical networks," Optoelectronics research center, Southampton, 2005.

[24] P. C. Becker, N. A. Olsson, J. R. Simpson, "Erbium-Doped Fiber Amplifiers, Fundamentals and Technology," 1999.

[25] Q. Mao, J. Wang, X. Sun, M. Zhang, "A theoretical analysis of amplification characteristics of bi-directional Erbium-doped fiber amplifiers with single Erbium-doped fiber," Optics Communications, Vol. 159 , pp.149–157,1999.

[26] G. P. Agrawal, "Non-linear fiber optics," Fourth edition, Academic Press, 2007.

[27] C. Headley and G. P. Agrawal, “Raman Amplification in Fiber Optical Communication Systems,” 2005.

[28] M. J. Guy, S. V. Chernikov, and J. R. Taylor, “Lossless Transmission of 2 ps Pulses over 45 km of Standard Fibre at 1.3 μm using Distributed Raman Amplification,” Elect. Lett. Vol. 34, No. 8, pp.793, 1998.

[29] X. He, S. Srinivasan, S. Wilson, C. Mitchell and R. Patel, “Fusion spliceable and high efficient Bi_2O_3-based EDF for short length and broadband amplification pumped at 1480 nm,” Electron. Lett.Vol. 34, pp. 21-26, 1998.

[30] S. Namiki and Y. Emori, “Ultrabroad band Raman amplifiers pumped and gain-equalized by wavelength-division-multiplexed high-power laser diodes,” IEEE J. Sel. Topics Quantum Electron. Vol. 7, pp. 3-16, 2001.

[31] L. Gruner-Nielsen, S. Nissen Knudsen, B. Edvold, T.Veng, D. Magnussen, C. Christian Larsen, and H. Damsgaard, “Dispersion compensating fibers,” Opt. Fiber Technol. Vol. 6, pp.164, 2000.

[32] Y. Akasaka, R. Sugizaki, and T. Kamiya, “High dispersion compensation ability and low nonlinearity of W-shaped DCF,” Digest of Optical Fiber Communication Conference, pp. 201–202, 1996.

[33] K. Mukasa, Y. Akasaka, Y. Suzuki, and T. Kamiya, “Novel network fiber to manage dispersion at 1.55 μm with combination of 1.3 μm zero dispersion Single-Mode fiber” Proc. 23rd European Conf. Opt. Comm. Vol.1, No.127 , Scotland, 1997.

CHAPTER 4

SINGLE AND MULTI-WAVELENGTH BISMUTH-BASED BRILLOUIN ERBIUM FIBER LASER

4.1 Introduction

Fiber lasers using EDFs have been widely investigated due to their advantages such as the higher power conversion efficiency and lower threshold powers. Stimulated Brillouin Scattering (SBS) is a nonlinear effect arising from the interaction between the intense pump light and acoustic waves in a medium, giving rise to backward-propagating and frequency shifted light [1]. The thermally excited acoustic waves generate an index grating that co-propagates with the pump light at the acoustic velocity in the medium. This moving grating reflects the pump light and causes a frequency downshift in the backscattered light owing to the Doppler effects. The frequency shift with respect to the pump is approximately 0.08 nm at the 1550 nm region for silica fibers. Although this scattering creates problems for some nonlinear signal processing applications that involve using a strong CW pump [2,3], the SBS can be used for amplification of light propagating in a direction opposite to the pump light. This has led to many applications, such as in Brillouin amplifiers, lasers, and microwave signal processors [4, 5]. Single-wavelength and multi-wavelength lasers can also be achieved using a hybrid Brillouin–Erbium Fiber Laser (BEFL) [6,7], which has recently became a topic of extensive study due to its potential applications in instrument testing and sensing and as optical sources for dense wavelength division multiplexing (DWDM) systems. The BEFL operates in such that a signal is injected and then locked in a

ring resonator, which in turn seeds the BEFL modes [6-8]. For instance, a figure-of-eight configuration is used to produce higher order multiple Stokes and anti-Stokes lines by exploiting the cascaded SBS process [9].

In applications involving the SBS process, it is desirable to have a medium that has a large Brillouin gain coefficient g_B to lower the power requirements and also to shorten the length of fiber devices. For instance, in an earlier work, a compact Brillouin Fiber Laser (BFL) has been demonstrated using a Chalcogenide fiber, which has the g_B coefficient of about 2 orders of magnitude larger than that of silica-based fibers [8]. However, the threshold for the Brillouin pump is much larger in this fiber compared with a silica fiber. Recently, a Bismuth-based Erbium-Doped Fiber (Bi-EDF) has been extensively studied for use in compact amplifiers with short-gain medium lengths. This fiber incorporates Lanthanum (La) ions to decrease the concentration quenching of the Erbium ions in the fiber [9], which in turn allows the Erbium ion concentration to be increased to more than 3000 ppm. A fiber with such a high Erbium dopant concentration is expected to have enormous potential in realizing a compact Erbium-doped fiber amplifiers (EDFAs) and EDFA based devices. The amplification characteristics of this fiber have been demonstrated in the previous chapter.

The Bi-EDF has also a very high fiber nonlinearity, which can be used for realizing a compact BEFL. In this chapter, a BEFL is demonstrated under a new approach using a piece of Bi-EDF as both linear and nonlinear gains media. The Stokes is generated in the Bi-EDF by the injection of a narrow linewidth Brillouin pump (BP). With the use of 1480 nm pumping on the Bi-EDF, the generated Brillouin Stokes is amplified to generate a BEFL. In the section, a single-wavelength BEFL is demonstrated using a ring configuration.

4.2 Single-wavelength BFL Using Bi-EDF in the Ring Cavity

A configuration of the proposed a single wavelength BEFL is shown in Figure 4.1, which consists of a circulator, a piece of Bi-EDF and an output coupler. In this experiment, the performance of the BEFL is demonstrated by using a reduced length of Bi-EDF. The properties of these fibers were discussed in chapter 2. The Bi-EDF used has a nonlinear coefficient of ~60 $(W/km)^{-1}$ in 1550 nm, an Erbium concentration of 3250 ppm, a cut-off wavelength of 1440 nm, and a pump absorption rate of 130 dB/m at 1480 nm. It is forward pumped using a 1480 nm laser diode to provide a linear gain in either C- or L-band region depending on the length used. A 1480/1550 nm WSC is used to combine the 1480 nm pump and the oscillating signal in the ring cavity. The Bi-EDF is also pumped by an external-cavity tunable laser source with a linewidth of approximately 20 MHz and a maximum power of approximately 8 dBm to generate a nonlinear gain or Stokes, which is injected into the ring cavity via optical circulator. In this study, the pump signal is called a Brillouin pump (BP). An optical isolator is used to block the BP from oscillating in the cavity and also to ensure a unidirectional operation of the BFL. The spacing between the BP and the BFL is obtained at approximately 10-11 GHz, which is equivalent to the Stokes shift in the silica fiber. The output of the linear cavity is tapped from the different coupler and characterized by an OSA with a resolution of 0.015 nm. The experiment is carried out for various coupling ratio of the output coupler.

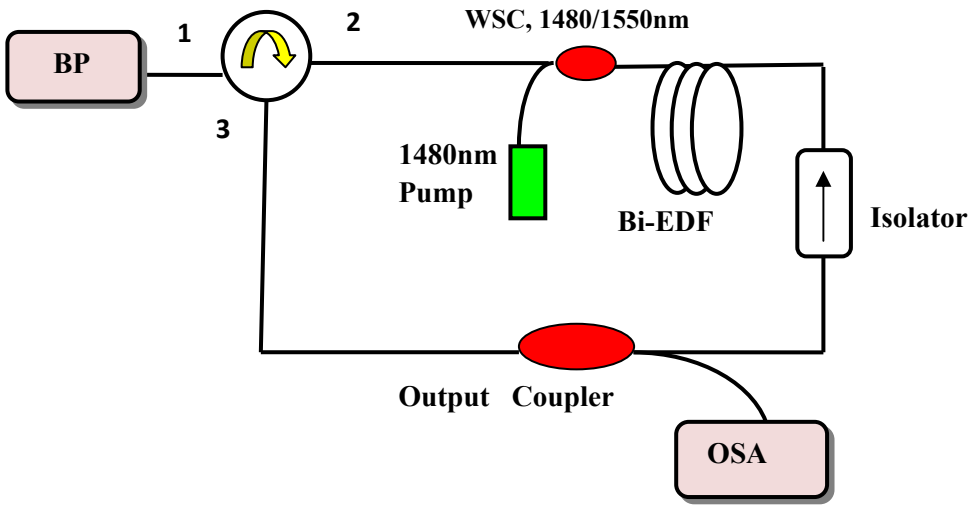

Figure 4.1: Configuration of the proposed BEFL.

The injected BP generates backward-propagating Brillouin Stokes, which is amplified by the linear Bi-EDF gain and oscillates in the loop to generate a BEFL in a counterclockwise direction. By using a single fiber for the linear amplification and Brillouin Stokes generation, the BP and Brillouin signal are simultaneously amplified in this cavity. This allows a shorter length of active fiber to be used for the BEFL generation, which in turn reduces a total cavity loss and increases the output power. The operating wavelength of the BFL is determined by the 1480 nm pumped Bi-EDF gain spectrum which covers the wavelength region from 1520 nm to 1620 nm as well as the cavity loss. The gain spectrum is strongly depended on the Bi-EDF length used.

Figure 4.2 compares the free-running spectrum (without BP) of the proposed BEFL of three different lengths of Bi-EDF. The free running BEFL spectra peak at the wavelength regions of 1567.0 nm, 1613.8 nm and 1615.7 nm with Bi-EDF lengths of 49 cm, 181cm and 215 cm, respectively. The spectrum has multiple peaks because, upon saturation, gain mode competition enables neighboring wavelengths to acquire a net gain to

oscillate, made possible by the inhomogeneously broadened gain medium. With Bi-EDF length of 181cm and above, the Bi-EDF laser operates at the extended L-band region owing to the use of Bismuth glass as a host material of the fiber, which is able to extend the amplification band to a longer wavelength compared to the conventional silica-based EDF. This is due to the vibration energy of the Bismuth glass lattice being smaller than that of silica, which contributes to larger emission and lower ESA in the extended L-band region [9].

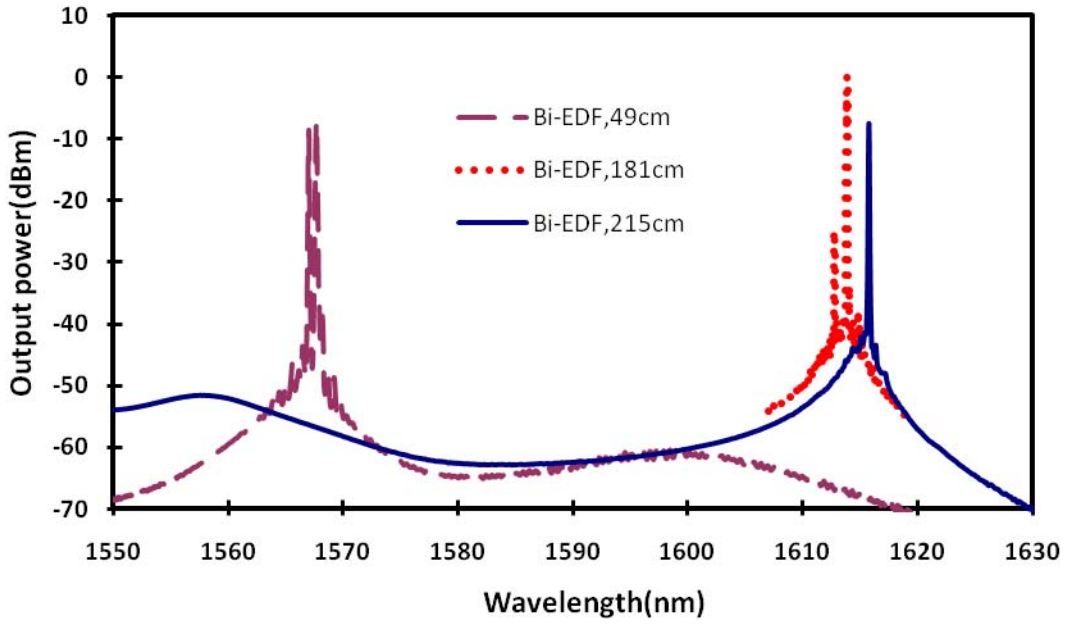

Figure 4.2: Free-running spectrum of three lengths of Bi-EDFA in 90/10 output coupler.

The Brillouin gain in the fiber is relatively very small. This necessitates that the wavelength for the operation of the BEFL be close to that at which the Bi-EDF laser would operate under a free-running condition. Therefore, the BP signals are launched into the Bi-EDF at wavelengths of 1567 nm, 1613.8 nm and 1615.7 nm for 49 cm, 215 cm and 181 cm

Bi-EDF, respectively; which is close to the EDF laser peak gains to generate a BEFL in either the L-band or extended L-band region. The free-running spectrum also exhibits peak powers of above -7 dBm. The operating wavelength of the BEFL shifts toward the longer wavelength with the longer Bi-EDF used as shown in Figure 4.2. This is attributed to the gain spectrum of the Bi-EDF amplifier, which peaks at the longer wavelength with the longer length of fiber.

Figure 4.3 shows a free running output spectrum of 215 cm Bi-EDF in different output coupler ratios (95/5, 90/10, 80/20 and 50/50). The ratio represents the oscillating laser power, which is extracted from the laser system by using the coupler while the remaining power is circulated back into the laser cavity. For this length, wavelength peaks regions are obtained in wavelength region from 1606.5 nm until 1615.7 nm, which is close to the extended L-band region. The 1480 nm pump power is fixed at 152 mW in this experiment. The operating wavelength shifts to a shorter wavelength as the extraction ratio or cavity loss increases. The operating wavelength shifts to a shorter wavelength to acquire more gain so that the cavity loss can be compensated.

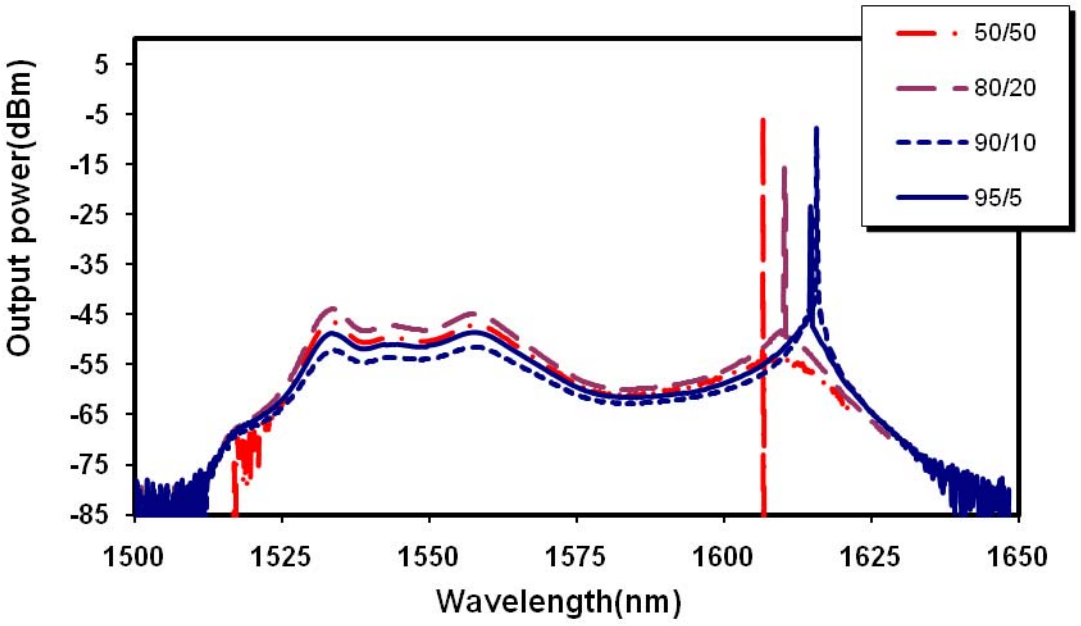

Figure 4.3: Output spectrum of the 215 cm Bi-EDF laser in different coupler ratio (Without BP).

The small Brillouin gain necessitates that the wavelength for the operation of the BFL be close to that at which the Bi-EDF laser would operate under a free-running condition. Therefore, the BP signal is launched into the Bi-EDF at a wavelength that is close to the EDF laser peak gain to generate a BFL in the extended L-band region. Figure 4.4 shows the output spectrum of the BEFL at various coupling ratio. A single line of Brillouin Stokes at 0.09 nm spacing shifted from the BP is achieved in the BEFL with 5%, 10% and 20% output couplers. However, no Brillouin laser is observed using the 50% coupling ratio as shown in Figure 4.4. It is shown that the BEFL operation is optimum with the use of 80/20 coupler, where 20% of the oscillating laser is tapped for the output.

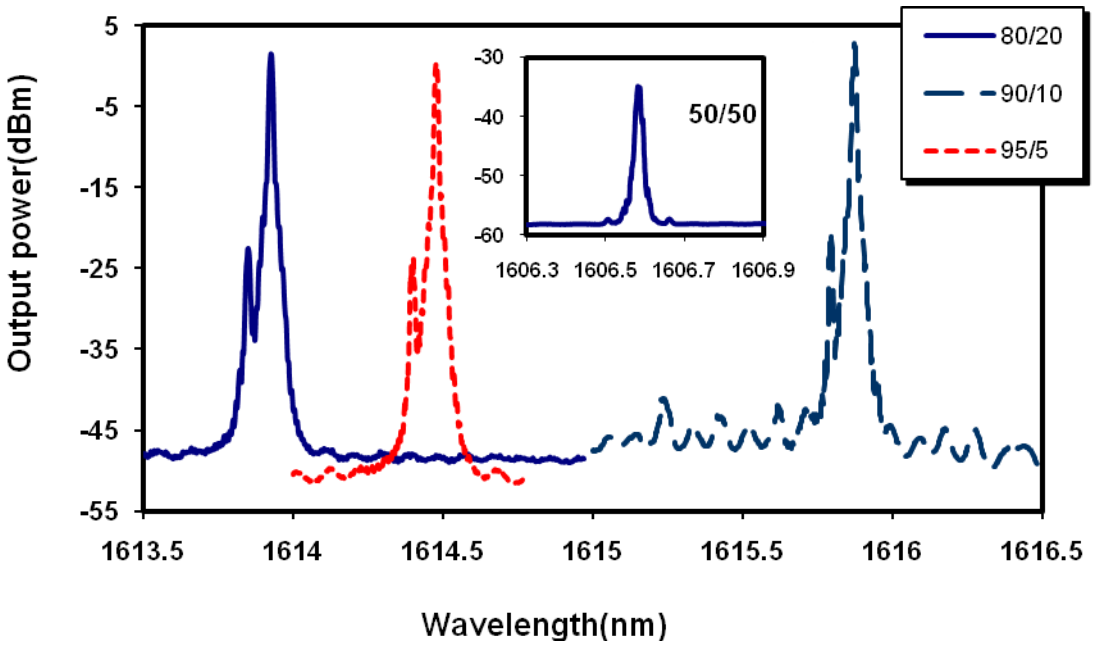

Figure 4.4: The output spectrum of the ring BEFL at different output coupler ratios.

Figure 4.5 shows the output spectra of the BEFL with the 80/20 coupler at different 1480 nm pump powers. The Brillouin laser with a separation of 0.09 nm from the BP could be easily observed when the 1480 nm pump power exceeded 115 mW, and it increased by more than 45 dB as the pump power was raised to 152 mW. According to this figure, the 1480 nm pump power threshold is approximately near to 115 mW. Below this pump power, the Erbium gain is very low and cannot sufficiently compensate for the loss inside the laser cavity, and thus no Stokes is observed. The generated BEFL power is observed to increase as the 1480 nm pump power increases, which is attributed to the increment of the Erbium gain with pump power. This situation provides sufficient signal power for SBS to generate Stokes, which is then amplified by the Erbium gain. At the maximum 1480 nm pump power, the BEFL has a peak power of 2 dBm and a side-mode suppression ratio (SMSR) which is defined as the power difference between the BFL's peak with the second highest

peak obtained of more than 22 dB. The incorporation of both optical isolator and circulator in the cavity ensure the uni-directional operation of the BFL and suppresses the residual BP. This prevents the FWM from happening and avoids the generation of anti-Stokes. The single-wavelength BEFL is expected to have a very narrow linewidth and low technical noise, which makes it suitable for sensing applications.

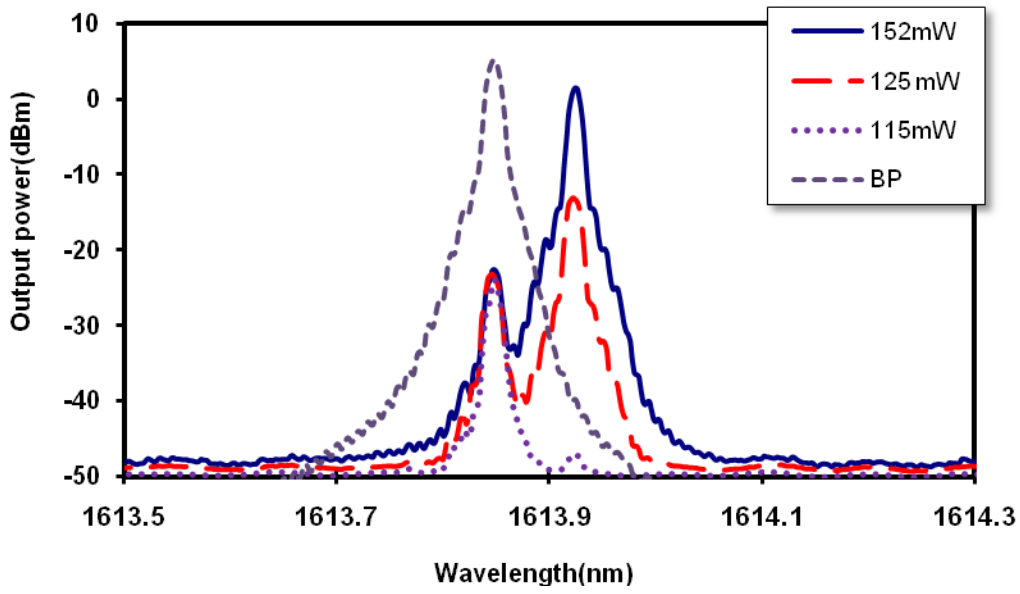

Figure 4.5: Output spectra of the BFL based on Bi-EDF at different power of 1480nm pump in 20% output.

Figure 4.6 proposes the output spectrum of the BEFL at various BP wavelengths. In this experiment, the BP and 1480 nm pump power as such as before are fixed at 5 dBm and 152 mW, respectively. As shown in the figure, the BP can be tuned from 1612 nm to 1615 nm to obtain the maximum output power of approximately 2 dBm. The Brillouin gain coefficient g_B for the Bismuth fiber is also calculated using the following well-known equation as discussed in chapter 2 [8]

$$g_B = \frac{21 A_{eff}}{P_{th} K L_{eff}} \tag{4.1}$$

Here P_{th} is power corresponding to the Brillouin threshold, A_{eff} is the effective cross-sectional area, L_{eff} is the effective length, and K is the constant. The peak Brillouin gain coefficient was determined to be 3.2×10^{-7} m/W (using K=0.5; for non-polarization maintaining fibers, A_{eff} =29.4 μm^2, L_{eff} =1.01 m, and P_{th}=3.2 mW), which is much higher than in the standard silica fibers (5×10^{-11} m/W).

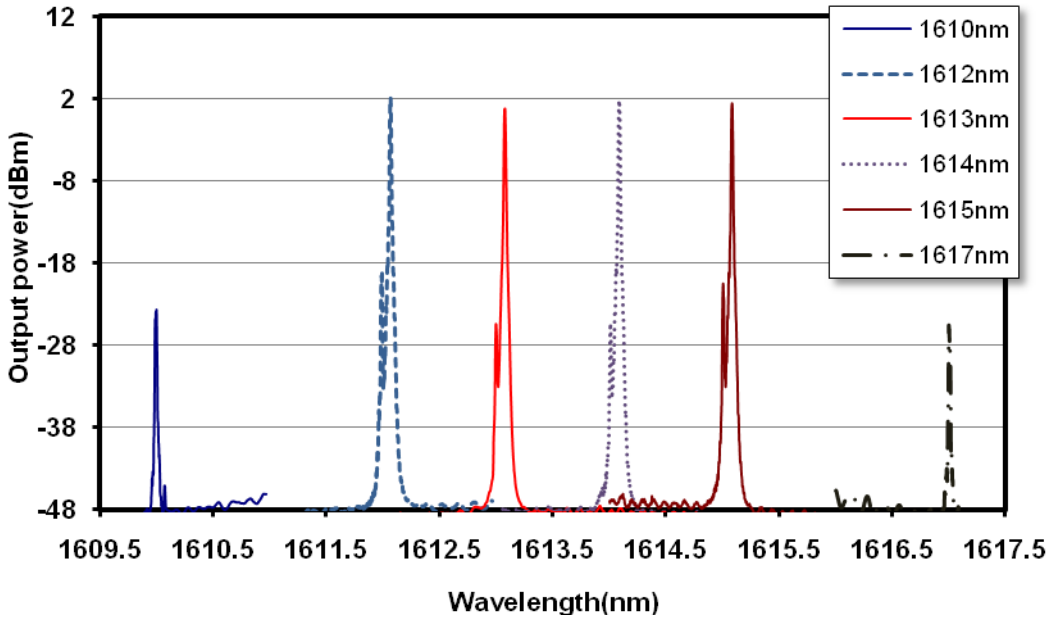

.

Figure 4.6: The output spectrum of the BEFL at various BP wavelength using 80/20 output coupler.

Figure 4.7 shows the output spectrum of the BEFL at various BP powers. In this experiment, 1480 nm pump power and BP wavelength are fixed at the maximum value of 152 mW and 1613.9 nm, respectively. As shown in the figure, the Brillion laser starts to lase at threshold BP pump power of 0 dBm. There is no SBS observed at pump power below 0 dBm and therefore the spectrum is not shown in the figure. The increase of BP

power from 0 dBm to 4 dBm slightly increases the output power and further increase of pump power do not changed the output power. On the other hand, the second Stokes and anti-Stokes is highest at the BP powers of 2 dBm.

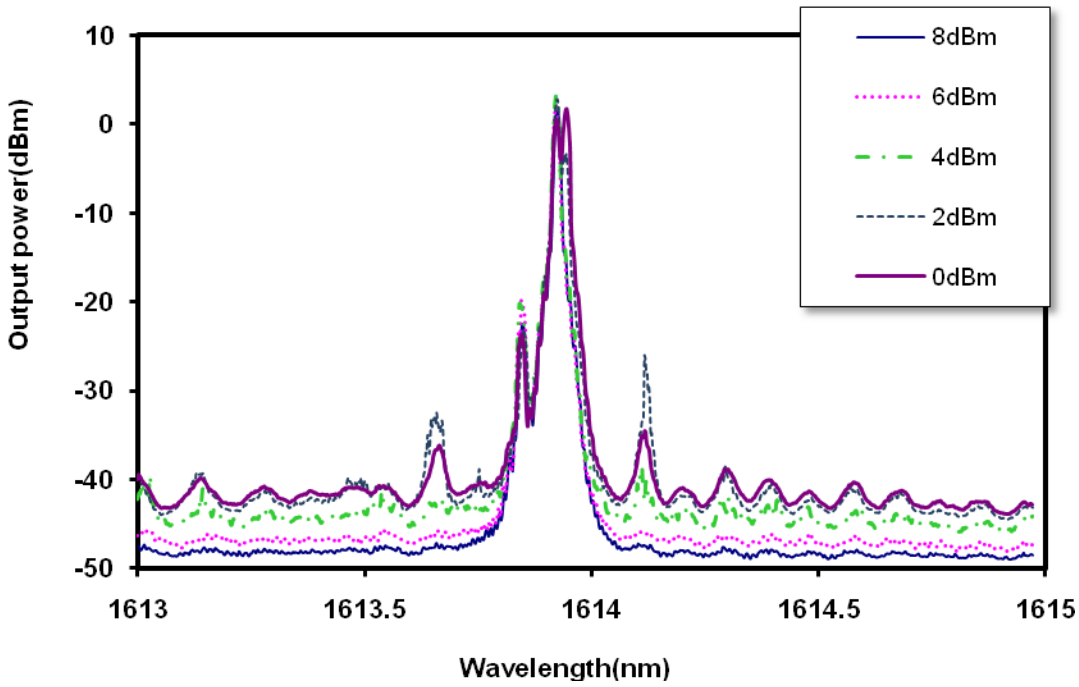

Figure 4.7: Output spectra of the BFL based on Bi-EDF at different signal input powers.

In conclusion, a single-wavelength BEFL is successfully demonstrated using only a very short length of Bi-EDF as both the linear and nonlinear gains medium. The BEFL is obtained at 1614 nm region with a SMSR of more than 22 dB with the BP and 1480 nm pump powers of 5 dBm and 152 mW, respectively. The spacing between the BP and the Stokes is measured to be approximately 0.09 nm. The multi-wavelength BEFL will be demonstrated in the next section. The Bi-EDF will also be used to generate multi-wavelength comb laser using the FWM effect, which will be explained in details in chapter 5.

4.3 Multi-wavelength BEFL Configuration with a Linear Cavity

Multi-wavelength lasers have recently become a topic of extensive study due to their potential applications in instrument testing and sensing, and as optical sources for DWDM system [10, 11]. The multi-wavelength operation can also be achieved through use of a BEFL. However, most of the previous research works on this topic used a long piece of fiber for both linear and nonlinear gain media in either ring or linear cavity configurations. In this section, a multi-wavelength BEFL is demonstrated using only a 215 cm long Bi-EDF as the gain medium in a linear cavity configuration. The Bi-EDF provides both nonlinear gain to generate SBS and linear gain to assist the multi-wavelength generation in extended L-band region, which is within the operating wavelength of the Bi-EDF amplifier.

Figure 4.8 shows the proposed multi-wavelength BEFL, which consists of a piece of 2.15 m long Bi-EDF, two circulators (OC1 and OC2) and two couplers (C1 and C2). The Bi-EDF is forward pumped through a WSC by a 1480 nm laser diode, and two circulators are placed at both ends of the laser cavity to act as fiber loop mirror. The Bi-EDF is also pumped through a 5/95 coupler, C1 by an external cavity TLS to generate a nonlinear gain or Stokes, which is injected into the linear cavity via optical circulator. An output coupler, C2 is used to extract the BEFL output, which is then characterized by the OSA. The effect of varying the output coupler on the BFL performance is also investigated in this experiment. The forward pumped Bi-EDF provides amplifications at wavelength region from 1565 nm to 1620 nm with the maximum gain of 12 dB (at 1610 nm). The Bi-EDFA operates at the extended L-band region due to the use of Bismuth glass as a host material of the fiber, which is able to extend the amplification band to a longer wavelength compared to the conventional silica-based EDF. The operating wavelength of the proposed BEFL

should be within this wavelength region since the Erbium gain will be used to amplify the Brillouin Stokes in order to assist the multi-wavelength generation in the linear cavity resonator.

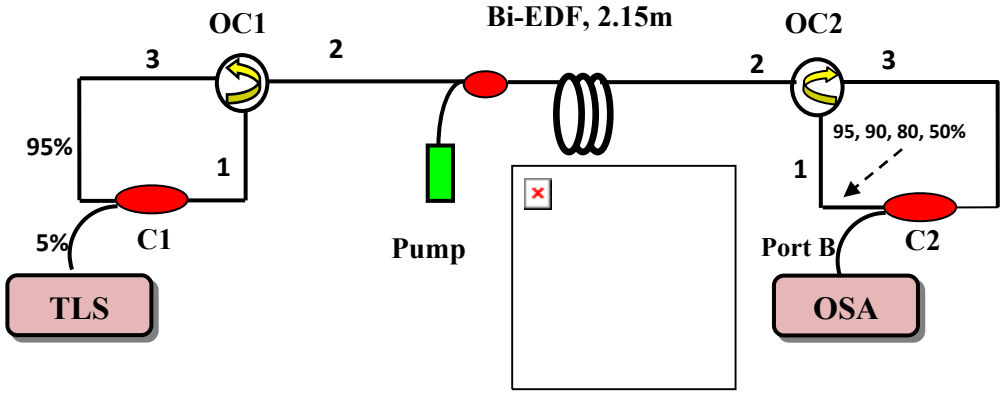

Figure 4.8: Configuration of the proposed multi-wavelength BEFL with a linear cavity configuration.

The Brillouin pump (BP) is injected into the Bi-EDF and the SBS in the fiber generates a Stokes-shifted signal in the opposite direction of the BP. In the linear cavity BFL system, the laser propagates through the Bi-EDF twice per oscillation trip. The first Stokes signal propagates in the opposite direction of the BP is reflected back into the cavity by the first fiber loop mirror, amplified again by the Bi-EDF amplifier to complete one oscillation. The oscillation continues till the first Brillouin Stokes reaches the threshold required to generate a second Stokes which is shifted further with a same frequency relative to the first Stokes signal. The double-pass through the Bi-EDF gain reduces the effective cavity loss and enables the multi-wavelength generation, which cannot be achieved by the ring system without a feedback loop. By using a single fiber for the linear Erbium amplification and Brillouin Stokes generation, we are simultaneously amplifying a BP and Brillouin signal in this cavity. This allows shorter length of active fiber to be used for the BFL generation, which in turn reduces a total cavity loss and increases the output power.

Figure 4.9 shows the output spectrum of the proposed BEFL for different output coupler (C2) ratio. In this experiment, the 1480 nm pump and BP powers are fixed at 155 mW and 5 dBm, respectively at room temperature. As shown in the figure, the highest number of lines is observed at 50% port B. As shown in Figure 4.9(a), more than 40 lines are obtained with a line spacing of 0.09 nm. The increment of output coupler ratio however reduces the reflectivity at the second loop mirror (OC2) which subsequently increases the loss in the linear cavity, which in turn reduces the number of comb lines at the output. The stability of the output is also worsened at the higher coupling ratio due to the inefficient phase matching condition in the laser cavity.

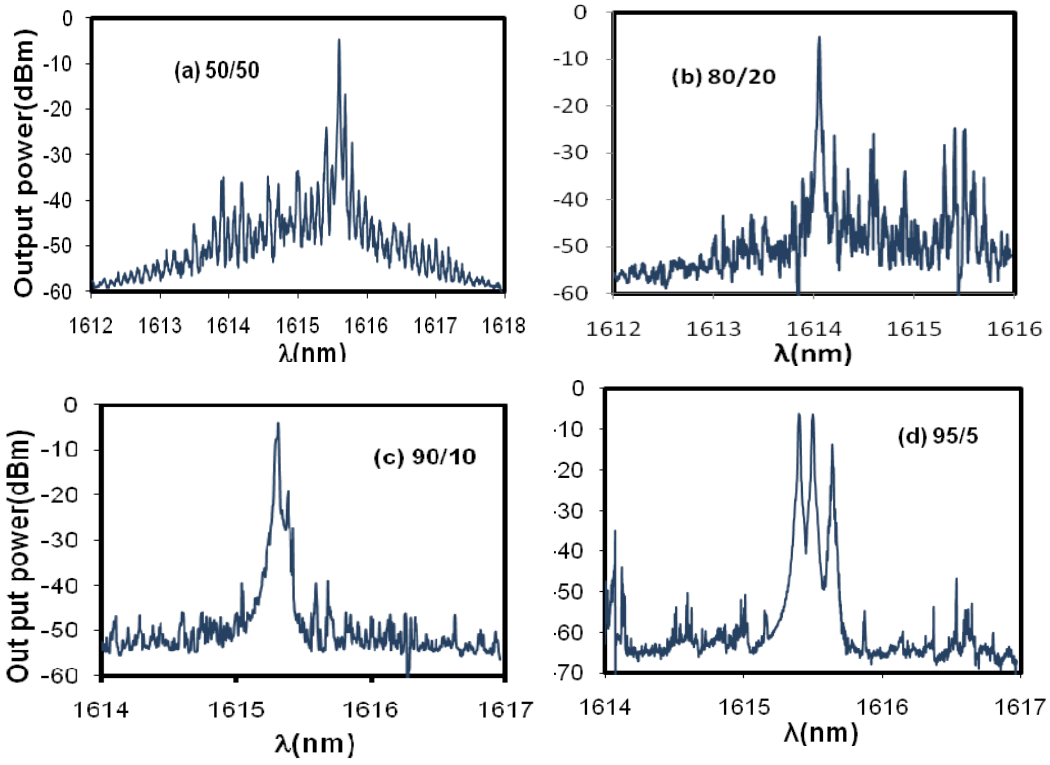

Figure 4.9: Output spectrum of BEFL at different C2 coupling ratios. The laser diode and BP powers are fixed at 155 mW and 7dBm, respectively at room temperature.

Figure 4.10 shows the output spectrum of the BEFL when the 1480 nm pump power is varied from 94 mW to 155 mW. As shown in the figure, a BEFL wavelength comb with

line spacing of approximately 0.09 nm at 1615 nm wavelength region could be easily observed when the 1480 nm pump power exceeded 124 mW, and it grew as the pump power was raised to 155 mW. Below this pump power threshold, the Erbium gain is very low and cannot sufficiently compensate for the loss inside the laser cavity and thus no Stokes is observed. The generated BEFL power is observed to increase as the 1480 nm pump power increases, which is attributed to the increment of the Erbium gain with pump power. This situation provides sufficient signal power for SBS to generate Stokes, which is then amplified by the Erbium gain. At the maximum 1480 nm pump power, more than 40 lines are obtained including the anti-Stokes. The anti-Stokes generation is due to FWM effects. Five strong FWM signals with spacing of 0.4 nm are also observed due to the dispersion characteristic of the Bi-EDF.

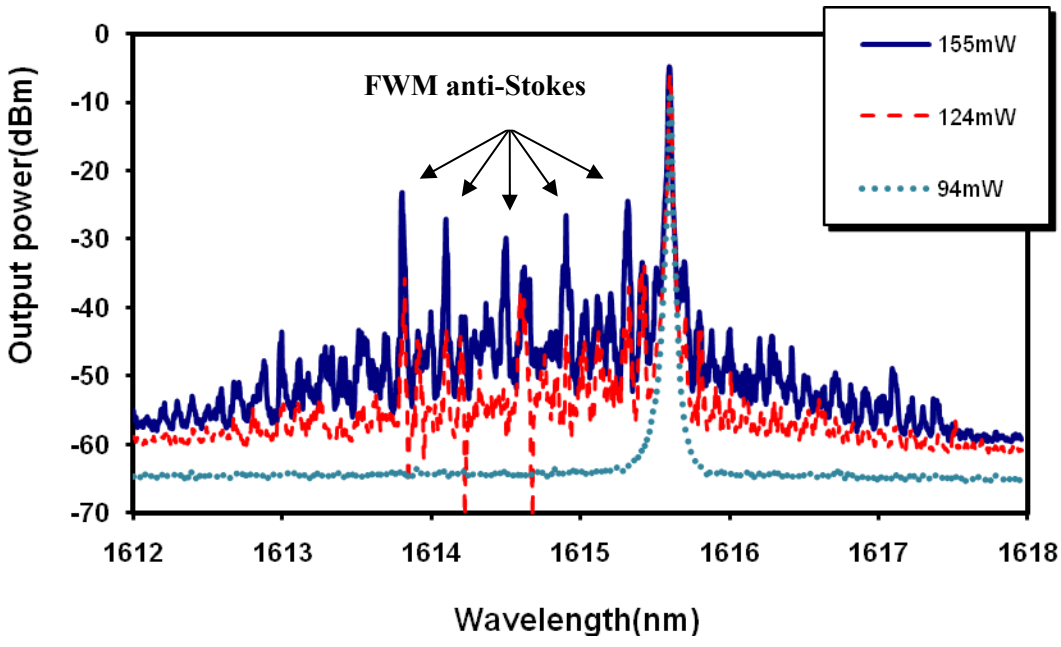

Figure 4.10: Multi-wavelength spectra at different combination 1480 nm pump powers. The BP power and wavelength is fixed at 5 dBm and 1615.6 nm, respectively.

In summary, a multiple wavelength source is demonstrated using only a short piece Bi-EDF as the gain medium. A stable output laser comb of about 40 lines is obtained at 1615.6 nm region with the BP power of 5 dBm and 1480 nm pump power of 155 mW. The proposed multi-wavelength BEFL is very compact and very narrow line-width by using only a piece of 215 cm long of gain medium.

4.4 New Configuration for the BEFL by Changing the Position of the Output Coupler

Brillouin multi-wavelength generation has two distinct advantages over other multi-wavelength method; a constant spacing and narrow linewidth. In the BEFL, a Bismuth-based EDF is used for both to generate and to amplify the SBS Stokes. In the previous section, a multiple wavelength source is demonstrated using only 215 cm long Bi-EDF as both linear and nonlinear gain media to operate in the extended L-band region. About 40 lines are achieved using that setup. In this section, the number of lines is further increased by using a new configuration in which the location of the output coupler is changed. The configuration of the proposed BEFL is shown in Figure 4.11. The similar gain medium and pump laser is used in this BEFL. The linear cavity was formed by using three optical circulators (OC1, OC2 and OC3) and a 3-dB coupler. Two optical circulators (OC1 and OC2) are placed at both ends of the laser cavity to act as fiber loop mirror. A TLS is used as a BP to generate a nonlinear gain or Stokes, which is injected into the Bi-EDF section via the OC3 and 3-dB coupler. The OC3 and 3-dB coupler are also used to extract the BFL output, which is then characterised using an OSA.

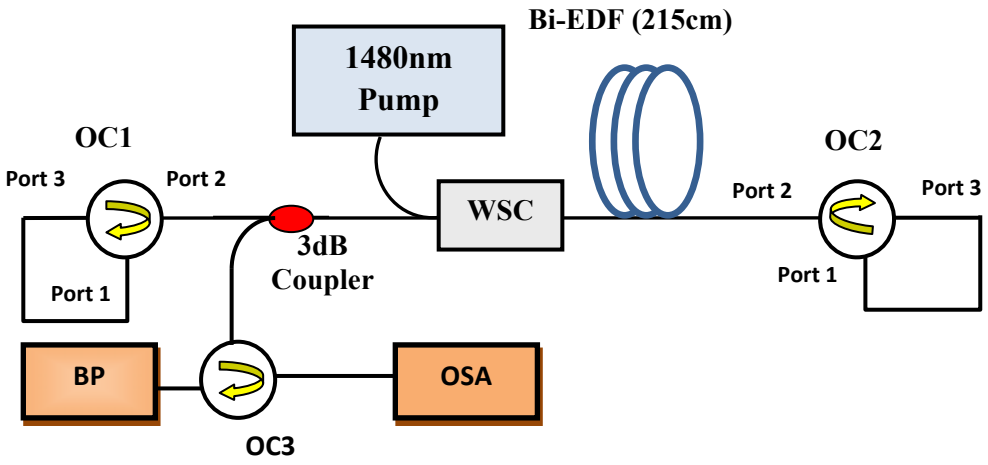

Figure 4.11: Configuration of the proposed new BEFL with the output coupler placed in the middle of linear cavity.

Although the injection of the Brillouin pump can create a Stokes signal and forces the laser cavity to lase at this particular wavelength, the laser cavity has its own cavity modes that oscillates freely in the laser system. In the initial stage, the first generated Stokes signal propagated in the opposite direction of the BP signal and is passed into the Bi-EDF for effective amplification. This signal traveled to the second optical circulator (OC2) and was recycled back into the Bi-EDF. The oscillation continued in this stage and when the intensity of the first Brillouin Stokes was higher than the threshold value for Brillouin gain, the second Brillouin Stokes is generated and oscillated in the cavity. This process continued and the cascaded Brillouin Stokes can be generated as long as the total gains of the Brillouin and Erbium media were equal to the cavity loss. In this experiment, the BP signal is launched into Bi-EDF at a wavelength of 1612.4 nm, which coincided to the free-running BEFL wavelength region and maximum gain profile. The wavelength shift was observed to be approximately 0.09nm, which is strongly dependent on the BP wavelength as governed by the following equation [1]

$$\nu_B = \frac{\omega_A}{2\pi} = \frac{2n\nu_A}{\lambda_p} \tag{4.2}$$

where ν_A is the acoustic velocity, λ_p is the BP wavelength, and n is the refractive index.

Figure 4.12 shows the output spectrum of the proposed BEFL for different 1480 nm pump power. In this experiment, the BP power is fixed at 5 dBm and the 1480 nm pump power is varied from 110 mW to 152 mW. As shown in the figure, a BFL wavelength comb with line spacing of approximately 0.09 nm at 1612.4 nm wavelength region could be easily observed when the 1480 nm pump power exceeded 110 mW, and it increased as the pump power was raised up to 152 mW. Below this pump power threshold, the Erbium gain is very low and cannot sufficiently compensate for the loss inside the laser cavity and thus no Stokes is observed. The generated BEFL power is observed to increase as the 1480 nm pump power increases, which is attributed to the increment of the Erbium gain with pump power. This situation provides sufficient signal power for the SBS to generate Stokes, which is then amplified by the Erbium gain. At the maximum 1480 nm pump power, about 50 lines are obtained including the anti-Stokes. The anti-Stokes generation is due to the FWM effect.

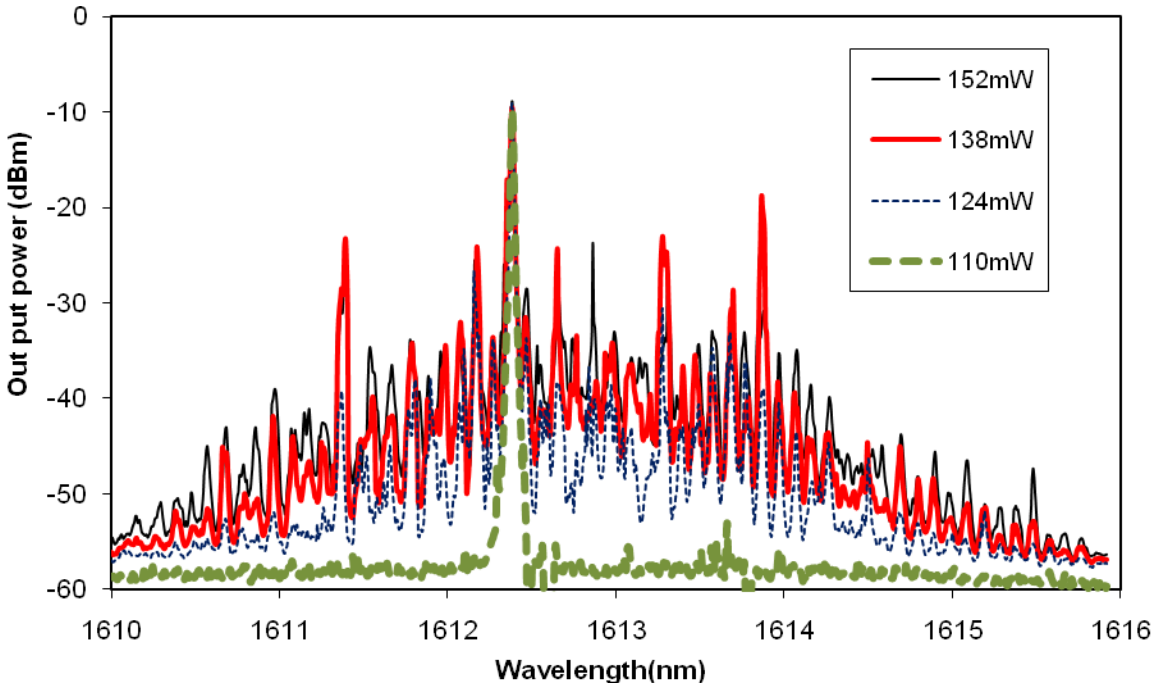

Figure 4.12: The output spectra of the proposed BEFL at various 1480nm pump powers.

The BEFL performance is also compared with the use of 181cm long Bi-EDF as shown in Figure 4.13. From the figure, the number of lines obtained is about the same (50 lines), however the comb operates at the shorter wavelength. This is attributed to the cavity loss which is smaller in the BEFL with 181cm Bi-EDF as compared to the other one with 215cm. However, this BEFL shows a slight fluctuation and instability in the comb spectrum and therefore 215 cm long Bi-EDF is used in the following works.

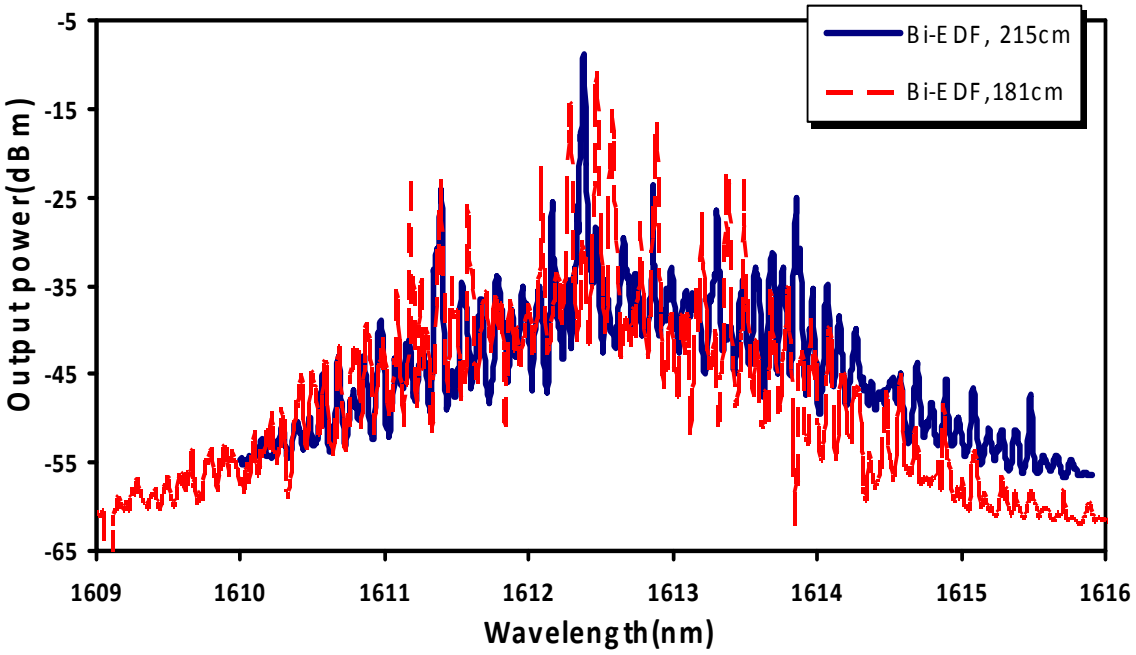

Figure 4.13: The comparison on output spectrum for different lengths of Bi-EDF.

The requirement of the internal active feedback to generate cascaded Brillouin Stokes was achieved by the proposed configuration. The novelty of this design proves that only a single gain medium (Bi-EDF) can be used in the linear cavity BEFL to amplify the Brillouin Stokes signal and support multiple wavelengths operation. Furthermore, only a single 1480 nm pump laser was deployed in this BEFL instead of two units of pump laser in the other works [6, 7]. In the next section, the effect of incorporating additional gain medium in the cavity will be investigated.

4.5 Multi-wavelength BEFL in a Ring Configuration

Photonic crystal fibers (PCFs) have generated great interest over the past few years, growing from a research-oriented field to a commercially available technology. The PCFs were first developed by Philip Russell in 1998, and can be designed to possess enhanced properties over (normal) optical fibers. They can be divided into two fundamental classes, solid-core and hollow-core as shown in Figure 4.14.

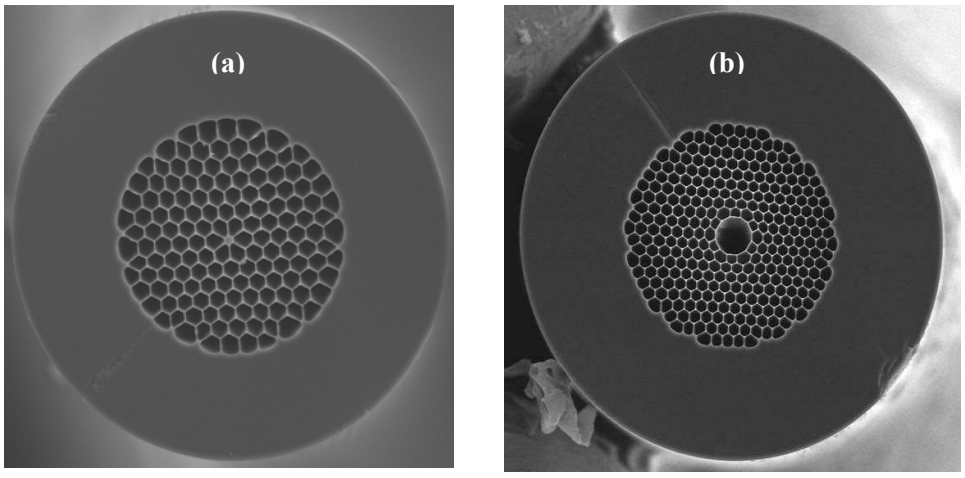

Figure 4.14: Photonic Crystal Fibers Types, **(a)** Solid core PCF, **(b)** Hollow core PCF.

The solid core PCF is used in this thesis that is two dimension (it has a periodic geometry in two directions and is homogeneous in the third) and we already introduced physical properties of that in table 2.2. Figure 4.15 shows an electron micrograph of the cross section of this solid core PCF. Despite the hexagonal structure of the cladding, the mode field is very similar to that of the fundamental mode of a conventional fiber. The optical properties of PCFs rely on the specification of the size, shape and arrangement of

the holes that surround a solid core to form a cladding. These parameters can easily be tailored to increase fiber nonlinearity, which is difficult to achieve using conventional fibers.

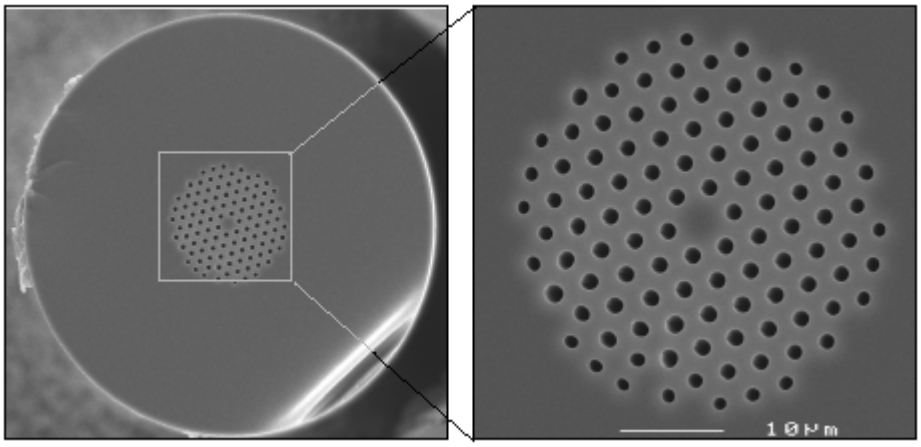

Figure 4.15: The Scanning Electron Micrograph (SEM) of the PCF cross section and an enlarged view of the central "holey" cladding.

The highly nonlinear PCFs have many applications such as wavelength conversion [12] and Brillouin fiber lasers (BFLs) [13]. So far, few reports have been published on the Brillouin effects in PCFs [12, 14, 15]. In BFL applications, the required gain medium length can be substantially reduced using a holey fiber to replace the conventional SMF-28 Fiber of Corning Inc.[13]. However, most of the earlier works on PCF based BFLs are mainly on a single wavelength operation [13]. In this section, a multi-wavelength BEFL operating in L-band region is demonstrated using a PCF in a ring configuration. In the ring configuration, a multi-wavelength operation cannot be achieved using a Bi-EDF alone as a gain medium. Therefore a very short length of PCF (20 m) is added in the ring cavity BEFL in the proposed configuration to achieve a multi-wavelength generation.

Figure 4.16 shows the experimental setup of the proposed PCF-based BEFL. The ring resonator consists of a circulator, a 20 m long PCF, a PC, two isolators and a bi-

directionally pumped 215 cm long Bi-EDF. The PCF used is a polarization maintaining type with a cut-off wavelength of 1000 nm, zero dispersion wavelength of 1040 nm, nonlinear coefficient of 11 $(W.km)^{-1}$ and a mode field diameter of 4.2 μm near zero dispersion wavelength. The Bi-EDF is pumped bi-directionally using two 1480 nm lasers. Optical isolators are used to block the BP from oscillating in the cavity and also to ensure a unidirectional operation of the BFL. The PC is used to control the birefringence (breakage of a light ray into two different directions therefore creating two separate light rays) of the ring cavity, so that the power of the laser generated can be controlled. The experiment executed using 3 different types of couplers the 80/20, 90/10 and 95/5 and the output for BFL is tapped from the leg with the smaller coupler ratio before it is characterized using an OSA.

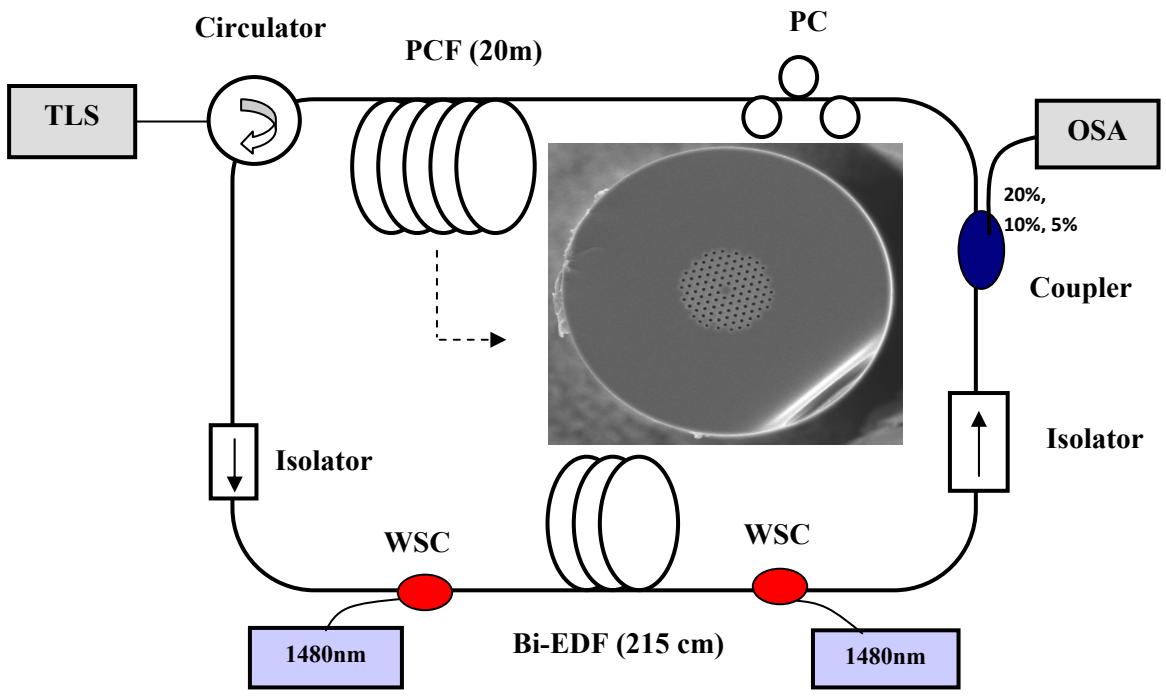

Figure 4.16: Configuration of multi-wavelength BFL.

The BP is injected into the ring cavity and then PCF via the circulator to generate the backward propagating Stokes light at opposite direction. However, since the PCF length is not sufficient enough, the back-scattered light due to Rayleigh scattering is relatively higher than the Stokes light. Both back-scattered pump and the Stokes lights are amplified by the bi-directionally pumped Bi-EDF and it oscillates in the ring cavity to generate first Stokes in an anti-clockwise direction. This oscillation continues and when the intensity of the first Brillouin Stokes is higher than the threshold value for Brillouin gain, the second order SBS is generated in clockwise direction and this signal is blocked by the isolator in the cavity. However, the back-scattered light from second SBS will be amplified by the Bi-EDF. Hence, the nonlinear gain by both PCF and Bi-EDF only amplifies the Stokes light and thus the Stokes light is more dominant and laser is generated at the Stokes wavelength. The spacing between the BP and the BFL is obtained at approximately 10 GHz, which is equivalent to the Stokes shift in the SMF.

The operating wavelength of the BFL is determined by the bi-directionally pumped Bi-EDF gain spectrum which covers the L-band region from 1560 nm to 1620 nm as well as the cavity loss. Figure 4.17 shows the free running spectrum of the BEFL, which is obtained by turning off the BP for three different output coupler ratios; 80/20, 90/10 and 95/5. The output laser is taken from the leg with a lower portion. The peak wave generated at approximately 1574 nm with bandwidth of approximately 3 nm due to the difference between Bi-EDF's gain and cavity loss is the largest in this region. The chosen BFL operating wavelength must be within or close to the bandwidth of free running BFL. Therefore, the BP is set within 1574 nm region which is within the lasing bandwidth of the free running BFL. At the coupling ratio of 80/20, the free-running BFL exhibits the highest

peak power of approximately -6 dBm with 20 dB bandwidth of approximately 1 nm. The cavity loss is the lowest with 80/20 coupler and therefore the peak power is the highest.

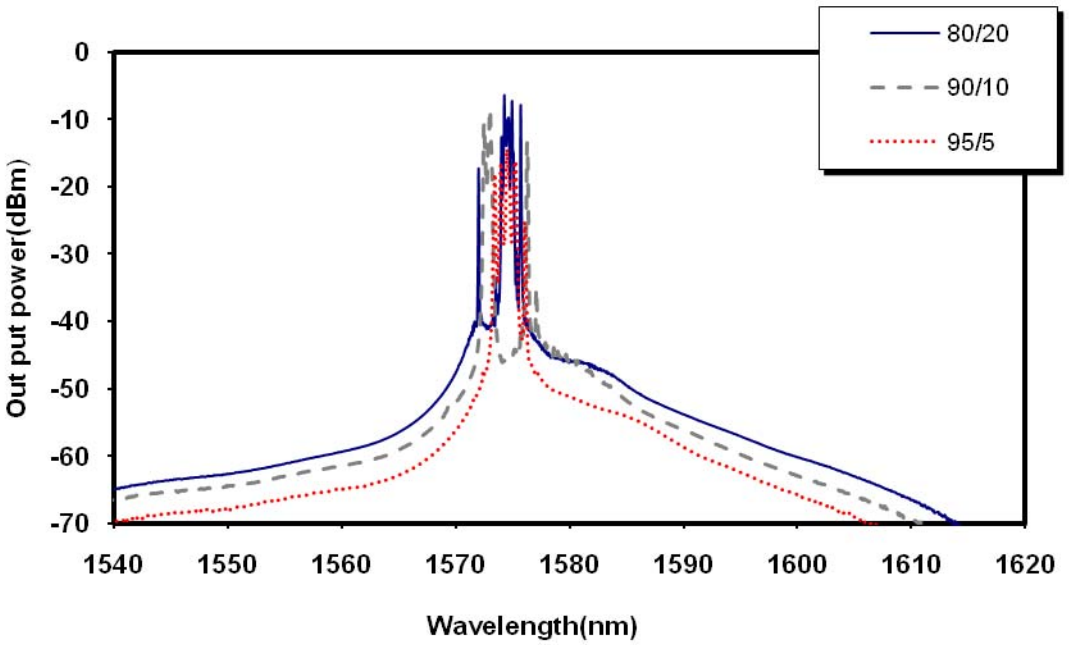

Figure 4.17: Free-running spectrum of the BEFL using 80/20, 90/10 and 95/5 couplers.

Figures 4.18 (a), (b) and (c) show the output spectra of the BEFL at different output coupler ratios of 80/20, 90/10 and 95/5, respectively. The experiment was carried out for three different pump powers. Both the 1480 nm pumps are set at the same power and power of each pump is varied from 60 mW to 135 mW. The threshold of the BEFL is observed to be around 60 mW for all setups. At pump power below of 60 mW (threshold) the Erbium gain is very low and cannot sufficiently compensate for the loss inside the laser cavity and thus no Stokes are observed. When increasing the 1480 nm pump power the number of wavelength generated is increased and the anti-Stokes wave also surfaced, which attributed to the increment of the Erbium gain with the pump power. This situation provides sufficient signal for SBS as well as the FWM to generate Stokes and anti Stokes.

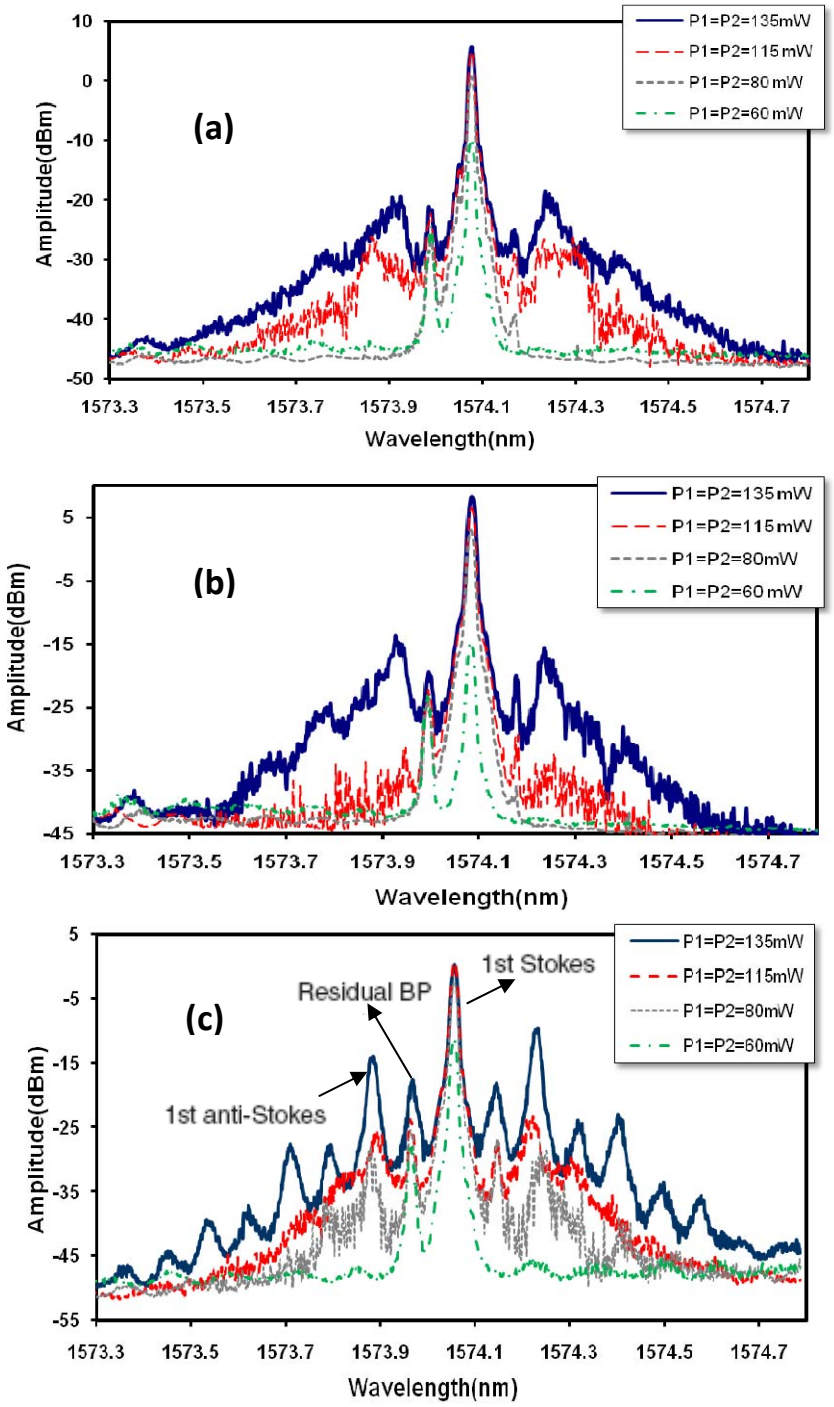

Figure 4.18: The BFL output spectrum for **(a)** 80/20 coupler, **(b)** 90/10 coupler and **(c)** 95/5 coupler. Both pumps are at the same power for each output coupling ratio.

In this experiment, more than 13 lines are obtained at the maximum 1480 nm pump power of 135 mW with wavelength spacing of approximately 0.08 nm for the BEFL

configured with 80/20 output coupler as shown in Figure 4.18(c). However, the number of lines significantly reduced as the cavity loss increases. For instance, only two Stokes are observed with 80/20 coupler as shown in Figure 4.18(a). The SMSR are obtained at approximately 27.0 dB, 26.9 dB, 18.8 dB for 80/20, 90/10 and 95/5 couplers, respectively as shown in Figure 4.18. The multi-wavelength output of the BFL is observed to be stable at room temperature with only minor fluctuations observed coinciding with large temperature variances. The side modes are mainly due to anti Stokes and additional Stokes of the BFL, which arises due to FWM effect in the PCF.

Figure 4.19 shows the output spectrum of the BEFL with and without PC. A 95/5 output coupler is used in this experiment. The PC is used to adjust the polarization state of the light inside the cavity. Proper adjustment of the birefringence or polarization of the light is important to achieve a multi-wavelength oscillation. As shown in the figure, a better spectrum is obtained by adjusting of PC. The anti-Stokes waves can also be observed in PCF-based BFL because of FWM between pump and Stokes waves or between different Stokes order. At the maximum pump power of 135 mW, FWM between the two first odd-orders Stokes waves leads to the generation of more than 13 spectral lines.

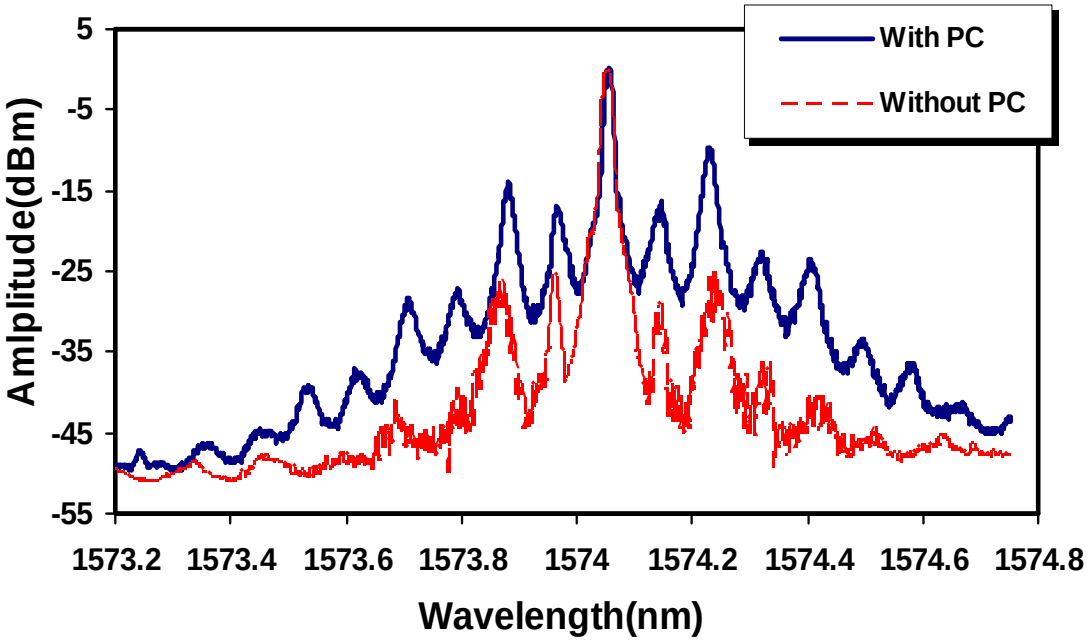

Figure 4.19: BFL output spectra with and without PC.

Figure 4.20 shows the peak power of the first Stokes for different couplers against the input 1480 nm pump power of each pump (total pump power is double). The BP power and wavelength is fixed at 5 dBm and 1574 nm, respectively. The BEFL starts to lase at 1480 nm pump power of 60 mW which is the threshold power. Below this power, the Erbium gain is very low and cannot sufficiently compensate for the loss inside the laser cavity and thus no Stokes is observed. The output power saturates at 135 mW. As shown in the figure, the peak power is highest with 80/20 coupler and lowest with 95/5 coupler. Inset of Figure 4.20 shows the peak power of the first Stokes against the BP power at various output couplers. This figure shows that the threshold power of around 4~5dBm is required to generate the Stokes with the use of 95/5 output coupler. The threshold power reduces as smaller portion of light is allowed to oscillate in the ring cavity. For instance the threshold is about 2 dBm with 80/20 output coupler.

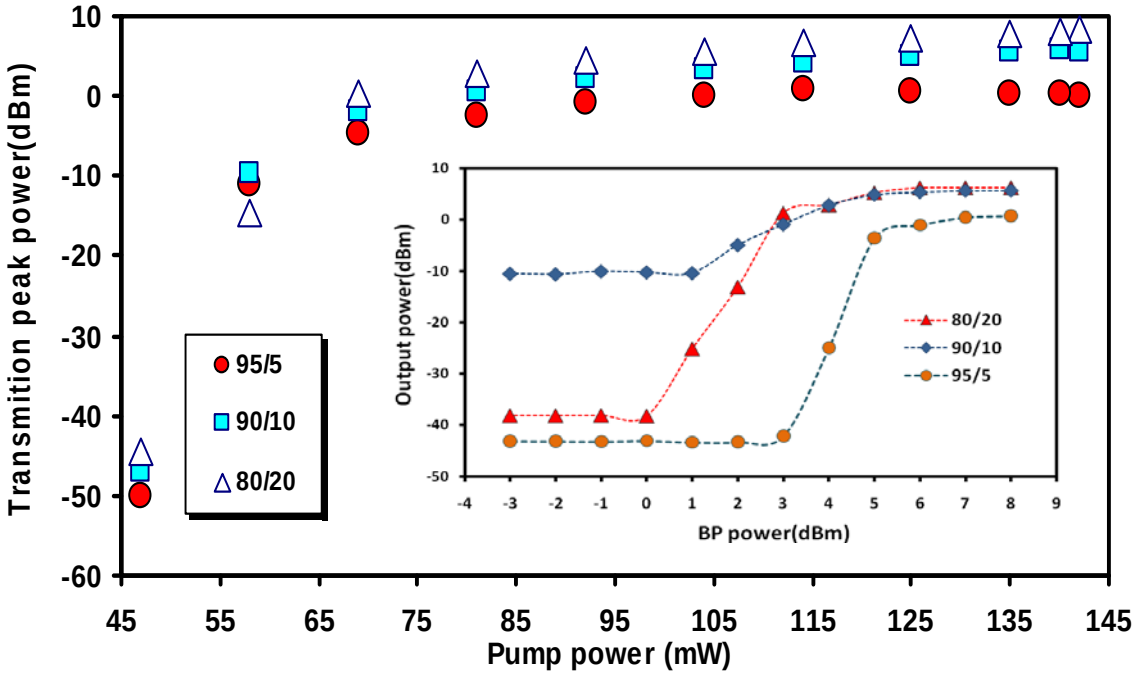

Figure 4.20: Output peak power as a function of 1480nm total pump powers. Inset shows the peak power against BP power.

In summary, a new configuration of multi-wavelength BFL is proposed and demonstrated using a PCF in conjunction with bi-directionally pumped Bi-EDF. The BFL uses a ring cavity structure to generate Stokes and anti-Stokes via SBS and FWM processes. The proposed BFL is able to generate up to 13 lines including anti-Stokes with a channel spacing of 0.09 nm at the 1574 nm region at a BP power of 5 dBm and the total 1480 nm pump power of 270 mW. The multi-wavelength BFL is stable at room temperature and also compact due to the use of only 20 m long of PCF and 215 cm long of Bi-EDF.

4.6 Self-excited Multi-wavelength BEFL Using a PCF

The use of highly nonlinear PCF to assist in multi-wavelength generation in a ring BEFL was demonstrated in the previous section. This section proposes a self-excited BEFL using a 20 m long PCF and 49 cm lenght of Bi-EDF as the gain media. Figure 4.21shows the schematic of proposed ring BEFL in which the resonator consists of two circulators, a bi-directionally pumped Bi-EDF, isolator, 90/10 output coupler, and PCF. Two circulators are used in conjunction with a PCF to acts as a mirror. This mirror doubles the SBS as light passes through the 20 m PCF twice during each round trip. The bi-directional Bi-EDF generates ASE, which oscillates in clock-wise direction in the ring cavity to achieve a narrow linewidth laser. The laser interacts with a PCF section to generate a Brillouin Stokes in opposite direction and is then further amplified and oscillates in the ring cavity to generate the first Stokes of Brillouin laser. The Stokes will acts as another BP to generate the subsequence Brillouin Stokes. This process is repeated to generate a BEFL comb as shown in Figure 4.22.

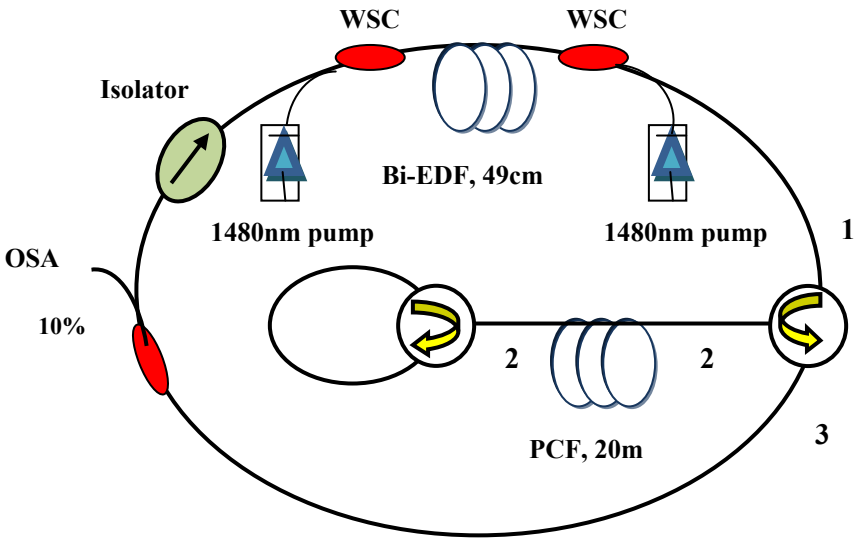

Figure 4.21: The BFL output spectrum of ring cavity resonator.

Figure 4.22 shows the output spectrum of the self-excited BEFL at different output couplers of 50/50 and 90/10. With 50/50 coupler, the BEFL achieved a comb spectrum over a bandwidth from 1558.1 nm to 1559.3 nm, which leads to multiple channels with the availability of different wavelengths, and the spacing between two consecutive peaks is 0.09 nm that correspond to 11GHz. The fluctuation of the peak power is due to reduced length of Bi-EDF and FWM effect between Stokes and pump powers. As the coupler is changed to 95/5 to route 5% of the oscillating light into the OSA and reflects back 95% to the ring cavity, the similar comb is also achieved with a smaller number of lines but still maintaining 0.09 nm wavelength spacing.

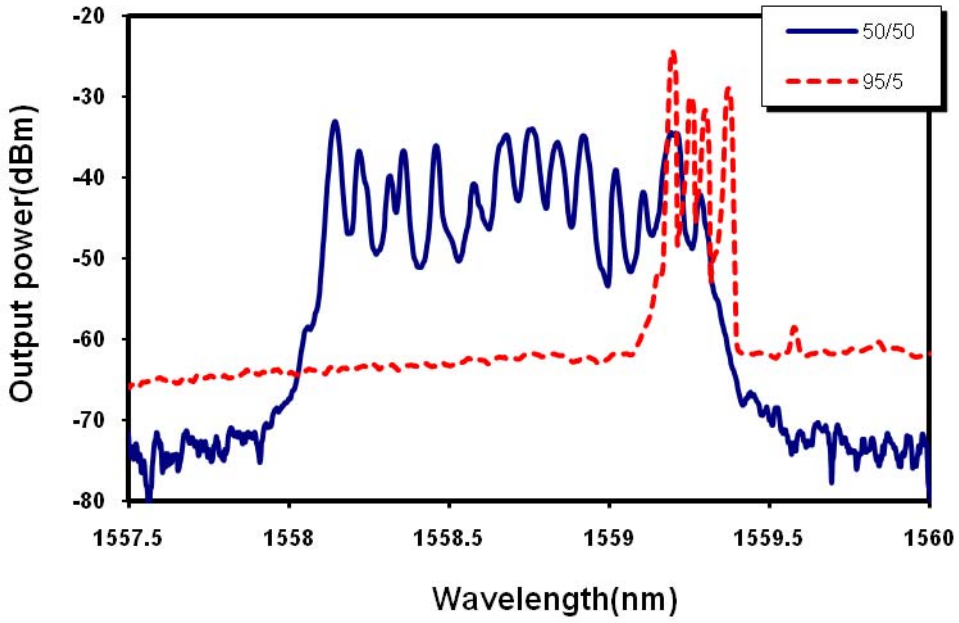

Figure 4.22: The output spectrum of the BEFL using PCF and sagnac loop filter.

Figure 4.23 shows the output spectrum obtained by varying the 1480 nm pump power. The 50/50 coupler is used in the experiment. As shown as in Figure 4.23, the 1480 nm pump power threshold is approximately 52 mW, below this pump power, the Erbium

gain is very low and can not sufficiently compensate for the loss inside the laser ring cavity and thus no Stokes is observed. The number of lines increases as the 1480 nm pump power increases. At the maximum 1480 nm pump power of 135 mW (total power of 270 mW), the BEFL comb with 13 lines at peak power around -33 dBm. This configuration is designed without external BP to demonstrate the upgradability of existing WDM networks with low costs.

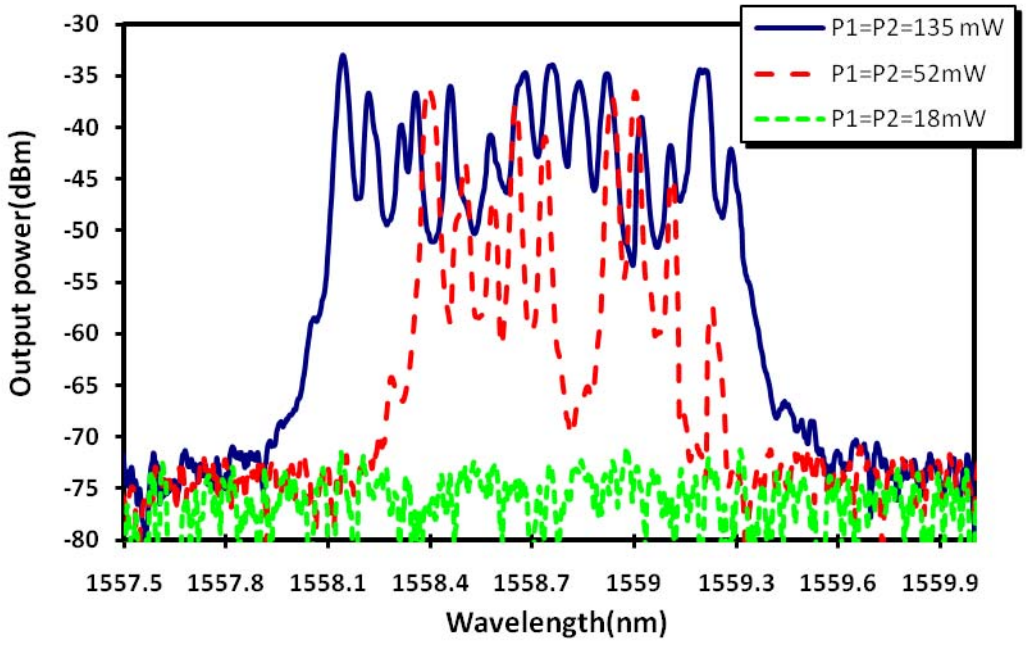

Figure 4.23: The output spectrum of the BEFL using PCF with different pump power.

4.7 Incorporation Effect of SMF in a Linear BEFL Cavity Configuration

Single mode fibers (SMFs) is used as transmission medium in an optical communication system due to their low loss characteristic that allow for a higher capacity compared to that of multimode fiber. The standard SMF (SMF-28) has also a small nonlinearity characteristics which is suitable for BFL generation. Since the Brillouin gain coefficient g_B in the standard SMF is about 4.5 ~ 5.0 $\times 10^{-11}$m/W, which is very small,

therefore the alternative materials such as PCF are used to reduce the gain medium length in this laser [12, 13]. In this section, we investigate the effect of SMF incorporation on the BEFL performance. Figure 4.24 shows the experimental setup of the linear cavity BEFL. A piece of SMF approximately 25 km in length is employed for studying of the multi-wavelength generation in BEFL. Two optical circulators are employed at both ends of system to act as a reflector in this Fabry Perot design. A 3-dB coupler is used to inject (or tap) the BP (or output) to (from) the linear cavity. The SMF is then replaced with a 20 m long PCF for comparison purpose.

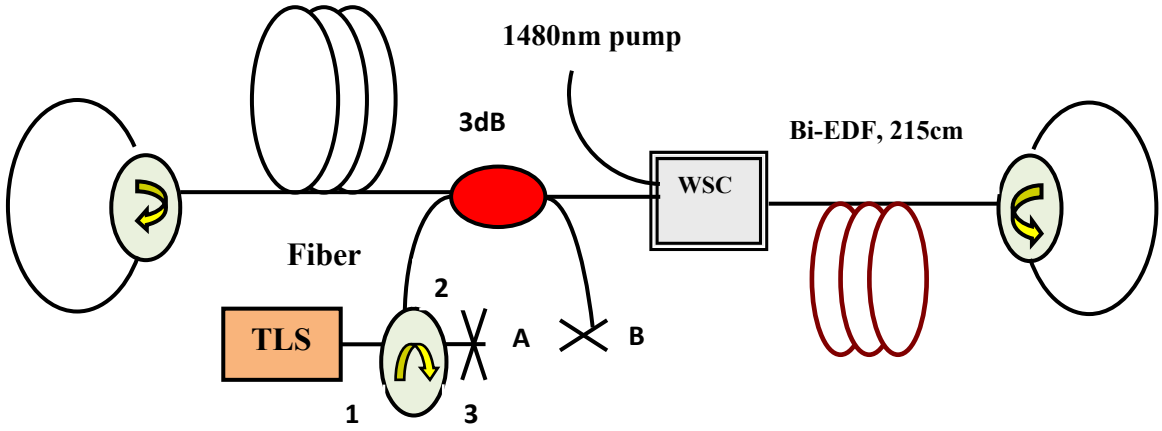

Figure 4.24: Configuration of the BEFL with a linear cavity.

Figure 4.25 shows the output spectrum of the BEFL using different gain medium in the linear cavity. The output spectrum is taken from port A of Figure 4.24. As shown in the figure, the BEFL operates within the wavelength region from 1605 nm to 1616 nm depending on the cavity loss. This wavelength region is in the extended L-band which falls within the amplification bandwidth of the Bi-EDF amplifier. The operating wavelength is moved towards a shorter wavelength as the cavity length increases as shown in Figure 4.25.

The comb bandwidth is smallest with the SMF due to the cavity loss. However, the quality of Stokes lines is better with the incorporation of SMF.

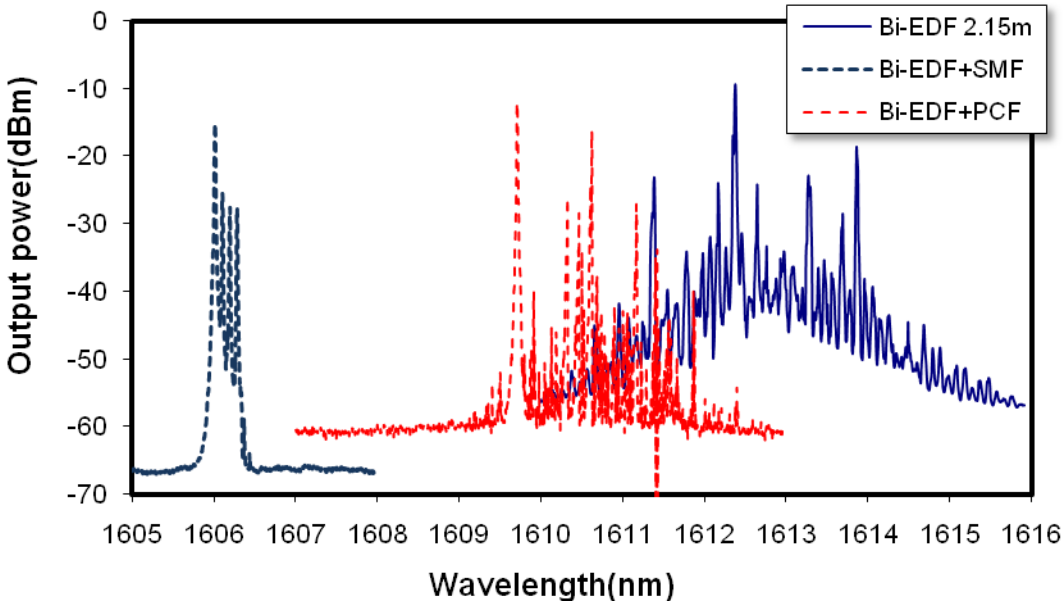

Figure 4.25: The output spectra of three types of gain media in port A.

Figure 4.26(a) and (b) show the output spectrum at different output ports A and B (see Figure 4.24) for both BEFLs with PCF and SMF, respectively. As shown in the figure, the output power is higher in port B in both cases due to the circulator loss at port A. With the SMF, the number of lines and its flatness is better at port B because the output is taken before Erbium amplification. Erbium amplification induces noise to the output comb and affects the flatness of the comb. With PCF, the comb generation is random and uncontrollable.

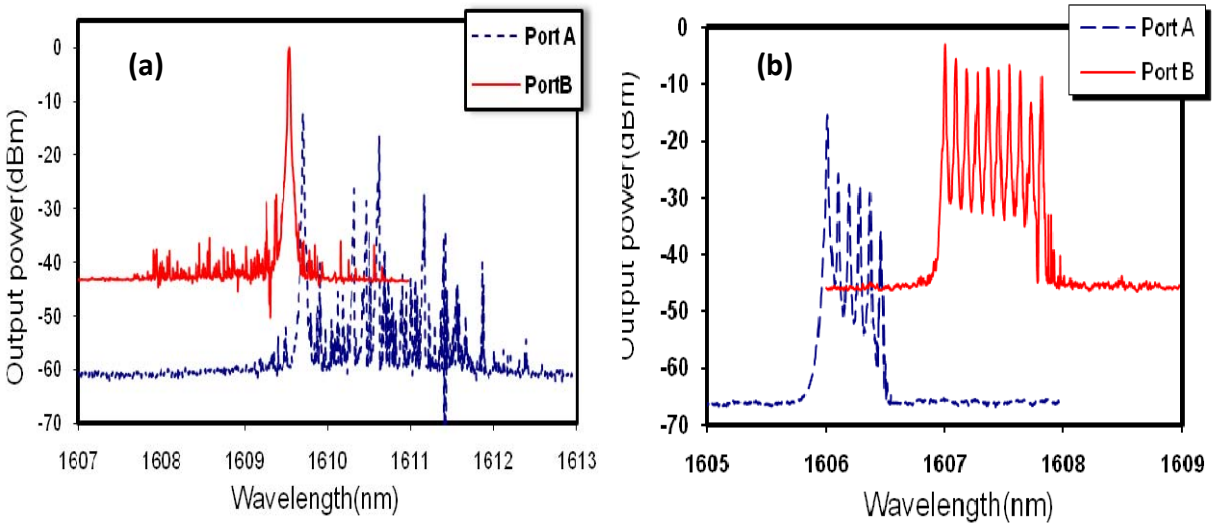

Figure 4.26: The comparison of output spectra of the BEFL with **(a)** PCF, **(b)** SMF at different output ports.

Figure 4.27 shows the peak power of the first Stokes against input BP power at different output ports with and without SMF. As shown in this figure, the Brillouin threshold of the proposed BEFL with SMF are obtained at approximately 0 dBm and 2 dBm for port A and port B, respectively. The threshold power is higher at port B due to the cavity loss which is higher on the left side of the configuration. Without the SMF, the threshold power increases to a higher level due to the smaller Brillouin gain as shown in Figure 4.27.

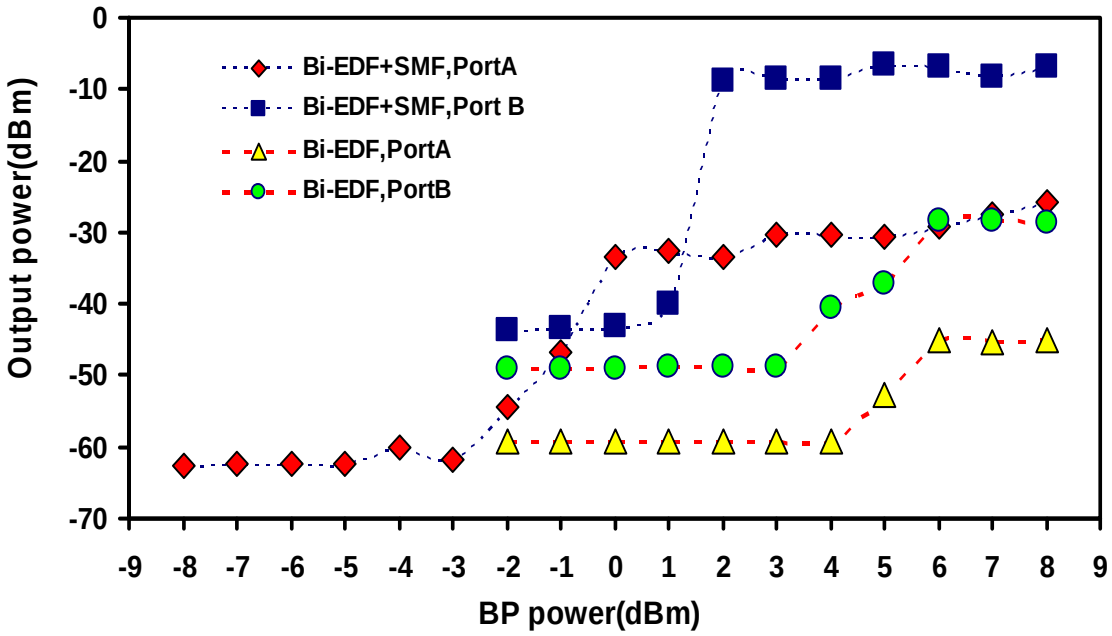

Figure 4.27: Output power against BP power for the BEFLs configured with and without SMF.

These results show that the above configuration is not efficient since the number of lines generated is limited. In the next section, an improved configuration of the BEFL is proposed. The new configuration is almost similar with this linear cavity design, which is arranged to reduce the cavity loss.

4.8 Enhanced Multi-wavelength BEFL with a Flat Output Spectrum

In the previous sections, we have demonstrated single and multi-wavelength BEFL with a Bismuth-based EDF in both a ring and linear cavity configuration. The linear cavity has shown to exhibit a lower threshold power compared with the ring configuration. In this section, a new multi-wavelength BEFL configuration based on linear cavity is proposed to increase the number of flat Stokes and anti-Stokes. This BEFL incorporates an optical

circulator at both ends to form a linear cavity for multi-wavelength light generation. This configuration is designed to have a lower cavity loss by injecting (tapping) a BP (output) from the side of the cavity. The configuration of the proposed BEFL is shown in Figure 4.28, which consists of a short Bi-EDF approximately 2.15 m in length with similar physical properties that was introduced earlier. The Bismuth based fiber is connected to the SMF and is pumped bi-directionally using two 1480 nm lasers. A SMF of 25 km in length is used as a nonlinear gain medium and WSC coupler is used to combine the pump and laser wavelengths. The coupler C1 is used to inject the signal BP from the TLS and C2 is used to tap the output signal for the OSA. The BP is injected into the linear cavity via C2 and is then amplified by the bi-directionally pumped Bi-EDF. The amplified BP is then coupled into the SMF to generate the first Stokes signal propagating in the opposite direction of the BP signal. The Stokes signal is then amplified by the Bi-EDF amplifier before being re-circulated by the OC2 ring cavity back towards the SMF. The 1st Stokes then travels towards OC1 where it is tapped by the coupler C1 for viewing at the OSA. As it travels, the 1st Stokes also generates the 2nd Stokes in the SMF, which will also travel towards OC1 and be re-circulated into the system, much like the 1st Stokes. This generation process continues as the incoming Stokes exceeds the threshold values for Brillouin gain, thereby providing cascaded Brillouin Stokes. The number of Stokes generated depends on the total gain of the Brillouin/ Bi-EDF amplifier over the cavity loss. The output of the linear cavity BEFL is tapped from the 5% port of C1 at OC1 and characterized by an OSA.

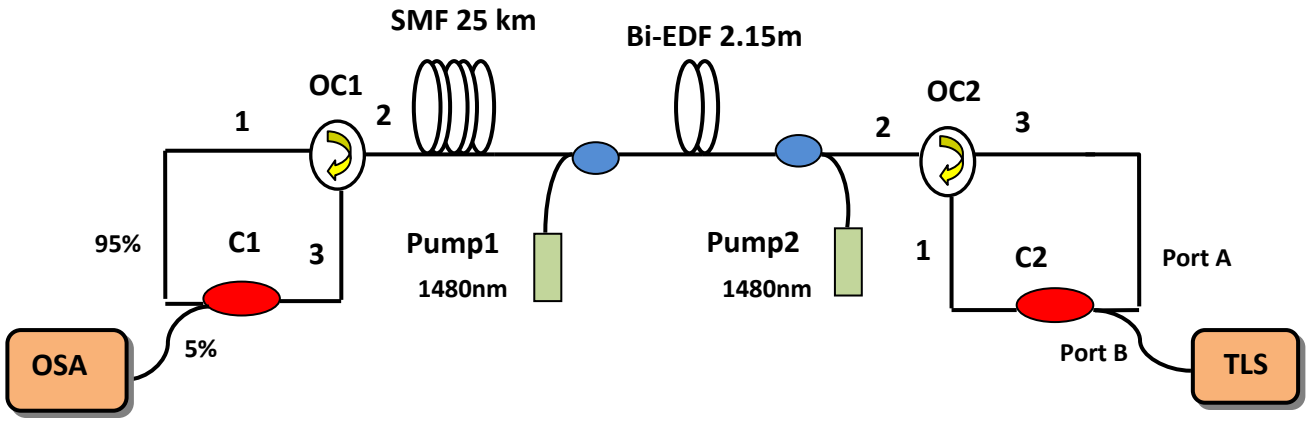

Figure 4.28: Experimental configuration of the proposed linear cavity BEFL.

The operating wavelength of the BEFL is determined by the gains of the bi-directionally pumped Bi-EDF over its cavity loss and this covers the L-band region (1560 nm–1600 nm). The free-running spectrum of the BEFL, which is taken without BP at a pump power of 120 mW for the two 1480 nm pumps is shown in Figure 4.29. In this experiment, C2 is a 99/1 coupler with the 99% output designated as port B. The peak wavelength is generated at the 1570 nm region, where the difference between the Bi-EDF gain spectrum and cavity loss is the largest. The free-running BEFL exhibits a peak power of approximately -30dBm with bandwidth of approximately 3 nm centered at 1570.5 nm. The chosen BEFL operating wavelength must be within or as close as possible to the bandwidth of the free-running BEFL (Figure 4.29).

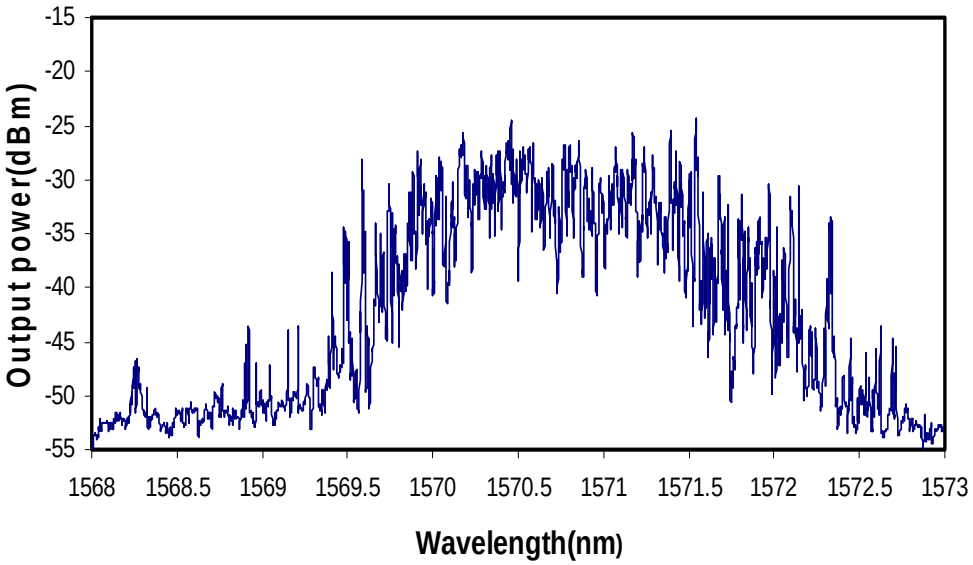

Figure 4.29: Free-running spectrum of the BEFL (without BP). The powers of P1 and P2 are fixed at 120 mW.

The impact of the coupling ratio of C2 on the number of Stokes and anti-Stokes generated by the BEFL is depicted in Figure 4.30. The 1480 nm pump and BP powers are fixed at 120 mW and 7 dBm, respectively. The BP wavelengths are optimized to 1570.7 nm, 1570.3 nm and 1568.5 nm for the coupling ratios of 50/50, 80/20 and 99/1, respectively. The coupling ratio of C2 controls the amount of BP power that is injected into the cavity which determines the reflectivity at OC2. A higher ratio at port B translates into a higher injected BP power and lower reflectivity of OC2. As shown in Figure 4.28, an increment of the port B ratio (50%, 80% and 99%) increases the number of lines of the BEFL output, but reduces the peak power of these lines. The reduction of the peak powers are due to the reflectivity of the OC2 ring, which subsequently increases the cavity loss. This also has the effect of shifting the operating wavelength of the BEFL which travels to the shorter wavelength region.

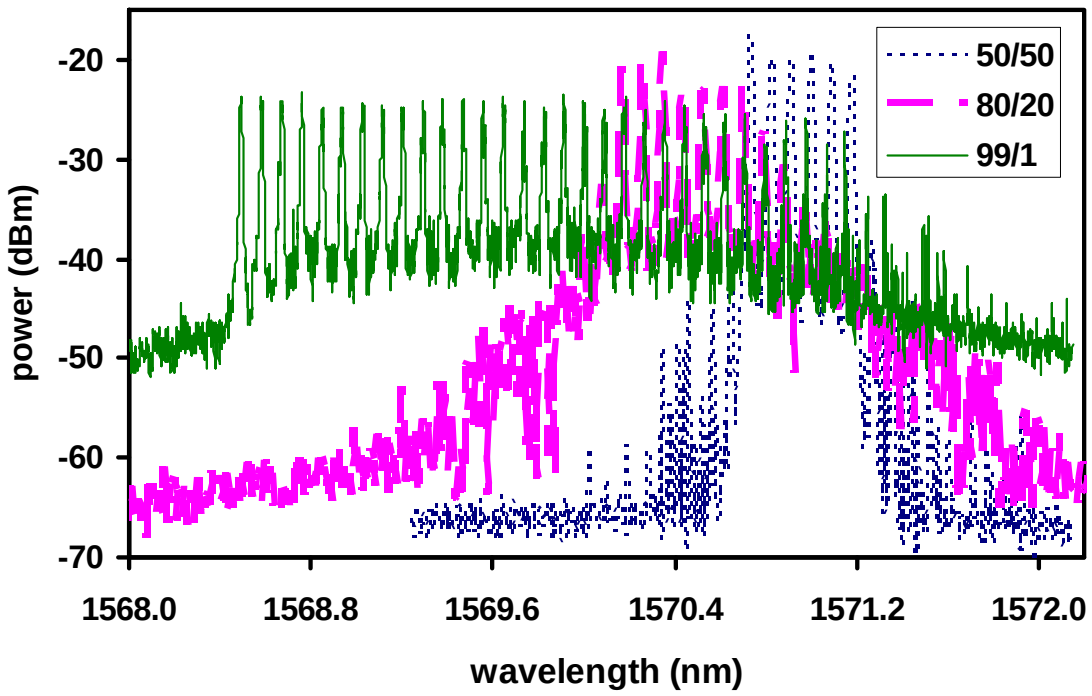

Figure 4.30: Output spectrum of BEFL at different C2 coupling ratios. The P1, P2 and BP powers are fixed at 120 mW, 120 mW and 7 dBm, respectively.

The impact of the 1480 nm pump power on the number of Stokes generated by the BEFL is depicted in Figure 4.31. The BP is set at a wavelength of 1569.0 nm, which is close to the lasing wavelength of the free-running BEFL and the BP power is fixed at 7 dBm. Both the 1480 nm pump powers are varied from 60 mW and 120 mW. Lower pump powers will not give any Stokes due to the low EDFA gain, and thus the minimum pump power is 60 mW. At a pump power combination of 60 mW and 100 mW, the least number of lines are generated as shown in Figure 4.31(c). However, as the combination pump power increases, the number of lines generated also increases. This can be attributed to the increment of the Erbium gain with increase in the pump power as this situation provides sufficient signal power for higher order Stokes signal to pump the SMF and maintain the cascading of the Stokes into multiple Stokes. As shown in the figure, the highest number of

lines is obtained with a pump power of 120 mW. The number of lines is higher in Figure 4.31(d) as compared with that in Figure 4.31(c) even though two pump power combinations are almost similar, due to gain characteristics of the bi-directionally pumped Bi-EDF amplifier. A higher gain is obtained if the signal is injected from the side with higher pump power.

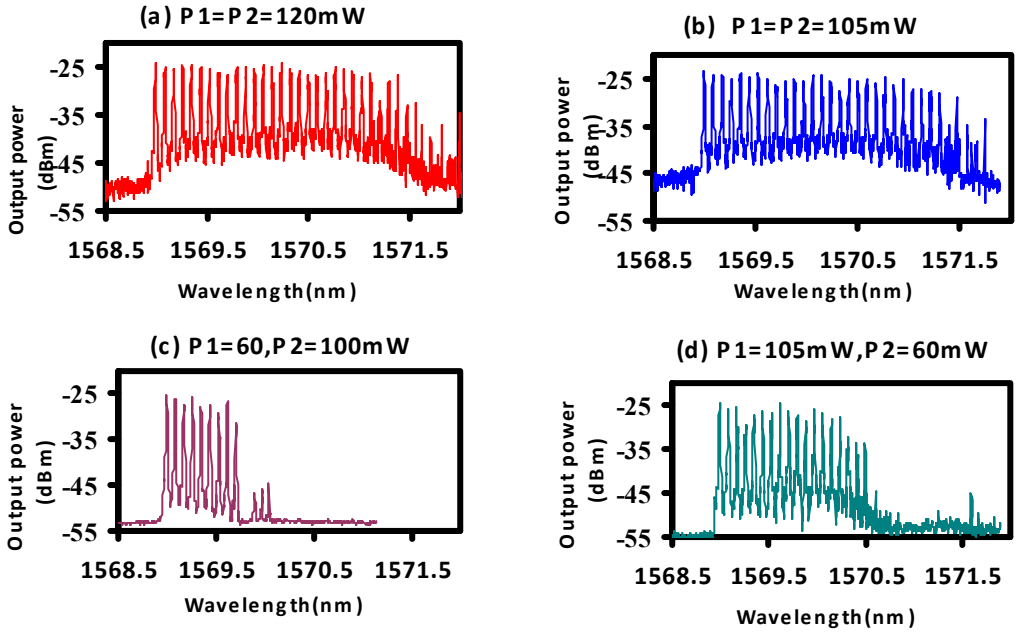

Figure 4.31: Multi-wavelength spectra at different combination 1480nm pump powers. The BP power and wavelength is fixed at 7dBm and 1569.0 nm, respectively. **(a)** P1 = P2 =120 mW, **(b)** P1 = P2 =105 mW, **(c)** P1 =60 mW, P2 = 100 mW and **(d)** P1 =105 mW, P2 = 60 mW.

Figure 4.32 shows the number of multi-wavelength lines as a function of BP wavelength at different BP powers. In the experiment, the BP wavelength is varied from 1568 nm to 1570 nm, which is close to the lasing bandwidth of the free-running BEFL and the BP power is varied from 3 dBm to 7 dBm. Both of the pump powers are fixed at 120 mW. Below a BP power of 3 dBm, the BEFL system operates with the presence of the free-running Bi-EDF laser cavity modes within the cascaded Stokes bandwidth. Therefore, the

experiment is not continued for BP powers below this power since the BEFL system is observed to be working in an unstable domain. The optimum BP wavelength is moving towards longer wavelength as the BP power reduces. The maximum multi-wavelength line of 50 is obtained at BP wavelength of 1568.2 nm and BP power of 5 dBm. As the BP moves farther away from this wavelength (1568.2 nm), less and less Stokes and anti-Stokes lines are observed as the gain decreases and becomes less and less sufficient to support the cascading process. If the BP is considerably far from the lasing bandwidth of the free-running BEFL, there is no gain to support the cascading process, and thus no Stokes lines are observed. The number of lines increases as the BP power increases from 3 dBm to 5 dBm as is expected when the BP power is increased as now more Stokes can be generated before the cascading process stops. But by increasing the BP power to 7 dBm, the number of Stokes decreased in the peak region. On the contrary, the number of Stokes was proportional to the intensity of Brillouin pump outside this wavelength range. This relationship to the intensity of Brillouin pump has its limit whereby the number of Stokes starts to reduce due to gain compression from the Brillouin gain.

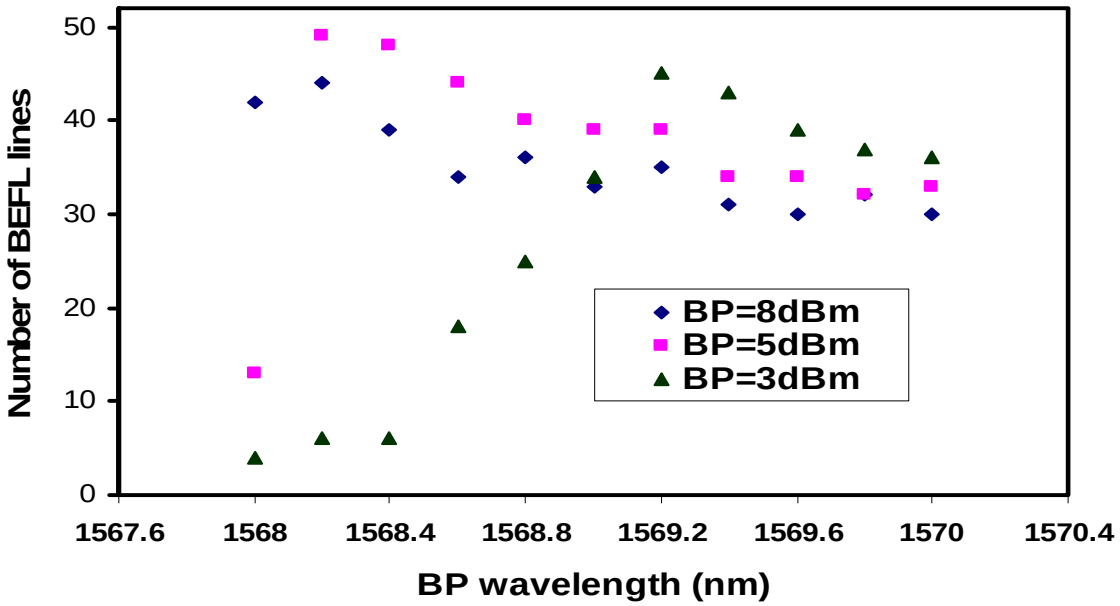

Figure 4.32: Number of BEFL lines against BP wavelength at different injected BP power. Both the P1 and P2 pump powers are fixed at 120 mW.

Figure 4.33 shows the output spectrum of the multi-wavelength BEFL at BP wavelength of 1568.2 nm and a BP power of 5 dBm. In this experiment, 50 multi-wavelength lines are obtained at the maximum pump power of 120 mW. However, a higher number of Stokes is expected at a higher pump power. The line spacing is approximately 0.09 nm in the wavelength domain and 11 GHz in the frequency domain while the 3 dB bandwidth of each line is about 0.02 nm, limited by the OSA resolution of 0.015 nm. Additionally, the power of each subsequent Stokes line is typically lower than that of the previous Stokes line, as each subsequent Stokes is generated with the energy of the previous Stokes, slightly reducing the Stokes line's power. However, some of the lines have a peak power, which is higher than the previous lines as shown in Figure 4.33. This is attributed to other phenomenon such as FWM, which will transfer energy from neighboring lines to this line. The multi-wavelength output of the BEFL is observed to be stable at room

temperature with only minor fluctuations observed coinciding with large temperature variances. The number of lines obtained in the proposed BEFL is higher as compared with the previous ring cavity BEFL configuration [16]. The linear cavity BEFL allows the lasing wavelength to pass the Bi-EDF gain twice per oscillation and thus increases the net gain per oscillation. This resulted in the linear cavity BEFL to exhibit a lower threshold power and achieves a larger number of Stokes and anti-Stokes compared with the ring configuration. The proposed BEFL using a short-length Bismuth-based EDF gain medium will allow for the development of compact BEFL devices. Further reductions in size can be obtained if the SMF is replaced with highly nonlinear fibers such as PCFs which will be discussed in next chapter. A PCF with a core diameter of ~1.6 μm would require less than 100 m to obtain the SBS effect desired [17] and FWM applications.

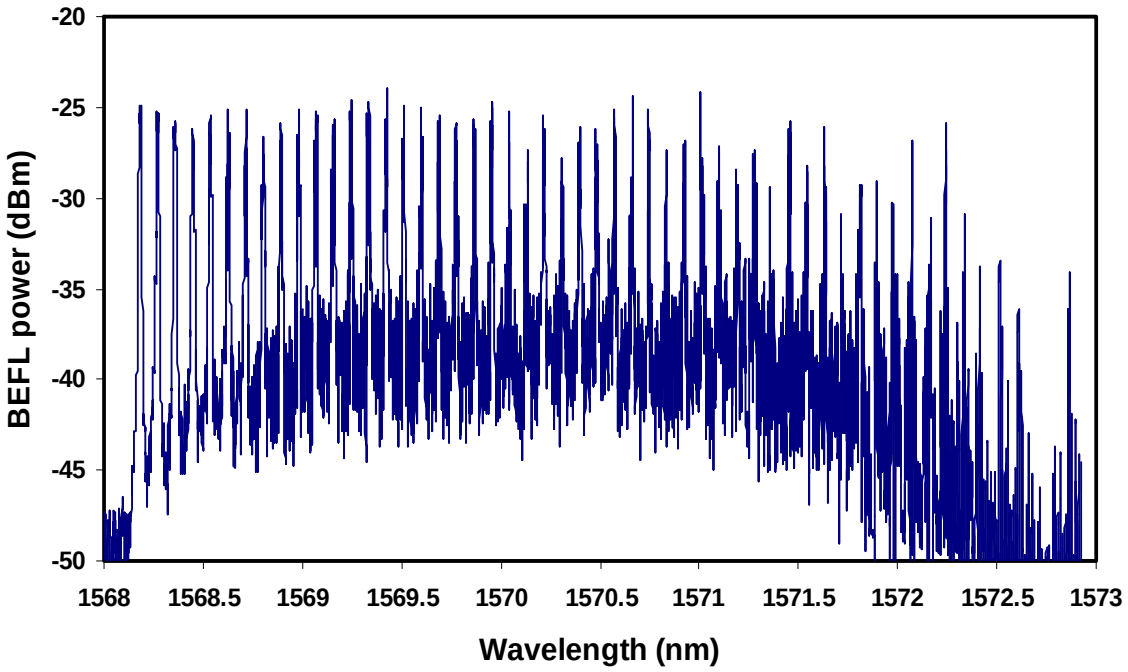

Figure 4.33: BEFL output spectra at BP wavelength of 1568.2nm and BP power of 5 dBm.

4.9 Multi-wavelength BEFL with Assistance of Raman Amplification

Various configurations have been proposed for multi-wavelength generation of BEFL in the earlier sections and also in many other literatures [18-21]. However, all these past approaches have to employ either a closed ring or Fabry-Perot cavity with efficient feedback mechanism. In this section, a new and simple multi-wavelength fiber laser configuration is proposed and demonstrated using a Brillouin-Rayleigh scattering with the presence of distributed Raman gain. In this setup, only one reflector is incorporated in the cavity while the DCF is used as a nonlinear gain medium. Figure 4.34 shows the configuration of the proposed hybrid multi-wavelength BEFL. It consists of two parts where the first is a forward pumped Bi-EDF and the second a midway isolator, a forward pumped DCF and a broadband FBG. The 49 cm long Bi-EDF is pumped by a 1480 nm laser diode via 1480/1550 nm WDM to provide amplification for the BP. A 7.7 km long, small core size DCF is used as a low threshold highly nonlinear Raman/Brillouin gain medium. Raman gain in 1540 nm region is provided using a 1440 nm Raman pump with the maximum power of 350 mW. The WDM is also used to combine the 1440 nm pump with the 1550 nm signals. A broadband FBG with a center wavelength of 1540 nm and a 3-dB bandwidth of 40 nm is used as a reflector at the output end of the BFL. The 10 dB output coupler is used to tap the output which is then characterised by an OSA.

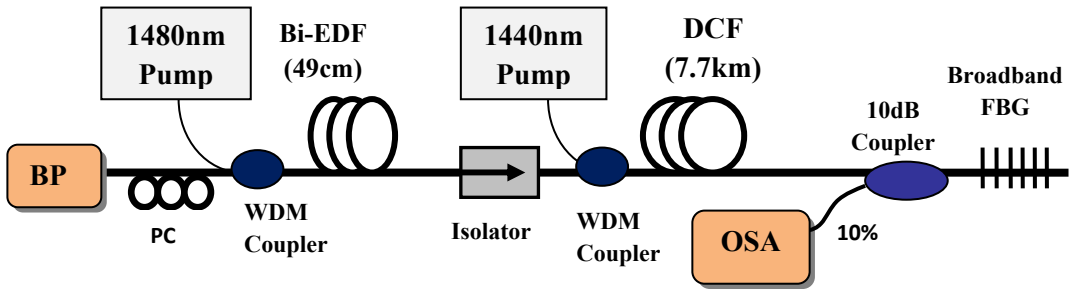

Figure 4.34: Experimental setup for multi-wavelength comb generation based Bi-EDF.

The principle of multi-wavelength generation can be explained by the coupling interaction between Brillouin and Rayleigh scattering processes, which is assisted by the Raman amplification. To intiate the SBS process, a TLS with a linewidth of approximately 20 MHz is employed as a BP. The BP is amplified by the forward pumped Bi-EDF and is then injected into the DCF. The FBG allows the injected BP to propagate twice in the DCF to generate a frequency shifted Brillouin Stokes. As the power of Raman pump increases, the Brillouin signal power exceeds the Brillouin threshold and generates another Brillouin Stokes in the opposite direction. Both forward and backward propagating Stokes oscillates and are then amplified by the Raman gain in the DCF section to generate a multi-wavelength comb as shown in Figure 4.35. This figure illustrates the measured output spectrum of the proposed BFLs with and without Raman pump when the BP signal power is fixed at 1mW. The Raman pump power is fixed at 350 mW. As depicted in the figure, the number of Stokes obtained is increased from 1 to more than 27 lines with the presence of Raman pump. Because of fast power growth and the increased interaction length that results from distributed Raman gain, the Brillouin scattered light works as a new BP source for the subsequent Brillouin Stokes generation. Rayleigh components that are concurrent with Brillouin Stokes components grow as well with Raman gain. Their coupled presence in this process reduces the threshold power for the subsequent Brillouin Stokes beams. The balance between these three scattering processes led to a flattened comb generation. Inset of Figure 4.35 shows the measured output spectrum of the BFL configured without the FBG. Without the FBG, the number of flat-amplitude lines obtained is only 17 lines, which is smaller than the proposed BFL. This is attributed to the reflectivity at the output end of the laser which is relatively lower without the FBG and thus reduces the number of lines. However, the reflectivity at both ends of DCF is more balance without the FBG which contributes to a flatter comb generation as shown in inset of Figure 4.35. We observed

power discrepancies in the odd and even numbered Stokes lines in the first 10 lines with FBG, after which the balance between the three types scattering leads to a flattened comb generation.

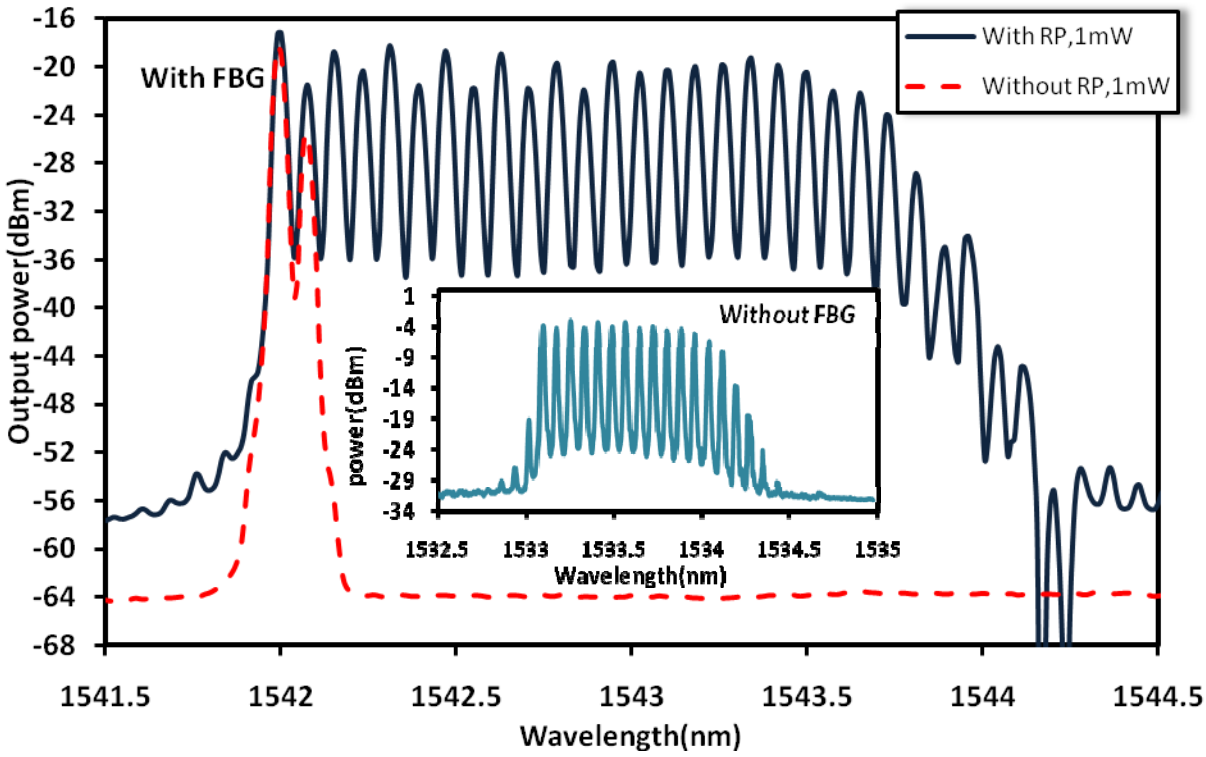

Figure 4.35: The multi-wavelength comb generation that includes and excludes Raman pump for the proposed BFL. Inset shows the comb spectrum for the BFL configured without the FBG.

Figures 4.36 (a) and (b) show the number of lines and flat-amplitude bandwidth of the proposed BFL against the BP wavelengths. In the experiment, the Raman pump power is also fixed at 350 mW and the BP signal power is varied from 0.15 mW to 4.5 mW. As shown in Figure 4.36 (a), the higher number of lines is obtained at BP wavelengths region which is close to the Raman peak gain. The highest number of lines of 27 (Figure 4.36 (a)), according to flat-amplitude bandwidth (Figure 4.36 (b)), is obtained at BP wavelengths of

1544 nm, 1542 nm and 1538 nm for the BP powers of 0.15 mW, 1 mW and 4.5 mW, respectively. This shows that the optimum BP wavelength shifts to a shorter wavelength, which is nearer to the Raman peak gain as the input BP signal power is increased. This is attributed to the Brillouin and Rayleigh scatterings, which is more pronounced at the higher BP power. Therefore, a higher Raman gain is required to balance the effect of these three scattering processes to obtain a wider bandwidth of flattened comb. The line spacing of the proposed BFL is measured to be approximately 0.09 nm.

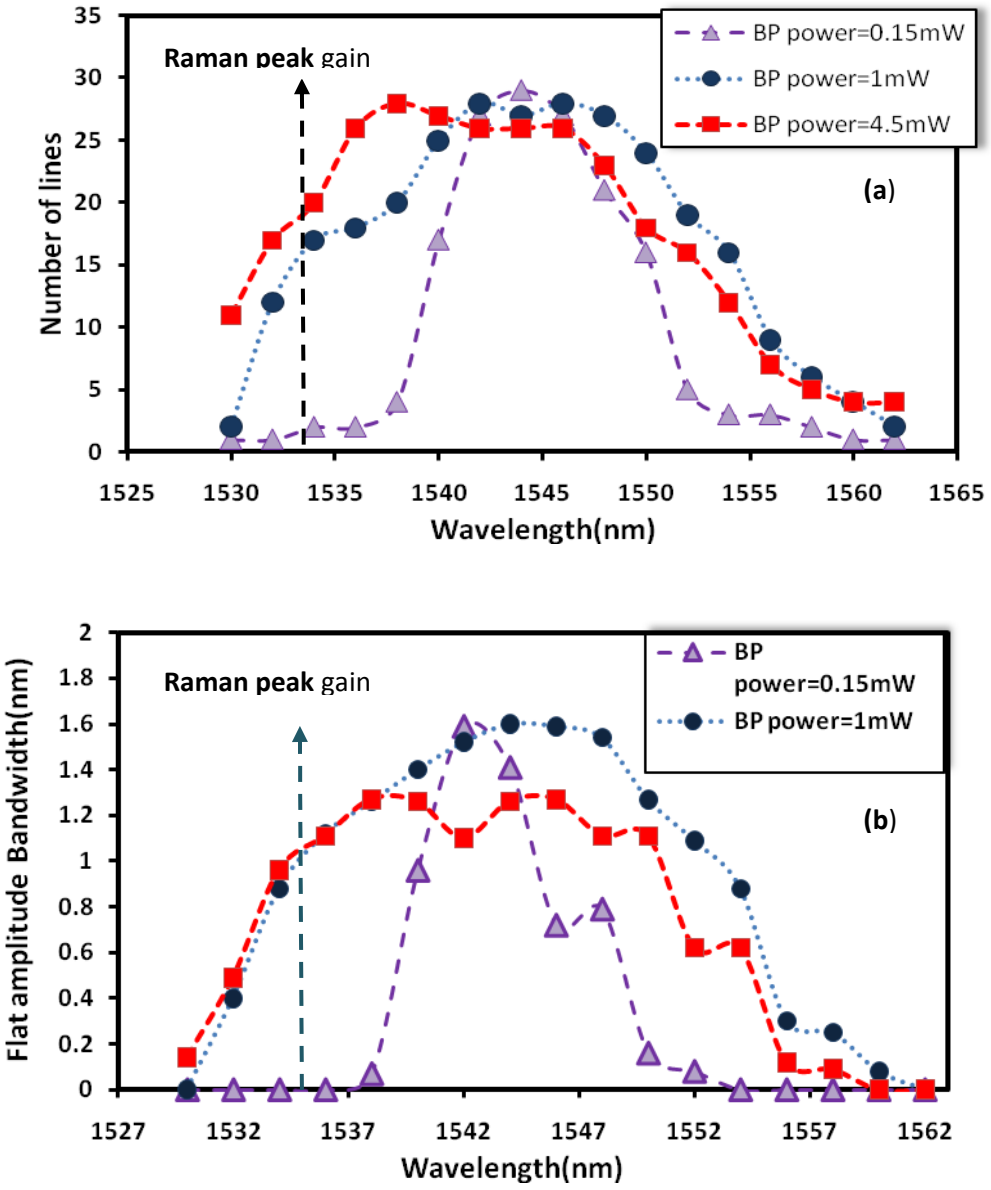

Figure 4.36: (a) The number of lines and **(b)** flat amplitude bandwidth against the injected BP wavelengths at various BP powers.

REFERENCES

[1] G. P. Agrawal, "Nonlinear Fiber Optics," Fourth edition, Academic Press, 2007.

[2] A. R. Chraplyvy, J. Lightwave Technol, "Limitations on Lightwave Communications Imposed by Optical-Fiber Nonlinearities," Vol. 8, No. 10, pp. 1548-557, 1990.

[3] M. R. Shirazi, S. W. Harun, M. Biglary, and H. Ahmad, "Linear cavity Brillouin fiber laser with improved characteristics," Opt. Lett. Vol.33, pp.770, 2008.

[4] S. Norcia, S. Tonda-Goldstein, D. Dolfi, and J. P.Huignard, " Two-wave mixing in an Erbium-doped fiber amplifier for modulation depth enhancement of optically carried microwave signals," Opt. Lett. Vol. 28, pp.1888, 2003.

[5] A. Loayssa, D. Benito, and M. J. Garde, "Optical carrier-suppression technique with a Brillouin- erbium fiber laser," Opt. Lett., Vol. 25, pp.197, 2000.

[6] G. J. Cowle, D. Yu, and Y. T. Chieng, J. LightwaveTechnol. "Multi-wavelength generation of L-band brillouin/erbium fibre laser," Vol.15, pp.1198, 1997.

[7] M. H. Al-Mansoori and M. A. Mahdi, "Brillouin-Erbium fiber laser with enhanced feedback coupling using common Erbium gain section," Opt. Express, Vol.16, pp. 7649, 2008.

[8] K. S. Abedin, "Single-frequency Brillouin lasing using single-mode As_2Se_3 chalcogenide fiber," Opt. Express , Vol.14, pp.4037, 2006.

[9] B. O. Guan, H. Y. Tam, S. Y. Liu, P. K. A. Wai, and N.Sugimoto, B. O. Guan, H. Y. Tam, S. Y. Liu, P. K. A. Wai, and N. Sugimoto, "Ultrawide-band La-codoped Bi_2O_3based EDFA for L-band DWDM systems IEEE Photon," Technol. Lett.,Vol.15, pp.1525, 2003.

[10] M. H. Al-Mansoori, M.K. Abdullah, B. M. Ali, M. A. Mahdi, "Hybrid Brillouin/Erbium fibre laser in a linear cavity for multi-wavelength communication systems," Optics & Laser Technology 37, pp.387–390, 2005.

[11] S. W. Harun, S. Shahi, H. Ahmad**, "**A compact Brillouin /Erbium fiber laser," Opt. Lett, Vol.33, pp.770-772, 2008.

[12] J. H. Lee, Z. Yusoff, W. Belardi, M. Ibsen, T. M. Monro, B. Thomsen, and D. J. Richardson, Conference on Lasers and Electro-Optics, Long Beach, USA, May 19–24, (CLEO 02), Technical Digest, Vol. 2, pp. CPDB5-1–CPDB5-3, 2002.

[13] Z. Yusoff, J. H. Lee, W. Belardi, M. Ibsen, T.M. Monro, and D.J. Richardson, Conference on Lasers and Electro-Optics, Long Beach, USA, May 19–24, (CLEO 02), Technical Digest, Vol. 1, pp. 50–51, 2002.

[14] R. K. Pattnaik, S. Texier, J. Toulouse, E. J. H. Davies, P. S. J. Russell, B. J. Mangan, CLEO 2003, Paper CWJ2, Baltimore, June 2003.

[15] C. J. S. de Matos , J.R. Taylor, K.P. Hansen, "All-fibre Brillouin laser based on holey fibre yielding comb-like spectra," Optics Communications, No.238, pp.185–189, 2004.

[16] N. S. Shahabuddin, S.W. Harun, M.Z. Zulkifli, K. Thambiratnam and H. Ahmad, "Bismuth-based Brillouin/Erbium fiber laser," J Modern Opt,Vol.55, No.8, pp.1345-1351, 2008.

[17] J. H. Lee, Z. Yusoff, W. Belardi, M. Ibsen, T.M. Monro, D.J. Richardson, "Investigation of Brillouin effects in small-core holey optical fiber: lasing and scattering," Opt Lett; Vol. 27, pp. 927–929, 2002.

[18] S. W. Harun, M. R. Shirazi and H. Ahmad, "A new configuration of multi-wavelength Brillouin fiber laser," Laser Phys. Lett., Vol. 5, pp. 48–50, 2008.

[19] M. R. Shirazi, N. S. Shahabuddin, S. N. Aziz, K. Thambiratnam, S. W. Harun and H. Ahmad, “A linear cavity Brillouin fiber laser with multiple wavelengths output,” Laser Phys. Lett., Vol. 5, pp. 361–363, 2008.

[20] M. N. Mohd Nasir, Z. Yusoff, M. H. Al-Mansoori, H. A. Abdul Rashid and P. K. Choudhury, Broadly Tunable Multi-wavelength Brillouin-Erbium Fiber Laser in a Fabry-Perot Cavity" **,** Laser Phys. Lett., Vol. 5, pp. 812-816, 2008.

[21] M. N. Mohd Nasir, Z. Yusoff, M. H. Al-Mansoori, H. A. Abdul Rashid and P. K. Choudhury, “Low threshold and efficient multi-wavelength Brillouinerbium fiber laser incorporating a fiber Bragg grating filter with intra-cavity pre-amplified Brillouin pump,” Laser Phys. Lett., Vol. 6, pp. 54-58, 2009.

CHAPTER 5

MULTI-WAVELENGTH BISMUTH ERBIUM DOPED FIBER LASER ASSISTED BY FOUR-WAVE MIXING EFFECT

5.1 Introduction

Optical nonlinear effect in fiber optics is one of the interesting topics which has many applications in the development of optical fiber devices. This effect is originated from the nonlinear refractive index (optical Kerr effect) and is responsible for many phenomenon such as self-phase modulation (SPM), cross phase modulation (XPM) and four-wave mixing (FWM) [1-2]. In the FWM process, light is generated at new frequencies through the conversion of optical power from the original signal wavelengths, or in quantum-mechanical terms FWM occurs when photons from one or more waves are annihilated and new photons are created. These new photons are created when two or more frequencies of light propagate through a nonlinear medium, provided that the condition known as phase matching is satisfied. The phase-matching is a function of pump power, signal spacing and chromatic dispersion [3]. Two photons of the pump source generate two sidebands (Stokes and anti-Stokes or signal and idler waves [1]), which must be phase matched along the fiber length for optimum efficiency. However, it is difficult to maintain the phase matching over a long length of fiber. Therefore, many research works have been focused on achieving FWM effect in the highly nonlinear fibers such as dispersion shifted

fiber (DCFs) and photonic crystal fibers (PCFs) [4, 5]. These fibers have a large nonlinear coefficient and the FWM can be achieved using a very short fiber segment.

The FWM effect can be used to achieve multi-wavelength laser operation that is useful for applications in wavelength converters [6], optical parametric oscillator (OPO) as well as laser source for the WDM system. In the previous chapter, Bismuth-based Erbium-doped fiber (Bi-EDF) was demonstrated to have a very high nonlinear characteristic. In this chapter, a FWM effect is demonstrated in various types of fibers including the Bismuth-based EDF, where the interaction between a pump and probe signals generate sidebands. The FWM effect is then employed to produce a multi-wavelength laser source using a Bi-EDF as a gain medium. This effect is also used to estimate some of the nonlinear parameters such as nonlinear coefficient and refractive index coefficient of the Bi-EDF.

5.2 FWM Effects in Open-loop Cavity System Using Various Gain Medium

The schematic diagram of the proposed experimental setup to generate FWM signals in various fibers is shown in Figure 5.1. Two input pump waves from two tuneable laser sources (TLS1 and TLS2) are combined by a 3-dB coupler before they are injected into a 49 cm long Bismuth Erbium doped fiber (Bi-EDF). The Bi-EDF is optically pumped by a 1480 nm laser diode (LD) with maximum power of 160 mW through a wavelength selective coupler (WSC). Polarization controllers (PC) are used to adjust the input waves into the same state of polarization and optimize the FWM efficiency. Finally, the output from the Bi-EDF is monitored by an OSA. In this experiment, the wavelength of TLS1 is fixed and TLS2 was tuned within a C-band wavelength region. The Bi-EDF has a nonlinear coefficient of ~60 $(W \cdot km)^{-1}$ at 1550 nm. The other physical properties of this fiber have

been discussed in the previous chapters. The experiment is repeated for L-band region by replacing the Bi-EDF to a length of 215 cm.

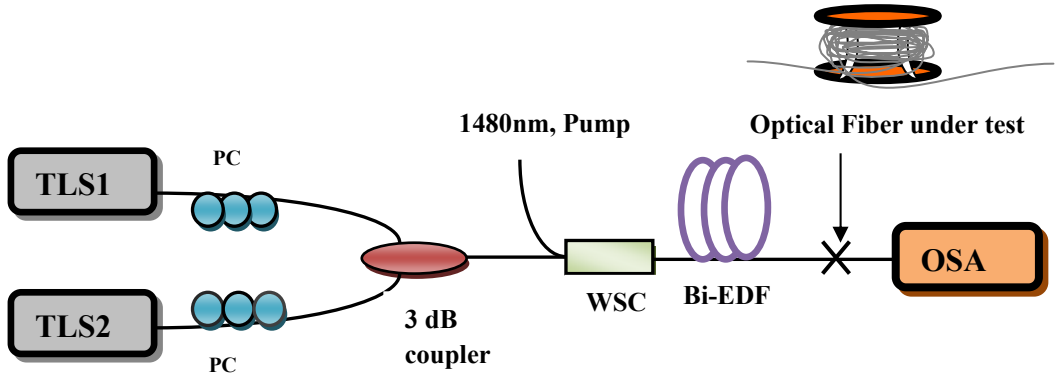

Figure 5.1: Experimental setup for the observation of FWM induced sidebands in different fibers under test.

Figures 5.2 show the output spectrum after the Bi-EDF where the spectral spacing of the two wavelengths was fixed at 0.5 nm. However, sideband signals are not observed with only 49 cm length of Bi-EDF at C-band region in comparison with 215 cm Bi-EDF at L-band region. The output powers of the dual signals are obtained at approximately 9 dBm for both C-band and L-band Bi-EDFA (Figures 5.2(a) and (b)). With 215 cm long Bi-EDF, the small sideband signals are observed due to the increased interaction length in this system. The dual input signals interact with each other to generate a sideband using FWM phenomena.

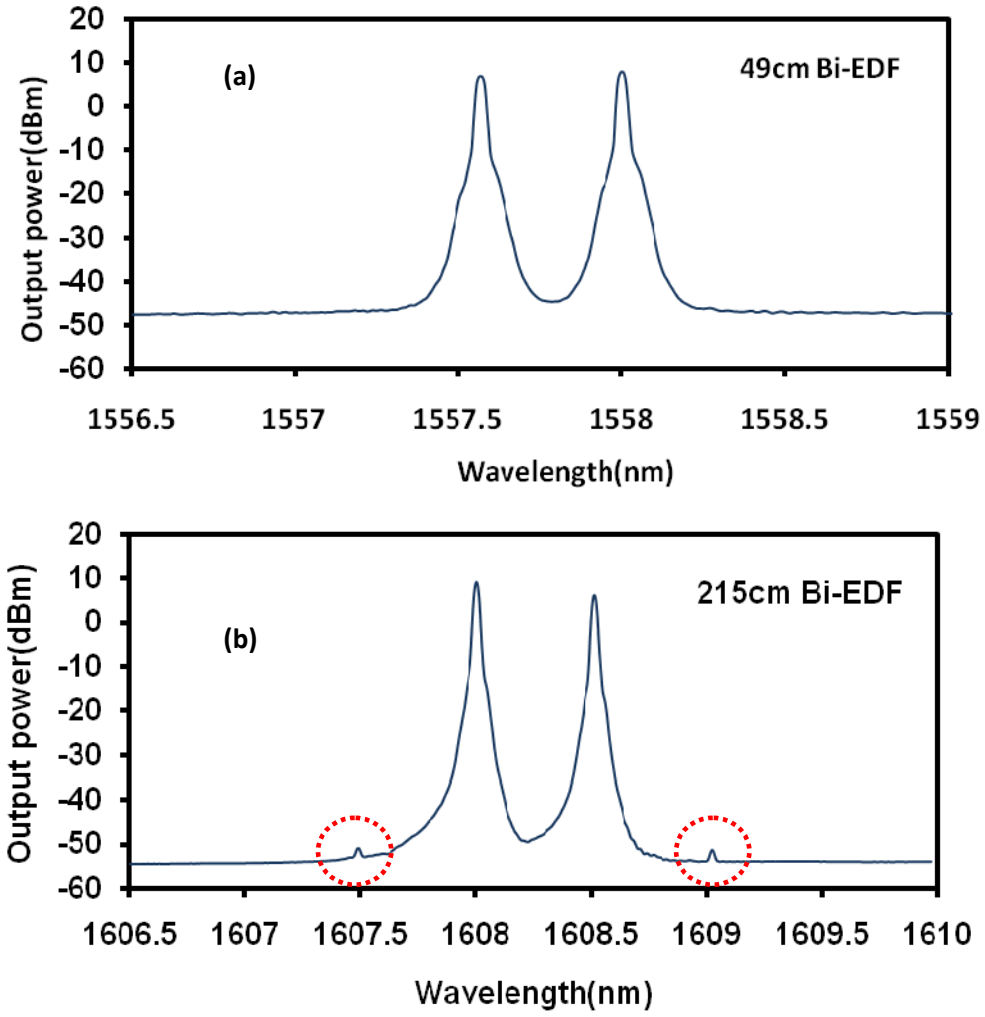

Figure 5.2: A comparison of dual-wavelength output spectrum at 0.5 nm spacing of **(a)** 49 cm and **(b)** 215 cm Bi-EDF in C- and L- band region, respectively.

In continuing of our analysis, we incorporate a piece of fiber after the Bi-EDF (49cm) to investigate the FWM effect inside the fibers. The optical spectra of dual-wavelength outputs of SMF, PCF and Bismuth-based fiber are compared in Figure 5.3. In this experiment, the spectral spacing has been tuned from 0.3 nm to 1 nm. As shown in the figure, many sideband signals are observed especially with 25 km long SMF. The

sidebands are more pronounced as the spacing of the dual input signals reduced. The noise power level is lower with the SMF by about 5 dB as shown in Figure 5.3. This is due to the insertion loss of the SMF which is about 0.2 dB/km. As also shown in Figure 5.3, the SBS effect is more pronounced in SMF to generate multi-wavelength comb with 0.08 nm spacing. This is attributed to the extremely long length used (25 km) and lower nonlinear coefficient in this fiber which contributes to the SBS generation. A small sideband is also observed with a short length of PCF (20 m) and Bismuth-based fiber (2 m). The Bismuth-based fiber is an un-doped fiber with a numerical aperture of 0.2.

Figure 5.4 compares the sideband (idler) peak power against the channel spacing for all types of fiber tested. As shown in the figure, the PCF and Bismuth have stable idler peak power against spacing. The idler peak power is highest at 0.3 nm spacing with SMF but the peak power significantly reduces as the spacing increases. This is attributed to the group velocity dispersion (GVD) as well as the insertion loss characteristics of the fiber, which increases with the increasing of the fiber length. It is very difficult to maintain the phase matching characteristic in a very long fiber and therefore the FWM is more pronounced in the PCF and Bismuth-based fiber as shown in Figure 5.4 especially at a wider spacing.

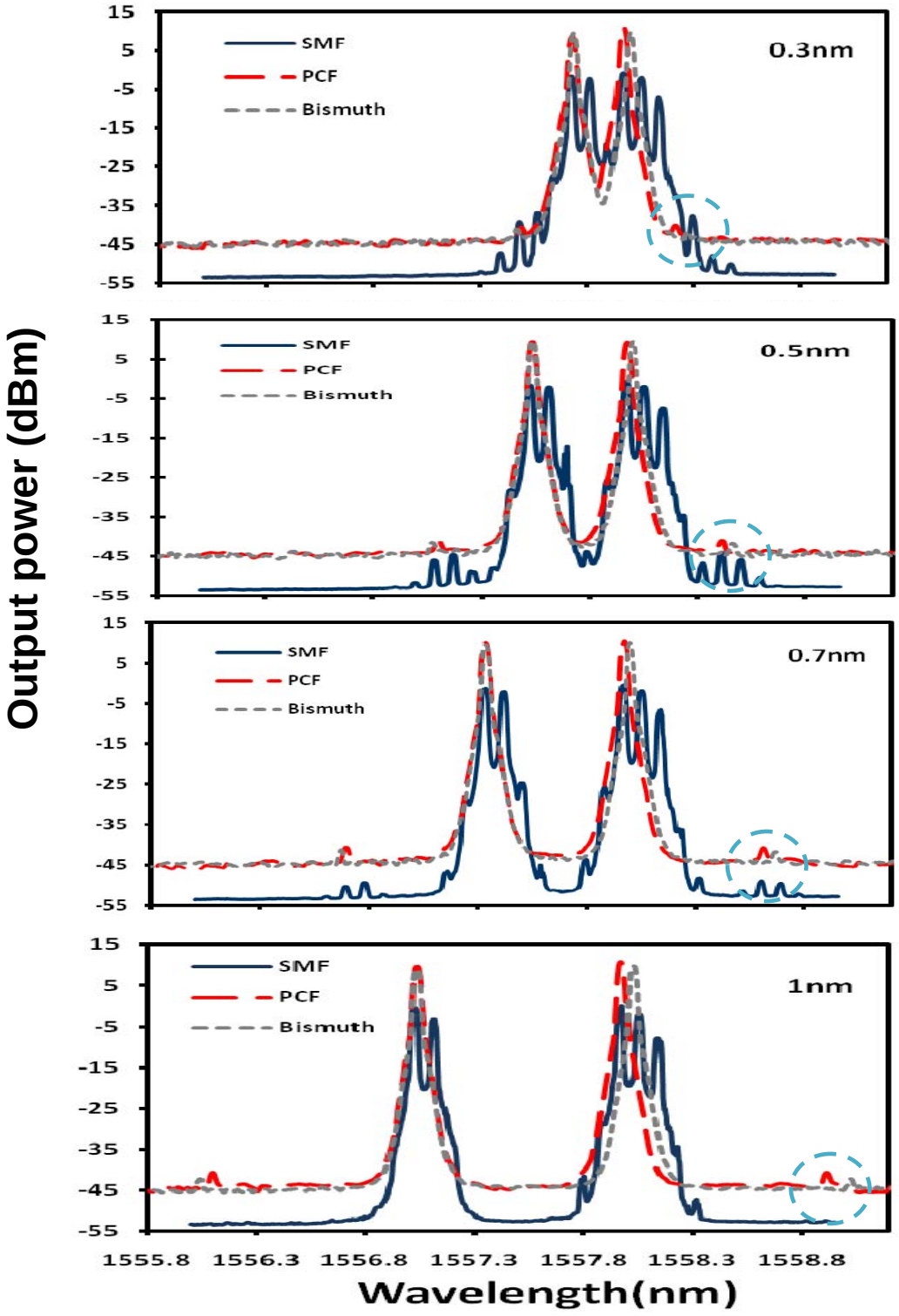

Figure 5.3: Optical spectra obtained from the different spacing tunable dual-wavelength source using SMF, PCF and Bismuth.

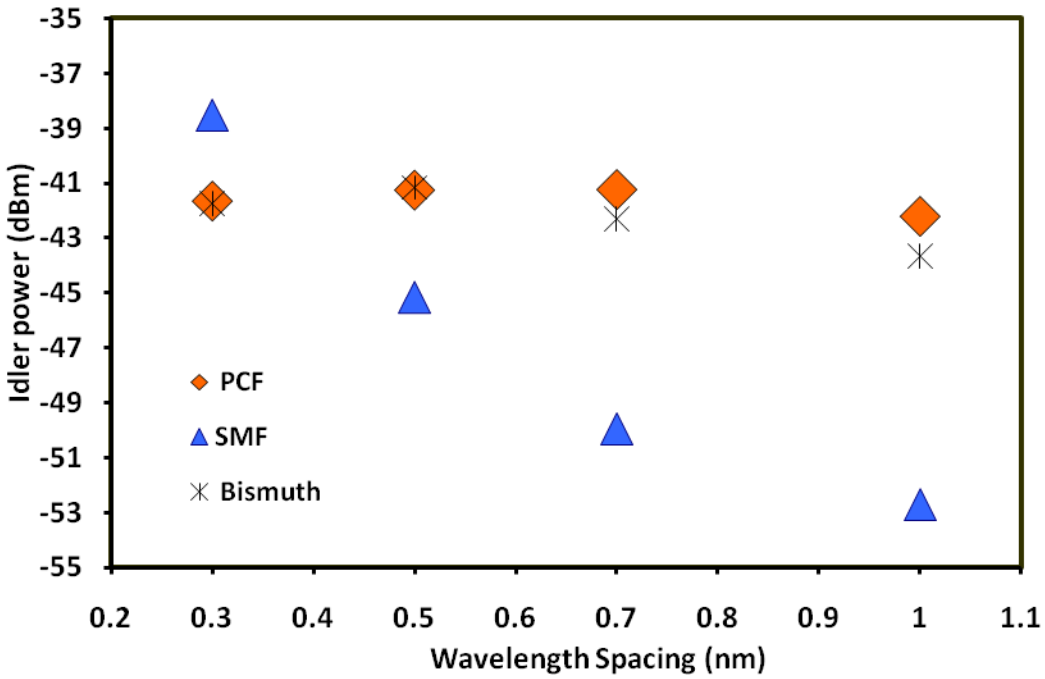

Figure 5.4: A comparison of idler output power of three fibers as a function of wavelength spacing.

Figure 5.5 proposes the power ratio of the generated idler wave over the input signal, which determine the conversion efficiency of the FWM process for all the fibers tested. The conversion efficiency is maintained for every channel spacing (of maximum 1nm) for both PCF and Bismuth-based fiber. However, the efficiency reduces as the channel spacing increases from 0.3 nm to 1 nm for the SMF. The highest conversion efficiency is obtained with the 20 m of PCF as shown in the figure. As discussed in chapter 2, the PCF has a high Kerr nonlinearity, n_2 which can securely confine light within the core. Therefore, the FWM effect is sufficiently large in this fiber.

.

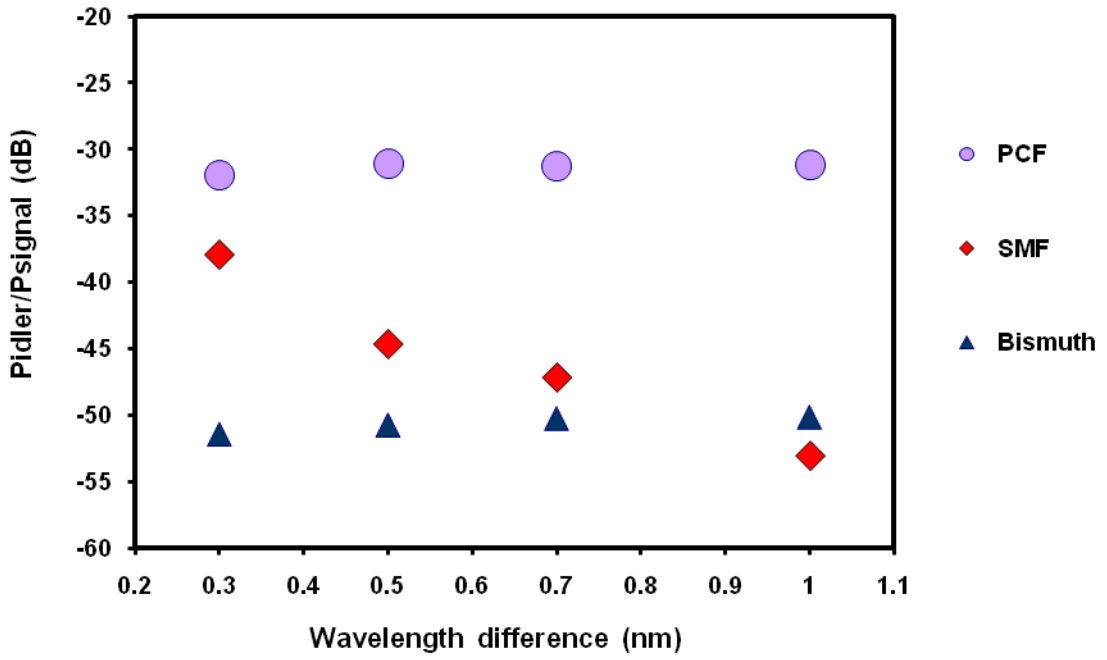

Figure 5.5: Ratio of idler power to input signal power as a function of the different spacing wavelength signals.

The experiment is also repeated with the use of 215 cm Bi-EDF in conjunction with PCF. The amplification region of 215 cm long Bi-EDF cover the extend L-band when pumped with a 1480 nm laser pump, and therefore two input signals are selected approximately 1608 nm, which is near to the peak gain region of the Bi-EDFA. Figure 5.6 shows the measured output optical spectrum with and without the 20 m long PCF. As shown in the figure, weak FWM signals are observed for both spectra. The ratio of idler to signal power is also improved with the PCF. However, the peak power and noise level of the spectrum is lower with the PCF due to the insertion loss of the fiber and connectors used.

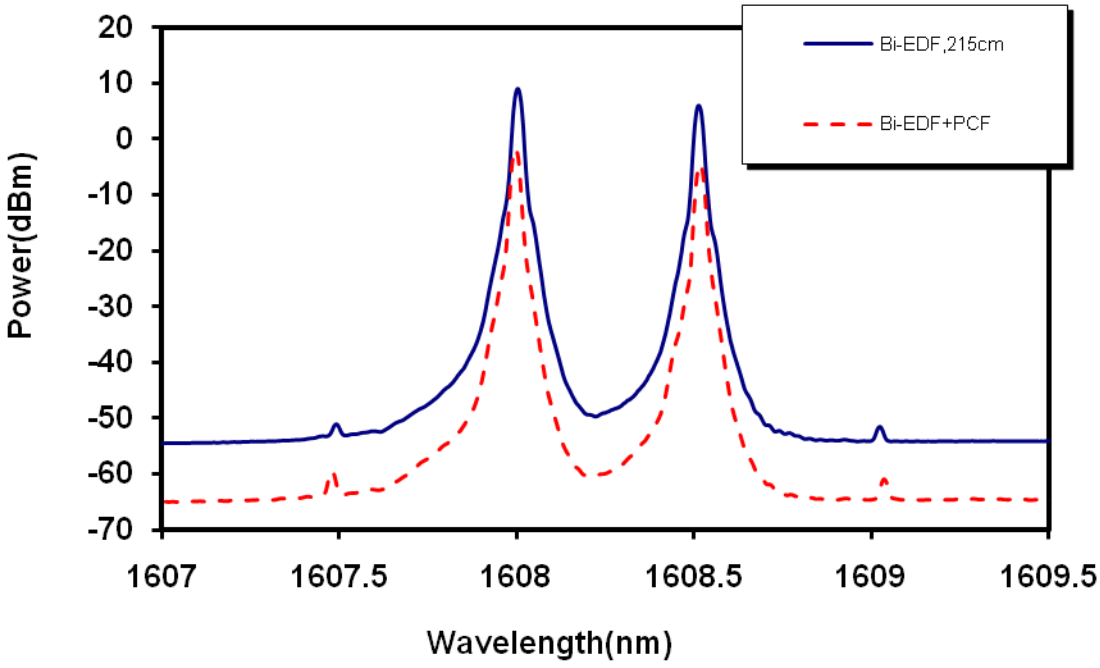

Figure 5.6: Measured optical spectrum in 0.5 nm spacing between two signals.

Figure 5.7 shows the ratio of the idler power to the signal power as a function of wavelength for both system configured with and without the PCF. In this signal, the input signal spacing is fixed at 1nm and the wavelength of the idler signal is varied from 1607 nm to 1613 nm, which covers most of the gain region of the Bi-EDFA. As shown in Figure 5.7, the ratio is improved with the PCF especially at a shorter wavelength region. At wavelength of 1611.5 nm and above, the Erbium gain and ASE levels are the highest and therefore the degenerative FWM signals are suppressed by the noise. The optical properties of the fiber such as nonlinear coefficient can be evaluated from the degenerative FWM signals as described in chapter 2. In comparison with conventional optical fibers, the significant FWM in PCF can occur at relatively low peak powers and over short propagation distances, and such processes can be possible in a much wider wavelength range [7]. In the next section, the FWM effect in a ring resonator will be investigated.

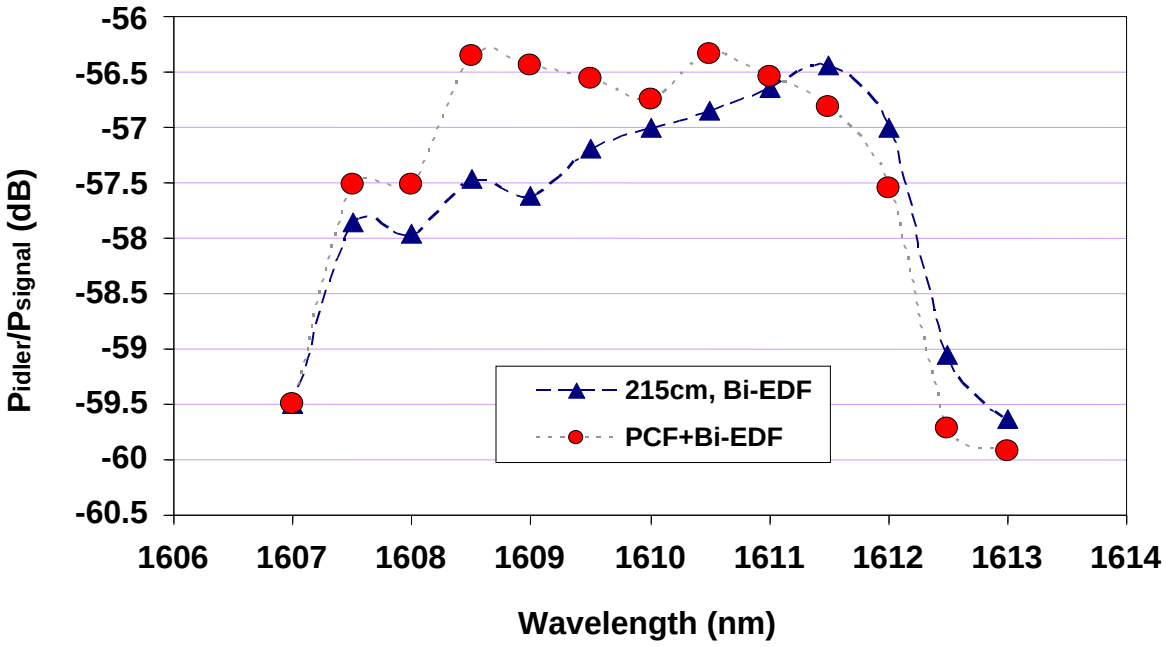

Figure 5.7: The ratio of the idler power to the signal power as a function of wavelength for the system configured with and without the PCF.

5.3 Enhanced FWM Efficiency of Bi-EDF in a New Ring Configuration for Determination of Nonlinear Parameters

In our earlier work, Bi-EDF was demonstrated to have a very high nonlinear characteristic, which creates a possibility to implement a range of nonlinear optical signal processing devices with only a meter or less of the fiber. Recently, Bi-EDF based ring fiber lasers have also been demonstrated with a tunable single wavelength operation [8]. These lasers provide a wide tuning range as well as a high signal to noise ratio. In the previous section, a FWM effect has been demonstrated in open loop using a piece of 215 cm long Bi-EDF. The FWM can be used to evaluate nonlinear coefficient γ, a function of nonlinear refractive index n_2 which is usually used to define the nonlinearity of the fiber. In this section, a ring fiber laser is proposed using a reduced length of Bi-EDF to generate FWM

signals and determine the nonlinear parameters of the fiber. The proposed method is based on CW dual-wavelength measurement technique [9, 10] in the L-band region. It is possible for this method to give accurate values of nonlinear parameters of the fiber using only a simple measurement setup.

Figure 5.8 shows the schematic diagrams for the proposed experimental setup to generate FWM signals in Bi-EDF using a ring configuration. Two input pump waves from two tunable laser sources (TLS1 and TLS2) are combined by a 3-dB coupler before they are injected into a 215 cm long Bi-EDF. The Bi-EDF is optically pumped by a 1480 nm laser diode (LD) with maximum power of 150 mW through a wavelength selective coupler (WSC). The PCs are used to adjust the input waves into the same state of polarization and optimize the FWM efficiency. The two combined pump waves are injected into the ring resonator using an 80/20 coupler. In this experiment, the two pump wavelengths with the spacing of 1nm are optimized at 1612 nm and 1613 nm wavelength region, respectively, which are near to peak power of free running spectrum (without signal) of the ring laser. Then, an isolator is employed to block the backward ASE power generated by the Bi-EDFA in ring. The 90/10 coupler is used for monitoring and tapping out the laser to OSA. The experiment is also repeated for the open configuration of Figure 5.1 using the same gain medium.

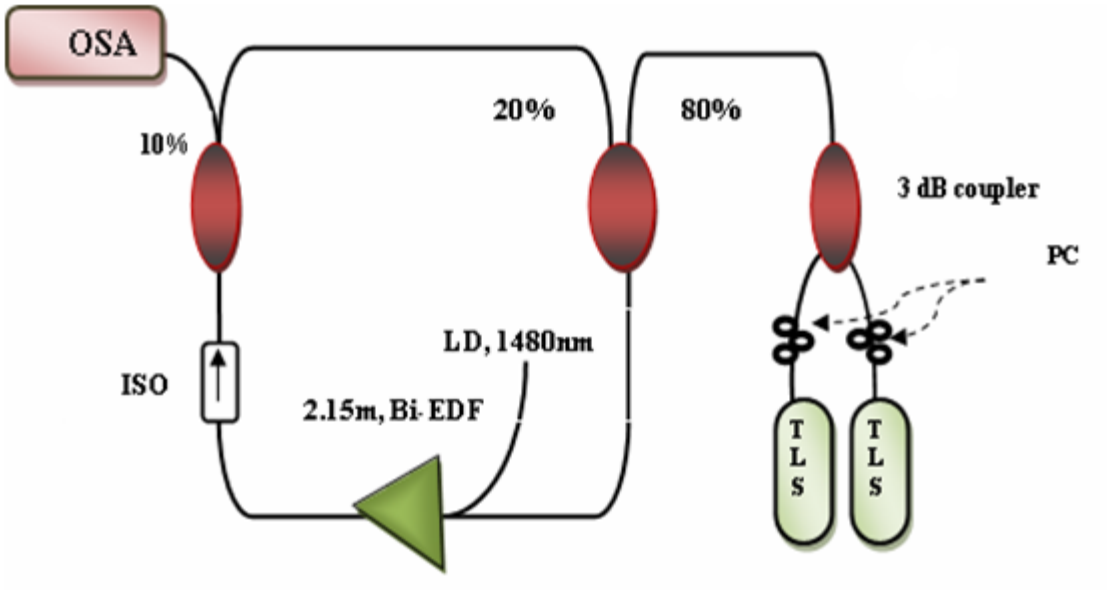

Figure 5.8: Experimental setup based on CW dual-wavelength method in ring Bi-EDF laser configurations.

In the experiment, the two input waves are deliberately set at 1612 nm and 1613 nm with a detuned wavelength of 1 nm in both open and ring configurations. The output spectra of the two configurations are shown in Figure 5.9. In the comparison of sideband power between the two setups, ring cavity achieves a higher power value which is approximately 9 dB higher than that of the sideband power generated in the open configuration. Two types of FWM may happen due to the interaction between signal wavelengths selected in Erbium gain region or free running laser area. The first type of FWM generates a new wave at the frequency of $\omega_4 = \omega_1 + \omega_2 - \omega_3$, whenever three waves of frequencies ω_1, ω_2 and ω_3 are co-propagate inside the fiber and three photons transferring energy to a single photon at frequency ω_4. Another type corresponds to the case in which two photons at frequencies ω_1 and ω_2 are annihilated, while two photons at frequencies ω_3 and ω_4 are created simultaneously such that $\omega_1 - \omega_3 = \omega_2 - \omega_4$ that

correspond to this work. The degenerate case ($\omega_1 = \omega_2$), which often occurs in optical fibers, can be initiated with a single pump beam. A strong pump wave at ω_1 creates two sidebands located at frequencies ω_3 and ω_4 with frequency shift of $\Omega_S = \omega_1 - \omega_3 = \omega_4 - \omega_1$ (we assumed $\omega_3 < \omega_4$). If a weak signal at ω_3 is also launched into the fiber with the pump, the signal is amplified while a new idler wave at ω_4 is generated [1]. Furthermore, the maximum FWM efficiency (MFE) wavelength is equal to the center frequency between v_1 and v_2, i.e., $(v_1 + v_2)/2$, when the generation efficiencies at $2\,v_1 - v_2$ and $2\,v_2 - v_1$ are equal [11], similar to the results in Figure 5.9.

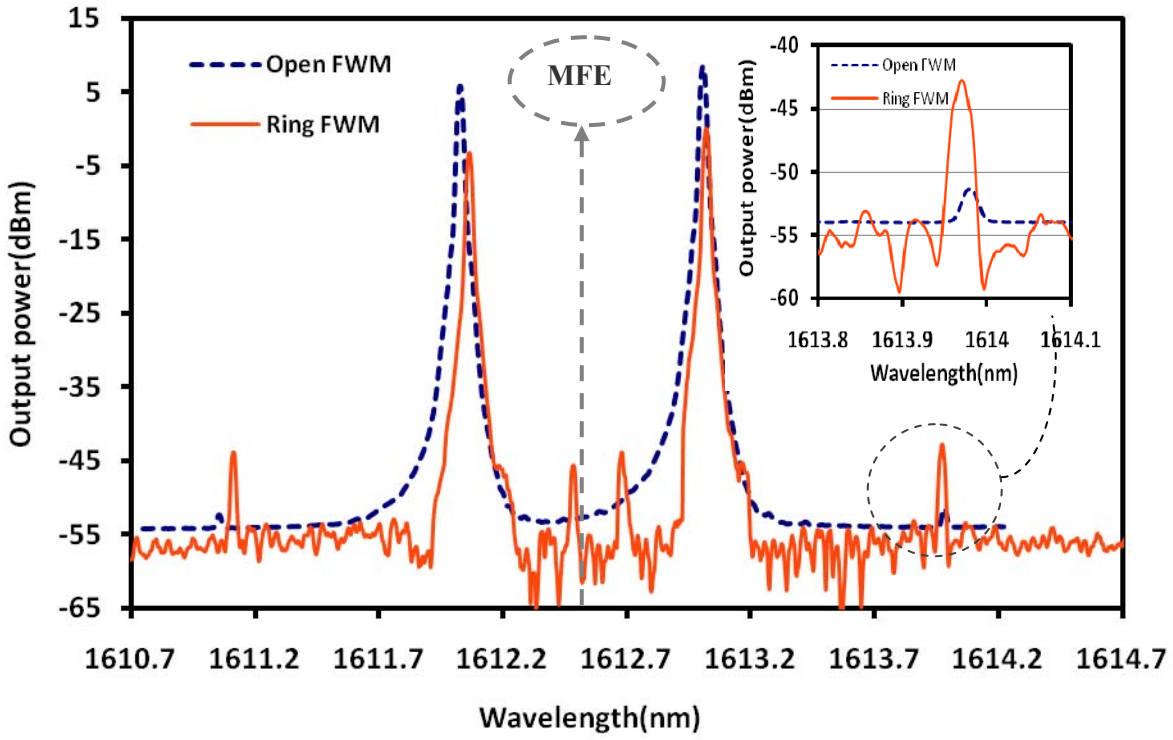

Figure 5.9: Output spectrum of the CW FWM method in ring based only Bi-EDF, spacing between two signals (1612 nm and 1613 nm) is 1nm.

The sidebands travel along with the original waves and develop at the expense of the signal strength input [12]. The existent of optical sidebands can be determined by using Eq. (5.1)

$$M = \frac{N^2}{2}(N-1) \tag{5.1}$$

where N is the number of optical waves pumped into a fiber [13]. When channels are not equally spaced, most FWM components fall in between the channels and add to the overall noise [14]. This phenomenon is shown in Figure 5.9 by employing only 215 cm of Bi-EDF in the ring cavity fiber laser. In the open configuration, the power difference of two signal lasers λ_1 and λ_2 was in interval power of 2.9 dB ~ 3.7 dB that is due to systematically error of the two TLS. If two intense signals with small wavelength separation are launched into a single fiber, SPM acts on the beat envelope to create sidebands in the wavelength domain. Then, the optical power ratio of the input signals to the idler is related to the nonlinear phase shift φ_{SPM} [14].

The magnitudes of optical Kerr effects are depend on the non-linear parameters like γ and n_2 or n_2/A_{eff}, where A_{eff} is the effective area of the light mode. It is therefore important to have a simple and accurate method for the determination of these parameters. The nonlinear refractive index n_2 in optical fibers is responsible for a large variety of nonlinear effects, such as SPM, XPM, FWM and soliton formation. One of the important properties of n_2 is its dependence on the polarization state of the field that in a long fiber, where the polarization state varies during its propagation along the fiber [15].

FWM effect produces sidebands whose amplitudes and frequencies depend on the nonlinear parameter γ (Figure 5.9). When the input wave is degenerated (λ_1 close to λ_2), then the power of FWM as mentioned by Eq.(2.32) [16]

$$P_{FWM}= \eta\, P_s\gamma^2\, P_p^2\{1-\exp(-\alpha L)/\alpha\}^2= \eta\, P_S\gamma^2\, P_P^2\,(L_{eff})^2 \qquad (5.2)$$

where P_P, P_S and L is the input pump power, transmitted signal power and the interaction length between the pump and signal, respectively. η is the FWM efficiency and it is dependent on the wavelength difference between the pump and signal. The efficiency is higher if the two selected input pump waves are close and near to zero dispersion wavelengths. From Figure 5.9, the P_P, P_{FWM} and P_S values are obtained at 150 mW, 3.14×10^{-5} mW and 0.39 mW, respectively. By replacing the power values into the Eq. (5.2), γ is estimated to be around 59.16 ($W^{-1}Km^{-1}$) for 215cm length of Bi-EDF. The γ value is also theoretically calculated to be approximately 58.3 ($W^{-1}Km^{-1}$) with material parameters of Bi-EDF in 1550 nm using Eq. (2.40).

Furthermore, the powers of the FWM sidebands were measured and used to estimate a value of n_2/A_{eff} which is equal to 1.51×10^{-8} (W^{-1}) at an input signal of 1612 nm using the Eq.(2.40) for the test fiber. Finally, the nonlinear index coefficient n_2 is measured to be approximately 4.40×10^{-19} (m^2/W), which is more than 10 times larger than that of silica. This parameter in the 1550 nm region is about 4.23×10^{-19} (m^2/W) when calculated by the theoretical method. However, the experimental and systematical errors in single mode fibers and another components in the configuration have contributed to the small discrepancy for these two estimated values of γ and n_2. By obtaining γ and n_2, it is possible to find another parameter like the nonlinear phase shift φ_{SPM}, conversion efficiency, phase mismatch Δß, chromatic dispersion coefficient and figure of merit (FOM = $\gamma.L_{eff}$) that is beyond our aims in this research.

Later, the power ratio between the idler (left hand) and signal waves was plotted for the 215 cm long Bi-EDF in Figure 5.10 as a function of the first input signal wavelength (λ_1) at the extended L-band wavelength region from 1606 nm to 1614 nm. In this case, the spacing between two signals (λ_1 and λ_2) is fixed at 1 nm. As shown in the figure, the average difference between power ratios between the two configurations is approximately 16 dB. However, the ring cavity design which allows a longer interaction between matter and light covers greater efficiency especially in Erbium gain area at the extended L-band region. Furthermore, MFE is theoretically and experimentally confirmed to be located within 1612 nm ~ 1613 nm region as shown in Figure 5.9 and also discussed in reference [11].

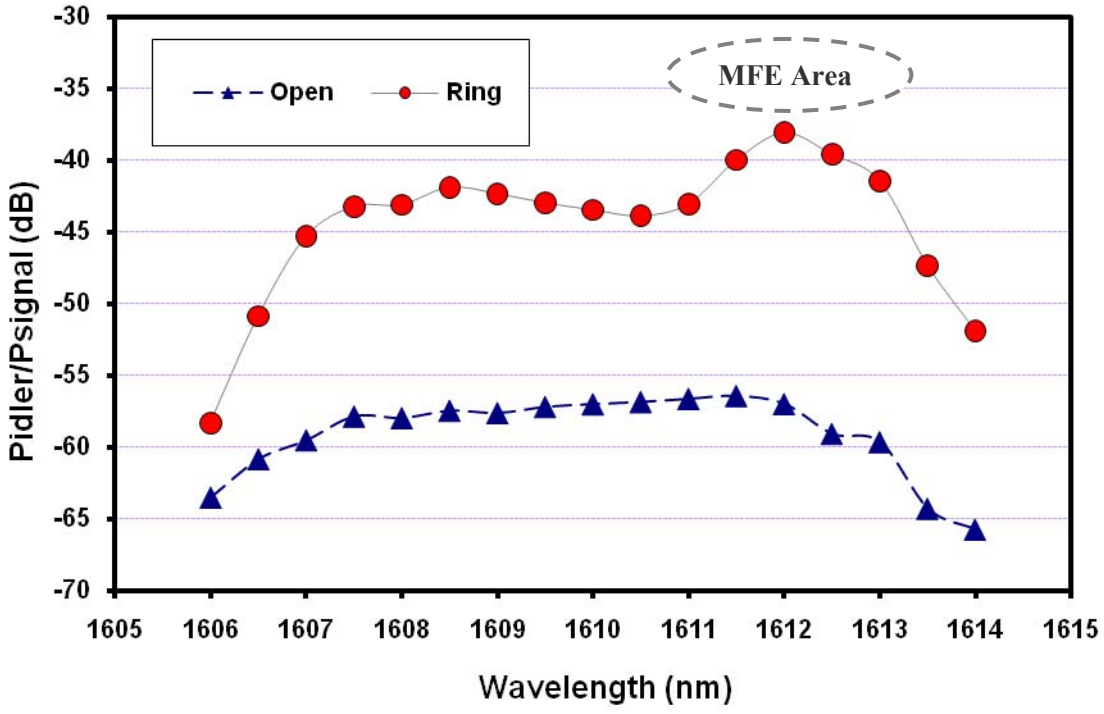

Figure 5.10: Measured ratio of the idler power to the first signal power as a function of wavelength in the two design based Bi-EDF.

Finally, to evaluate more of the FWM efficiency, a comparison of the FWM efficiency within dual-wavelength method based on three lengths of Bi-EDF with near physical properties is conducted. FWM efficiency can be also defined as [15]

$$\eta = P_{idler1}/(P^2_{sig1}P_{sig2}) \quad (5.3)$$

where P_{idler1} is the power of idler, P_{sig1} and P_{sig2} are the power of output signals. FWM efficiency is plotted in Figure 5.11 for 49 cm, 181 cm and 215 cm long of Bi-EDF. The maximum FWM efficiency is observed to be about -28.32 dB for 49 cm of Bi-EDF, which operates in the C-band region. In this region, the coherence length value is higher because of the higher gain in the shorter wavelength region and also the phase match which is easier to maintain within a shorter fiber length used. Furthermore, the FWM is more significant if the fiber length satisfies the condition of $L<L_{coh}$ [1]. The FWM efficiency in the L-band region is obtained at -37.6 dB and -46.7 dB for 215 cm and 181 cm long of Bi-EDFs, respectively as shown in Figure 5.11. These values are lower than that of C-band (49cm) because of increasing mismatching in higher length that led to shorter L_{coh} and lower FWM efficiency. However, 215cm shows a better efficiency than that of 181cm due the longer interaction length and optimum phase matching condition, which increases the efficiency. By having n_2/A_{eff} value, other nonlinear parameters for instance nonlinear phase shift (φ_{SPM}) can also be estimated. Moreover, by neglecting the dispersion effect in the reduced length Bi-EDF, the relationship between φ_{SPM} and nonlinear index coefficient can be expressed as [1]

$$\Phi_{SPM} = \frac{2\omega_0}{c} \cdot \frac{n_2}{A_{eff}} L_{eff} \overline{P} \qquad (5.4)$$

where $\overline{P}$ shows the average launched power. Inset of figure 5.11 shows the nonlinear phase shift against pump powers for the three lengths of Bi-EDF. As shown in the figure, nonlinear phase shift is lowest in the 49 cm Bi-EDF, which shows that phase match condition is satisfied and this increases the FWM efficiency as well as closing to zero dispersion wavelength. The increment of CW φ_{SPM} resulted in the decrease of idler power and FWM efficiency. The lowest FWM efficiency is obtained at only -46.7 dB for 181 cm Bi-EDF. This is attributed to the Erbium gain of this fiber which is highest in the L-band region. To confirm this, the last experiment is done on the amplification characteristic whereby a higher value flat gain (20 dB in the extended L-band region) is obtained with this fiber in comparison with the 215 cm one. However, this parameter value (φ_{SPM}) in these three lengths of Bi-EDF is very low and it can be practically ignored in the experiments. In the next section, the multi-wavelength generation will be demonstrated using the FWM phenomena.

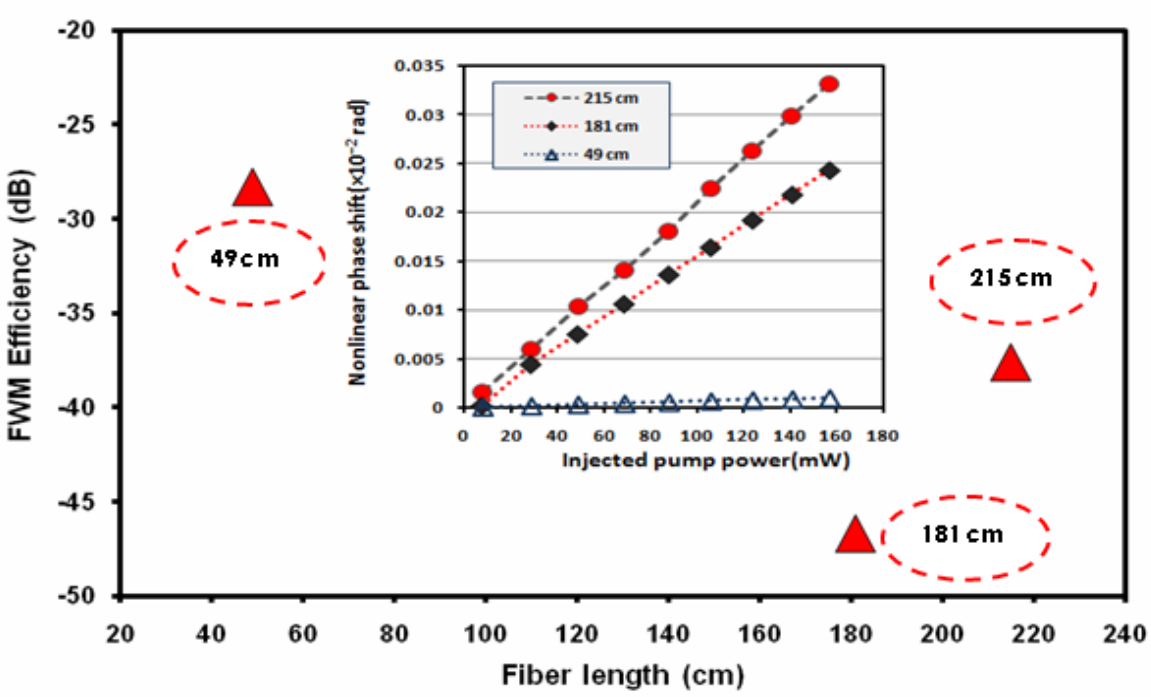

Figure 5.11: FWM efficiency as a function of fiber length. Inset shows that nonlinear phase shift as a function of input power.

5.4 FWM-based Ring Laser Using 49cm of Bi-EDF for Multi-wavelength Laser Generation

This section describes a multi-wavelength laser using a Bi-EDF assisted by FWM process in a simple ring configuration. Figure 5.12 shows the experimental setup for the ring laser, in which the resonator consists of a piece of 49 cm long Bi-EDF, a piece of 20 m long PCF, two isolators, a PC and a 90/10 output coupler. The Bi-EDF is forward pumped by a 1480 nm laser diode via a WSC to produce a stimulated emission in C-band region. The polarization maintaining PCF is used as a nonlinear gain medium to assist Bi-EDF laser in a multi-wavelength generation. Optical isolators are used to ensure unidirectional operation of the laser. PC is used to control the birefringence of the ring cavity, so that the power of the laser generated can be controlled. In this section, the operation of the FWM-

based Bi-EDF ring laser is investigated with and without the PCF in the cavity. The output of the cavity is tapped from the 90/10 coupler and characterized by an OSA.

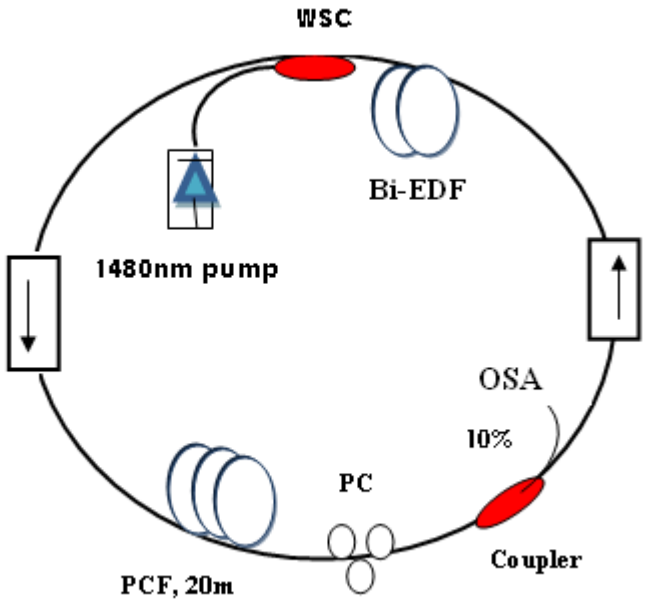

Figure 5.12: Proposed configuration of ring cavity based Bi-EDF.

Figures 5.13 (a) and (b) show the output spectra of Bi-EDF laser without and with the PCF, respectively at the maximum pump power of 150 mW. Without the PCF, the output spacing is obtained at around 0.50 nm at 1568 nm region as shown in Figure 5.13(a). The spacing is determined by the cavity length as well as the birefringence state in the cavity, which can be controlled by the PC. With the PCF, the larger spacing of 0.57 nm was obtained due to the incorporation of the PCF, which changes the cavity loss and dispersion parameter, which had been mentioned in chapter 2. The incorporation of PCF also improves the FWM characteristics of the laser due to the longer interaction length between the signals and medium in the cavity. However, the number of lines obtained is limited to only three lines due to the availability of the pump power, erbium gain and insufficient

coherence length in Bi-EDF. The performance of the FWM-based Bi-EDF laser in linear cavity will be presented in the next section.

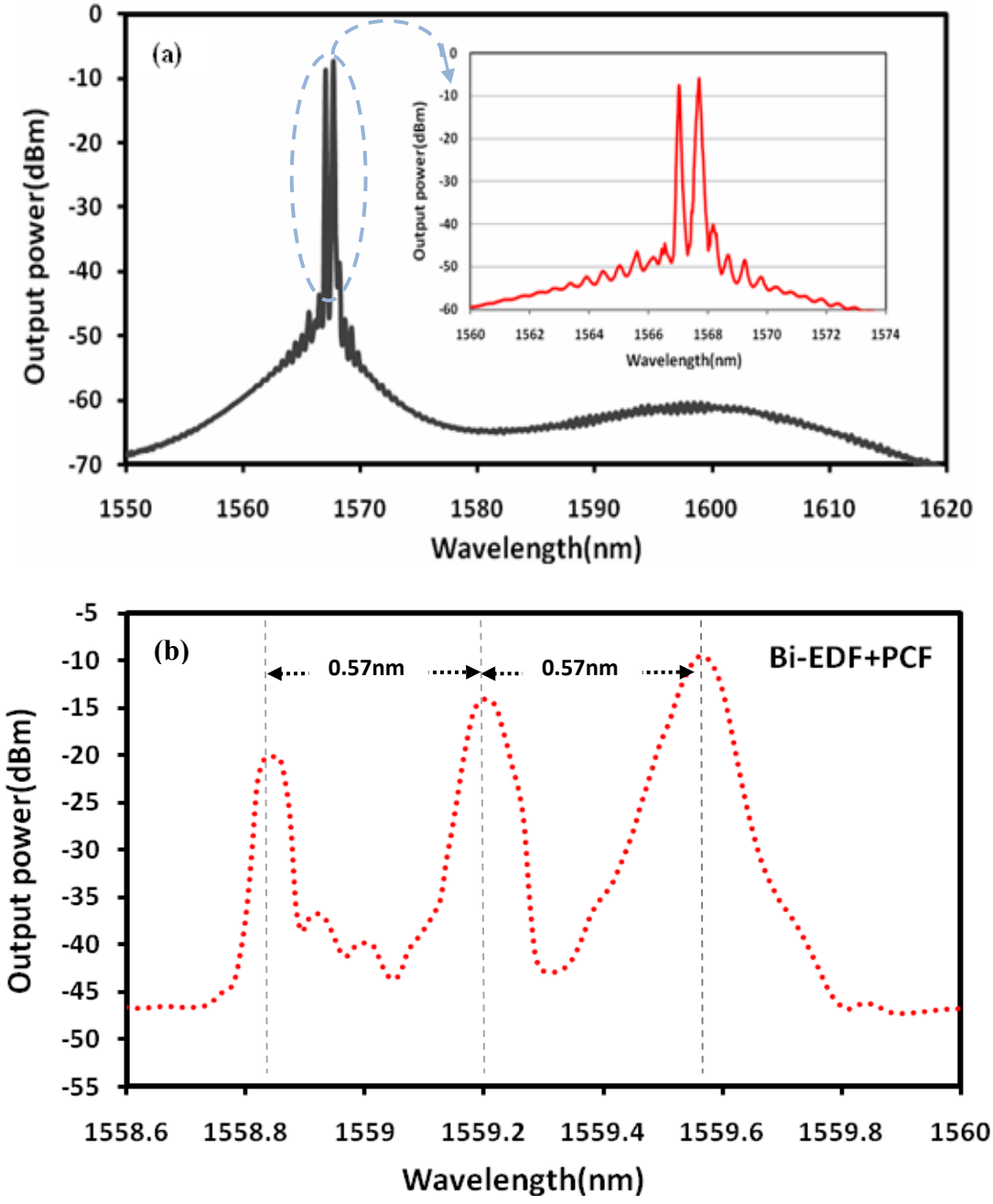

Figure 5.13: The output spectrum of the Bi-EDF laser **(a)** without and **(b)** with the PCF at 150 mW pump power from 1480 nm laser source.

5.5 FWM-based Bi-EDF Self-seed Multi-wavelength Laser in the Linear Cavity

In this section, a multi-wavelength laser is demonstrated using only 49 cm long Bi-EDF assisted by FWM process in a linear cavity. The forward pumped Bi-EDF acts as both linear and nonlinear gain media. The linear gain will generate Erbium laser lines which interact with each other in the same medium to generate a multi-wavelength comb. The experimental setup for the multi-wavelength laser is shown in Figure 5.14, which uses the 49 cm long Bi-EDF that we introduced in chapter 2. The Bi-EDF is forward pumped using a 1480 nm laser diode where the pump and laser wavelengths are combined using the WSC. Two optical circulators designated as OC1 and OC2 in which port 3 is connected to the coupler and then to port 1 is used at both ends of system to act as a reflector. A 3-dB coupler is used to tap the output of the laser via Port A and Port B as shown in Figure 5.14, which is then characterized by an OSA.

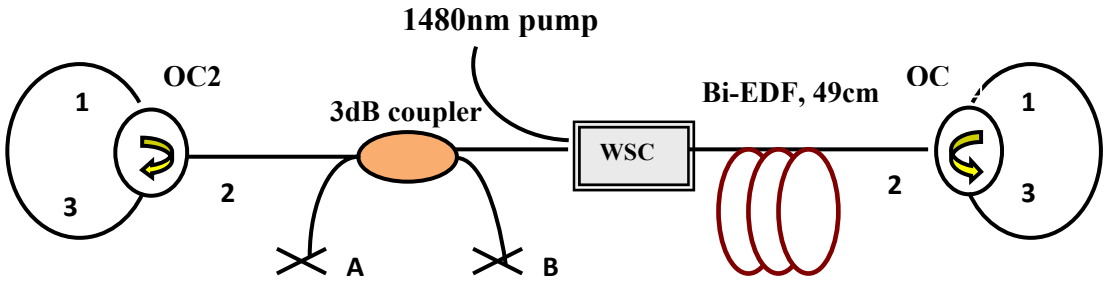

Figure 5.14: Experimental setup for the proposed a Bi-EDF based multi-wavelength laser.

The operating wavelength of the multi-wavelength laser is determined by the forward pumped Bi-EDF gain spectrum which covers the conventional band (C-band) region from 1525 nm to 1570 nm as well as the cavity loss. The output spectrum of the

multi-wavelength laser at Ports A and B is investigated as shown in Figure 5.15, in which the oscillating laser lines are observed in the 1565 nm region. The 1480 nm pump power is fixed at 160 mW. The laser operates at this region due to the cavity loss which is lower at the longer wavelength. The forward pumped Bi-EDF generates amplified spontaneous emission at C-band region which oscillates in the linear cavity to generate at least two oscillating lines while the spacing is determined by the cavity length and the birefringence characteristic in the linear cavity. The multi-wavelength laser generation with a constant spacing is assisted by the FWM process. A PC has been used to control the polarisation and the birefringence inside the cavity, which in turn controls the number of line generated, channel spacing and the peak power. As shown in Figure 5.15, the output lines are more pronounced at Port A with optical signal to noise ratio (OSNR) higher than 44 dB as compared to the Port B.

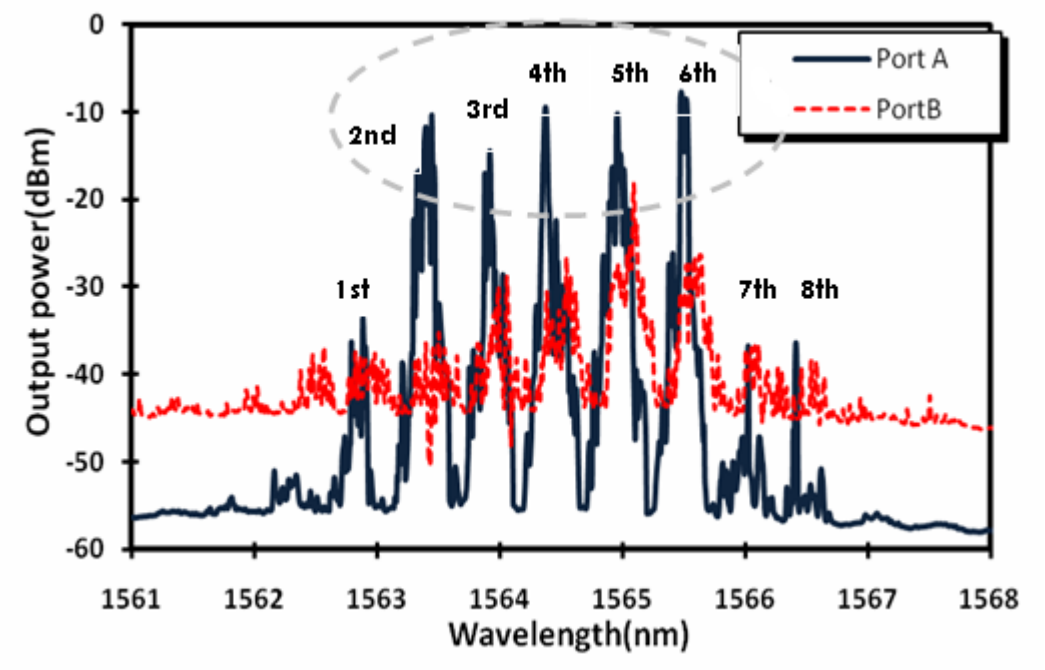

Figure 5.15: Output spectrum of the proposed Bi-EDF based multi-wavelength laser at different output ports.

Figure 5.16 shows the output spectrum of the multi-wavelength laser at Port A for different pump power of 1480 nm. At the minimum pump power of 28 mW, the Erbium gain is very low and the peak power of the oscillating laser lines is below the threshold of the FWM process and thus only two lines were observed. The number of generated line as well as the peak power is observed to increase as the pump power for the 1480 nm laser diode increases which is attributed to the increment of the Erbium gain with pump power. This situation provides sufficient signal power for the FWM process to generate additional lines. In this experiment, 8 lines are obtained within a bandwidth of approximately 5nm at the maximum 1480 nm pump power of 160 mW with 5 of these lines have a peak power above -15 dBm and the lines spacing is measured around 0.52 nm. The pump threshold of the laser is approximately 30 mW. The number of lines are limited by the availability of the 1480 nm pump power or Erbium gain, fiber nonlinearity and polarisation filtering effect in the linear cavity resonator. The multi-wavelength output is observed to be stable at room temperature with only minor fluctuations observed coinciding with large temperature variances.

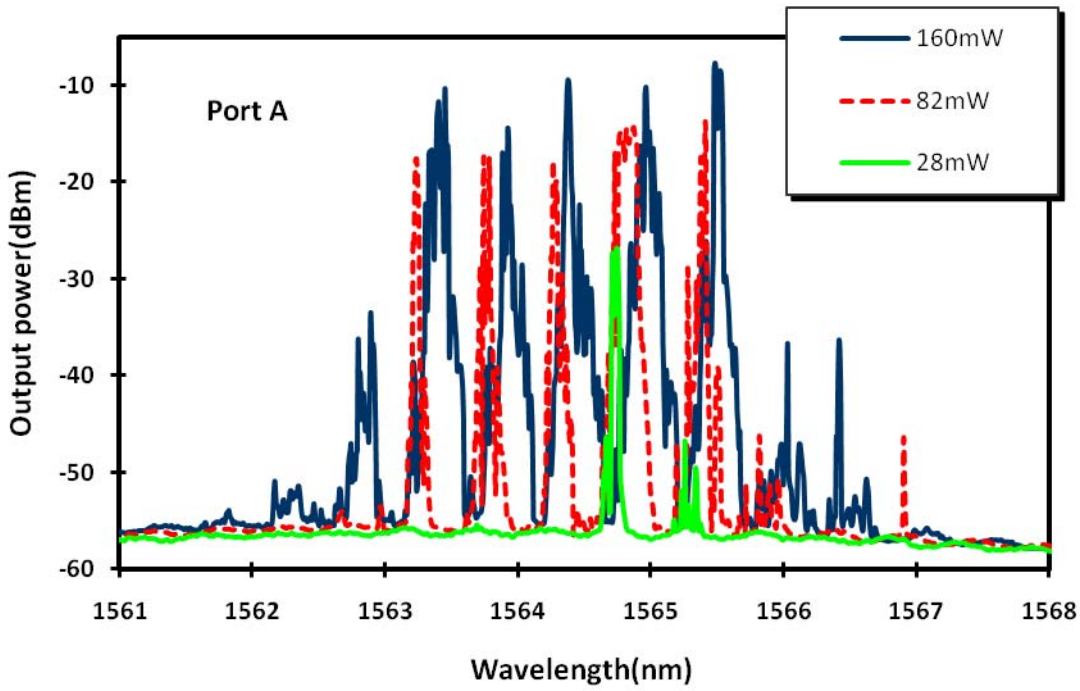

Figure 5.16: Output spectrum of the proposed Bi-EDF based multi-wavelength laser at1480 nm of different pump powers.

Figures 5.17(a) and (b) compare peak power of five middle lines of the output comb against 1480 nm pump powers which were obtained at port A and B, respectively. As shown in Figure 5.17, the peak powers of the lines are suddenly increased as the 1480 nm pump power reach to 40 mW especially at Port A. This is attributed to the Erbium gain which is start to be positive at this pump power level and thus assists in multi-wavelength generation. After this threshold power, the average output powers of port A (Figure 5.17(a)) are observed to be higher than that of port B (Figure 5.17(b)) by at least 10 dB. At Port A, the FWM lines 5^{th} and 6^{th} shows a higher power compared to the rest due to the Erbium gain which is highest at this wavelength region. The FWM lines are unstable at Port B due to variation in cavity loss, Rayleigh scattering and interference between the ASE and output signals.

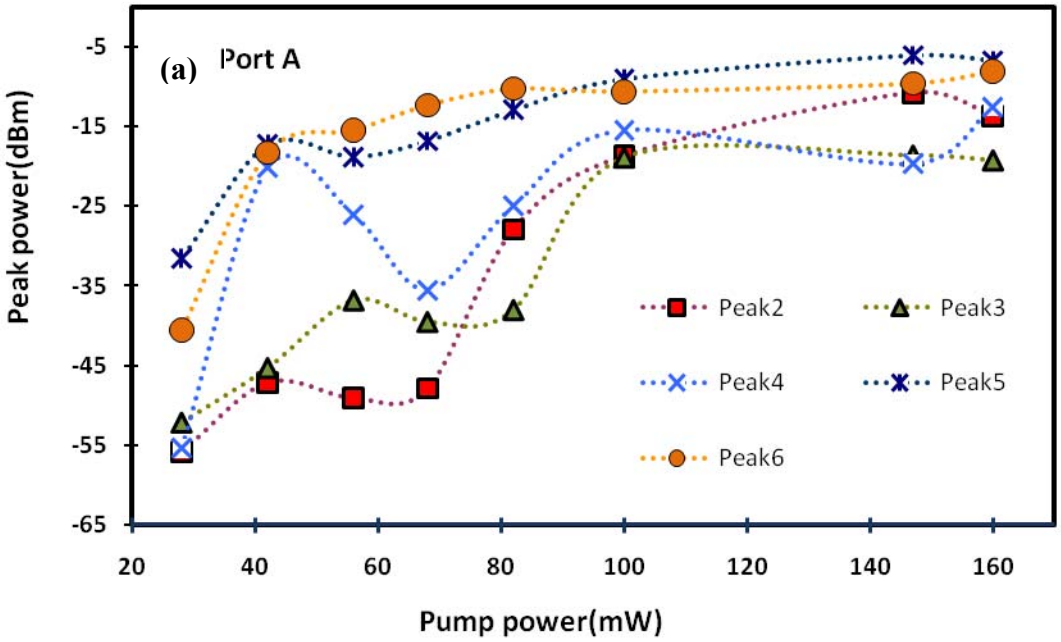

(a) Port A

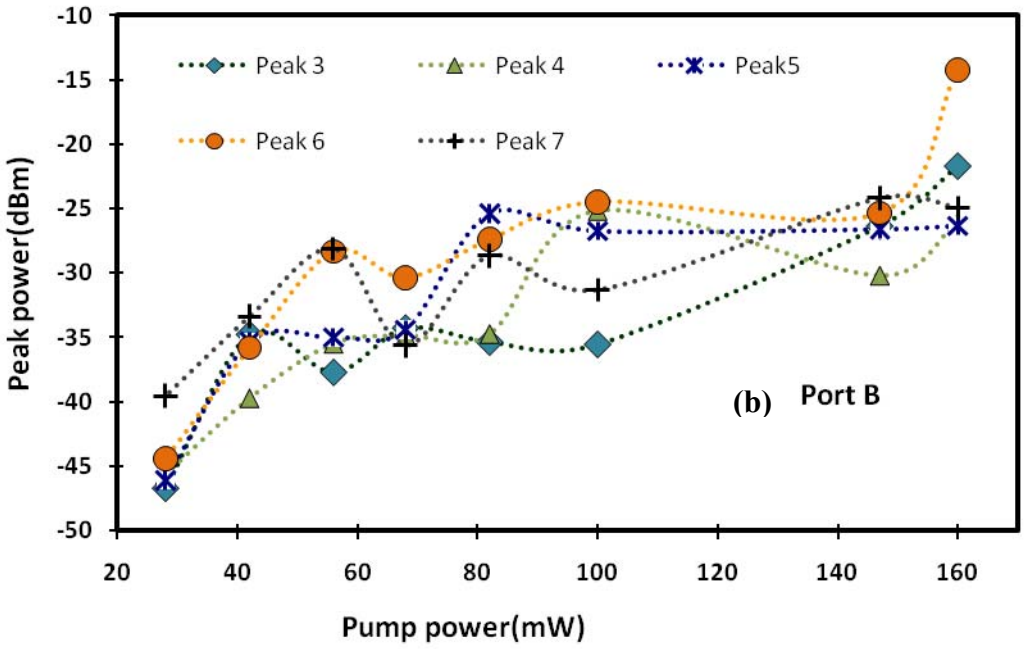

(b) Port B

Figure 5.17: Peak powers of 5 middle lines of the output comb against 1480nm pump power at **(a)** Port A and **(b)** Port B.

5.6 Multi-wavelength Laser Generation with Bi-EDF in Extended L-band Region

A multi-wavelength laser is demonstrated using the Bi-EDF assisted by FWM process in a ring cavity resonator. The backward pumped Bi-EDF acts as both linear and nonlinear gain media. The linear gain will generate Erbium laser lines which interact with each other in the same medium to generate a multi-wavelength comb with a constant spacing. The experimental setup of the proposed multi-wavelength laser is shown in Figure 5.18. It uses a ring resonator containing a 215 cm long Bi-EDF, optical isolators, PC and 10 dB output coupler. The Bi-EDF is backward pumped using a 1480 nm laser diode to generate gain in extended L-band region. The WSC is used to combine the pump and laser wavelengths. To control the birefringence inside the cavity, which in turn control the number of lines generated, channel spacing and the peak power, the PC is used so that the output laser generated can be optimized. Two optical isolators are used in our case to block the spurious back reflection from each component and to ensure unidirectional operation of the laser. A 10-dB coupler is used to tap the output of the laser via 10% port as shown in Figure 5.18, which is then characterized by an OSA. The total cavity length of the ring resonator is approximately 7m. As discussed in chapter 3, the forward ASE by 215 cm long Bi-EDF covers the long-wavelength band (L-band) region from 1570 nm to 1620 nm and peaks at approximately 1615 nm. The gain spectrum of the amplifier follows the ASE spectrum and peaks also at 1615 nm. At 150 mW pump power, the Erbium gain is obtained at around 15dB at 1615 nm region. The operating wavelength of the multi-wavelength laser is determined by the Bi-EDF gain spectrum as well as the cavity loss. The insertion losses of the isolators, PC, WSC and coupler are slightly wavelength dependent.

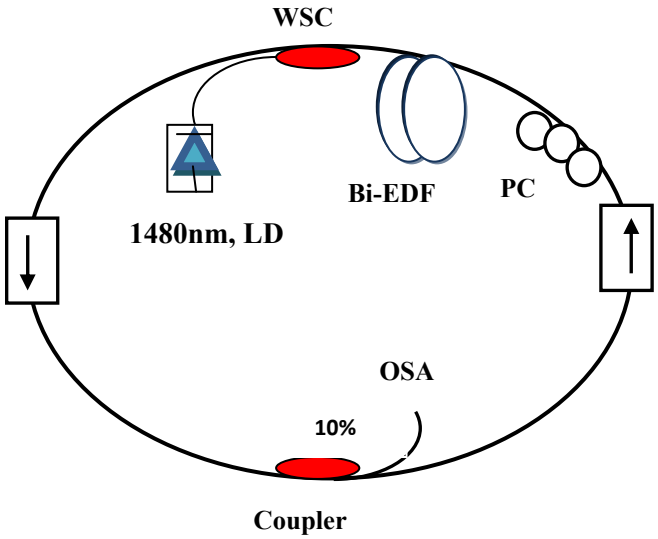

Figure 5.18: Experimental setup for the proposed a Bi-EDF based multi-wavelength ring laser.

Figure 5.19 shows the output spectrum of the multi-wavelength laser for different 1480 nm pump power. As shown in the figure, the oscillating laser lines are observed in the 1615.5 nm region, which falls within an extended L-band region. The amplification bandwidth of the Bi-EDF is extended to this region because of the suppression of excited-state absorption (ESA). The laser operates at this region due to the cavity loss which is lower at the longer wavelength. The backward pumped Bi-EDF generates amplified spontaneous emission at this region which oscillates in the ring cavity to generate at least two oscillating lines with a constant spacing due to the longitudinal modes interference. The strong forward oscillating laser generates a backward propagating reflected light in the gain medium (due to Rayleigh scattering and Fresnel reflection) to form a standing wave which interferes with each other to form multiple modes. The multi-wavelength laser generation with a constant spacing is assisted by the FWM process, which annihilates photons from these waves to create new photons at different frequencies.

As shown in Figure 5.19, more than 10 lines are obtained at the maximum pump power of 147 mW. At the minimum pump power of 100 mW, the Erbium gain is lower and only one strong oscillating laser is generated. Since another oscillating laser line is below the threshold of the FWM process, no additional frequencies lines were observed. The number of generated line as well as the peak power is observed to increase as the pump power for the 1480 nm laser diode increases which is attributed to the increment of the Erbium gain with pump power. This situation provides sufficient signal power for the FWM process to generate additional lines. In this experiment, the strongest line has a peak power of approximately -2dBm and the line spacing is measured to be approximately 0.41nm, which is determined by the cavity length and the birefringence in the ring cavity. According to Eq. 2.39 of Chapter 2, the dispersion parameter of the Bi-EDF can be determined from the fixed length of the Bismuth fiber, channel spacing and operating wavelength of the generated FWM signals. In this case (L=215cm, $\Delta\lambda$=0.41nm and λ=1615nm), the fiber dispersion parameter D is estimated to be approximately 95 (ps/nm.km), which is comparable with other reports in this wavelength region [17, 18]. Figure 5.20 also shows the output spectrum when the polarisation state in the ring cavity is un-optimised. In this case, 5 simultaneous lines like mirror images are obtained with a constant spacing of approximately 1.23 nm.

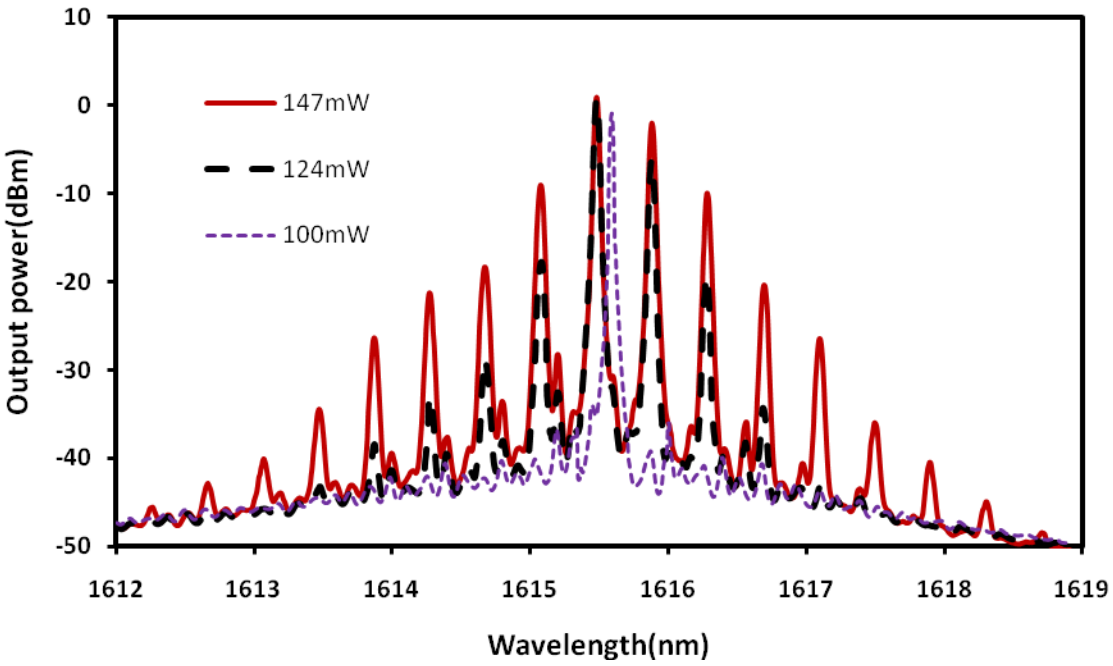

Figure 5.19: Output spectrum of the proposed Bi-EDF based multi-wavelength ring laser at different 1480 nm pump powers.

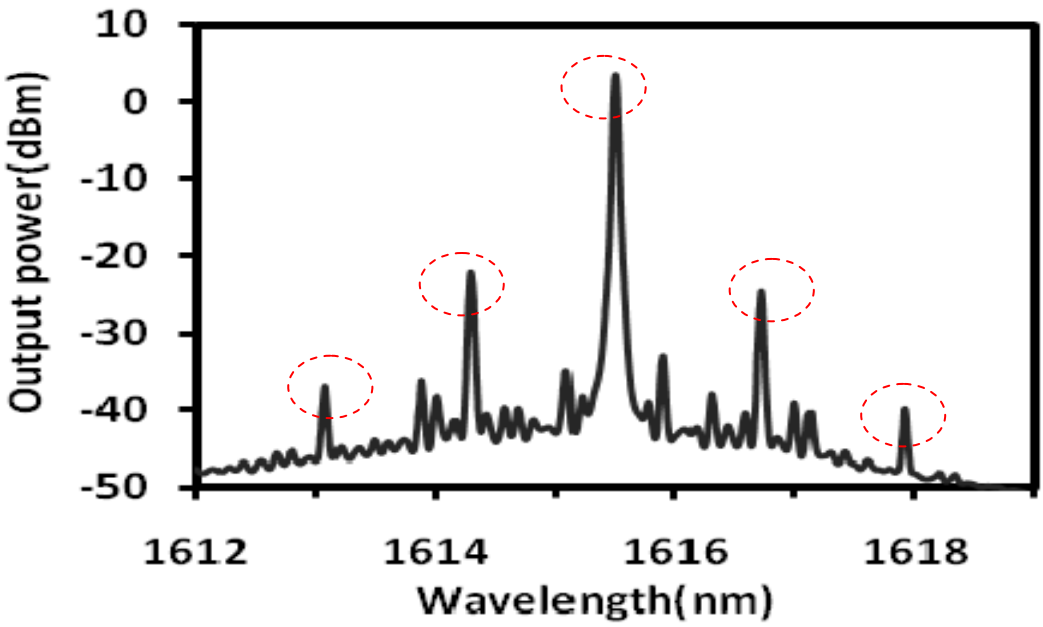

Figure 5.20: The output spectrum when the polarization is un-optimized.

Figure 5.21 shows the peak power against 1480 nm pump power for the best 4 lines of the laser comb. As seen in this figure, the pump threshold for the additional lines to be generated is approximately 100 mW and the peak power increases with the pump power. The number of lines are limited by the availability of the 1480 nm pump power or Erbium gain, fiber nonlinearity and polarisation filtering effect in the linear cavity resonator. The multi-wavelength output is observed to be stable at room temperature with only minor fluctuations observed coinciding with large temperature variances.

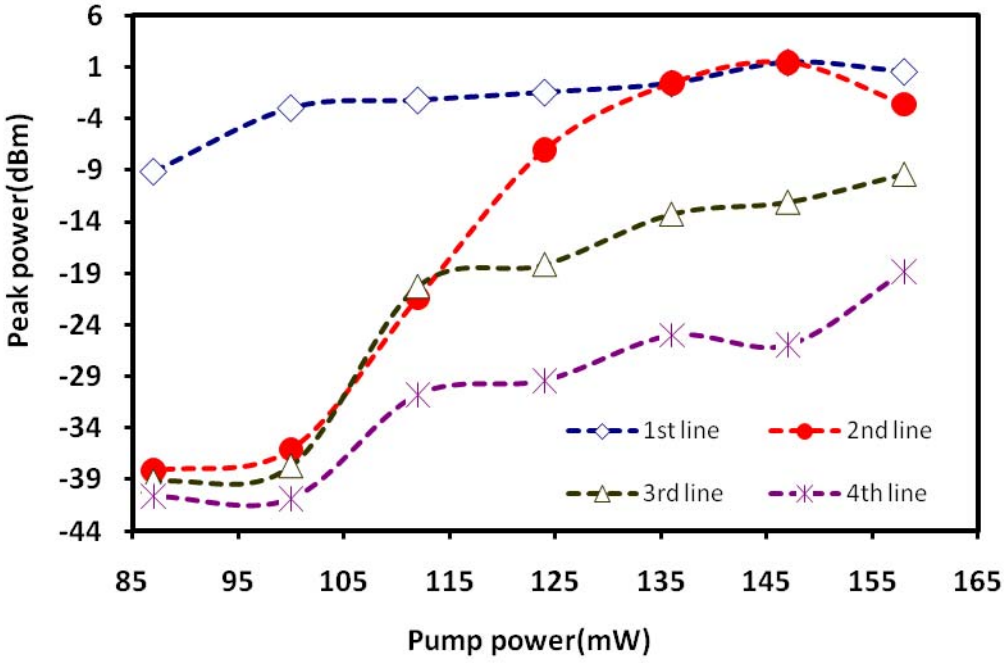

Figure 5.21: Peak power against pump power of the 1480 nm laser diode for first 4 lines in the multi-wavelength laser spectrum.

In this study, we also examined the effect of incorporating 20 m long PCF in the ring cavity on the performance of the multi-wavelength laser. In this case, the PCF was incorporated in between the isolator and output coupler. The output spectrum of the laser is

shown in Figure 5.22 at various 1480 nm pump power. As shown in the figure, the FWM comb is observed with a channel spacing of 0.12 nm. The comb obtained is worst in this case compared to that of previous setup (without PCF). This is due to the phase mismatch in the ring cavity with a longer and hybrid nonlinear gain medium. In addition, the operating wavelength of this laser is within the extended L-band region that is very far from zero dispersion wavelength of the PCF. The zero-dispersion wavelength plays an important role in FWM Stokes generation and the value is around 1040 nm for this length of PCF. In the next section, the effect of incorporation of PCF is studied for linear Bi-EDF laser. The linear cavity is used in conjunction of bi-directional pumping to reduce the cavity loss and enhance the gain in the configuration.

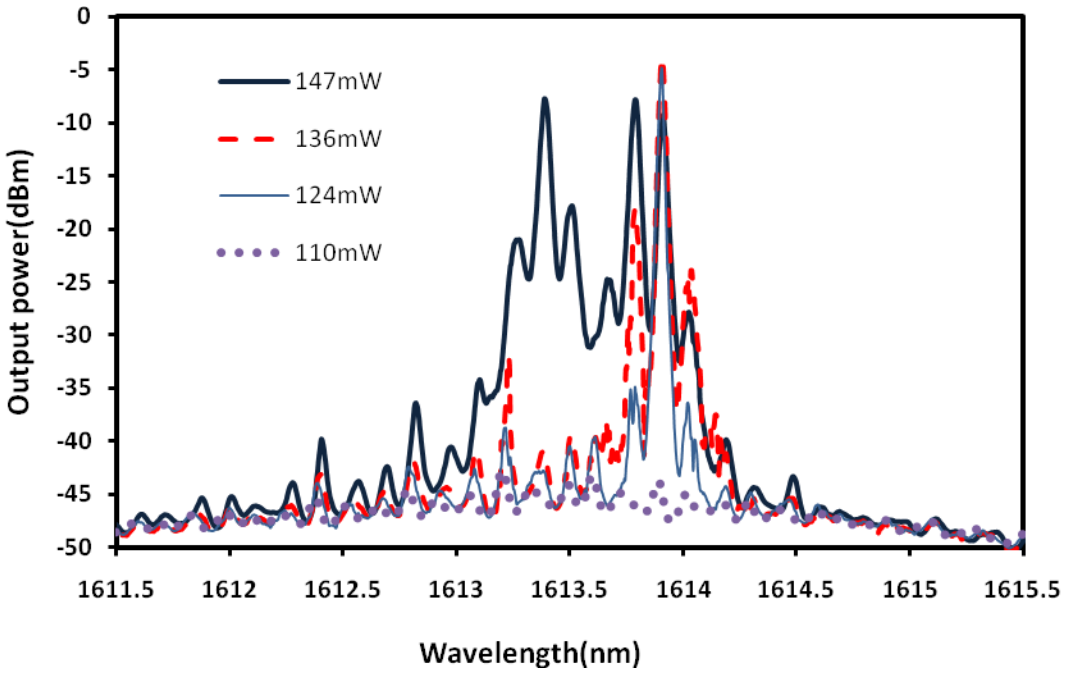

Figure 5.22: Multi-wavelength spectra of the ring laser with incorporation of PCF at different 1480 nm pump powers.

5.7 FWM-based Multi-wavelength Laser with Incorporation of PCF in Linear Cavity Configuration

The technology of photonic crystal fiber (PCFs) has rapidly progressed in recent years, with many successful applications such as nonlinear optical devices for fiber-optic communication systems. PCFs can have much higher nonlinearity per unit length than conventional fibers, and devices based on such fibers can thus be much shorter in length, and/or operate at lower power levels. As the FWM can be very efficient at the zero-dispersion wavelength, the use of PCF would allow the operation of these nonlinear devices in the wavelength regime outside the possibility of using conventional fibers (besides the obvious advantage of shorter fiber requirement). This is because the PCFs, unlike DSFs, can have a zero dispersion wavelength ranging from 550-1550 nm [16]. In this section, a PCF based multi-wavelength laser is demonstrated using a FWM effect in a linear cavity resonator. A bi-directionally pumped Bi-EDF is used in the resonator to generate an Erbium laser which interacts with a tunable laser source signal in the PCF to generate a multi-wavelength comb.

The experimental setup for the PCF-based multi-wavelength laser is shown in Figure 5.23. It consists of a Bi-EDF approximately 2.15 m in length. The Bi-EDF is pumped bi-directionally using two 1480 nm lasers. A 20 m long PCF is used as a non-linear gain medium and a WSC is used to combine the pump and laser wavelengths. The PC is used to control the birefringence of the linear cavity so that the power of the laser generated can be controlled. Two optical circulators designated as OC1 and OC2 in which port 3 is connected to the coupler and then to port 1 is used at both ends of system to act as a reflector. Two couplers, designated as C1 and C2, is incorporated at OC1 and OC2 to tap the output and inject a pump signal respectively as shown in Figure 5.23. An external

cavity TLS with the maximum power of 6 dBm is used as the pump signal. The output of the linear cavity BEFL is tapped from the output coupler C1 and is characterized by an OSA. The output ratio of C1 is fixed at 5% and the coupling ratio of C2 port to inject pump power from TLS is varied from 1 to 50%.

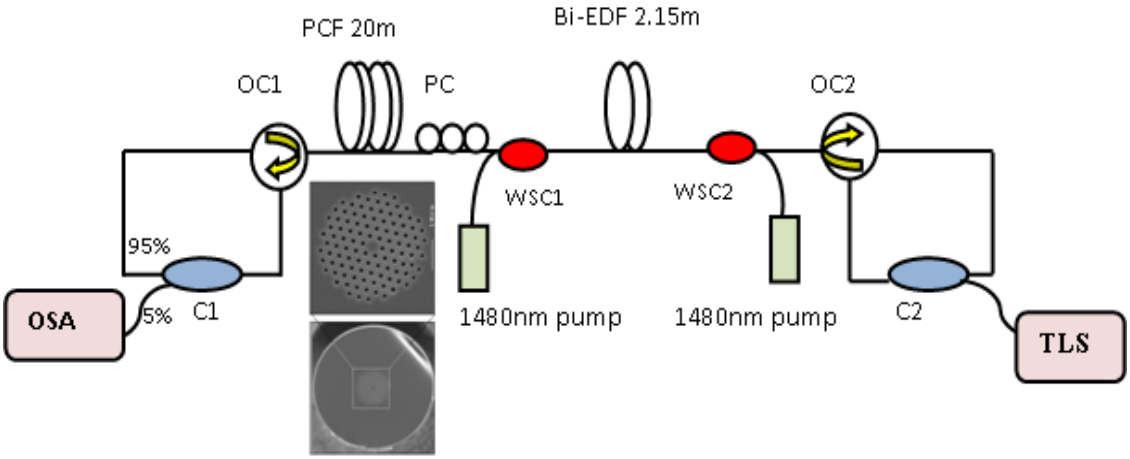

Figure 5.23: Experimental FWM setup for the proposed PCF-based multi-wavelength laser.

The operating wavelength of the multi-wavelength laser is determined by the bi-directionally pumped Bi-EDF gain spectrum which covers the long wavelength band (L-band) region from 1565 nm to 1620 nm as well as the cavity loss. The Bi-EDFA has a small signal gain of approximately 30 dB at 1585 nm with a total 1480 nm pump power of 270 mW. The free running spectrum of the Bi-EDF laser (without BP) is also investigated in which the oscillating laser is observed in the 1585 nm region. Therefore, the pump signal is injected at this wavelength region into the linear cavity via C2 and OC2. The

Erbium laser and the amplified pump signal oscillate in the cavity and interact in the PCF to generate a multi-line spectrum as shown in Figure 5.23.

Figure 5.24 compares the output spectrum of the multi-wavelength laser at different C2 coupler ratio. The pump power for each 1480 nm laser diode and TLS is fixed at 135 mW and 6 dBm, respectively. As shown in Figure 5.24, more than 10 lines are obtained for all coupling ratios of C2. The multi-wavelength comb is obtained by precisely varying the TLS signal wavelength from 1583.0 nm to 1585.2 nm and controlling the polarisation state of the light inside the linear cavity using a PC. The injected TLS signal is shown in the spectrum as the highest peak. The wavelength spacing between the lines varies from 0.34 nm to 0.39 nm. The multi-wavelength generation is attributed to the FWM effect, which annihilates photons from both waves to create new photons at different frequencies. At 50/50 coupling ratio, the peak power of most of the lines is lowest compared to other coupling ratios. The reduction of power is due to the reduction of reflectivity at OC2, which subsequently increases the cavity loss and reduces the overall output power of the laser. Although output power and optical signal to noise ratio (OSNR~35dB) in 99/1 port is higher than others, the line spacing does not have the same value.

One of the interesting applications of FWM is spectral inversion. Consider a case that involves the input of a strong single-frequency pump wave along with a relatively weak wave having a spectrum of finite width positioned on one side of the pump frequency. FWM leads to the generation of a wave whose spectrum is the “mirror image” of that of the weak wave, in which the mirroring occurs about the pump frequency [19]. The representation of this image can be observed in Figure 5.24(a) where the spectrum is symmetry with the use of 50/50 coupler.

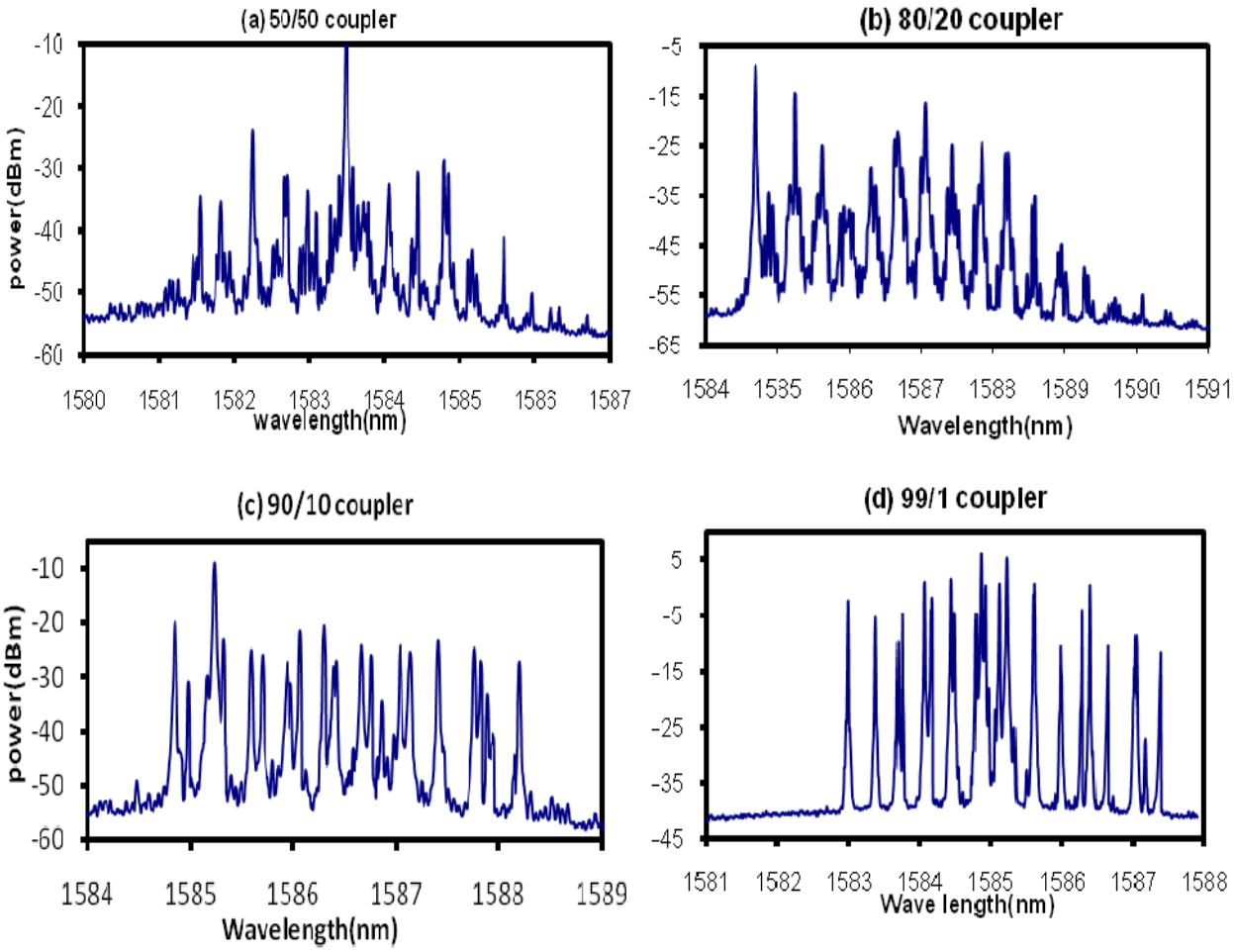

Figure 5.24: The output spectrum of the multi-wavelength laser at different coupling ratios of C2.

Figure 5.25 shows the output spectrum of the multi-wavelength laser at different power of each 1480 nm laser diode. The coupling ratio of C2 is fixed at 80/20, in which 20% of the TLS power is injected into the cavity and 80% of the oscillating light is reflected back into the linear cavity. The peak power of each line increases with the 1480 nm pump power increment. At pump power of 69 mW, no multi-wavelength comb is observed as shown in this Figure. This is attributed to the Erbium gain which is very low at this pump power and cannot sufficiently compensate for the loss inside the linear cavity and

thus no laser is generated at 1585 nm region. The number of FWM signals increases as the 1480 nm pump powers are further increased as shown in Figure 5.25. In every FWM peak, a weak Brillouin scattering is also observed with channel spacing of 0.09 nm.

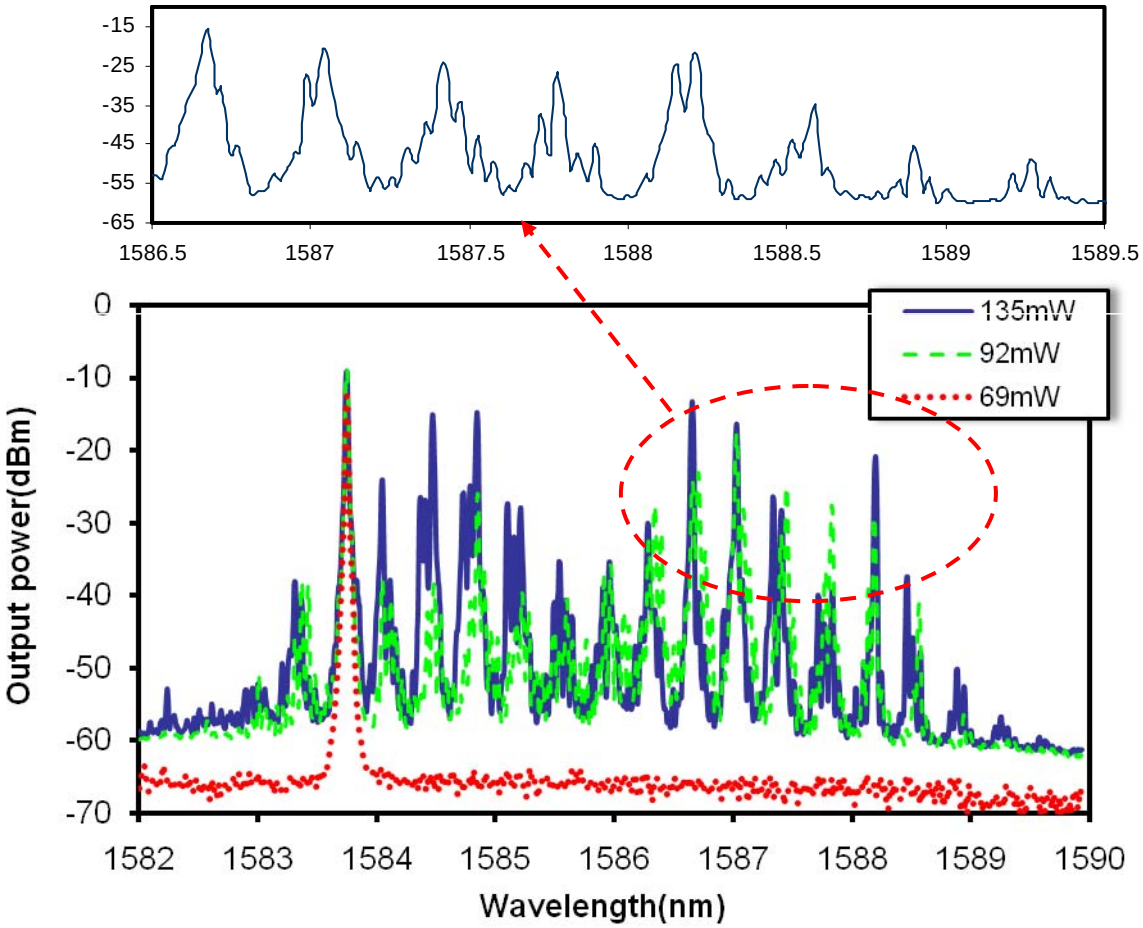

Figure 5.25: Multi-wavelength spectra 80/20 coupler at different combination 1480 nm pump powers, P1=P2 (mW) at the same time.

In quantum-mechanical terms, FWM can be defined as a phenomena that occurs when photons from one or more waves are annihilated to create new photons at different frequencies. In this process, the net energy and momentum are conserved during the

parametric interaction [1]. Hence, during the degenerate FWM process of $2\omega_1 = \omega_2 + \omega_3$, two photons at frequency ω_1 are annihilated in order to create a photon at frequency ω_2 and another photon at frequency ω_3 as described in Figure 5.26. Then, in the total nonlinear processes, the photon-exchanging number of ω_2 is equal to that of ω_3 and to a half of the photon-exchanging number of ω_1. Taking into account $\omega_1 \approx \omega_2 \approx \omega_3$, the total transfer energy of ω_1 is as twice as that of ω_2 and ω_3, respectively. According to the energy conservation, the decreased (or increased) power of ω_1 should be equal to the sum of the increased (or decreased) powers of ω_2 and ω_3, i.e., $\delta P_1 + \delta P_2 + \delta P_3 = 0$ [12], which can be observed in Figure 5.27.

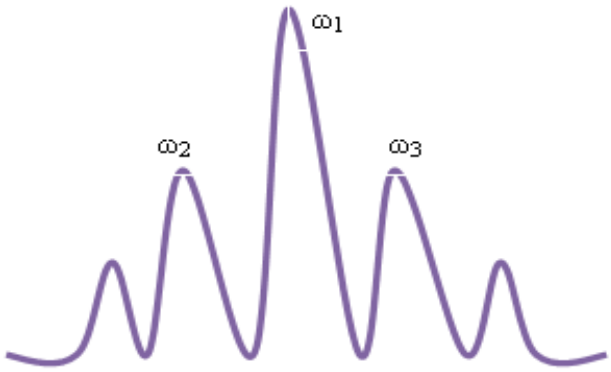

Figure 5.26: Schematic of degenerate FWM effect.

Figure 5.27 shows the output spectrum at various BP power. As shown in the figure, by varying the BP power from -6 dBm to 6 dBm, the power of the lines increases at a certain area but decreases in another area with constant line spacing. This proves the conservation of energy during the process.

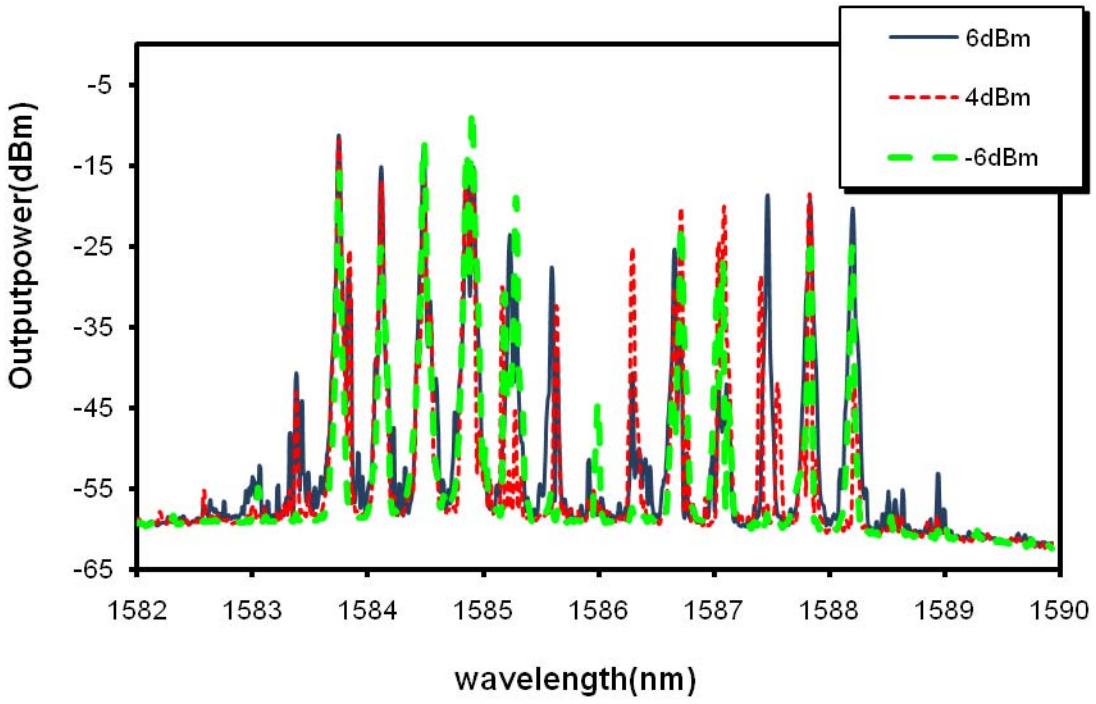

Figure 5.27: Conservation of multi-wavelength energy in different pump power of BP at 1583.75 nm signal and 80/20 output coupler ratio.

We have demonstrated a multi-wavelength comb using a FWM process in PCF based on Bi-EDF configuration. The comb generation is due to the interaction between an Erbium laser from a Bi-EDF pumped by 1480 nm laser and a TLS signal. The comb has more than 13 lines with channel spacing varying from 0.34 nm to 0.39 nm. However besides this application, the FWM effect can also be employed for signal amplification, phase conjugation, wavelength conversion and high-speed optical switching.

REFERENCES

[1] G. P. Agrawal, "Nonlinear Fiber Optics," Fourth edition, Academic Press, 2007.

[2] M. B. Mashade and M. N. Abdel Aleem, "Analysis of Ultra-Short Pulse Propagation in Nonlinear Optical Fiber," Progress In Electromagnetics Research B, Vol.12, pp. 219-241, 2009.

[3] H. Ahmad, S. Shahi and S. W. Harun, "Multi-wavelength laser generation with Bismuth based Erbium-doped fiber," Optics express, Vol.17, No.1, pp. 203-207, 2009.

[4] S. Pachnicke, J. Reichert, and E. Voges, "Impact of polarization-mode dispersion and fiber nonlinearities on four-wave mixing efficiency, " OECC, 5F2-2-2, 2006.

[5] W. Belardi, J. H. Lee, K. Furusawa, P. Petropoulos, M. Ibsen, T. M. monro, and D. J. Richardson, "A 10 Gbit/s tunable wavelength converter based on four-wave mixing in highly nonlinear holey fiber," ECOC, PD1.2, Copenhagen, Denmark, 2002.

[6] K. Inoue and H. Toba, "Wavelength conversion experiment using fiber four-wave mixing," IEEE Photon. Technol. Letts.Vol. 4, pp. 69-72, 1992.

[7] G. Keiser, "Optical Fibre Communications," McGraw Hill, pp. 498-499, 2000.

[8] H. L. Liu, H. Y. Yam, W. H. Chung, P. K. A. Wai, and N. Sugimoto, "La-codoped Bismuth-based Erbium doped fiber ring laser with 106-nm tuning range," IEEE Photon. Technol. Letts., Vol. 17, pp. 297–299, 2005.

[9] A. Boskovic, S. V. Chernikov, J. R. Taylor, L. Gruner-Nielsen, and O. A. Levring, "Direct continuous-wave measurement of n_2 in various types of telecommunication fiber at 1.55 μm," Opt. Lett., Vol. 21, pp. 1965–1967, 1996.

[10] T. Omae, K. Nakajima, and M. Ohashi, "Universal conditions for nonlinear refractive index n_2 estimation of dispersion compensating fibers by CW-SPM method," Optical fiber conference (OFC), TuH3, Anaheim, USA, 2001.

[11] K. Inoue, "Experimental Study on Channel Crosstalk Due to Fiber Four- Wave Mixing Around the Zero-Dispersion Wavelength, " J. Light-wave tech., Vol. 12, No. 6, 1994.

[12] X. M. Liu, "Four-wave mixing self-stability based on photonic crystal fiber and its applications on Erbium-doped fiber lasers," Optics Communications 260, pp.554–559, 2006.

[13] G. Keiser, "Optical Fibre Communications, " McGraw Hill, pp. 498-499, 2000.

[14] G. P. Agrawal, "Applications of Nonlinear Fiber Optics, " Academic Press, San Diego, California 92101-4495, USA,2001.

[15] S. Ohara, N. Sugimoto, K. Ochiai, H. Hayashi, Y. Fukasawa,T. Hirose, T. Nagashima, M. Reyes, "Ultra-wideband amplifiers based on Bi_2O_3-EDFAs," Optical Fiber Technology 10, pp. 283–295, 2004.

[16] J.C. Knight, J. Arriaga, T. A. Birks, A. Ortigosa-Blanch, W. W. J, and P. S. J. Russell, "Anomalous dispersion in photonics crystal fiber, " IEEE Photon. Technol. Letts. 12, pp. 807-809, 2000.

[17] N. Sugimoto, "Erbium doped fiber and highly non-linear fiber based on bismuth oxide glasses, " Journal of Non-Crystalline Solids, No.354, pp.1205–1210, 2008.

[18] D. K. Mynbaev and L. L. Scheiner, "Fiber optic communications technology," 2001.

[19] J. A. Buck, "Nonlinear effect in optical fiber," J. Opt. Soc. Am., Vol.5, No.4, pp.103, 2001.

CHAPTER 6

CONCLUSION AND FUTURE WORKS

6.1 Conclusions

In this thesis, a thorough study on Bismuth-based Erbium-doped fiber (Bi-EDF) is carried out for optical amplifiers and nonlinear fiber laser applications. Various configurations on the continuous-wave (CW) multi-wavelength fiber lasers have been proposed and demonstrated using the Bi-EDF as both the linear and nonlinear effects. Nonlinear effects such as the stimulated Brillouin scattering (SBS) and four-wave mixing (FWM) in the fiber lasers to generating stimulated fiber laser and multi-wavelength comb lines either through a Brillouin/Erbium fiber laser (BEFL) or FWM-based fiber laser are the novel features of this research. Another target of this work was producing compact nonlinear fiber laser device.

Bi-EDF based optical amplifier

Erbium-doped fiber amplifier (EDFA) is used in the optical networks such as wavelength-division multiplexing (WDM) system to amplify the weak signals which propagate through it. After traveling in a specific distance, the signal becomes weak, then this signal enters the EDFA, into which light at 980 nm or 1480 nm is injected using a pump laser to stimulate the Erbium to achieve the amplification through photon emission at 1550 nm, so that the signal gets stronger, as it travels down the fiber. One of the objectives of this study is to characterize the performance of the reduced lengths of Bismuth-based

EDFA (Bi-EDFA) in terms of amplification bandwidth, conversion efficiency, gain and noise figure in various condition including pump powers, amplifier configurations, signal powers and signal wavelengths. The use of Bi_2O_3 in the Bi-EDF allows high Erbium ions concentration to be doped without a significant concentration quenching effect. The high refractive index of Bi_2O_3 broadens the emission spectrum of Erbium ions to achieve a broader flat gain profile compared to normal silica-based EDF. Much shorter length of Bismuth-based EDFA exhibits better performance with less ripples for amplification in both C- and L-band regions (1530 nm to 1620 nm) compared to silica-based EDFA. From the results, double pass and bi-directional pumping presented higher flat gain signals in comparison with uni-directional pumping. Therefore it plays an important role in the development of a compact EDFA that operates in this area. Although, we used C-band Bi-EDFA for double pass pumping to produce multi-wavelength Brillouin Erbium fiber laser applications with average gain more than 10 dB but it suffers a higher noise figure penalty at higher input signal powers. Thus, in most of the configurations, it is preferred to employ a single-pass configuration to improve the signal to noise ratio.

The gain and noise figure spectra are compared at different input signal powers as a function of different input wavelengths and pump powers for applications in C- and L-band regions. With 49 cm long Bi-EDF, the maximum gain of approximately 26 dB was achieved at the input signal power of -30 dBm for 1535 nm signal using a backward pumping scheme. The gain value is approximately 4 dB higher than forward pumping. With practical pump power level of 150 mW, the noise figure varies from 4.0 dB to 9.4 dB at input signal of -30 dBm with the backward pumping. At the input signal power of 0 dBm, a flat gain spectrum is achieved with an average gain of 11.2 dB using either forward and backward pumping. The forward pumping scheme produces a relatively lower noise

figure compared to the backward pumping especially for the small input signals. The noise figure is also relatively higher at high input signal power due to the domain of output ASE level factor which reduces the population inversion at input power of the amplifier.

The L-band Bi-EDFA has been also demonstrated using a piece of 215 cm long Bi-EDF as the gain medium. The amplifier performances have been investigated in terms of PCE, QCE, gain and noise figure. The highest QCE and PCE for 215 cm long of Bi-EDF are estimated to be approximately 23.7% and 25.7%, which is obtained at 1605 nm. The lowest QCE and PCE are calculated to be 11.1% and 11.7%, respectively at 1570 nm. The backward pumping provides a better gain compared with the forward pumping with the expense of noise figure. Therefore, the forward pumping is more desirable in optical network. With the forward pumping, the maximum gain of the L-band Bi-EDFA is obtained at the extended L-band region, which peaks at 11.5 dB and 7.29 dB for input signal powers of -30 dBm and 0 dBm, respectively. The peak gains are obtained at wavelengths, which coincides with the maximum emission and absorption coefficient of the Erbium ion. At input signal of 0 dBm, the 3 dB bandwidth of the gain spectrum covers more than 45 nm region from 1575 nm to 1620 nm) that shows the suitability of the Bi-EDFA for L-band amplifier application. At input signal power of -30 dBm, the maximum noise figure of around 12 dB is also observed at 1560 nm and reducing with the increment of signal wavelength. The minimum noise figure of 3.2 dB is obtained approximately 1620 nm region. These results show that the excited state absorption (ESA) of Erbium ion in Bi-EDF is shifted to longer wavelengths compared to other host. This enables Bi-EDF to exhibit high gain and low noise figure operation in the extended L-band. Therefore, the Bi-EDFA is suitable for the flat-gain operation, which covers both L-band and extended L-band regions.

In order to improve the gain of the Bi-EDFA in both C- and L-band region, bi-directional Bi-EDFA is also proposed using a 215 cm long Bi-EDF. The Bi-EDF is bi-directionally pumped by two 1480 nm laser diode at pump power of 120 mW. The maximum gain is obtained at 34 dB at around 1570 nm. The operation of the bi-directional Bi-EDFA covers from C-band to the extended L-band regions. This shows that the Bi-EDFA is a promising candidate for practical wideband amplifiers. Furthermore, the bi-directional Bi-EDFA has a higher gain compared to uni-directional pumping because it reduces the under-pumped fiber length significantly.

Raman amplifier

Distributed Raman amplifier is also demonstrated in this thesis because it will be used to assist in comb generation in Brillouin fiber laser. In contrast to an EDFA which uses a specially constructed fiber for the amplification medium, a Raman amplifier makes use of the transmission fiber itself. In this thesis some pieces of different types of fibers are examined as a gain medium for the distributed Raman amplifier. We have compared the performance of Raman amplifiers with four types of fiber pieces (49 cm long Bi-EDF, 20 m long PCF, 25 km long SMF and 7.7 km long DCF). The highest gain of 5.1 dB is obtained with the DCF at 1540 nm region.

Bismuth-based Brillouin Erbium fiber laser (BEFL)

This thesis demonstrates the enhanced SBS phenomenon in the Bi-EDF and investigates the performance of a ring and linear cavity BEFL based on this fiber for producing single- and multi-wavelength lasers. Firstly, the single wavelength BEFL was demonstrated using only 215 cm long Bi-EDF in a ring cavity. The laser operates at a wavelength of 1613.93 nm with a peak power of 2 dBm as well as the SMSR of more than

22 dB when the BP and 1480 nm pump powers are fixed at 5 dBm and 152 mW, respectively. The same length of Bi-EDF is also used to generate a multi-wavelength comb laser with a constant spacing. A stable output laser comb of 40 lines was observed at a BP of 1615.59 nm and 7dBm and 1480 nm pump at 155 mW. Besides that, in another design of linear cavity, the 215 cm of Bi-EDF produced more than 50 lines by changing the coupler location to reduce the cavity loss. The number of generated Stokes and anti-Stokes lines increases as the 1480 nm pump power increases. The proposed BEFL can be considered as a compact device since it only uses a short piece of Bi-EDF as the gain medium.

When another gain medium such as SMF and PCF is incorporated together with the Bi-EDF, the operation wavelength of the BEFL shifts to a shorter wavelength region, which is near to C-band. The laser produces a better quality multi-wavelength comb with a spacing of approximately 0.09 nm. Multi-wavelength BEFL has been demonstrated using a PCF in conjunction with Bi-EDF in a simple ring resonator. This BEFL is able to generate up to 13 lines including anti-Stokes at 1574 nm region. The PCF-based BEFL is stable in room temperature and also compact due to the use of only a 20 m long PCF. The enhanced BEFL is then demonstrated using a 2.15m long Bi-EDF together with a 25 km long SMF in a linear cavity. This laser uses a pair of optical circulators at the input and output ends of the cavity to form a resonator for multi-wavelength generation in conjunction with optical couplers to inject the BP and to tap the output at the two ends. A stable output laser comb of 50 lines is obtained at a BP of 1568.2 nm and 5 dBm and two 1480 nm pumps at 120 mW. The injected BP wavelength and power as well as the 1480 nm pump powers have a great effect on the number of lines and output power of the BEFL. This configuration can be made more compact by replacing the single-mode fiber with highly non-linear fibers such as PCFs.

A new multi-wavelength BEFL operating in C-band region is also demonstrated using a shorter length of Bi-EDF (49cm) with a corporation of dispersion compensating fiber (DCF). In this work, an efficient laser comb can be achieved using a self feedback mechanism of Brillouin-Rayleigh scatterings with the presence of distributed Raman gain. The balanced of these three scatterings generates a laser comb more than 27 lines with a relatively flat amplitude and constant spacing of 0.09 nm. This is realised using a 7.7 km long DCF as the nonlinear gain medium, an amplified Brillouin pump and a broad-band fiber Bragg grating as a reflector. The number of flat-amplitude lines obtained is strongly dependent on the balance between Brillouin, Rayleigh, and Raman scattering processes

Bi-EDFL assisted by Four-wave mixing (FWM)

Multi-wavelength fiber laser comb can also be demonstrated using a FWM effect where the interaction between a pump and probe signal generates sidebands. This thesis also demonstrates the FWM effect in various types of fibers including the Bi-EDF. This effect is also used to estimate some of the nonlinear parameters such as nonlinear coefficient and nonlinear refractive index of the Bi-EDF. Firstly, a FWM effect in a short length of Bi-EDF is investigated using a open and ring configurations. The generated FWM signals are used to determine the nonlinear properties of the Bi-EDF based on two CW dual-wavelength measurement methods. By employing this method, the nonlinear parameter of γ and nonlinear index coefficient of n_2 for the 215 cm long Bi-EDF are estimated to be 59.16 ($W^{-1}km^{-1}$) and 4.40 $\times$ 10^{-19} (m^2/W), respectively at 1612 nm. The n_2 value per effective area A_{eff} is estimated to be 1.51×10^{-8} (W^{-1}). The FWM efficiency is obtained at -28.32 dB and -37.6 dB with 49 cm and 215 cm of Bi-EDF, respectively, which shows that the use of Bi-EDF is suitable for signal amplification in both C- and L-band

regions as well as for the various FWM applications such as wavelength conversion and high-speed optical switching.

The multi-wavelength fiber laser has been demonstrated for the first time based on a Bi-EDF assisted by a FWM process. Using a simple linear cavity resonator scheme cointaining a 49 cm long Bi-EDF, an optical comb with 8 lines with a line spacing of approximately 0.52 nm can be obtained using 1480 nm pump power of 160 mW. The laser operates in 1565 nm region, which is within the amplification region of the C-band Bi-EDFA. The number of lines is limited by the avaiability of the 1480 nm pump power or Erbium gain, fiber nonlinearity and polarisation filtering effect in the linear cavity resanator. The multi-wavelength output observed to be stable at room temprature with only minor fluctuations observed coinciding with large temprature variances. A multi-wavelength laser comb operating in L-band region is demonstrated using a FWM effect in a backward pumped Bi-EDF for the first time also. It uses a ring cavity resonator scheme containing a 215 cm long Bi-EDF, optical isolators, polarization controller and 10 dB output coupler. The laser generates more than 10 lines of optical comb with a line spacing of approximately 0.41 nm at 1615.5 nm region using 146 mW of 1480 nm pump power. The multi-wavelength generation is due to oscillating Bi-EDF laser lines which interacts each other to create new photons at other frequency via FWM process. A multi-wavelength Bi-EDFL is also demonstrated with incorporation of a 20 m long PCF in the linear configuration. The generated comb has more than 13 lines spaced in between 0.34 nm to 0.39 nm in the 1585 nm region with a total 1480 nm pump power of 270 mW.

6.2 Future Works

The comb generation can be further investigated using more enhanced configurations such as hybrid of two stages or more amplifier systems. The investigation should also focused to reduce further the length of Bi-EDF or to replace the Bi-EDF with other enhanced rare earth dopant fibers likes Zarconia-Yttria doped fiber that can maintain high flat gain per length coefficient of compact amplifiers. Furthermore, the study of hybrid high power Raman fiber amplifier and Bi-EDFA is also required to increase the efficiency of this amplifier in broad-band regions. In the future, a development study can be done by employing a state of the pump-signal technique which is useful for determine the Brillouin linewidth with high frequency resolution near to 1 MHz.

Besides that, the compact devices for multi-wavelength fiber laser generation can be improved with the existence of suitable Fiber Bragg Grating (FBG) and highly nonlinear reduced length fibers such as Chalcogenide fiber and sufficient length of high nonlinear PCF with properly pump power. However, the study of nonlinear and micro-structure fibers such as PCF and Bi-EDF with a low value of dispersion can improve the performance of the FWM based multi-wavelength fiber laser with suitable wavelength tuning. The FWM in the compact fiber such as Bi-EDF and PCF can also be used to study wavelength convertor. These days, the wavelength conversion technology is an attractive subject but as yet not well developed. The use of highly nonlinear fibers for many applications lead to reduce power and fibre length requirements compared to conventional fibers, the power length product has been reduced by 5-40 times. The various reduced nonlinear fiber devices products mean cheaper, potentially more stable, efficient and practical products. It seems that an interesting area of research in applications of nonlinear fiber optics remain as an important issue of the future.

APPENDIX A

LIST OF PUBLICATIONS

ISI Journals

1. S. W. Harun, **S. Shahi**, H. Ahmad, "A compact Brillouin /Erbium fiber laser," **Optics Letters**, Vol. 34, No. 1, pp. 46-48, 2009.

2. **S. Shahi**, S. W. Harun, N. S. Shahabuddin and M.R. Shirazi , H. Ahmad, " Multi-wavelength generation using a Bismuth-based EDF and Brillouin effect in a linear cavity configuration," **Optics & Laser Technology**, Vol. 4, No. 2, pp.198-201, 2009.

3. H. Ahmad, A. H. Sulaiman, **S. Shahi**, and S. W. Harun, "SOA-based multi-wavelength laser using fiber Bragg gratings," **Laser physics**, Vol. 19, No. 5, pp. 1002–1005, 2009.

4. H. Ahmad, **S. Shahi**, S. W. Harun, " Multi-wavelength laser generation with Bismuth-based Erbium-doped fiber," **Optics Express**, Vol. 17, No. 1, pp. 203-207, 2009.

5. **S. Shahi**, S. W. Harun, A. H. Sulaiman, K. Thambiratnam, H. Ahmad, " Multi-wavelength source based on SOA and EDFA in a ring cavity resonator," **Microwave and optic laser technology**, Vol. 51, No. 1, pp.110-113, 2009.

6. S. W. Harun, **S. Shahi,** H. Ahmad, " Bismuth Erbium-doped fiber based multi-wavelength laser assisted by four-wave mixing process," **IEICE Electronics Express,** Vol. 6, No. 1, pp. 40-43, 2009.

7. **S. Shahi**, S. W. Harun, and H. Ahmad, " Multi-wavelength Brillouin fiber laser using a holey fiber and a Bismuth-oxide based Erbium-doped fiber," **Laser Phys. Lett**. 6, No. 6, pp. 454- 457, 2009.

8. S. W. Harun, N. Tamchek, **S. Shahi**, and H. Ahmad, " L- band amplification and multi-wavelength lasing with Bismuth-based Erbium doped fiber," **Progress In Electromagnetics Research**, Vol. 6, pp. 1-12, 2009.

9. **S. Shahi**, S. W. Harun, K. Dimyati and H. Ahmad, " Brillouin fiber laser with significantly reduced gain medium length operating in L-band region," **Progress In Electromagnetics Research Letters**, Vol. 8, pp.143-149, 2009.

10. **S. Shahi**, S.W. Harun, and H. Ahmad, " Multi-wavelength Brillouin fiber laser using Brillouin-Rayleigh scatterings in distributed Raman amplifier," **Laser physics letters**, Vol. 6, No. 10, pp. 737–739, 2009**.**

11. **S. Shahi,** S. W. Harun, and H. Ahmad, " The comparison nonlinearity behavior of PCF with two reduced length of Bi-EDF in ring cavity," **Nonlinear optics and material journal (JNOPM),** Vol.18, No.3, pp.521-527, 2009.

12. S. W. Harun, **S. Shahi,** H. Ahmad, " Brillouin fiber laser with a 49 cm long Bismuth-based Erbium-doped fiber," **Laser Physics Lett.** Vol.7**,** No.1, pp. 60-62, 2009.

13. **S. Shahi,** S. W. Harun, K. S. Lim, A.W. Naji and H. Ahmad, " Enhanced four-wave mixing efficiency of Bi-EDF in a new ring configuration for determination of

nonlinear parameters," **J. of Electromagn. Waves and Appl. (JEMWA)**, Vol. 23, pp. 2397–2407, 2009.

14. **S.Shahi**, S.W.Harun, S.F.Norizan, M.R.A.Moghaddam and H.Ahmad, "Brillouin/Raman Multi-Wavelength Laser Comb Generation Based On Bi-EDF By Using Dual-Wavelength In Dispersion Compensating Fiber," **Nonlinear optics and material journal (JNOPM),** Vol. 9, No.1, pp.123-130, 2010.

15. H.Ahmad, **S.Shahi**, and S.W.Harun, "Bismuth based erbium doped fiber as a gain medium for L-band amplification and Brillouin fiber laser", **Laser physics**(fiber laser), Vol. 20, No. 3, pp. 716-719, 2010.

16. **S. Shahi**, S.W.Harun, K.Dimyati, M.R.Tamjis, and H.Ahmad, "Multiple Brillouin stokes generation with Bismuth –based erbium doped fiber," **MICROWAVE AND OPTICAL TECHNOLOGY LETTERS** , Vol. 52, No. 6, pp.1416-1418, 2010.

Conferences

1. S. W. Harun, **S. Shahi**, A. H. Sulaiman, H. Ahmad, " Multi-wavelength generation in ring cavity resonator based on SOA and EDFA, " 4th Mathematics and Physical Sciences Graduate Congress, Faculty of Science National University of Singapore, 17-19 December, 2008.

2. H. Ahmad, **S. Shahi** and S. W. Harun, " Multi-wavelength Brillouin fiber laser with Bi-EDF," Advance materials science and nanotechnology Conference, Nha Trang Vietnam, Dec 2008.

3. H. Ahmad**, S. Shahi** and S. W. Harun, "Bismuth-based Erbium doped fiber as a gain medium for L-band amplification and Brillouin fiber laser," Barcelona, Spain, 13-17 July, 2009.

4. N. S. Shahabuddin, A. Adamiat, Z. Yusoff, H. A. Abdul Rashid, **S. Shahi**, "An enhanced ring cavity photonic crystal fiber laser, " SEIT-126, Proceedings of the 2nd seminar on Engineering and Information Technology, Kota Kinabalu, Sabah, 8 - 9 July, 2009.

5. **S. Shahi,** S. W. Harun, K. S. Lim, R. Parvizi, M. R. A. Moghaddam and H. Ahmad, "Application of Four-Wave Mixing For Determination of Nonlinear Parameter Based on Bi-EDF," 5th Mathematics and Physical Sciences Graduate Congress, Faculty of Science, Chulalongkorn University, Bangkok, Thiland, 6-9 December, 2009.

6. **S. Shahi**, R. Parvizi, S. W. Harun, R. Jafari , and H. Ahmad, " Nonlinear Applications of Compact Bismuth Erbium Doped Fiber Amplifier, " Yazd, Iran, 26-28 January, 2010.

APPENDIX B

SELECTED PAPERS